UNIVERSITY OF SOUTHAMPTON

Faculty of Engineering and the Environment

Civil, Maritime and Environmental Engineering and Science

Experimental Investigations into the Motions of Vessels, Less Than Twenty Metres in Length, Stationed at Single Point Moorings.

Catherine Jayne Hollyhead

Thesis submitted in partial fulfilment for the degree of Doctor of Engineering.

January 2019

ABSTRACT

FACULTY OF ENGINEERING AND THE ENVIRONMENT

Civil, Maritime and Environmental Engineering and Science

Doctor of Engineering

EXPERIMENTAL INVESTIGATIONS INTO THE MOTIONS OF VESSELS, LESS THAN TWENTY METRES IN LENGTH, STATIONED AT SINGLE POINT MOORINGS.

by Catherine Jayne Hollyhead

The Royal National Lifeboat Institution (RNLI) is an independent charity whose purpose is to save lives at sea and end preventable loss of life. In order to achieve these goals 21 of their all-weather lifeboats are moored permanently to a single point mooring (SPM) and a further 19 lifeboat stations have a reserve secondary mooring. On the 23rd March 2008 a Trent class lifeboat slipped her mooring and was damaged beyond economic repair and there are also numerous media reports of vessels breaking free from their coastal harbour SPMs resulting in damage and/or rescue crews being called out. The motivations for the experimental work presented in this thesis are the reported loss of human life and damage to vessels together with the lack of consistent SPM configurations.

This project is aimed at an improved understanding of the motions experienced by a lifeboat and buoy in order to gain insight into the key factors which effect a SPM in order to provide guidance for full scale. Three changes in SPM configuration have been investigated namely: three changes in mooring line (hawser) length, two scales of mooring buoy and five shapes of mooring buoy.

The novel contributions of this research include: (1) a detailed breakdown of the literature examining the motions of vessels at SPMs, (2) the creation and validation of a portable method of motion capture which can be used for small scale laboratory testing and in-situ full scale data recording, (3) experimental data on the effects of changes in buoy shape and size upon the motions experienced by a lifeboat the results of which suggest that the introduction of a twice scale buoy reduces the risk of mooring failure by reducing the motions of a lifeboat at a SPM, (4) investigations into the coupling of the 6 degrees of freedom motions of a model lifeboat moored in regular waves the results of which show that increasing the wavelength to longer than the length overall of the model leads to a breakdown in the coupling between surge-pitch, surge-heave and heave-pitch and (5) in-situ motion data, for both vessel and buoy, from a full scale lifeboat at a SPM the results of which indicate that it is passing harbour traffic that produces the peak excursions and therefore the RNLI's SPMs should be positioned as far as is operationally practical from shipping routes.

These experimental results and in situ measurements will contribute to improving the RNLI's design and operation of its SPM. Furthermore these techniques are of use to Harbour Commissions monitoring the safe mooring of vessels e.g. the validated algorithm could be used to notify of extreme motions at a SPM via video surveillance.

Table of Contents

List of Figures:

List of Tables:

DECLARATION OF AUTHORSHIP

I, Catherine Jayne Hollyhead declare that this thesis entitled "Experimental Investigations into the Motions of Vessels, Less Than Twenty Metres in Length, Stationed at Single Point Moorings" and the work presented in it are my own, and has been generated by me as the result of my own original research. I confirm that:

- This work was done wholly or mainly while in candidature for a research degree at this University;
- Where any part of this thesis has previously been submitted for a degree or any other qualification at this University or any other institution, this has been clearly stated;
- Where I have consulted the published work of others, this is always clearly attributed;
- Where I have quoted from the work of others, the source is always given. With the exception of such quotations, this thesis is entirely my own work;
- Parts of this work have been published as listed in Section 1.4.

Signed:

Date:

ACKNOWLEDGEMENTS

Firstly, I am very grateful for the generous financial support of both the Engineering and Physical Sciences Research Council (grant EP/G036896/1) and the Royal National Lifeboat Institution (RNLI). I appreciate the support of the staff at the RNLI in particular Steve Austen who helped to set up this EngD, Charlie Cooke who always responded to my queries and Chris Noble who so very nearly pulled off a full scale sea trial.

My decision to undertake an Engineering Doctorate was driven by a desire to gain an insight and apply academic experimental techniques to a real world engineering issue. With the unwavering support, guidance and patience of my academic supervisors Drs. Nicholas Townsend and James Blake I have been able to achieve this goal. I would like to offer my appreciation and thanks to Dr Christopher Philips for allowing me to use and adapt his motion tracking Matlab code which enabled me to experiment at small scales in the University of Southampton's circulatory flume. I am also indebted to my internal examiners, Prof. Grant Hearn and Dr. Mingi Tan, for the time they have kindly given up to appraise, examine and provide invaluable feedback on my research.

I would like to add a personal thank you to Dr. Adam Sobey for his guidance for the first year of my EngD whilst sat next to me in our old home of the Froude Building. My experimental research would not have been possible without the time so willingly given by my fellow postgraduate students and I would particularly like to thank James Bowker, Trewut Anurakpandit and Apostolos Grammatikopoulos. In addition I gratefully acknowledge the support I received from the various Learning Support Assistants provided by the Enabling Services team in particular Jan Stubbington who has been assisting me since August 2014. A heartfelt thanks to skipper Peter Lemonius who so generously gave up his time and allowed us to rig up his Mersey lifeboat and refused to take a penny.

Finally Paul, Mum and Dad I send my love and kisses.

Definitions and Abbreviations

Roman symbols

A .....effective cross-sectional area (m^2)
c .....wave celerity (m/s)
d .....half horizontal distance between suspension ropes (m)
E_{FS} .....Young's modulus at full scale (N/m2)
E_M .....Young's modulus at model scale (N/m2)
F_N .....Froude number
F_{Nchan} .....Froude number for channel flow
$_{FS}$.....full scale quantities
f .....wave frequency (Hz)
g .....acceleration due to gravity (m/s^2)
H.....vertical distance between model and suspension ladder (m)
H_s.....significant wave height (m)
h_h.....hydraulic depth (m) (Froude Number)
h_r.....hydraulic radius (m) (Reynolds Number)
K .....yaw radius of gyration (m)
k .....wave number (m^{-1}) (2π/wavelength)
KW.....Kruskal-Wallis test statistic
L.....length (m)
L_{FS} .....length full scale (m)
L_H .....hawser length (m)
L_M.....length model scale (m)
L_V .....length to a reference point along its centerline (m)
$_M$.....model scale quantities
$\dot{M}$ .....mass flow rate (kg/s)
N.....number of frequency components with a signal
N_K.....total number of observation in Kruskal-Wallis test
n_K.....total number of observations per sample for Kruskal-Wallis test
R .....dimension scaling ratio (full scale length/model scale length)
Re .....Reynolds number (inertia force/viscous force)
R_{echan} .....Reynolds number for channel flow
R_{HF}.....scale of hydrodynamic forces
S_S .....scope of mooring line (m)
t.....time or temperature difference
T .....period (s)
T_{KW}.....the sum of the ranks in the Kruskal-Wallis test
U.....velocity (m/s)
U_{FS}.....full scale velocity (m/s)
U_M.....model velocity (m/s)
v.....recorded flow velocity (m/s)
W_1.....maximum load to be measured
WP.....wetted perimeter
x,y,z .....axes of right handed co-ordinate system

Greek symbols

Δ .....change in accompanying quantity
δ .....change in accompanying quantity
ϵ.....compound single error measurement
ϵ_H .....hysteresis error of load cell (%)
ϵ_L .....nonlinearity error of load cell (%)
ϵ_R .....repeatability error of load cell (%)
ϵ_S .....temperature effect on span of load cell (%)
ϵ_Z .....temperature effect on zero balance of load cell (%)
Θ.....angle between the vessel's centre of gravity and the vertical from bow fairlead (degrees)
λ .....wavelength (m)
μ .....dynamic viscosity (Pa·s)
μg.....submerged weight per unit length (N/m^3)
π .....mathematical constant
ρ .....density (kg/m^3)
θ .....yaw angle (degrees)
ϕ.....roll angle (degrees)
ϕ.....angle between hawser and the vertical from the buoy (degrees)
ψ.....pitch angle (degrees)
ω .....angular frequency (rad/s) (2π/wavelength)

Acronyms

ABS .....American Bureau of Shipping
ADBx.....Additional different shapes buoys test number
BBx .....Big Buoy test number
BST .....British Summer Time
CV .....Coefficient of Variation
DFT .....Discrete Fourier Transform
DSBx .....Different Scale and shape buoys text number
FBx.....Fixed Buoy test number
GPS .....Global Positioning System
GRT.....Gross Register Tonnage
IMU.....Inertial measuring unit
ITTC .....International Towing Tank Conference
LOA.....Length Overall
NBBx.....No Boat or Buoy test number
OCIMF .....Oil Companies International Marine Forum
RAO .....Response Amplitude Operator
RGB.....Red, Green, Blue
RMS .....Root Mean Square
RNLI .....Royal National Lifeboat Institution
SBx.....Small Buoy test number (x)
SPM .....Single Point Mooring
STD .....Standard Deviation
WEC.....Wave Energy Converter

Chapter 1: INTRODUCTION

1.1 Background and motivation

The Royal National Lifeboat Institution (RNLI) is an independent charity funded by voluntary contributions. The institution is committed to providing lifeboat cover out to 100 miles off the coast and to reach "at least 90% of all casualties within 10 nautical miles of the coast, within 30 minutes of a lifeboat launch – in any weather" (RNLI, 2015). In order to achieve these goals 21 of their all-weather lifeboats are moored permanently to a single point mooring (SPM) as indicated in Figure 1. A further 19 lifeboat stations have a reserve secondary SPM mooring for use when the lifeboat stations are inaccessible due to weather or repairs and maintenance. The particulars and statistics for each classification of lifeboat are presented in Table 1.

The location and configuration of these SPMs has been determined by local knowledge of wind, tide, current, fetch and topography (J. Deas personal communication, 27 May 2015). Since the loss of a lifeboat, whilst secured on its mooring is unacceptable, experimental data is needed to improve our understanding of how such a mooring can fail. Then steps can be taken to prevent such an occurrence and reduce the risk of potential loss of life as a result of no local lifeboat capability.

Figure 1: The Robert Charles Brown, an 11.77m Mersey class all-weather Lifeboat at a SPM.

Table 1: Class, dimensions and number of RNLI all-weather lifeboats located at SPM.

	Length	Beam	Draught	Displacement	Total Fleet	Primary mooring	Secondary mooring
	(m)	(m)	(m)	(kg)	(no.)	(no.)	(no.)
Severn	17.3	5.9	1.78	42,300	35	9	0
Trent	14.3	4.9	1.45	28,000	29	9	0
Tyne	14.3	4.4	1.45	27,000	16	2	1
Tamar	16.3	5.3	1.40	32,000	16	1	14
Mersey	11.6	4.0	1.02	14,000	31	0	3
Shannon	11.6	4.5	1.00	18,000	1	0	1

Primary moorings are permanently used mooring, secondary moorings are reserve moorings for use in rough weather conditions or when work is done on the pontoons.

On the 23rd March 2008, in Dunbar's Torness harbour, the *Sir Ronald Pechell BT* a Trent class lifeboat slipped her mooring and was damaged beyond economic repair during a force 8 storm (Lost Dunbar, 2009). This prompted the RNLI to begin an organisation wide audit to review its SPM design and quality in order to reduce the risk of any further incidents. The main focus of the recommendations was the quality, monitoring and replacement of chains, shackles and swivels all of which have now been acted upon by the RNLI, but there still remains a lack of understanding of the motions experienced by a moored lifeboat.

During the review a standard template, an example of which is presented in Figure 2, was created to record specific mooring configuration and environmental conditions for each SPM. An examination of these revealed a wide variety of configurations a breakdown of which is provided in Appendix A. For example the number of mooring ground chains varied with one station having 1 chain, four with 2 chains, twenty one with 3 chains (e.g. Figure 2), twelve with 4 chains and one with 5 chains. The majority (thirty three) are secured via mooring anchor, four using a sinker and the remaining a combination of the two. The hawser is the mooring line between SPM itself and moored vessel. The upper and lower hawsers of the RNLI (see items 4 and 5 in Figure 2) also vary in length as do both the riser and mooring ground chains (see items 10 and 13 in Figure 2).

Environmental characteristics were recorded separately, a summary of which is presented in Appendix B. The six recorded environmental factors are: water depth (m), maximum wave height (m), highest astronomical tide (m), available boat swing (m) in the horizontal plane, wind fetch (Nm) and current flow (m/s).

These recorded configurations and environmental conditions were used to determine the depth, current and wave heights in the model experiments performed.

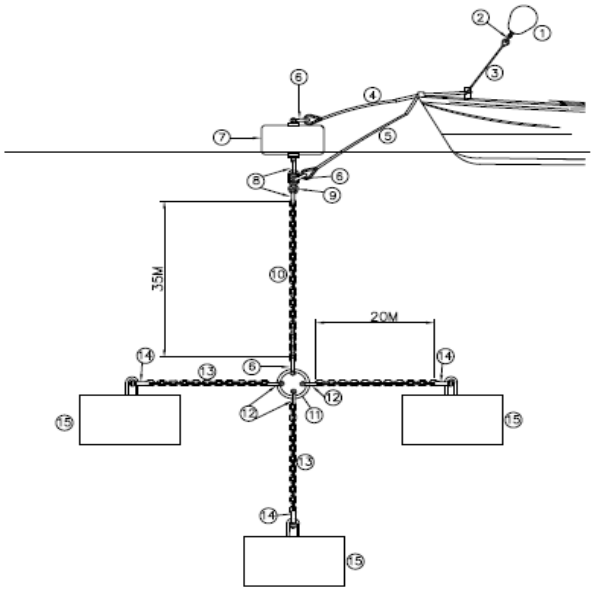

1	Buoy marker
2	Forelock shackle
3	Pickup rope
4	Polypropylene hawser (strop rope)
5	Polypropylene hawser (strop rope)
6	Forelock shackle
7	Hippo buoy with fixed chain rings
8	Swivel forelock shackle
9	Lloyds swivel
10	Chain riser
11	Mooring ring
12	Forelock shackle
13	Mooring ground chain
14	Anchor forelock shackle
15	Sinker/Anchor

Figure 2: Example of a RNLI single point mooring configuration.

In order to reveal any trends in the RNLI's SPM configurations correlations of the three SPM parameters of upper hawser length, number of ground chains and length of chain riser have been investigated for the environmental parameters of water depth, wave height, tidal flow, lifeboat class and available boat swing.

The results presented in Figure 3 show no correlation and, according to the Operations Manager of the RNLI, the main criterion for configuration has been the topography and material composition of the seabed (J. Deas personal communication, 27 May 2015). There are four pairs of SPM with the same configurations namely: Alderney and St Peters Port (both Channel Islands), Barra and Sheerness, Fishguard and Portree and Moeltre and Mumbles. It is therefore clear that there has been little co-ordinated scientific basis to these SPM configurations and it appears that no account has been taken of the variety of tide or wave conditions.

In addition to those of the RNLI there are significant numbers of SPM moored boats around the world, including 391 listed marinas in the U.K (Which-Marina, 2015). These moorings employ a variety of hawser lengths and buoy shapes, including spherical, cylindrical, barrel and modular buoys (Budder, 2017). Thus buoy size and shape also provides a potential parameter for scientific investigations.

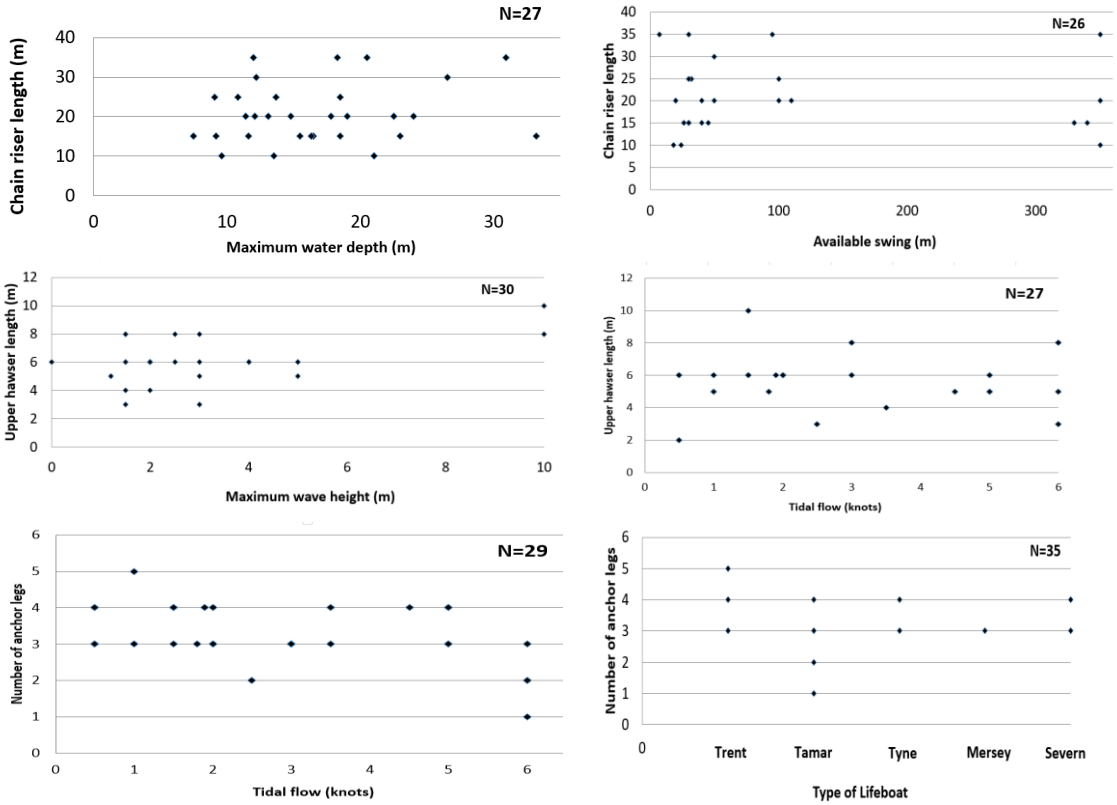

Figure 3: Investigated correlations between mooring configurations and external parameters. N is the number of RNLI's SPM where data were available.

The SPM of vessels less than 20m in length in coastal harbours are, to date, not a significant part of academic research despite the risks involved to human life. In 2001 the Marine Accident Investigation Branch published its findings from its ten year database of all accidents reported to them under the UK's Merchant Shipping (Accident Reporting and Investigation) Regulations. During this period 85 fishermen's lives were lost of which 6 were reported due to "mooring and towing lines" accidents (Lang, 2001). Deaths included; whiplash from failed mooring line, mooring line slipping from fairlead and struck by failed mooring rope. A further report into analysis of fishing accident data between 1992 to 2000 states that 5 out of 171 deaths at sea were due to "Mooring or Towing Gear and Equipment." (Lang, 2002). These statistics highlight the need to better understand the motions and forces experienced by a moored vessel in order to reduce fatigue and failures.

Due to the adverse publicity SPM failures are not readily reported by Harbour Commissions but some examples of publically available incidents are presented in Table 2. These incidents further illustrate that there is value to be gained from a better understanding of the factors that impact the total excursions and velocity of a boat attached to a SPM.

Table 2: Examples of reported SPM mooring failures.

Date	Location	Incident	Website
February 2008	Isle of Sheppey	30ft yacht which broke its mooring in high winds.	(BBC, 2008b) http://news.bbc.co.uk/1/hi/england/kent/7272434.stm
June 2010	South Cornwall	"Concern of number of mooring failures in the past few years … evidence of significant variation in the configuration of moorings."	(Percuil River Mooring Ltd. 2010) http://www.percuilriver.co.uk/implementation-mooring-contractor-guidelines
April 2012	Isle of Wight	5 Daring class yachts sunk on their SPM during 48-53knots north-easterly gales in Cowes harbour, on the south coast of UK. The Harbour Commission subsequently reduced the number of swing moorings by 5.	(IWCP, 2012) http://www.iwcp.co.uk/news/news/boats-sink-in-heavy-seas-44153.aspx
July 2012	Isle of Man	32ft yacht was washed ashore after its mooring failed.	(BBC, 2012) http://www.bbc.co.uk/news/world-europe-isle-of-man-18952895
March 2013	Guernsey	36ft yacht broke from its moorings.	(BBC, 20013) http://www.bbc.co.uk/news/world-europe-guernsey-21739188
November 2013	Dorset	Several vessels broke their moorings, some cases badly damaged and at least one was written off.	(SeaSurveys, 2013) http://www.turbolink.co.uk/seasurveys2011/news.html
June 2016	Scottish Highlands	36ft yacht was washed ashore after its mooring failed.	(Yachting and Bating World, 2016a) http://www.ybw.com/news-from-yachting-boating-world/may-dream-aground-plockton-23755
August 2016	Dorset	Yacht believed to have broken free from its mooring.	(Yachting and Bating World, 2016a) http://www.ybw.com/news-from-yachting-boating-world/yacht-smashes-and-sinks-in-portland-harbour-39858

1.2 Motivation, aims and objectives

The motivations for the experimental work performed for this Engineering Doctorate were the reported loss of human life and damage to vessels together with the lack of consistent mooring configurations and emphasis in the current research on the motions of moored tankers. The following are the bases for the chosen experimental parameters:

- Hawser length appears in the two dimensional equations for sway and surge (Halliwell & Harris, 1988) which suggests this would impact boat motion.
- In initial experiments the observed flow patterns around the buoy indicated that its shape and size may influence boat motions as well as its own motions.
- The size and weight of the buoy will impact the catenary shape of its mooring chain which may impact the motions of the buoy and the vessel.

This project is aimed at an improved understanding of the motions experienced by a lifeboat and buoy in order to gain insight into the key factors which effect a SPM in order to provide guidance for full scale. This was achieved through a combination of:

1. Ascertainment of the current level of knowledge regarding the motions of vessels at single point moorings through a literature review.
2. Sourcing an accurate and repeatable method of motion capture.
3. Performance of a systematic series of experiments, using a free standing SPM, incorporating changing line length, buoy shape and buoy size whilst recording the motions of a lifeboat and the buoy in current and regular waves
4. Recording of full scale motions of a lifeboat and its buoy at a SPM.

1.3 Outline structure of thesis

This thesis is split between three experimental methodologies namely: experiments on the motions of a model lifeboat at a SPM in a circulatory flume, experiments of a model lifeboat at a SPM in regular waves and data acquisition at full scale of a lifeboat at a SPM.

Chapter 2 reviews the literature relating to boats stationed at SPM. It is divided into sections describing the current knowledge for vessels in deep off-shore waters and shallower coastal regions. For each the literature for model and full scale testing is presented along with an example of a currently available computer simulation. Finally the published research into mooring buoy shape is presented.

Chapter 3 details the experimental investigations of the effect of changes in line length, buoy shape and buoy size upon the motions of a 1:40 scale lifeboat, at a SPM, in steady current. Chapter 4 details the experimental investigations of the effect of changes in buoy shape and buoy size upon the motions of a 1:10.67 scale lifeboat, at a SPM, in regular waves. Chapter 5 presents the in situ motion data acquisition of a Mersey class lifeboat at Yarmouth Harbour.

Chapter 6 draws the thesis Chapters together by discussing the validated experimental methodologies, the effects of buoy size in the two different experimental set-ups and the implications of the in-situ data recording. Finally Chapter 7 presents the conclusions of this thesis.

1.4 Novel contributions

The outcomes and novel contributions of this research are:

- A detailed breakdown of the literature examining the motions of vessels at single point moorings.
- Creation and validation of a simple, adaptable, consistent, inexpensive and portable method of motion capture which can be used for small scale testing, without the need of cabled instrumentation, and for in-situ full scale motion capture.
- Provision, of currently unavailable, experimental data on the effects of changes in buoy shape and size upon the motions experienced by a lifeboat and buoy itself (Hollyhead et.al., 2017). Results suggest that the introduction of a twice scale buoy may reduce the risk of mooring failure by reducing the motions of a lifeboat and therefore the mooring fatigue experienced at a SPM in a tidal coastal harbour.
- Investigations into the coupling of the 6 degrees of freedom motions of a model lifeboat moored in different regular wave frequencies. Results showed that increasing the wavelength to longer than the length overall of the model lead to a breakdown in the coupling between surge-pitch, surge-heave and heave-pitch.
- In-situ motion data, for both vessel and buoy, from a full scale lifeboat at a SPM in a coastal harbour whilst providing further validation of motion capture systems. Results indicate that it is passing harbour traffic that produces the peak excursions and the RNLI's SPMs should positioned as far as is operationally practical from shipping routes.

These experimental results and in situ measurements will contribute to improving the RNLI's design and operation of its SPM. The novel validated experimental techniques can be applied to record motion data in a variety of laboratory and full scale testing. Furthermore these techniques are of use to Harbour Commissions monitoring the safe mooring of vessels e.g. the validated Matlab algorithm could be used to notify of extreme motions at a SPM via video surveillance or a motion tracking mobile phone application can be written utilising the accelerometers now built into them.

This research has been published and/or presented in the following mediums:

1. Hollyhead, C.J., Townsend N.C. and Blake J.I.R., (2017). Experimental investigations into the current-induced motions of a lifeboat at a single point mooring. *Ocean Engineering,* 146, 192-201. (Bibliography 1.1)
2. Hollyhead, C.J., Townsend N.C. and Blake J.I.R., (in preparation). Experimental investigations into the wave-induced motions of a lifeboat at a single point mooring. *Ocean Engineering.* (Bibliography 1.2)
3. Presentation at 5th UK Marine Technology Postgraduate Conference, Newcastle, 9th June 2014. "The motion and security of moored floating bodies."
4. Presentation at EngD conference 2014 – 'Solving Global Engineering Challenges', St Mary's Stadium, Southampton, 20th November 2014. "Observational and experimental investigations into the behaviour of Lifeboats at single point moorings."

Bibliography 1.1 and Bibliography 1.2 are provided after Appendix G.

Chapter 2: LITERATURE REVIEW

"Anchoring seems not to be so much a lost art as one which never caught up with the times" (van Dorn, 1974).

This chapter presents the literature review. The motions of a vessel at a single point mooring (SPM) are described in Section 2.1. The published model and full scale experiments performed for offshore depths (over 50m) and coastal waters are outlined in Sections 2.2 and 2.3 respectively. Section 2.4 presents the published research found regarding buoy shape and the chapter concludes with a summary of the literature in Section 2.5.

2.1 The motions of a vessel at a single point mooring

A rigid floating body moves with six degrees of freedom – these modes of motion are typically defined using the right-handed Cartesian coordinate system shown in Figure 4. The translational movements of surge (x), sway (y) and heave (z) are defined along these axes and rotations around each defines the roll (ϕ), pitch (ψ) and yaw (ϑ) angles. These motions are traditionally subdivided into oscillatory (heave, pitch and roll) which invoke restoring forces (due to a change in the vessel's equilibrium displacement) and nonoscillatory (surge, sway and yaw), (van Dorn, 1974). The attachment of a boat to a SPM creates restraining (restoring) forces which can lead to boat oscillations in surge, sway and yaw. Each of these motion modes has distinct natural frequencies with the potential to lead to large amplitude motions at these resonant frequencies (van Dorn, 1974).

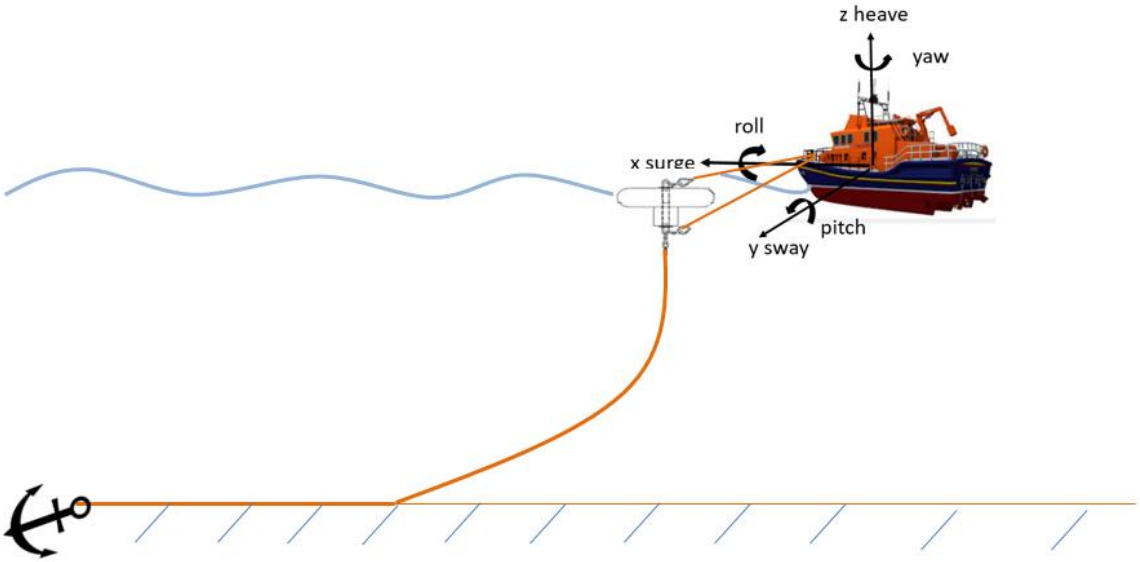

Figure 4: The right-handed coordinate system and six degrees of freedom of a rigid floating body.

Assuming that a mooring line attached at the bow will not appreciably restrain the vessel's roll motion van Dorn categorises the remaining 5 modes into three groups as follows and illustrated in Figure 5a:

1. Coupled pitch and heave – affected by the vertical component of mooring line tension which, in turn, is equal to the suspended line weight.
2. Surge – in response to waves and wind gusts. There should be enough compliance in the SPM such that the vessel's natural period in surge is larger than the maximum expected period of the waves in which case the vessel will surge "by less than the horizontal component of wave particle movement."
3. Coupled sway and yaw – vessels are dynamically unstable in yaw when moored at the bow with a yaw angle up to 60° from the wind direction. The oscillation period "increases with anchor scope, decreases with increased wind force and is roughly independent of vessel displacement; typical periods are one to five minutes" (van Dorn, 1974).

The scope of a mooring riser (S_S) is defined as the chain length from the point it rises from the seabed up to the point at which it is attached to the buoy as illustrated in the schematic in Figure 5b.

(a)

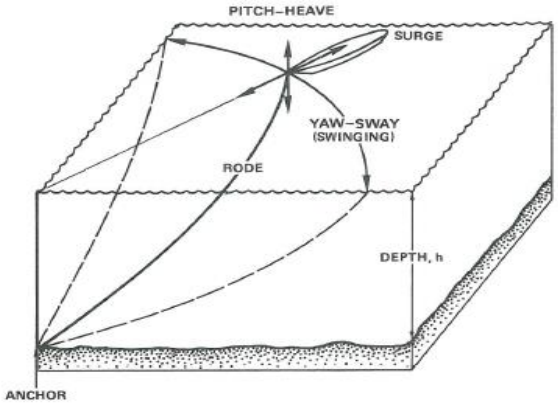

(b)

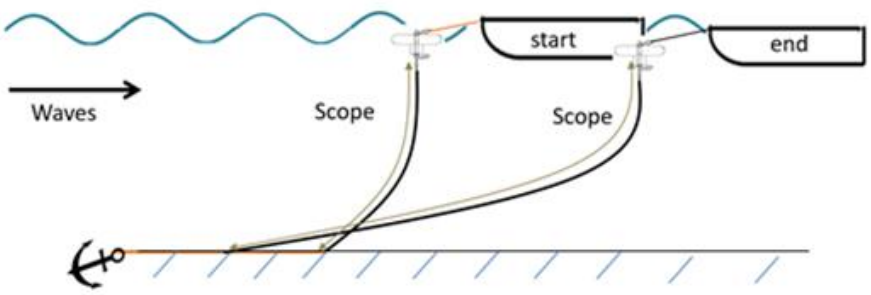

Figure 5: Single point mooring; (a) Three significant modes of motion of a moored vessel, adapted from van Dorn (1974), (b) schematic of change in scope.

A SPM is defined by the American Bureau of Shipping (ABS) as “a system which permits a vessel to weathervane while the vessel is moored to a fixed or floating structure anchored to the seabed by a rigid or an articulated structural system or by catenary spread mooring” (ABS, 2014). A moored vessel is subject to the external forcings of wind, wave and current. The SPM allows it to self-align to the prevailing wind or current often referred to as weather-vaning. A floating elongated body will slowly drift in the direction of wave propagation and turn broadside to the waves (Wehausen, 1971) thereby reducing the load in the mooring hawser compared to that if the heading was constrained (Schellin, 2003).

The motions of a moored ship in waves and current can be split into (1) high frequency 1^{st} order that are linearly proportional to wave height and due to oscillations with the wave frequency and (2) low frequency 2^{nd} order motions, in the order of 0.01 to 0.05Hz (Simos et al., 2001, Gaythwaite, 2004), which are proportional to the square of the wave height (Wichers, 1988) and are the result of unstable equilibrium positions and the low frequency excitation from wind and waves (Sorheim, 1980).

A mooring line suspended from a vessel forms one half of a catenary chain the mechanics of which were derived independently by Leibnitz, Huygens, and Johann Bernoulli in response to a challenge posed by Jacob Bernoulli around 1690 (Behroozi, 2014). The restoring force comes primarily from changes in the shape of the catenary line and due to the coupling between the horizontal force and the vertical restoring force, the longer the distance from the anchor to the touch down point the safer the mooring (Oppenheim and Wilson, 1982). In shallower water the dynamic tension of the mooring depends strongly on the ratio of elastic stiffness to catenary stiffness and typical horizontal motions are 4-10% of water depth (Isaacson and Baldwin, 1996).

Unlike a taut configuration a catenary SPM maintains its security by changes in suspended line weight in order to optimise itself to the varying forces (O.C.I.M.F., 2008). The catenary shape (mooring chain suspended in the water) is held in place by the tension at the top of the mooring chain. The motions of structures attached to catenary moorings are inherently nonlinear due to significant viscous damping, non-linear static restoring forces as well seabed friction; at low frequencies the mooring behaves like a spring but as frequencies increase inertia and drag forces begin to take significant effect (Fitzgerald and Bergdahl, 2008).

An engineering analysis of a SPM is usually split into three stages which are illustrated in Figure 6: (a) the initial equilibrium position taking into account the configuration and line tensions with an analysis of each cable based on the equations for an elastic catenary; (b) the displacement of the ship via a static analysis from the current drag and wave drift force to obtain the steady state

offset; and (c) the effects of the oscillatory wave forces and slowly varying wave drift forces via a dynamic analysis (Isaacson and Baldwin, 1996). This is elaborated into a five step process by Schelfn and Östergaard (1993) who describe the steps to numerically predict the non-linear motions of a moored ship in the time domain including the forces in the mooring lines as set out in Figure 7.

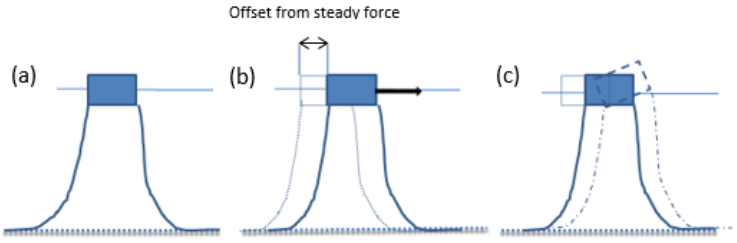

Figure 6: Component steps in SPM analysis.
(a) equilibrium –principal loads due to self-weight of mooring lines no environmental loads (b) static – steady offset due to static components of environmental loadings (c) dynamic – fast varying motions from wave loading and slowly varying motions from wave drift force. Adapted from Isaacson and Baldwin (1996).

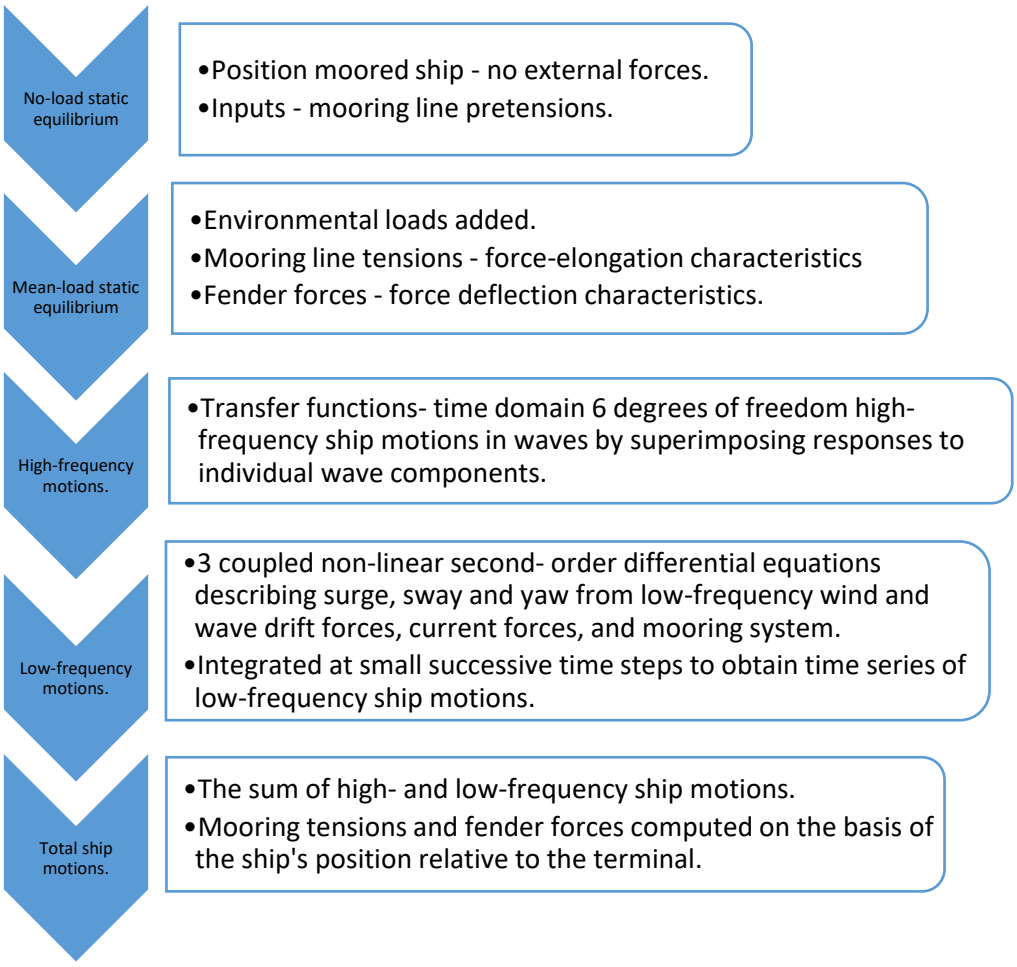

Figure 7: Steps to numerically predict the non-linear motions of a moored ship.
Forces in the mooring lines, adapted from text in Schelfn and Östergaard (1995).

Orcaflex is one example of a 3 dimensional, non-linear time domain finite element program which uses a lumped mass element to simplify the mathematical formulation. It can be used for a static or dynamic analysis of offshore systems including SPMs and wave power systems. The environmental parameters available include water depth, seabed, waves, current and wind and their website gives examples of the in-built software applications including a section on moorings (Orcaflex, 2018). The SPM simulation incorporates three legs and a short chain connecting a 3D buoy, thus allowing the dynamics of a catenary chain to be modelled. Since the simulation assumes the mooring system motion will be dominated by the hydrodynamics of the lines the buoy is modelled as a simple weight minus buoyancy influences. This means that simulation results for the effects of changes in the size and shape of the buoy upon the motions of the buoy and vessel would not be available in the current version. With further programming work this may be possible as another example of an Orcaflex inbuilt simulation details that it is possible to change the size and shape of an oceanographic measurement buoy moored in deep water.

Due to restrictions on the availability of classified RNLI design specifications the use of any simulation package is beyond the scope of this thesis and therefore the following literature review is restricted to publications detailing model scale and full scale SPMs.

2.2 Vessels located in deep offshore waters

2.2.1 Model scale experiments

A review of the role of model test procedures in the design of SPM that were available in the mid 1970's is presented by Pinkster and Remery (1975). They discuss Froude scale factors, the required input parameters, suggested measurements, errors and limitations. Since then the expansion of offshore oil and gas extraction has led to the publication of numerous experiments observing the patterns of behaviour in waves and current, of large scale tankers stationed at SPM in offshore waters. One of the observed behaviours in wind and current, both in experiments and from mathematical modelling, is termed "fishtailing" (e.g. Aghamohammadi and Thompson, (1990), Luai and Zhi, (2013), Schellin, (2003), Sharma et al., (1988), Wang et al., (2007), Wichers, (1988)). This slowly varying drift motion, in the horizontal plane, is described by a combination of the oscillatory motions of surge, sway and yaw around the buoy as set out in Figure 8. The addition of this motion onto the existing forces created by the wave induced motions can lead to high peak loads on the vessel's hawser (Wichers, 1976). Additionally this motion increases the chafing at points where ropes meet chains making this a primary cause of mooring failure (van Dorn, 1974).

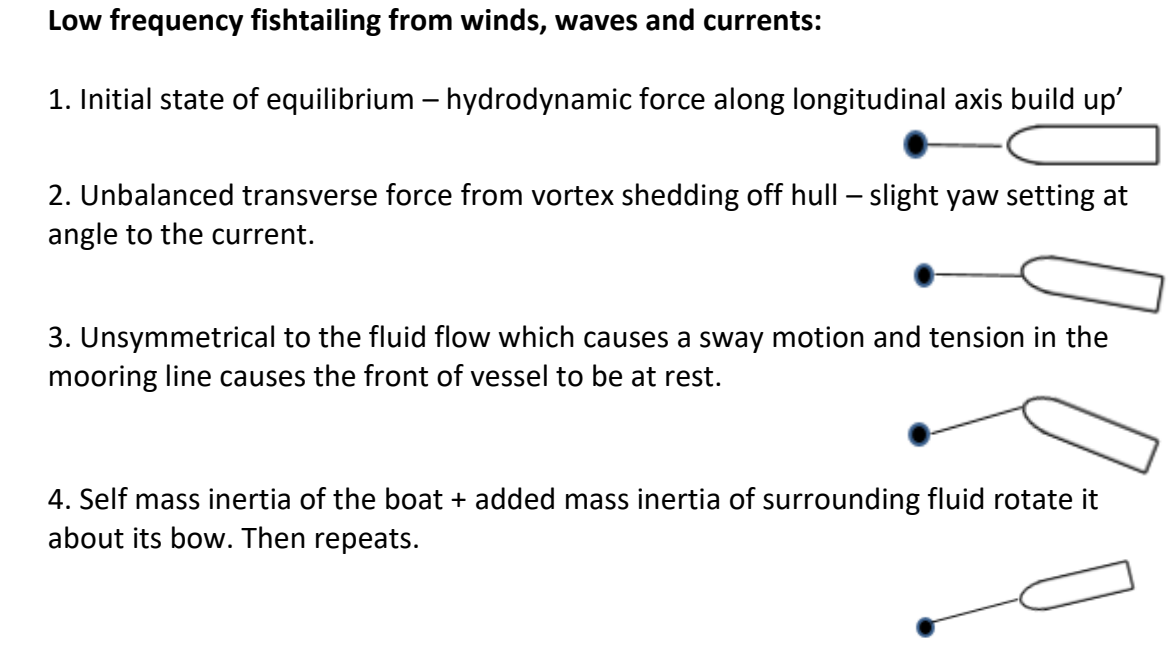

Figure 8: Fishtailing motion of a vessel at a single point mooring, adapted from Aghamohammadi and Thompson (1990).

Fishtailing observations from model tests show that loaded tankers exhibit slow oscillating motions in the horizontal plane about the mooring point which is determined by the height, period and direction of the waves and the speed and direction of current and wind (Pinkster and Remery, 1975). In their tests a yaw orientated fishtailing motion occurred in current speeds of around 0.77m/s when the vessel took an average position in line with the bow hawser. This swinging motion can be reduced by reducing the hawser length (Pinkster and Remery, 1975) or increasing the hawser tension (Sorheim, 1980). As the wind's speed increases it passes a critical point which reduces the effective mooring line damping to zero and the vessel becomes unstable (Aghamohammadi and Thompson, 1990).

Model tests, scaled for tankers with lengths between perpendiculars in the range 316 to 363.5m, in wind and current exhibit slow fishtailing movements in the horizontal plane which are dampened upon the introduction of a wave drifting force (Wichers, 1988). If the wind speed is below a critical value a tanker assumes an equilibrium position when the wind and current forces are in balance with the hawser. As wind speed increases the effective damping of the mooring line is reduced until the tanker motion reaches a limit cycle (Aghamohammadi and Thompson, 1990). Ignoring these destabilising effects of time varying forces in the stability analysis of an offshore mooring could result in mooring design unfit for service (Paton et al., 2006).

The influence of length and elastic properties of a hawser attached to a 300,000 DWT tanker have been investigated in a 1:100 model experimental programme of 400 tests, using a fixed mooring point, in regular waves with no wind and current (Halliwell and Harris, 1988). Their main conclusions are summarised as:

- Low frequency yaw- sway-surge pendulum motions exhibited in waves having periods of less than 9s.
- Amplitudes of surge, sway and yaw do not change with changes in wave height.
- The hawser load increases with wave height.
- The elastic properties of the hawser do not affect the low frequency motion, but increases in hawser length lead to increased loads because the amplitude of yaw and sway motions are increased.
- An increased draught increases the period of low frequency motion, but has no effect on amplitudes or loads.

The stiffness and damping characteristics of a catenary mooring line are affected by a multitude of intrinsic factors such as: its material composition, diameter and length relative to water depth as well as the external factors of wind, wave and current (Chakrabarti, 2005). Results from tank tests on a large (1:16) and a small (1:70) scale catenary mooring line moored in a depth of 82.5m have shown that the relationship between the point of suspension and the scope to be highly nonlinear and extremely sensitive to water depth, line pretension and wave conditions (Kitney and Brown, 2001). Their research showed that line tensions exceeded those that would be

predicted from a static analysis only and therefore suggest a dynamic approach is required to fully understand the mechanisms of mooring line damping.

Huang and Lee (2012) tested a 1:25 model scale of a rectangular floating platform in a wave tank and reported, for the open sea, that the amplitude of the heave response was almost identical to the amplitude of the incoming incident wave. In higher current speeds (full scale 1.75m/s) the drag forces acting downwards on the structure caused pitch and surge motions to be supressed. Peak mooring line tension recorded in current alone was 5N, when waves and current were combined this rose to 28N which is the full scale equivalent of 440kN at a depth of 20m with a current speed of 1.75m/s and a wave height of 2.5m (Huang and Lee, 2012). This recorded maximum load is 2.7 times the maximum break load of RNLI hawsers which are rated at 164kN.

Wang et.al. (2007) analysed the response of a SPM for a 289m long tanker in wind, waves and current using a nonlinear coupled analysis model verified by physical model tests. Their 30 minute simulation showed sway to be most sensitive to wind, surge to current and heave induced mainly from random waves (model parameters were water depth 50m, mean wind velocity 20m/s, a JONSWAP wave spectrum with significant wave height 5.2m and current velocity 1.20m/s). Significant wave height (H_s) is defined as the mean wave height (trough to crest) of the highest third of the waves. In the tests the mooring line tension peaked at a value of 3,500kN. After 22 minutes the simulation was presented in the OXY plane, as shown in Figure 9, although described as “obvious” the authors do not relate the surge and sway motions with the fishtailing phenomenon and present no graphs of the yaw motion. The author’s figure has been adapted by adding the blue arrows to aid interpretation of the vessel’s simulated path. However without any information regarding the vessels orientation with respect to its buoy it is difficult to visualise its fishtailing motion.

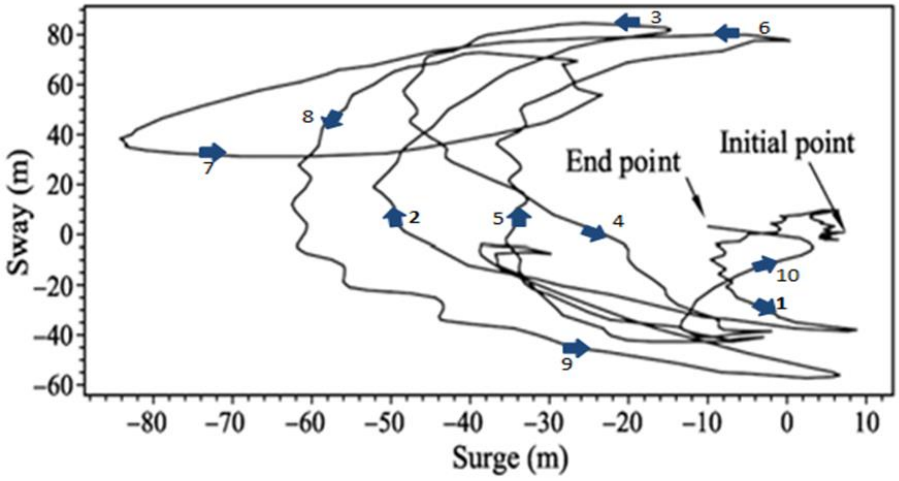

Figure 9: Simulated track in an SPM coupled model of a SPM 289m tanker.
The tanker is modelled in 50m water depth, mean wind velocity 20 m/s, current velocity 1.20 m/s, a JONSWAP wave spectrum with significant wave height 5.2m and peak period 10 s run over a 30 minute simulation. Adapted from Wang et al., (2007).

During the 14th International Ship and Offshore Structures Congress of 2000 the Technical Committee I.2 identified the potential "important issue" for ships at SPM to be the highly peaked loads in the mooring hawser (Schellin, 2003). Subsequently research to numerically predict the mooring load of two supertankers moored to a catenary leg buoy in deep water (length between perpendiculars 290m and 325m) in current was undertaken internationally by three industrial companies, one research laboratory and three universities. The participants and models used are detailed in Schellin (2003) along with graphed results of mooring load and horizontal motions. Overall the results exhibited a high degree of variability. For example, at current velocities of 2.0m/s one simulation predicted a maximum mooring load of 3,200kN whilst another predicted 500kN. It should be noted that only one of the participants attempted to directly verify their simulations by specifically designed model tank experiments. Furthermore: "To assess the resulting numerical predictions, comparative experimental data, preferably obtained from full scale measurements, are required. However, such data were not available for the problem under investigation here" (Schellin, 2003).

2.2.2 Full scale measurements

Experiments on different mooring line materials for a deep sea oceanographic mooring were performed in the United States for the National Oceanic and Atmospheric Administration (Pattison, 1977). Results were reported for load response ratios: defined as the ratio of measured horizontal and vertical dynamic load to the measured equilibrium tension. For flexible models the ratio increased with increased pretension in the mooring line, but for stiff systems increasing the pretension decreased the ratio. Load response ratios were also found to increase with increased current and scope of mooring line. Furthermore the stiff models exhibited more peaked load responses thereby concluding the best mooring line material is flexible combined with chain anchor lines on the seabed. This recommendation was based upon the desire for a deep sea oceanographic mooring to minimise its "watch circle", which is the diameter of the area on the ocean surface where the buoy can move about while still anchored to the ocean bottom.

Observations of the motions of a tanker moored to a quay in the Japanese port of Yokkaichi were recorded in the years 1980 and 1981 (Viggosson, 1988). The vessel was not at a SPM, but moored by thirteen synthetic ropes and the vessel's heave was measured by camera and surge via scales on the hull. In the 1980 test (with maximum wind speeds of 28m/s and wave heights of 0.75m) surge was recorded between 0.19m to 0.29m and in the 1981 test (with maximum wind speeds of 19m/s and wave heights reduced to less than 0.10m) surge was recorded between 0.52m to 1.08m (Viggosson, 1988). These measurements indicate that the reduction in wave height and wind speeds leads to larger amplitude motions in surge.

In summary the literature reviewed for SPM vessels in offshore waters have all researched the motions and load experienced by large tankers of lengths exceeding 200m (see Section 2.5 and Table 3) which has been driven by the expansion of oil and gas exploration.

2.3 Vessels located in coastal harbour waters

2.3.1 Model scale experiments

Tank experiments in regular waves measuring the motion and tensions of a 200mm diameter PVC spherical buoy of weight 5N anchored to a concrete block were performed by Sundaravadivelu et.al. in 1991. The load cells were held vertically on a taut mooring chain and so there was no catenary effect during the 25 tests performed. Their conclusions drawn were (Sundaravadivelu et al., 1991):

- "…for lower relative water depths the increases in surge and heave acceleration are significant.
- The normalised dynamic tensions increase significantly with increase in wave steepness for intermediate water depth conditions. Such a significant increase is absent in higher relative water depth conditions.
- The dynamic effects on the mooring line are predominant in lower relative water depths."

The number of experiments performed (with no repeats) for the six different relative water depths meant that these conclusions are based upon the number of data points per depth ranging from a very limited 3 to 6.

Measurements of surge, heave and pitch of a three anchor SPM model tanker in shallow water (0.16m and 0.20m) were performed by Troesch and Beck (1974). The results were compared to a theoretical model based upon slender body theory. The model is reported as 7 feet (2.13m) but no scale ratio is given. Comparisons were close for surge motions but there was poor agreement for heave and pitch. Motions recorded showed little variation between the two depths tested implying that, in shallow water, viscosity is not altering the flow between the model and bottom of the tank (Troesch and Beck, 1974).

A comparison of tank experiments and bespoke time domain numerical software simulations of the motions and forces of a container ship moored to a dock wall for a 1:50 scale model in full scale depths of 15.24m was performed in 2013 at Texas A&M University by Luai and Zhi. Once again the vessel is not attached to a SPM and is a large tanker (216m) but the investigated parameters and conclusions drawn (regarding motions and forces) plus methodology used provide useful insight into current technological advances available in tank experimentation. For the model tanker tested in waves and berthed at a dock wall (Luai and Zhi, 2013) concluded:

- Translational motions are proportional to significant wave height and period.
- Rotational motions are proportional to significant wave height but show a variable effect of wave period.
- Sway, heave and roll are the more prevalent motions.
- As wave height increases mooring line forces increase.

2.3.2 Full scale measurements

Observations were made in 1983 of the motions of a 30 Gross Registered Tonnage (1 GRT = 2.83m^3) fishing boat (LOA 17.4m) in the Icelandic fishing harbour of Akranes and in the Thorlakshofn harbour all berthed at the quayside (Viggosson, 1988). The 17.4m fishing boat was subject to a significant wave height of 3.7m and average wind velocity of 22.1m/s and the recorded maximum excursions were surge 0.32m, sway 0.71m, yaw 6.35° and roll 2.34° (Viggosson, 1988). Once again these data are not related to a SPM but do provide some guidance for planning the recording of lifeboat RNLI data in the field and tank experiments.

Issues regarding interruptions to cargo handling and berthing work under varying climate conditions over a two month period were investigated in the harbour at Punta Langosteira Port, Spain (Ferreras et al., 2013). Motions of a 72m controlled vessel berthed at the quayside were recorded using a Global Positioning System **(**GPS) system, a tri-axial accelerometer, a gyroscope and mooring rope tension using three load cells. Whilst the 2013 conference paper details the data recorded the authors have yet to publish their results.

Tyrberg et. al. (2011) measured the motions of a 4.0m diameter buoy using a buoy based accelerometer system on May 27th 2009, in a water depth of 25m at the Lysekil Research Site, off the Swedish west coast. The recorded wind speed was 12m/s and a significant wave height of 2.5m. The sideways motion of the buoy in the buoy's reference system is reproduced from their publication in Figure 10.

The literature for experiments in coastal harbours water is lacking in volume compared to offshore water studies and once again the vessels investigated are large tankers (see section 2.5 and Table 3).

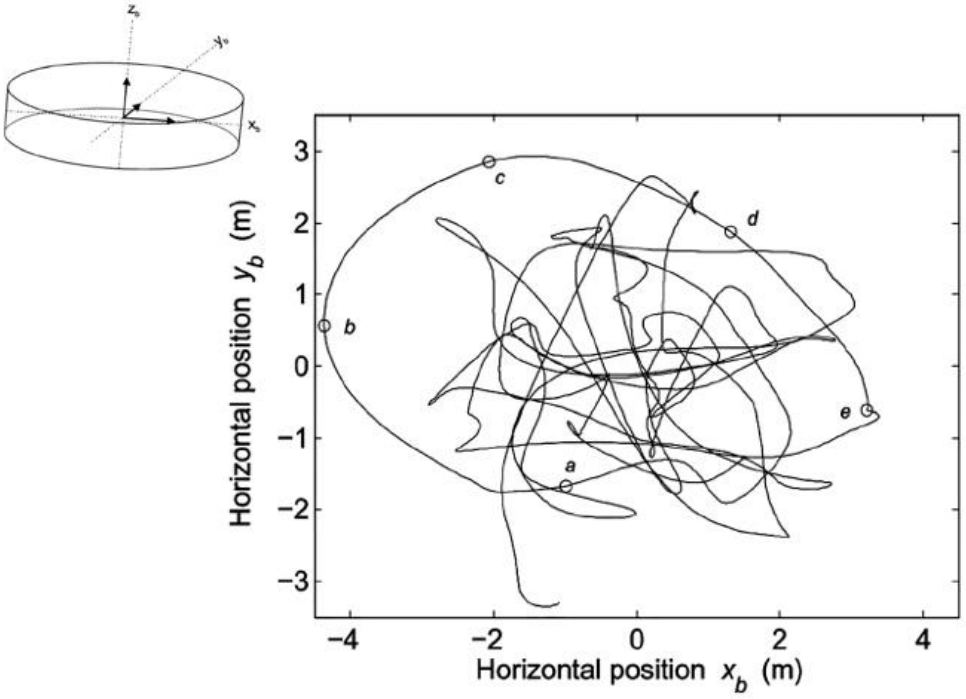

Figure 10: Measured buoy motions (Tyrberg et.al, 2011).
The path of the buoy from a point to e point takes 9s.

2.3.3 Ship – ship interactions

A further subject which provides relevant published research is the ship - ship interactions in harbours and ports from passing vessels. The additional created wave action causes increased motions of the moored vessel which in turn induce additional forces on the mooring lines. Full scale measurements of a 12,000t barge moored against piles in a water depth of 10.5m were made in July 2003 by the Ministry of Transport and Waterways. It was located in the Noordzee canal which is on the route to the Port of Amsterdam, Netherlands (Pinkster, 2004). The increases in surge force on the barge were recorded as 40kN from the passing of a bulk carrier travelling at 2.98m/s and 85kN from the passing of a cruise liner travelling at 4.58m/s (Pinkster, 2004).

Field observations of the waves generated by a conventional passenger ferry travelling at 8.74m/s (17knots) and a high speed ferry travelling at 13.63m/s (26.5knots) have been made at a micro-tidal beach located around the Greek island of Lesbos (Velegrakis et al., 2007). The data, collected at a water depth of 2m in "calm wave conditions" in late September 2005, showed the high speed ferry generated higher wave heights with a maximum of 0.74m compared to 0.24m from the passenger ferry. Also the wave packets generated by the high speed ferry lasted an order of magnitude longer at 680s than those of the passenger ferry which lasted 65s (Velegrakis et al., 2007). The wave energies peaked at two frequencies (0.22 and 0.46Hz) for the conventional ferry and four frequencies (0.16, 0.25, 0.32 and 0.39Hz) for the high speed ferry (Velegrakis et al., 2007).

2.4 Buoy shape

No published experimental investigations have been found that examine the effect of buoy shape or buoy size upon the motions of vessels less than 20m in length stationed at a SPM in a coastal harbour. However, due to the increased global interest in wave energy extraction prototypes, there has been research conducted into the impact of the shapes of buoys as components of energy extraction devices.

When optimising the geometric shape of a wave energy converter (WEC) the following design criteria should be considered (Goggins and Finnegan, 2014):

- Extraction of maximum available energy at the incumbent wave frequencies.
- Adaptation of the device to the changing wave direction.
- Minimisation of the probability of the device slamming in excessive conditions.

The optimum underwater shape for a heaving WEC, using numerical simulation methods, indicates that the surface shape with the highest hydrodynamic damping combined with a submerged mass in tune with the system's resonant frequency provides the highest potential power take off (Alves et al., 2007). Modelling and numerical simulation to optimise the geometry of an oscillating water column device shows that the size of the chamber, the immersion depth and orientation versus the flow direction all have a very significant impact on the performance (Bouali and Larbi, 2013).

Goggins and Finnegan (2014) used the average energy spectrum data from the west coast of Ireland to establish the optimum structural geometric configuration of a floating buoy. The tested shapes are presented in Figure 11a. The data were used within a configuration algorithm to determine the most efficient axisymmetric geometric shape and device radius by inputting the specific Response Amplitude Operator (RAO) to obtain the response velocity. Their results showed the most efficient was a truncated vertical cylinder of radius 8m with a hemisphere attached to its base and a total draught to radius ratio of 2.5 (Goggins and Finnegan, 2014).

McCabe (2013) used a genetic algorithm to compare differently shaped and sized WEC, operating in surge, for a given wave climate on the West Shetland shelf in the North-East Atlantic Ocean. The algorithm predicted that: (a) when there was no restriction on size the larger, simpler virtually hemispherical shape performed better and (b) the smaller more complex (pointed prows and sterns) shapes with pronounced asymmetry in the direction of the wave propagation showed better performance compared to a benchmark box shaped collector (McCabe, 2013). Examples of the simpler and more complex shapes are presented in Figure 11b.

Two different shaped heaving point absorbers, shown in Figure 11c, with a variety of diameters between 1.5 and 6.5m and three draughts (2,2.5,3m) have been numerically modelled in the frequency domain in sea states typical of offshore waters of the North Sea at 50m depth (Pastor and Liu, 2014). The simulations predicted power in the region of 150kW per buoy and conical shape resulted in larger power absorption than the hemispherical shape with an optimal draught of 2m and as large a diameter as possible taking into account available space and cost. Additionally power absorption efficiency of three heaving model buoys, in wave periods from 1.4 to 1.6s, show that a concave surface consistently performed better than a convex or straight edge facing the direction of the waves (Hager et al., 2012).

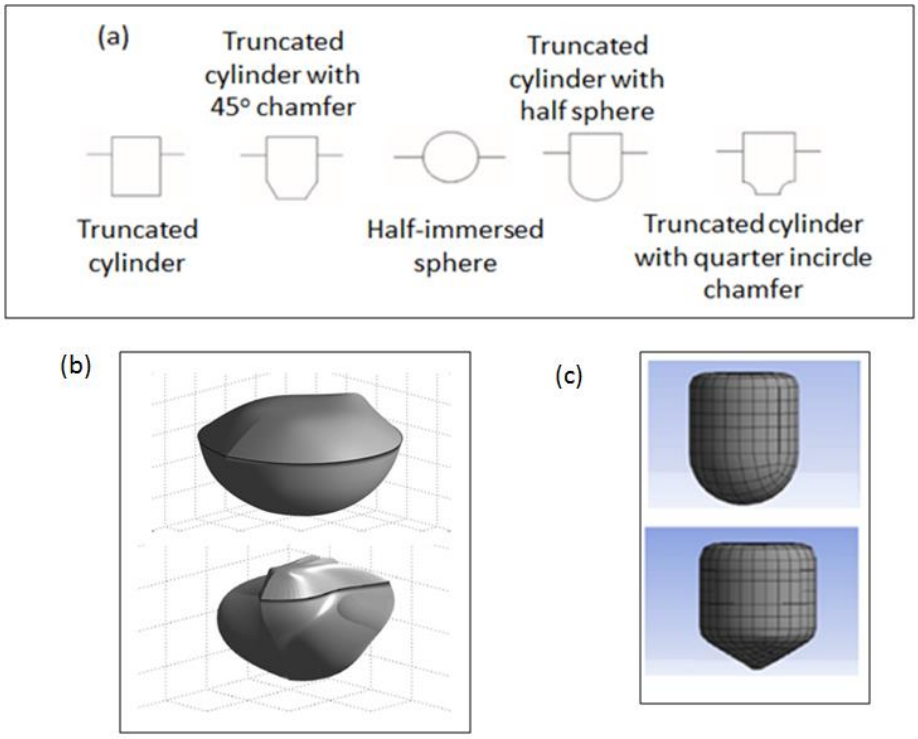

Figure 11: Published investigations into buoy shapes.

(a) Six geometric shapes of heaving wave energy converters tested in an optimisation algorithm (Goggins and Finnegan, 2014). (b) Examples of simple and complex shapes (McCabe, 2013) (c) Hemispherical and conical shape heaving point absorbers (Pastor and Liu, 2014).

2.5 Summary

There are many factors which affect the motion and forces experienced by a vessel at its mooring. In the case of a coastal SPM the roll, pitch and yaw will depend upon the resonance period of the ship, the wave spectrum and its reflective pattern as well as its freedom to self-align to the prevailing wind and current. The results of the literature review are that experiments and mathematical modelling of motions and forces have been predominantly based upon large scale oil and gas tankers moored in deep offshore waters in order to assess the reliability and operational efficiency of their moorings (a summary of which is presented in Table 3). All the journals found for coastal waters have again been for large tankers and all are moored alongside quay walls. Only one publication, Viggosson (1988), has been found that collects in situ data for a vessel less than 20m in length and this was berthed and not at a SPM and in significant wave height of 3.7m.

Table 3: Summary of the literature review for tank experiments and simulations of SPMs.

Reference	**Type**	**Vessel/platform /mooring line**	**Depth (m)**	**Measurement**
Deep				
Pinkster and Remery, 1975	Tank	Tankers	45	Forces and Motion.
Sorhiem, 1980	Simulation	250m tanker	150	Forces and Motion.
Aghamohammadi and Thompson, 1990	Tank	Tanker	'Deep'	Motion.
Wichers, 1988	Tank	316 and 364m tankers	82.5	Motions.
Halliwell and Harris, 1988	Tank	292 and 300m tankers	150	Forces and Motion.
Kitney and Brown, 2001	Tank	Mooring line only	82.5	Forces.
Schellin, 2003	Simulation	290 and 352m tankers	'Deep'	Forces and Motion.
Paton et. al., 2006	Simulation	65m Turret	800	Motion.
Wang et. al., 2007	Tank and simulation	289m tanker	50	Forces and Motion.
Huang and Lee, 2012	Tank	Floating platform	30	Forces and Motion.
Shallow				
Troesch and Beck, 1974	Tank and simulation	2.13m model tanker	0.16, 0.2 tank depth	Motion.
Sundaravadivelu et.al. 1990.	Tank and simulation	Buoy only 200mm	10	Forces and Motion.
Luai, 2013	Tank and simulation	216m tanker	15	Forces and Motion.

This thesis presents two sets of model scale experimental investigations into the effect of hawser length, buoy scale and shape on small boats (considered sub 20m) with free catenary SPM configurations (i.e., without the use of fixed spring-mass-damper mooring line). The work addresses the gaps in the literature, for small vessels at SPM in coastal waters. The first set was at 1:40 scale in a circulatory flume at Chilworth research laboratory and the second at 1:10.67 scale in regular waves at Solent University. The presented results and discussion highlight the dominant motions and examine whether changing the size and shape of a SPM buoy impacts upon the motions of the attached lifeboat. Additionally the motions of a full scale lifeboat have been recorded at a SPM in Yarmouth Harbour, Isle of Wight.

Chapter 3: SPM FLUME EXPERIMENTS AT 1:40 SCALE

> "A physical model is a physical system reproduced (usually at a reduced size) so that the major dominant forces acting on the system are represented in the model in correct proportion to the actual physical system." (Hughes, 2005).

This chapter details the experimental investigations into the impact of line length, buoy size and buoy shape upon the motions of a 1:40 scale lifeboat in steady current. Section 3.1 includes an introduction to model scale testing and scaling requirements. The experimental design of the model lifeboat, at its single point mooring, is outlined in Section 3.2 together with the test facility, key parameters, data acquisition systems and procedures. Sections 3.3, 3.4, 3.5 and 3.6 present the data acquisition verification, test results, discussion and summary respectively.

3.1 Introduction

The use of scientific investigation and full scale measurements at sea in terms of both financial and time scale investments is usually prohibitive and so physical interactions are best modelled at a smaller scale giving the advantage of a controlled environment to test new hypotheses. The advantages and disadvantages of scaled model tests according to Hughes (2005) are presented in Table 4.

In order to assess the impact of different physical parameters upon the motion experienced by a lifeboat interacting with its mooring buoy, at a SPM, a systematic series of scaled model experiments have been performed in current as set out in Table 5 and Appendix D. In Appendix D each of three series of experiments are summarised: Series 1 (August 2014) was designed to evaluate the effect of flow speed and hawser length using a 1:40 and 1:20 scale buoys. Series 2 (April 2015) used 1:40 scale buoys of differing shapes ranging from a circle to a wing shape whilst maintaining the same volume. Series 3 concluded the investigations in current in August 2015 with a set of experiments at 1:20 scale with differently shaped buoys attached to the boat and with the buoys in the flume without the boat attached.

Table 4: Some advantages and disadvantages to model scale testing.

Advantages	**Disadvantages**
Integration of governing equations without the simplification required for numerical analysis.	Scale effects – impossible to scale all relevant variables e.g. larger viscous forces on a small scale model leads to difference in prototype and model response.
Smaller sizes facilitate a range of cheaper data collection simultaneously.	Laboratory effects – necessary approximations such as wave spectra.
High degree of environmental control. Allows verification of computer output.	Inability to replicate all forcing terms simultaneously e.g. wind, wave and current.
Instantaneous visual feedback of behaviours which can be used to focus future research.	More expensive to run physical model tests than established computer simulations.
Advances in data processing techniques facilitate more complex relationships to be investigated.	
Physical manipulation of fluid interactions allows creativity beyond the output of theory or computer predictions.	

Table 5: Test performed in current, figures in brackets are the hawser length (m).

Test set up	**Buoy shape and hawser length**
No buoy	(0.125)
Normal buoy size (1:40)	circle (0.125,0.150,0.200) octagon (0.150) hexagon (0.150) square (0.150) wing (0.150)
Large buoy size (1:20)	circle (0.125,0.150,0.200,0.300) octagon (0.300) square (0.300) wing (0.300)
Large buoy (1:20) and no boat	circle, octagon, hexagon, square, wing

3.1.1 Scaling for experiments in current

When conducting tank tests the experimental conditions need to be "scaled to ensure the model's motions are an accurate reproduction of the motions which would have been experienced by the ship at full scale" (Lloyd, 1989). The full and model scale can be compared by geometric (linear dimensions), kinematic (velocity) and dynamic (forces) similarities. Floating structures are subject to gravitational, inertia, elastic, surface tension, and viscous shear forces and to model the behaviour the dominant forces must be identified (Hughes, 2005).

In order to further examine the scaling requirements two non-dimensional ratios are defined as (Lloyd, 1989):

Froude number = F_N = resistance of a partially submerged object moving through water

$$= \sqrt{\frac{\text{inertia force}}{\text{gravity force}}} = \sqrt{\frac{(\text{mass x acceleration})}{(\text{mass x gravity})}} = \sqrt{\frac{\rho L^2 U^2}{\rho\, g L^3}} = \frac{U}{\sqrt{gL}} \quad (1)$$

where ρ= density, L= length, U= velocity, g= acceleration due to gravity.

Reynolds number = R_e = determination of smooth laminar flow or chaotic turbulent flow

$$= \frac{\text{inertia force}}{\text{viscous force}} = \frac{(\text{mass x acceleration})}{(\text{viscousity x velocity grafient x area})} = \frac{\rho L^2 U^2}{\mu U L} = \frac{\rho U L}{\mu} \quad (2)$$

where ρ= density, L= length, U= velocity, μ= viscosity.

Equality of F_N for model scale ($_M$) and full scale ($_{FS}$) requires:

$$\frac{U_M}{\sqrt{gL_M}} = \frac{U_{FS}}{\sqrt{gL_{FS}}} \text{ thus } U_M = \frac{U_{FS}}{\sqrt{R}} \quad (3)$$

Indicating model speed should be reduced in proportion to the square root of the dimension ratio.

Equality of R_e for model scale ($_M$) and full scale ($_{FS}$) requires:

$$\frac{\rho_M U_M L_M}{\mu_M} = \frac{\rho_{FS} U_{FS} L_{FS}}{\mu_{FS}} \quad \text{thus } U_M = U_{FS} R \quad (4)$$

Indicating model speed should be increased in proportion to the dimension ratio.

This analysis demonstrates the experimental speed conundrum i.e. when testing in fluids of similar density and viscosity it is impossible to scale simultaneously at a Froude and Reynolds scale and therefore maintain the relationships between inertia, gravity and viscous forces. In practice for ship tank experiments Froude scaling is used as the gravitational forces are considered to be dominant over the viscous forces at a large enough scale. The current flow and the boat itself are scaled according to Froude criteria where the ratio of length scales, *R,* is defined as the dimension scaling ratio and is equal to the full scale length divided by the model length. Time and velocity are scaled by $1/\sqrt{R}$ and forces at $1/R^3$ multiplied by a correction factor for the difference in freshwater and seawater density as detailed in Appendix E.

In this particular case of model testing cables in water it is usual to violate exact geometric scaling for practical reasons however the correct value for the Young's modulus of the material should be used as its violation, in dynamic testing, is extremely significant (Papazoglou et al., 1990). The ground and riser chains and hawser were scaled using the Cauchy criterion which facilitates the similitude of the ratio of inertial to elastic forces using the Young's modulus of the material (Hughes, 2005). For tests run at a scale ratio *R* the required Young's modulus of the model is:

$$E_M = \frac{E_{FS} R^2}{R_{HF}} \qquad (5)$$

where E_{FS} is the Young's modulus at full scale and R_{HF} is the scale of hydrodynamic forces which is corrected for the ratio of specific gravities of fresh and sea waters (9.79kN/m^3 and 10.05kN/m^3 respectively.), i.e.:$R_{HF} = 0.97\ R^3$.

In practice it is not possible to source a material of the exact required Young's modulus and so the appropriate adjustment to the scaled diameter should be made to compensate: for example a smaller diameter than if Froude geometrical scaling is needed to compensate for the model hawser and chain when the material is stiffer than the ideal material (Hughes, 2005). The required diameter for the riser chain, via geometrical scaling, is 0.65mm and for the hawser rope is 1.1mm.

The Young's modulus of the materials used in the experiments is therefore required to calculate the required reduced diameter. These were obtained via tensile tests at the University of Southampton using an Instron E-Series Circumferential Extensometer. The stress/strain curves, linear regression lines and resultant calculations of the Young's modulus testing of the materials used in the tank tests are available in Appendix F. The ideal material for the hawser, based on these tests, was the rubber, however its mass resulted in a model hawser with insufficient tension to accurately reproduce the interaction between a full scale boat and its mooring and so suitably scaled fishing wire was used.

The calculation of Young's modulus dependent diameter for the chosen fishwire yielded a requirement of 0.11mm and the actual diameter was 0.20mm ± 0.05mm. The calculation of diameter for the sourced chain yielded a requirement of 0.92mm and the actual diameter was 0.80mm ± 0.05mm.

The range of flow speeds tested in the flume was a full scale equivalent of 1.02 to 2.23m/s which falls within the full scale range of 0.25 to 3.09m/s recorded at RNLI SPM as detailed in Appendix B. The range of depths tested was a full scale equivalent of 6.6 to 10.6 m which falls within those documented by the RNLI of 1 to 25m as set out in Appendix B.

3.1.2 Blockage effects

One further limitation of tank testing is known as the blockage effect i.e. the tank walls and floor interfere with the fluid flow which would not occur in unrestricted water at full scale. There is a trade-off between maximising the scale of a model, in order to reduce scaling effects, and reducing the blockage effect. In tank tests the established assumption is that "the model cross sectional area should not be more than 0.5% of the tank cross-sectional area" (Molland et al., 2011). This ratio for the 1:40 scale model at Chilworth is between 0.02 – 0.05% indicating that the blockage effects were negligible in the tests performed.

For the particular case of tank testing of moorings in current, the tank wall effects on the lateral forces are negligible when the ratio of tank width to vessel length is 5 but have a noticeable effect when this is reduced to 3 (Chakrabarti and Cotter, 1994). This ratio for the 1:40 scale model at Chilworth is 3.04 (1.4/0.46m) indicating that there may have been a marginal effect from the tank walls but this would be the same for all tests and therefore deemed not to have compromised the comparability between test configurations.

Furthermore for a water depth to vessel draught ratio of 5 or more, the shallow water effect is made negligible (Chakrabarti et al., 1995). The shallowest depth to draught ratio for the current tests was 6 (0.30/0.05m) indicating that the shallow water effects were negligible in the tests performed.

3.2 Experimental methodology

3.2.1 Test facility

Three series of tests have been performed at the indoor circulatory flume at the Chilworth research laboratory. The flume is 22m long, 1.4m wide and with a working depth up to 0.4m. The flume is a conventional gravity fed flume in which water is lifted from a large sump, via up to three centrifugal pumps, the fluid then returns to the sump at the upstream end of the working section (Myers and Bahaj, 2010). Flow rates are controlled by radial clock valves on each of the pumps and the water depth is controlled via a weir with the slope adjustable between zero and 1:200.

3.2.2 Model Severn class lifeboat

As detailed in Section 3.1.2 the size and therefore scale of the model is limited by the width of the tank and therefore a 1:40 scale was the largest that could be used in the Chilworth flume. The representative model used was of the Severn class lifeboat and a comparison of scale particulars are presented in Table 6. Although not all particulars were an accurate match the two deemed most important for the comparing the observed dominant motions of yaw and sway, i.e. length overall and yaw radius of gyration, were within a 2% error.

The yaw radius of gyration of the model was measured using a suspension rig where the model was suspended underneath a ladder and then oscillated in yaw. The time taken for 10 complete yaw oscillations was recorded and the test repeated ten times. The equation for the yaw radius is derived in Chapter 10 of "Seakeeping" Lloyd (1989) as:

$$K = \frac{Td}{2\pi}\sqrt{\left(\frac{g}{H}\right)} \qquad (6)$$

where K= yaw radius of gyration (m), T = the period of one oscillation (s), d = half the horizontal distance between suspension ropes (m), g = acceleration due to gravity (m/s^2) and H = the vertical distance between model and suspension ladder (m). The tests yielded a yaw radius of gyration of 0.11m which is equal to the value of 0.11m when using the estimation of 0.25% of the length between perpendiculars provided by the International Towing Tank Conference (ITTC, 2008).

The model was marked with 2 fluorescent ping pong balls one fore (referred to as bow) and the other aft (referred to as stern) to facilitate motion tracking from the video capture. The frame of reference and the position of the markers are depicted in Figure 12. It was moored to a four sinker and ground chain configuration as 55% of the RNLI's SPM have four sinkers compared to 35% with three.

Table 6: Principal particulars of RNLI Severn class lifeboat.

Particular	Full scale	Model actual	Percentage difference to 1:40 scale
Length overall (m)	17.30	0.443	2.4%
Beam (m)	5.90	0.164	10.1%
Draught (m)	1.78	0.0520	14.4%
Displacement (kg)	42,300	0.856	22.8%
Yaw radius of gyration (m)	4.32 (estimated)	0.1061 (measured)	-1.8%

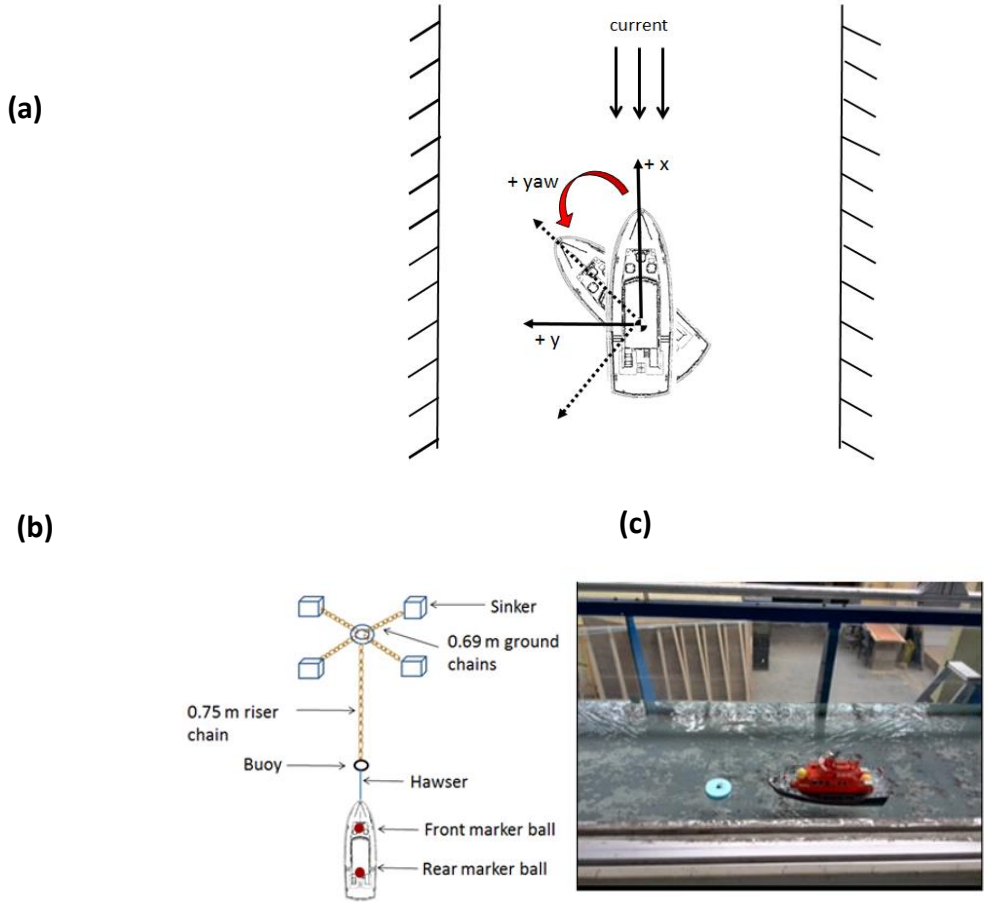

Figure 12: Flume layout (a) two-dimensional frame of reference and (b) aerial view and (c) side view.

3.2.3 Data acquisition

The parameters recorded, were are listed in Table 7, were the current flow (at the surface and at three depths), the motions of the boat and the motions of the buoy. Initial tests included the recording of ground chain load but subsequent data analysis revealed that the recorded tension was of a small magnitude so tests were performed recording the tension without the SPM attached to the ground mooring chains. The results show that there was little difference in the range recorded with and without the mooring (namely 0.086N and 0.003N difference in the two cells) as detailed in Appendix C. Furthermore plots of the recorded load also showed the dominant magnitudes to be at similar frequencies indicating that the force in the mooring chain could not be isolated and therefore all load acquisition and data is presented in Appendix C.

The surface flow velocity (± 0.1m/s) was measured by timing the movement of a ping pong ball, travelling at the water surface, past two marker strings placed across the tank one metre apart downstream from the test section. Ten measurements for flow velocity (v) were taken and then averaged for each individual test. The mass flow rate ($\dot{M}$), in kg/s, was calculated using the cross sectional tank area (A) and temperature dependent values for fresh water density (ρ) taken from tables published by the International Towing Tank Conference (ITTC, 2011):

$$\dot{M} = v\, A\, \rho \text{ (kg/s)} \qquad (7)$$

Spot velocity profiles for flow travelling down the flume were measured using a Valeport Model 801 Electromagnetic Flow Meter. The meter measures the flow twice every second, and calculates the real time flow every second as the average of the half second readings. The average speeds (m/s) are computed as the average of the one second real time values over the averaging period which was set at 60s; the standard deviation (STD) is also calculated. The 2Hz data is digitally filtered from raw data with an accuracy of ±0.5% of reading plus 5mm/s. Measurements were taken for tests with buoy only and with the boat attached in positions directly behind, to the side (as depicted in Figure 13) and upstream of the testing site. Readings were taken (in water depth of 0.20m) at distances from the tank floor of a top position 0.19m, middle position 0.10m and bottom position 0.05m.

Table 7: Parameters recorded for Series 1 to 4 at Chilworth flume.

Series	Motion using camera	Motion using Xsens	Surface flow	Flow at depth
1	✓	×	✓	×
2	✓	✓	✓	×
3	✓	✓	✓	✓

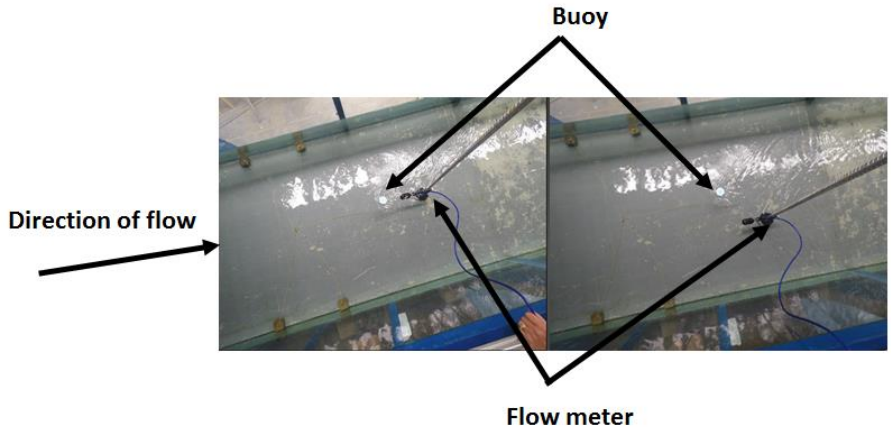

Figure 13: Aerial view of Valeport Flow Meter immediately behind and to the side of the buoy.

Motions of the boat and the buoy were recorded using a Go Pro Hero camera set at 30 frames per second and mounted at a fixed angle on a gantry above the tank capturing the motions in the x-y plane of both the boat and the buoy. A Matlab image tracking algorithm, written at the University of Southampton, was used to plot the paths of the buoy and the boat using the marker balls as depicted in Figure 12. Each object on the video has a unique colour combination of red, green, blue (RGB) values which range from 0 to 255. A Thresholding Tool was used to isolate an object by selecting its unique RGB values and a video created in which the only image that remains is the required object. This enabled the location of an object's centroid to be tracked in terms of its x and y pixel co-ordinates, an example, isolating the 1:20 scale circular buoy, is depicted in Figure 14.

For a selection of tests in Series 2 and 3 the accelerations, roll, pitch and yaw angles of the model boat were recorded using an Xsens Mtw wireless inertial measurement unit (IMU) housing a gyroscope and triaxial accelerometer. This unit has a mass of 20g which added 0.02% additional mass to the model. It has an angular resolution of 0.05^{o} and static accuracy to < 0.5^{o} and uses a bespoke Kalman Filter algorithm to minimise drift for static and dynamic movements.

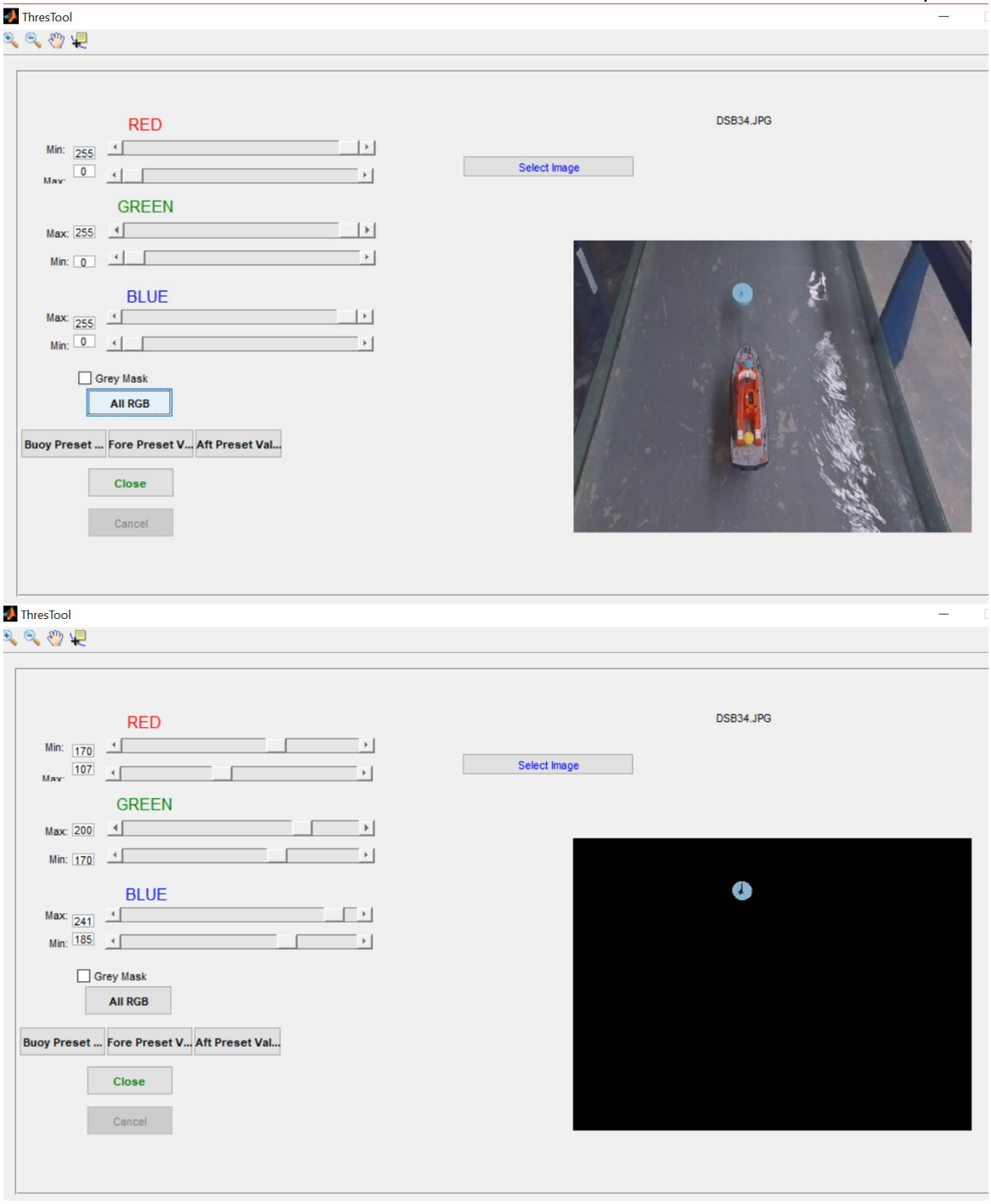

Figure 14: Image from test DSB34 showing mask created from RGB values.

3.2.4 Signal processing

All signal processing, in this thesis, was performed using Matlab software. When applying the Discrete Fourier Transform (DFT) for a signal, in a finite domain, it assumes that there is a whole number of periodic signals within the sample. So for a signal length of T with N frequency components between frequencies of 0 and $(N-1)/T$ the DFT are calculated for components that are integer multiples of $1/T$. Signals which have frequencies which are not integer multiples of $1/T$ are not identified by the DFT and spectral leakage will occur. Furthermore those that are outside the range $\pm N/2T$ will be missed (termed 'aliasing'). To avoid the distortion of these phenomena the sampling frequency was set at 0.03Hz which was at least twice the expected frequency rate observed from initial experiments.

The noise in the signal was removed by the implementation of a 10^{th} order Butterworth filter set to a low pass normalised frequency cut-off of 0.05π radians per sample. The normalized cut-off frequency is between 0 and 1, where 1 corresponds to the Nyquist frequency which is half the sampling frequency (i.e. for samples uniformly spaced by Δt it is $1/(2\Delta t)$. The 10^{th} order was chosen as it has a high cut-off slope and the point 0.05 because from this point on the signal was of negligible magnitude, as shown in Figure 15.

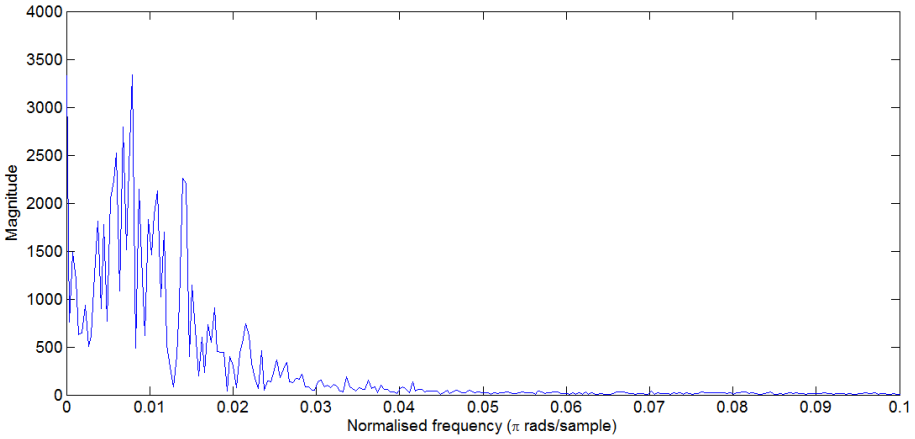

Figure 15: Example of yaw angle Discrete Fourier Transform for 1:40 scale circular buoy (ADB25).

3.2.5 Test programme

The full program of experiments performed in current at the indoor flume at Chilworth research laboratory is detailed in Table 5 and Appendix D. The buoys used in the experiments were model scales of the “mushroom Hippo” buoys used by the RNLI which have a lower cylinder underneath an upper ellipsoid as shown in the schematic in Figure 16.

Series 1: tests with different hawser lengths attached to scale and twice scale buoys and tests with no buoy:

This series of tests were designed to investigate if changes in hawser length or buoy size has an impact upon the motions of a model lifeboat in steady current.

The tests comprised of:

- Three weir settings and two pump settings yielding full scale equivalent water depths from 6.6 to 11m and full scale surface flow rates between 1.03 and 2.31m/s.
- A scale and a twice scale buoy were used each with three different hawser line lengths the full scale equivalent of which being 8m, 6m and 5m. Full test run parameters are detailed as SB1-18 and BB19-36 in Appendix D.1.
- These tests were designed to investigate if the presence of a mooring buoy had an impact on the model vessel’s motions. For the tests, with no buoy, three hawser lengths of 8, 6 and 5m (full scale equivalent) were attached to a ring that was free to find its equilibrium position along the vertically suspended wire rope, a control test with no boat was also run. The test run parameters are detailed as FB1-26 in Appendix D.1.

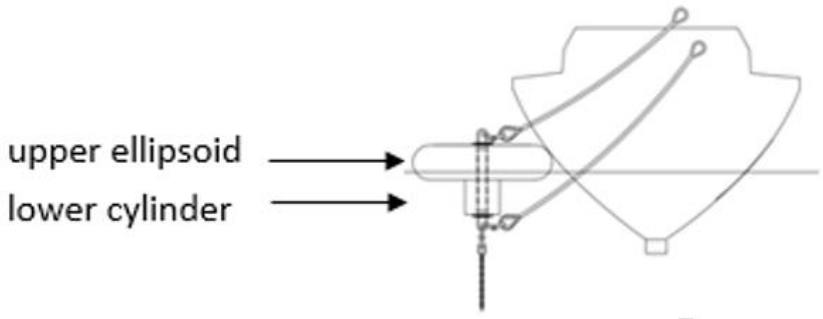

Figure 16: Schematic of an RNLI buoys - 245kg mushroom Hippo buoy (J. Deas personal communication, 27 May 2015).

Series 2: tests at constant flow and depth with different shaped buoys at 1:40 scale:

Having observed the flow patterns around the circular buoy in Series 1 this set of tests were designed to investigate if changing the shape of the mooring buoy impacted upon the motions of the model vessel or the buoy itself. Additionally Series 2 recorded the roll (°), pitch (°) and yaw (°) of the model lifeboat using the Xsens IMU, facilitating the validation of the motion measurements using the video camera and bespoke Matlab code. These tests comprised of:

- Constant pump and weir settings yielding full scale equivalent depth of 8 ± 0.06m and surface flow of 1.75 ± 0.15m/s.
- Five buoy shapes, pictured in Figure 17a, with a decreasing number of edges namely: circle, octagon, hexagon, square and wing, all with the equal immersed volume. The test run parameters are detailed as ADB1–12, ADB25-48 and ADB43-48 in Appendix D.2.
- Tests were run recording the motions of the buoy without the boat attached in order to assess if buoy shape had an impact upon its own motion in steady current. The test run parameters are detailed as ADB13-18 in Appendix D.2.
- Load measurements were taken to record the background load experienced by the anchor lines without either the boat or a riser and buoy attached in order to establish if load measurement was viable. The test run parameters are detailed as NNB1-5 in Appendix D.2.

(a)

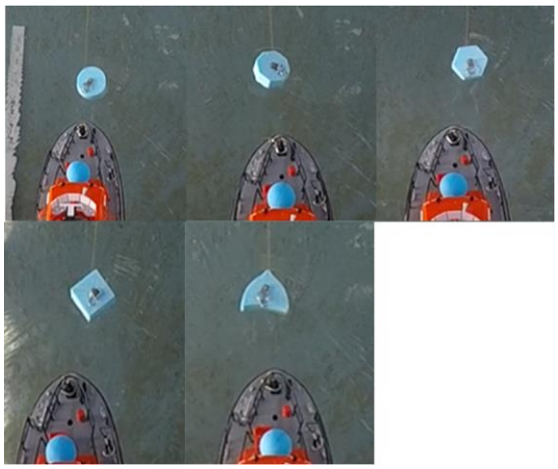

(b)

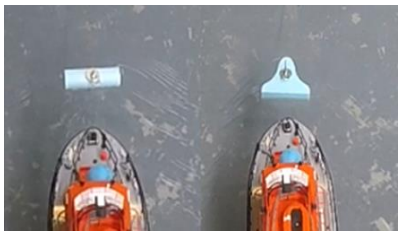

Figure 17: Different shaped buoys tested.
(a) Series 2 and (b) additional shapes in Series 3.

Series 3: tests at constant flow with scale and twice scale different shaped buoys attached and not attached to the model boat:

The program continued by testing different shaped 1:20 scale buoys. Flow meter readings were also recorded to establish the flow regime in the flume.

Series 3 comprised of:

- The pump and weir setting kept constant yielding full scale equivalent depth of 8 ± 0.06 m and surface flow of 1.85 ± 0.23m/s.
- In order to provide three repeat tests per shape, the first set of tests was a repeat of the 1:40 scale performed in Series 2 with an additional redesigned wing shape as shown in Figure 17b. The test run parameters are detailed as DSB1-6 in Appendix D.3.
- Flow readings only were taken behind the 1:40 scale buoys with an additional barrel shape, as shown in Figure 17b, as this is an alternative shape used by some of the RNLI SPM. The tests were repeated twice and the run parameters are detailed as DSB7-27 in Appendix D.3.
- The scale of the buoys and riser length was increased to 1:20 using the shapes of a circle, octagon, hexagon, square, barrel and wing and tests run with the buoys only i.e. the model lifeboat was not attached. The test run parameters are detailed as DSB28-33 in Appendix D.3.
- The boat was attached to the 1:20 scale buoys with a 1:20 scale hawser. The tests were repeated twice and the run parameters are detailed as DSB34-53 in Appendix D.3.

3.3 Verification of data acquisition

3.3.1 Flow

The experiments were designed to test the effect on vessel and buoy motions from changes in hawser length and buoy shape and buoy size at a constant flow speed which was measured as the Mass Flow Rate($\dot{M}$). This was calculated from the multiplication of the surface area (*A*) by the water density (ρ) and surface flow speed (*v*) assuming a uniform velocity down the water column. The error of the measurement is given by the addition of the fractional measurement errors in quadrature (the square root of the sum of the squares):

$$\dot{M}\ error = \sqrt{\{\left(\frac{\delta\rho}{\rho}\right)^2 + \left(\frac{\delta A}{A}\right)^2 + \left(\frac{\delta v}{v}\right)^2\}} \qquad (8)$$

The errors were a percentage measurement error ranging between 3.02% and 3.73%.

The mean, STD and coefficient of variation (CV), calculated as STD/mean, of the $\dot{M}$ for the tests performed and analysed are presented in Table 8. The tests with the highest degree of variability in $\dot{M}$, with a CV of 9.4%, were those comparing the 0.150m hawser length configuration across the different buoy scales. When comparing tests of a specific scale the highest CV is 3.6% for the 1:40 scale different shaped buoys, these levels of variation are considered acceptable for comparison of motion response.

As two different methods of flow measurements were used an attempt was made to correlate the two in order to be able to calculate the depth flow profile, recorded in Series 3 only, from the surface measurements which were recorded for every test. The flow speed for two sets of tests (DSB 49-53 and DSB 75-79), taken behind the test section by the speed of the ping pong ball, and at the front of the section using the flow meter were compared. The resultant plot, shown in Figure 18, shows no linear correlation between the two sets of readings and therefore a calibration curve between the two different types of measurements cannot be used (R^2 = 0.449 and 0.001). The plot also illustrates the degree of variation of the flow between tests run within a set of 5 experiments (during which the pumps were kept continually running) and comparison between days when they had been switched off and restarted.

Table 8: Mass flow rates measured during analysed tests at Chilworth flume
(a) changes in hawser length and (b) changes in buoy shape and size including repeated tests.

(a)

Hawser length (m)	**Mass flow rate (kg/s)**					
	1:40 scale buoy	1:20 scale buoy	no buoy	mean	STD	CV
0.125	77.70	78.87	89.35	81.97	6.42	7.8%
0.150	74.46	80.31	89.63	81.47	7.65	9.4%
0.200	79.61	79.08	89.19	82.63	5.69	6.9%
mean	77.26	79.42	89.39			
STD	2.60	0.78	0.22			
CV	3.4%	1.0%	0.2%			

(b)

Buoy shape	**Mass flow rate (kg/s)**								
Tests and repeats	1:40 scale buoy	1:40 scale buoy	1:20 scale buoy	1:20 scale buoy	1:20 scale buoy	buoy only	mean	STD	CV
circle	72.85	84.47	79.16	83.30	76.83	81.87	79.75	4.38	5.5%
octagon	78.45	84.47	79.43	79.99	73.73	84.35	80.07	4.02	5.0%
hexagon	78.06	81.65				80.69	80.13	1.86	2.3%
square	78.45	81.25	79.16	78.61	74.01	82.90	79.06	3.02	3.8%
wing	78.84	81.25	87.98	75.30	75.11	83.61	80.35	5.00	6.2%
mean	76.95	82.96	79.25	80.63	74.86	82.45	79.52	3.16	4.0%
STD	2.74	1.75	0.16	2.41	1.71	1.55	1.72	0.89	
CV	3.6%	2.1%	0.2%	3.0%	2.3%	1.9%			

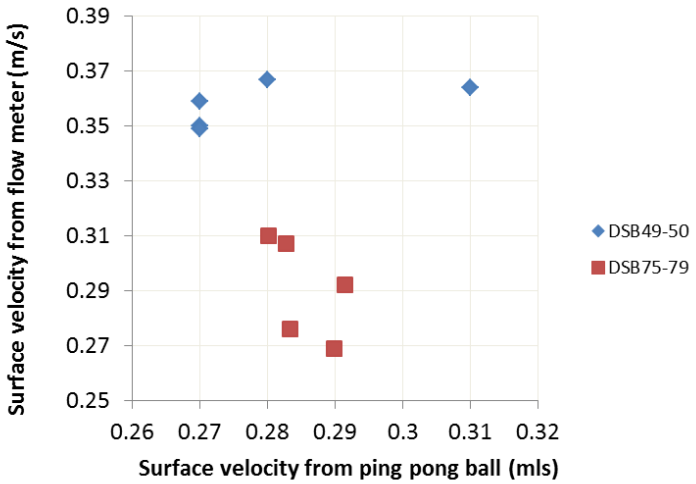

Figure 18: Lack of Correlation between flow velocity measurements.

The assumption made for the flow in the Chilworth flume is that of a steady uniform flow i.e. constant discharge and depth over the time interval recorded in the section containing the model and mooring. The variation in recorded velocity shows that there is variation in the flow velocity both within an experimental time slot when equipment was left running and between days when equipment was restarted. This assumption is therefore not without error. The range of depth, timing of the ping pong ball and $\dot{M}$ for the tests where it should have been constant are presented in Table 9. The variation was more pronounced when comparing between days as opposed within a specific test run where the pumps were left running all session e.g. the percentage difference in $\dot{M}$ for DSB28-33 was 4% and for DSB34-38 was 9%. The data analysed for comparing the effects in mooring configuration are the tests with the closest $\dot{M}$ values.

In order to test the uniformity of flow speed over time and depth a series of ten repeat flow measurements were taken upstream of the test site using the Valeport Flow Meter. The measurements were taken at three positions in the water column (bottom, middle and top) and the results are presented in Figure 19 and Table 10. Over the 10 sets of measurements the STD of the mean measurements shows little variability for the 15 minute duration of the tests at a specific depth, the average recorded STD being 0.006, 0.004 and 0.001m/s respectively for the three depths tested. The flow speed was recorded as decreasing with depth from a mean of the ten mean recordings of 0.36m/s at the top to 0.29m/s at the bottom of the tank.

Figure 19: Mean flow measurements at three depths.
Measurements are at 2Hz for 60s at depths from tank floor of 0.05m (bottom), 0.10m (middle) and 0.19m (top).

Table 9: Minimum, maximum and range mass flow rates of tests at Chilworth flume.
Calculated using measured velocity of ping pong ball travelling at water surface.

Parameter	Series	Minimum	Maximum	Range	% change
Depth (m)	2	0.201	0.204	0.003	1.5
	3	0.200	0.203	0.003	1.5
Time to travel 1m (s)	2	3.3	3.9	0.6	18.2
	3	3.2	3.8	0.6	18.2
$\dot{M}$ (kg/s)	2	72.02	83.86	11.84	16.4
	3	73.16	88.78	15.62	21.4

Table 10: Depth flow readings.

Readings taken at different depths in tank over a 15 minute slot per depth.
Measurements are at 2Hz for 60s at depths from tank floor of 0.05m (bottom), 0.10m (middle) and 0.19m (top).

	Bottom		Middle		Top	
Test	Mean	STD	Mean	STD	Mean	STD
	(m/s)		(m/s)		(m/s)	
1	0.300	0.017	0.339	0.018	0.358	0.007
2	0.294	0.024	0.331	0.017	0.357	0.007
3	0.297	0.020	0.340	0.024	0.357	0.007
4	0.297	0.019	0.336	0.012	0.358	0.006
5	0.287	0.019	0.327	0.015	0.360	0.005
6	0.292	0.023	0.331	0.015	0.357	0.006
7	0.290	0.018	0.337	0.017	0.356	0.007
8	0.284	0.020	0.337	0.015	0.359	0.006
9	0.284	0.020	0.338	0.014	0.355	0.007
10	0.298	0.020	0.333	0.018	0.358	0.007
STD of means		0.006		0.004		0.001

To further investigate the flow within the Chilworth flume the following ratio analysis was performed. When considering open channel flow, the characteristic length parameter used to determine whether flow is laminar or turbulent is the Reynolds Number (R_{echan}) based on the hydraulic radius (UDEL, 2015). The hydraulic radius is a measure of the channel flow and is defined as:

$$h_r = \frac{A}{WP} \qquad (9)$$

where *A* is the cross sectional area and *WP* is the wetted perimeter.

Flow is laminar for $R_{echan} < 500$, transient for $500 \leq R_{echan} \leq 2{,}000$ and turbulent if $R_{echan} > 2{,}000$. Taking the data recorded on 28th August 2015 for the tank width of 1.381m, at a water depth of 0.200m, water temperature of 17.9° C and flow velocity 0.341m/s (top position) this yields an hydraulic radius of 0.16m and a R_{echan} of 29,000 (to two significant figures) and therefore fully turbulent channel flow. Data for the density (998.7780kg/m^3) and kinematic viscosity of fresh water (0.001808Pa.s) used in the calculation was taken from values published by the International Towing Tank Conference (ITTC, 2011).

Examining the ratio of the gravitational forces to the inertial forces of the flow the Froude Number (F_{Nchan}) for channel flow is defined using the hydraulic depth (UEDL, 2015):

$$h_h = \frac{A}{T} \qquad (10)$$

where A is the cross sectional area and *T* is the top width of the channel. For $F_{Nchan} < 1$ it is subcritical flow, $F_{FNchan} > 1$ supercritical and $F_{Nchan} = 1$ critical flow. From the same data in the tank the $h_h = 0.2$ and the $F_{Nchan} = 0.24$ (to two significant figures) implying subcritical flow.

Both numbers are used to describe the flow regime (energy state) in the Chilworth open channel flow. The calculated Reynolds number describes the flow as turbulent implying that the water particles are not travelling along parallel paths at constant velocities however the results presented in Table 10 show a constant flow velocity at each depth tested (maximum differences of 0.016m/s, 0.013m/s and 0.005m/s respectively). The Froude calculation, examining the relationship between flow velocity and flow depth, is a low 0.24 and the subcritical conditions indicate that inertial forces are dominant resulting in deep and slow flow. The implication for these experiments is that the radiated waves generated by the model lifeboat are able to travel upstream against the oncoming low energy state flow and therefore have the potential to impact the motion of the buoy.

3.3.2 Motion

The yaw angle of the model is obtained from the x and y pixel coordinates of the bow and stern markers taken from the same Region of Interest from the GoPro video footage. As the camera was not positioned directly above the entire test site a degree of parallax occurred i.e. there was a distortion in the apparent position of images further down the tank which is illustrated in Figure 12 by the apparent change in distance between the side rails which were an equal distance apart. In order to quantify the amount of parallax, in the video footage, a calibration plot of the variation in millimetres per pixel for the various object lengths on the model lifeboat and the buoy is presented in Figure 20. There was a negligible degree of parallax with a difference of 0.7mm from the buoy to the vessel's transom and so no correction was deemed necessary for the distortion effect. For example the y value co-ordinate moved from minimum pixel position 522 to maximum position 539 during test ADB25.

Furthermore if there was no change in the point tracked by the software then the distance, for example, between the two balls fixed on the model should be a constant value. Footage from the test ADB25 gives pixel values for the distance between them to be between 175 and 172 pixels giving a 1.7% (0.4cm) error which scaled up at a pixel factor of 0.13 pixels per centimetre results in a 16cm error for the equivalent motion of a full scale lifeboat.

In order to verify the motion capture and Matlab algorithm the yaw angle of the model was also measured using a wireless Xsens MTw inertial motion unit for a sample of fourteen tests. The time domain plots for the yaw angle calculated from the video and measured by the Xsens IMU indicated that either measure can be used to record the rotational yaw of the boat. An example comparing the yaw angle using both methods is shown in Figure 21. The phase shift between the two data sets is a result of the manual starting of the two recording systems i.e. the camera and the Xsens. When comparing the tests the maximum difference of the detrended root mean squares was 0.67°, the minimum -0.05° and the standard deviation for all tests was 0.21° as detailed in Table 11.

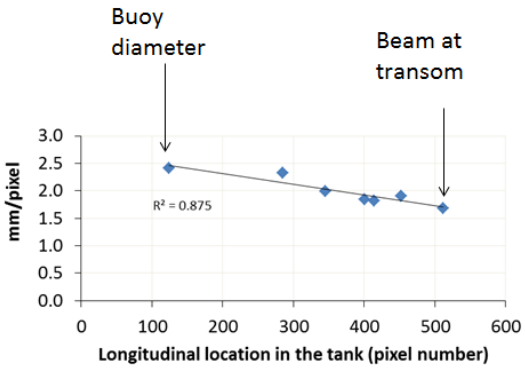

Figure 20: Calibration plot for parallax of camera angle in y direction.

(a)

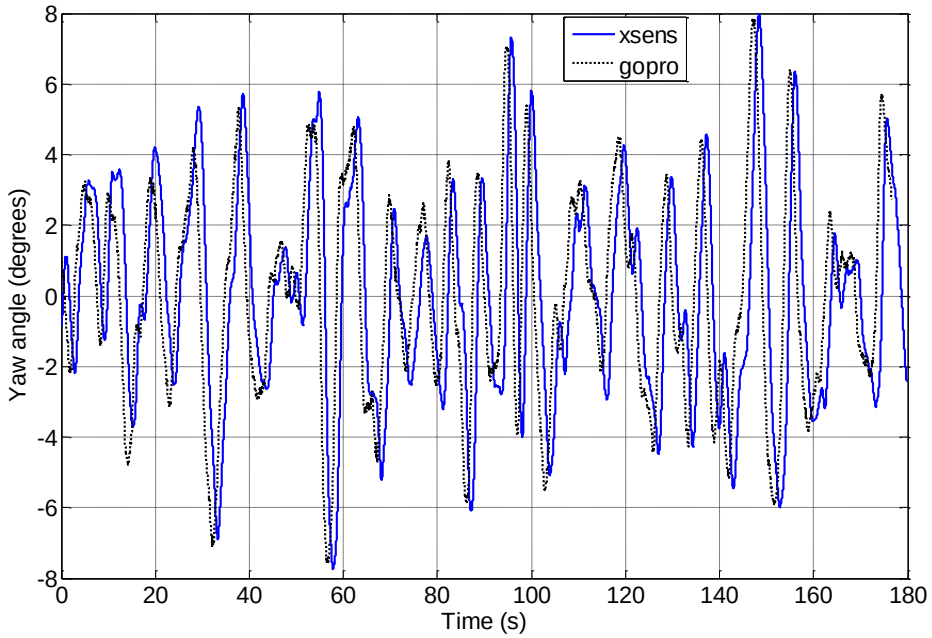

Figure 21: Comparison of yaw angles (a) ADB25 small circle (b) ADB30 small wing.

Angles are calculated from GoPro camera and Matlab code (solid line) and measured by Xsens IMU (dotted line).

Table 11: Comparison of yaw angle using video and IMU.

Test	**Shape**	**RMS from camera**	**RMS from IMU**	**Difference**
		(degrees)	(degrees)	(degrees)
First run 1:40 scale				
ADB25	circle	2.7	2.7	0.0
ADB26	octagon	2.9	3.0	-0.1
ADB27	hexagon	3.1	3.1	0.0
ADB28	square	3.2	3.6	-0.4
Repeat 1:40 scale				
ADB43	circle	2.6	3.2	-0.6
ADB44	octagon	2.5	2.9	-0.4
ADB45	hexagon	2.8	3.0	-0.2
ADB46	square	3.0	3.6	-0.6
1:20 scale				
DSB34	circle	2.1	2.3	-0.2
DSB38	octagon	2.0	2.1	-0.1
DSB37	square	2.5	2.8	-0.3

The verification of the Matlab code and yaw calculation also allows the calculation of other angles of rotation in the tank testing such as that between the buoy and the bow. Assuming that the hawser is rigid the dynamics of the vessel's motions, in a steady current, can be described by a pair of angles controlled by the hawser length (L_H) and the length to a reference point along its centerline (L_V) with the friction force on the hull playing the role of gravity (Tannuri et al., 2001).

Assuming a fixed hawser length and fixed mooring point the two degrees of freedom double pendulum motion can be defined in terms of: ϕ the angle between the hawser and the vertical from the buoy and θ the angle between the vessel's centerline and the vertical from the bow tip (yaw angle) as depicted in Figure 22. From this the following holds (Halliwell and Harris, 1988):

$$sway = L_H sin\varphi + L_V sin\theta \qquad (11)$$

$$surge = L_H(1 - cos\varphi) + L_V(1 - cos\theta) \qquad (12)$$

For the purpose of calculation the reference point on the centerline is the stern marker ball which yields an L_V of 0.44m. Using these formulae the sway and surge have been calculated additionally from the video footage using the pixel co-ordinates of the bow and stern marker balls and buoy.

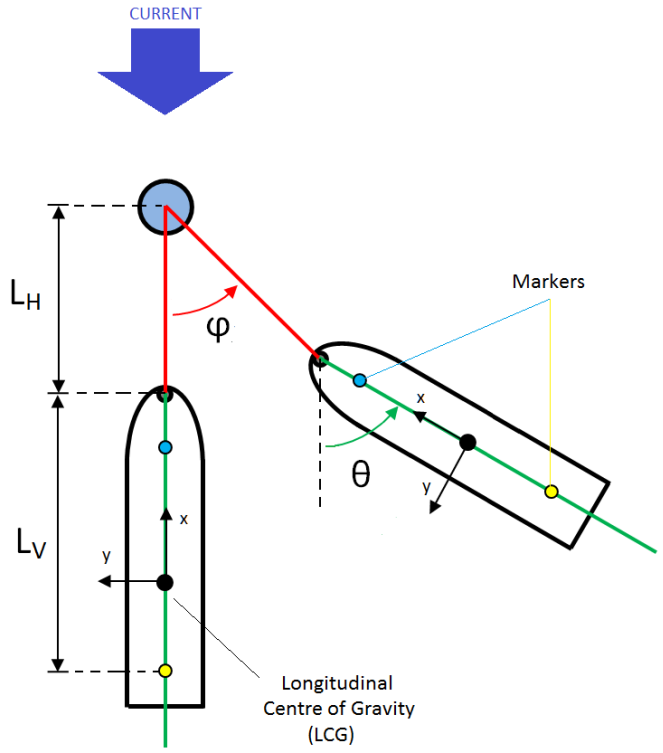

Figure 22: Double pendulum model with fixed hawser length (Hollyhead et al., 2017).

3.4 Results

3.4.1 Flow

For the Series 1 and 2 model test runs the effect of the size and shape of the buoy on the motions of the boat were investigated whilst keeping the pump rate and weir height constant. Although the depth remained constant with only a 3mm variation (1.5%) the surface flow velocity varied from 0.26m/s to 0.33m/s leading to a variation in $\dot{M}$ of 16% in Series 1 and 21% in Series 2, as detailed in Table 9.

In Series 2 of the tests, repeated twice, there were seven different shaped 1:40 scale buoys attached to the SPM only, i.e. with no boat attached (DSB7 –DSB27). During this time the flow was measured over a one minute period at three positions within the water column directly behind the buoy and to the side (e.g. Figure 13). The aims were to test repeatability of flow measurements and see if there was a significant difference between the flow profiles in the wake of the buoys. The results for the top measurement (0.19m from the tank floor in a depth of 0.20m) show that the octagon and barrel shape had the fastest flow and the square the slowest, as illustrated in Figure 23. Again there was some variability between test runs.

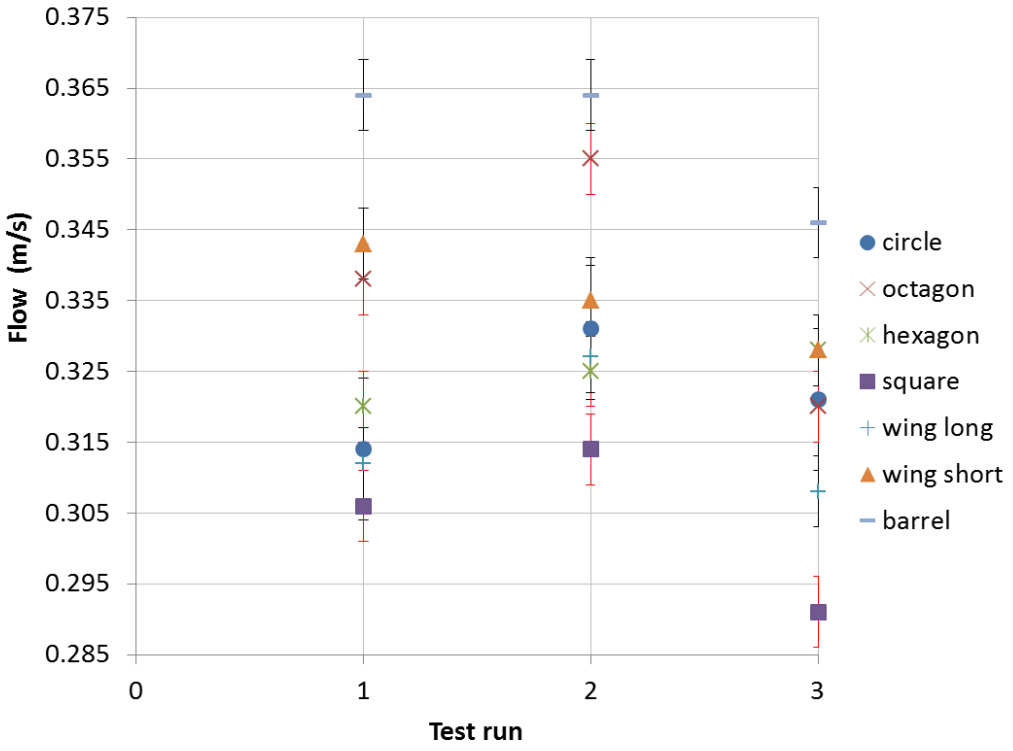

Figure 23: Comparison of flow rates behind the different shaped buoys. All are at 0.19m depth and 1:40 scale buoys. Test run 1 DSB7-DSB13, test run 2 DSB14-DSB20 and test run 3 DSB21-DSB27.

A significant factor influencing the repeatability of the results and therefore the interpretation of the effects of changing buoy shape and size on the motion of the model boat is the comparability of the $\dot{M}$ between test runs. Taking the repeated Series 2 tests for the different shaped buoys as an example the $\dot{M}$, calculated from the surface flow rate, varied between the tests comparing 1:40 to 1:20 scale by: circle 3.1%, octagon 0%, square 1.2% and wing -2.0% which is deemed to be within acceptable error levels.

3.4.2 Typical motion responses in steady current

Experimental results presented are for 170s which is a similar duration of those presented by Chakrabarti and Cotter (1994) and Huang and Lee (2012). With expected yaw and surge oscillations of a full scale tanker at a SPM subjected to steady current of 0.8Hz (Aghamohammadi and Thompson, 1990) this should provide sufficient detail to compare the effects of changes in hawser length and buoy characteristics. The coupled fishtailing motion, which is described in Figure 8, of the 1:40 scale lifeboat at its SPM was observed during all tests performed in current.

Frequency domain plots for all tests did not have a single significant frequency signal peak indicating a series of time signals in the lifeboats motion. However the time domain plots reveal the dominant translational motion to be sway and rotational motion yaw. For example the time and frequency domain for the lifeboat attached to a 1:40 scale circular buoy with a 0.15 m hawser (surface flow 0.26m/s) are presented in Figure 24. The yaw angle moves between -6° and +4° degrees with a frequency peak response range of 0.07 to 0.3Hz and the maximum sway excursion is 0.14 m with a frequency peak response range of 0.06 to 0.21Hz

The extent of the linear correlation between the dominant motions of the vessel's sway (m) and yaw (°) show a marked difference between the 1:40 and 1:20 scale buoys, as shown in Figure 25. Whilst a strong linear correlation does not imply that a sway motion is "causing" a yaw motion it does mean that the value of one variable can be used to determine the value of the other in an engineering analysis. The linear correlation coefficient for the 1:40 scaled buoys ranged from 0.76 to 0.81 over the four shapes but showed a deterioration in linear correlation for the 1:20 scale buoys ranging from between 0.29 and 0.41. (In these tests the hawser lengths were the same scale as the buoy size i.e. the 1:40 scale buoys had a 1:40 scale hawser length and the 1:20 buoys a 1:20 scale hawser length).

In order to compare the impact of the configuration changes the analysed data presented is on the dominant motions of yaw and sway using the three reference points of buoy, bow marker and stern marker balls as illustrated in Figure 24.

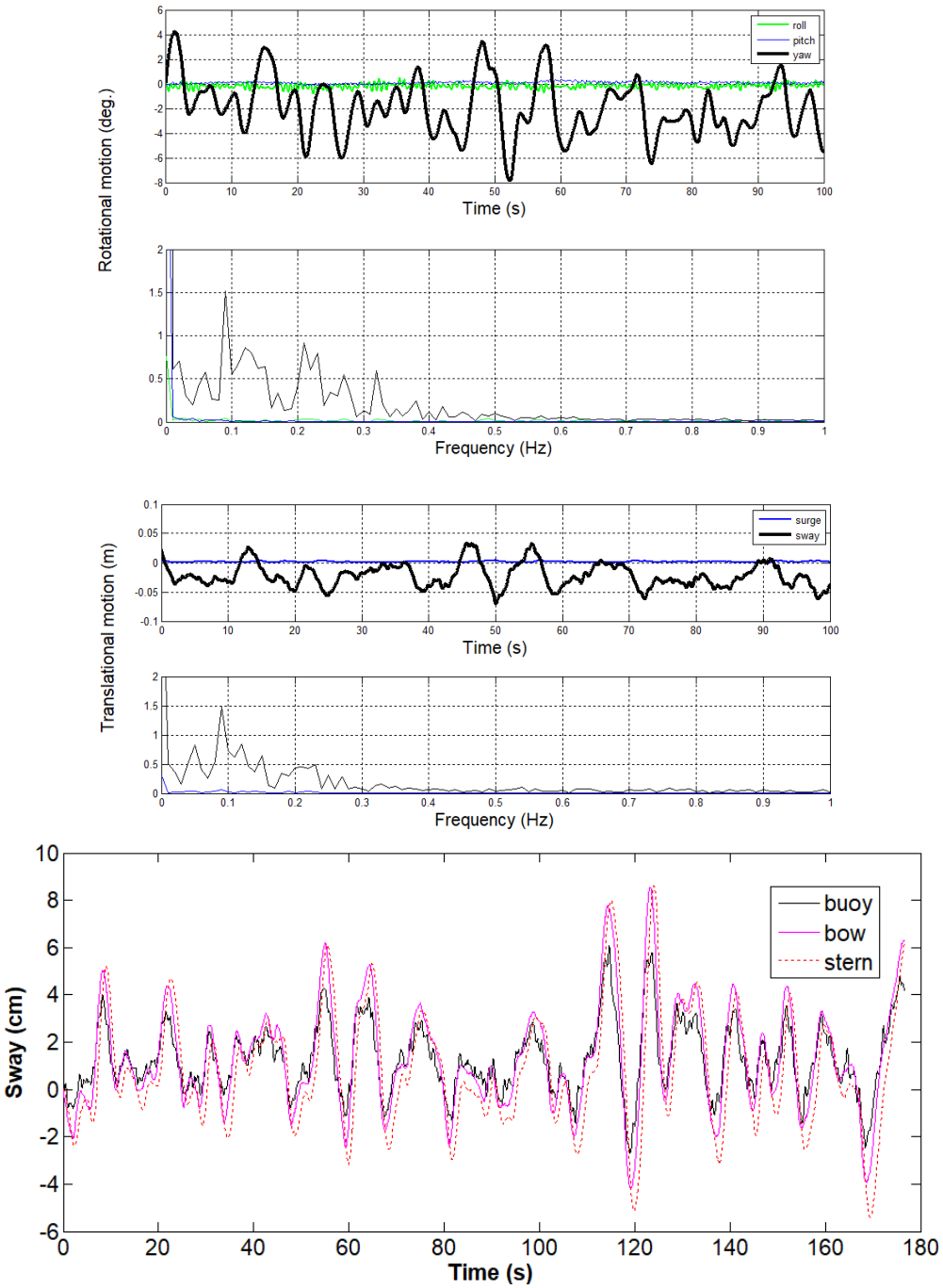

Figure 24: Motions of a 1:40 scale Severn lifeboat with a 1:40 scale circular buoy (test ADB25).

(a) **R^2= 0.81**

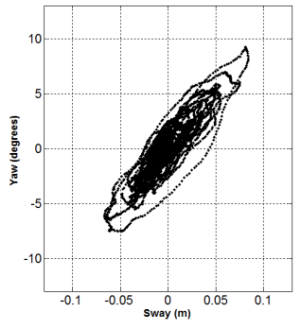

(b) **R^2= 0.32**

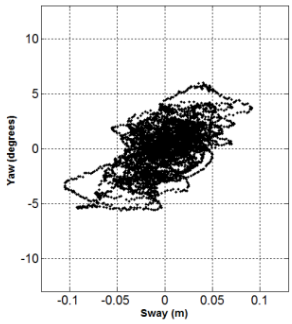

(c) **R^2= 0.76**

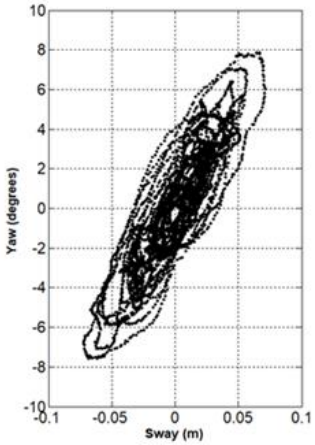

(d) **R^2= 0.41**

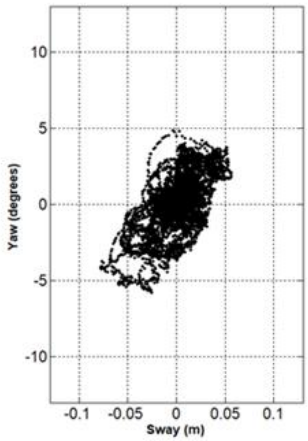

(e) **R^2= 0.79**

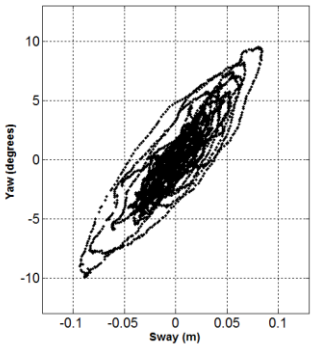

(f) **R^2= 0.35**

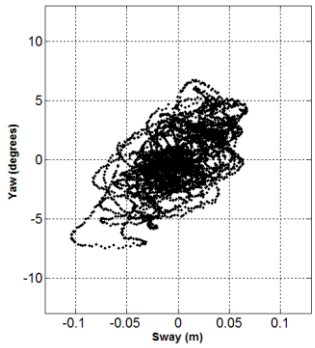

(g) **R^2= 0.81**

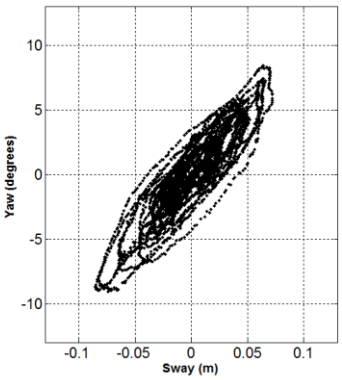

(h) **R^2= 0.29**

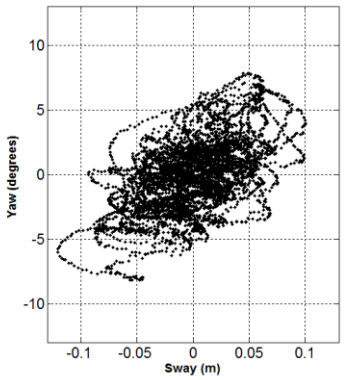

Figure 25: Sway vs. yaw phase plots at two buoy scales.
(a) 1:40 scale circular buoy (ADB25) and (b) 1:20 scale circular buoys (DSB34).
(c) 1:40 scale octagon buoy (ADB26) and (d) 1:20 scale octagon buoys (DSB38).
(e) 1:40 scale square buoy (ADB28) and (f) 1:20 scale square buoys (DSB37).
(g) 1:40 scale wing buoy (ADB30) and (h) 1:20 scale wing buoys (DSB35).

3.4.3 Effect of line length and buoy scale

The first series of experiments were designed to test the effect of hawser length (three lengths at a 1:40 scale of 0.125, 0.150 and 0.200m) and of the size of the circular buoy (three scenarios of no buoy, 1:40 scale and 1:20 scale). The tests that were analysed were the closest matched mass flow rates for the particular line length. For the 1:40 scale these were SB15 (77.70kg/s), SB12 (74.46kg/s) and SB4 (79.61kg/s). For the 1:20 tests these were BB32 (78.87kg/s), BB26 (80.31kg/s) and BB19 (79.08kg/s). For the tests where the boat was moored to a rigid pole FB5 (89.35kg/s), FB13 (89.73kg/s) and FB22 (89.19kg/s) were analysed.

Results show for the tests where no buoy was present (when the lifeboat was moored to a rigid pole) there is a stepwise decrease in the sway velocity for both the bow and stern marker balls as the hawser length was increased, as shown in Figure 26. The highest average sway velocities were using the shortest line length recording an average of 0.030m/s and 0.012m/s for the bow and stern markers respectively. The slowest average sway velocities were using the longest line length recording an average of 0.021m/s and 0.012m/s for the bow and stern markers respectively. There was no such pattern shown for the measurement of yaw.

The tests for line length using the scale and twice scale buoys show a lack of consistent trends i.e. there is no stepwise increases and decreases in average sway or yaw measurements as illustrated in Figure 26. What is more apparent from the data presented is that it is the presence and size of a mooring buoy that had a more pronounced effect on the model lifeboat's motion than hawser length. The sway and yaw velocities, over the 100 second interval, both show significantly higher values when there was no buoy attached to the boat. For example the tests using a 0.125m hawser recorded average sway velocities, for the bow marker, for the largest 1:20 scale buoy of 0.013m/s which increased to 0.017m/s for the smaller 1:40 scale buoy and increased still further to 0.030m/s when there was no buoy present. The yaw range (degrees) decreased by 48% when a 1:20 scale buoy was introduced compared to no buoy presence.

These findings directed the future experiments towards the examination of size and shape of mooring buoy and its effect on the model lifeboat's motions.

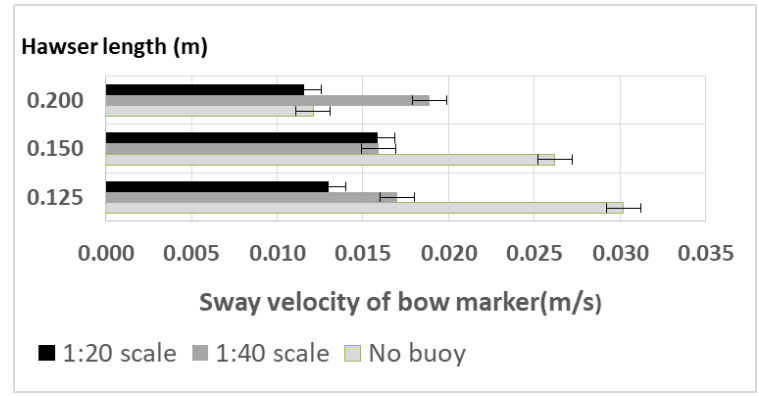

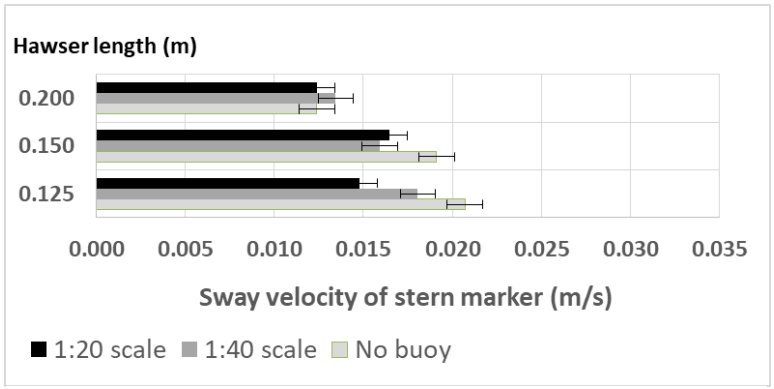

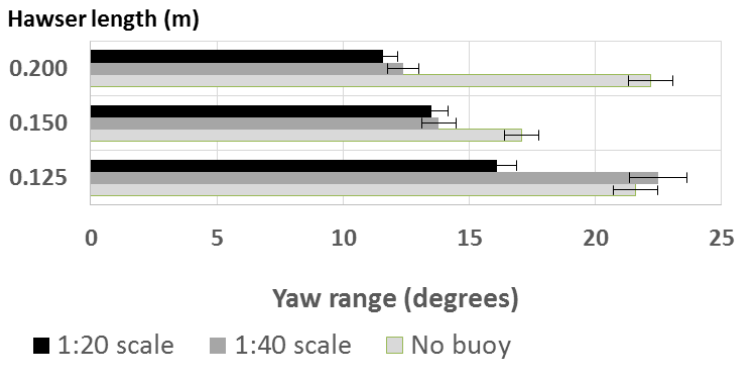

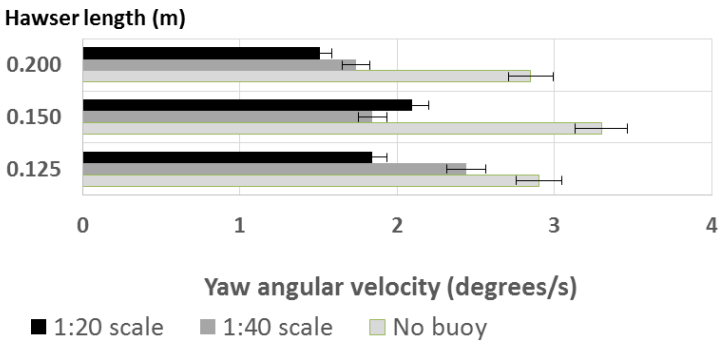

Figure 26: Effect of hawser length on sway velocity, yaw angle and velocity for a 100 second duration.

3.4.4 Effect of buoy shape at 1:40 scale with a 0.150 (m) hawser

Experimental observation and subsequent examination of the videos from the tests, using the scale and twice scale circular buoys, highlighted the different wave patterns radiating from the buoys towards the model boat lifeboat. The subsequent experiments were designed to test the hypothesis that changing the shape and size of the buoy, and therefore the wave patterns, would have an impact upon both the buoy's and lifeboat's motions. The five 1:40 scale buoy shapes, of equal volume and a constant hawser length of 0.150m, tested were; circle, octagon, hexagon, square and wing, examples of which as shown in Figure 17.

At this small scale, and within the calculated error bars, there was little difference between the sway velocities of the different shaped buoys or the resulting motions of the vessel as illustrated in Figure 27a. However for each different shape it consistently showed that the sway velocity of the buoy is slower than the bow marker ball which is slower than the stern marker ball on the model.

The distribution characteristics of the yaw motion of the lifeboat is compared via boxplots of the yaw angular velocity (degrees/s) as presented in Figure 27b. The plots are centred on the median value with associated interquartile boxes which show the ranges from the 1st to the 3rd quartiles. The upper whiskers extend to the maximum data point within 1.5 box heights from the top of the box and the lower 1.5 box heights away from the bottom. The crosses are individual outlier data points which lie above or below the whiskers. Overall there is little difference between the distributions of the yaw angular velocities of the lifeboat due to a change in buoy shape at this scale, as demonstrated by the fact the boxes are of very similar size and equally distributed about the median. The square and the wing shape exhibited the fewest outliers.

To test the null hypothesis that the individual tests had the same distribution of yaw velocities (that is to say that the velocities are from identical populations) the non-parametric Kruskal-Wallis test was performed. This test was chosen as the distributions were not normally distributed and therefore a ranking of data and comparison of medians is required rather than a comparison of means. The test uses ranks of the data, rather than numeric values, to compute the KW test statistics. It finds ranks by ordering the data from smallest to largest across all groups, and taking the numeric index of this ordering. The test statistic is calculated using the formula:

$$KW = \left(\sum \frac{{T_{KW}}^2}{n_K} * \frac{12}{N_k(N_K + 1)} \right) - 3(N_K + 1) \qquad (13)$$

where KW = Kruskal-Wallis test statistic, N_K = total number of observation, n_K = total number of observations per sample and T_{KW} = sum of the ranks in the Kruskal-Wallis test.

The resultant test statistic is a chi-square statistic and the null hypothesis is accepted if this value is less than the tabulated chi-squared value at the relevant alpha value and degree of freedom for the test. The alpha value is the acceptable probability of rejecting the null hypothesis when the null hypothesis is true and for this test was set at 5%. As there are 5 tests and so the degree of freedom is 4 and the relevant chi-squared statistic is 9.49. The calculated *KW* was 4.87 and the null hypothesis is accepted that all tests have equal distribution of yaw velocities, i.e. there is no difference in the effect of buoy shape.

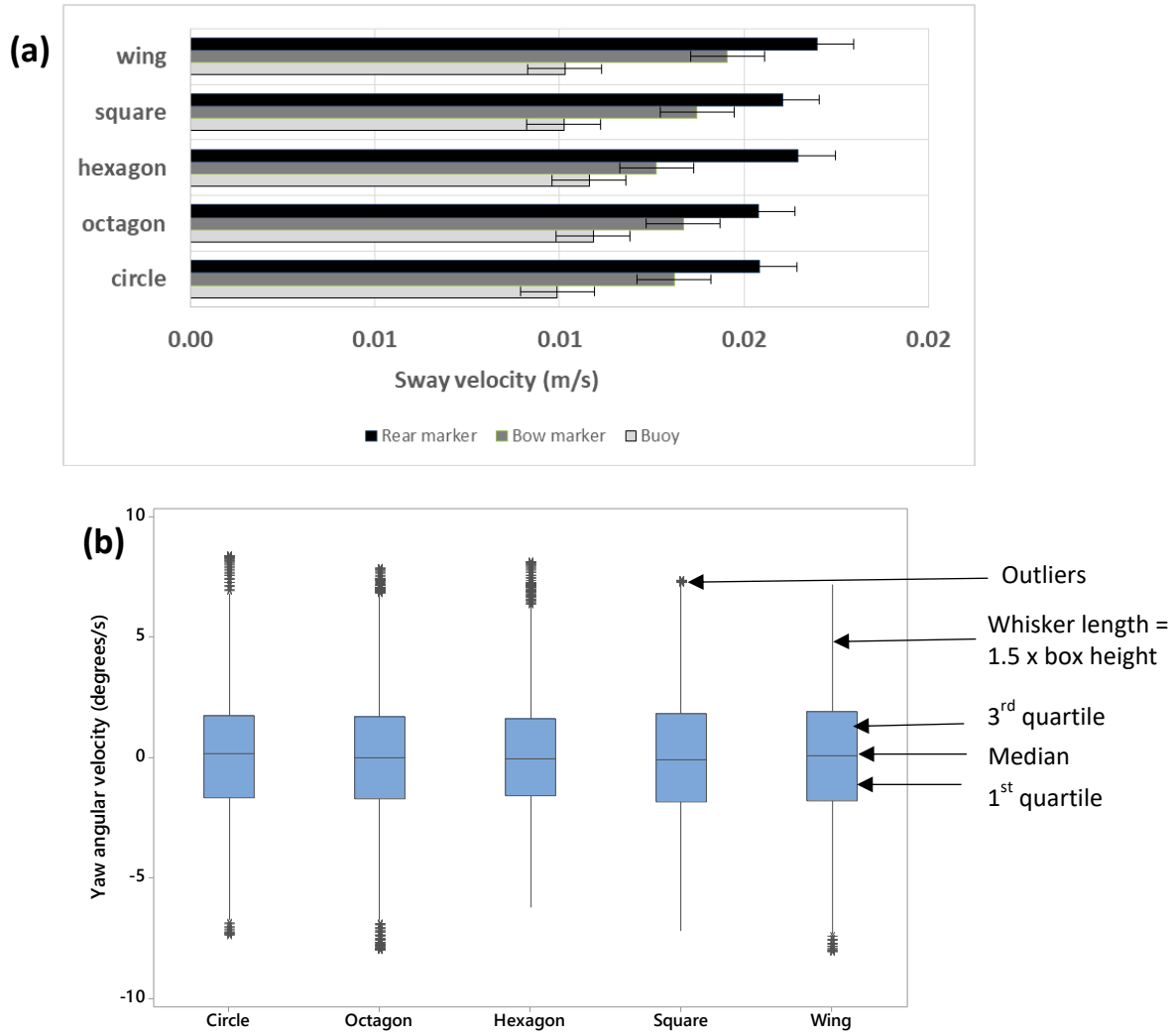

Figure 27: Effect of change in buoy shape at 1:40 scale on (a) sway (mean of two test runs ADB25-30 and ADB43-48) and (b) yaw boxplots of the ADB25-30.

3.4.5 Effect of buoy shape at 1:20 scale with a 0.300m hawser

The next set of experiments again tested the impact of buoy shape keeping the model, depth and flow scales at 1:40 but increasing the hawser length and buoy scale to 1:20. Due to time constraints one shape (the hexagon) was sacrificed in order to perform 2 repeat tests: DSB34-38, DSB45-47 and DSB49-52.

The results of the mean of the three runs show the interaction between buoy and lifeboat is now changed to be the buoy being the fastest in sway whilst at the 1:40 it was the slowest and the differential between the bow and stern marker balls has been reduced as illustrated in Figure 28a. When comparing the sway velocities of the 1:20 scale buoys to those of the 1:40 scale they had increased significantly namely the circle by 138%, octagon by 73%, square by 128% and wing by 191%.

Furthermore, at this larger buoy scale, there is now a significant difference between the velocities for the different shapes tested. In all three tests the wing shape had the fastest sway velocity and the octagon the lowest. So this series of tests showed that using a larger scale of buoy the buoys themselves behaved differently when comparing shapes. Again there was no significant difference in vessel motion from a change in buoy shape however, as shown in Figure 28, there is a difference in the sway velocities of the buoys themselves at this larger scale.

The boxplots of the first set of tests showed, once again, that the yaw angular velocities have similar distributions for all shapes tested as illustrated in Figure 28b and equal median values were proven by a Kruskal Wallis test with a null hypothesis that the data are from equal distributions. The alpha value was set at 5% and there are 4 tests and so the degree of freedom is 3 and the relevant chi-squared statistic is 7.82. The calculated *KW* was 5.49 and the null hypothesis is accepted that all tests have equal distribution of yaw velocities, i.e. there is no difference in the effect of buoy shape.

Comparing the results of the two different scaled buoys revealed that both the yaw angular velocities and range of yaw angles experienced by the vessel consistently decreased when the scale of the buoy was increased; percentage differences in mean values are given in Table 12. Thus showing again that an increase in buoy size reduced the motions experienced by the model lifeboat.

These observed difference in buoy motions lead to the set of experiments, at a 1:20 scale, where the motion of the buoys in steady current were tracked when not attached to the vessel. This also provides data useful to the RNLI who have 20 of their SPM which are secondary moorings and as such are only occasionally used to moor their lifeboats as a more stationary buoy would result in reduced fatigue on the SPM.

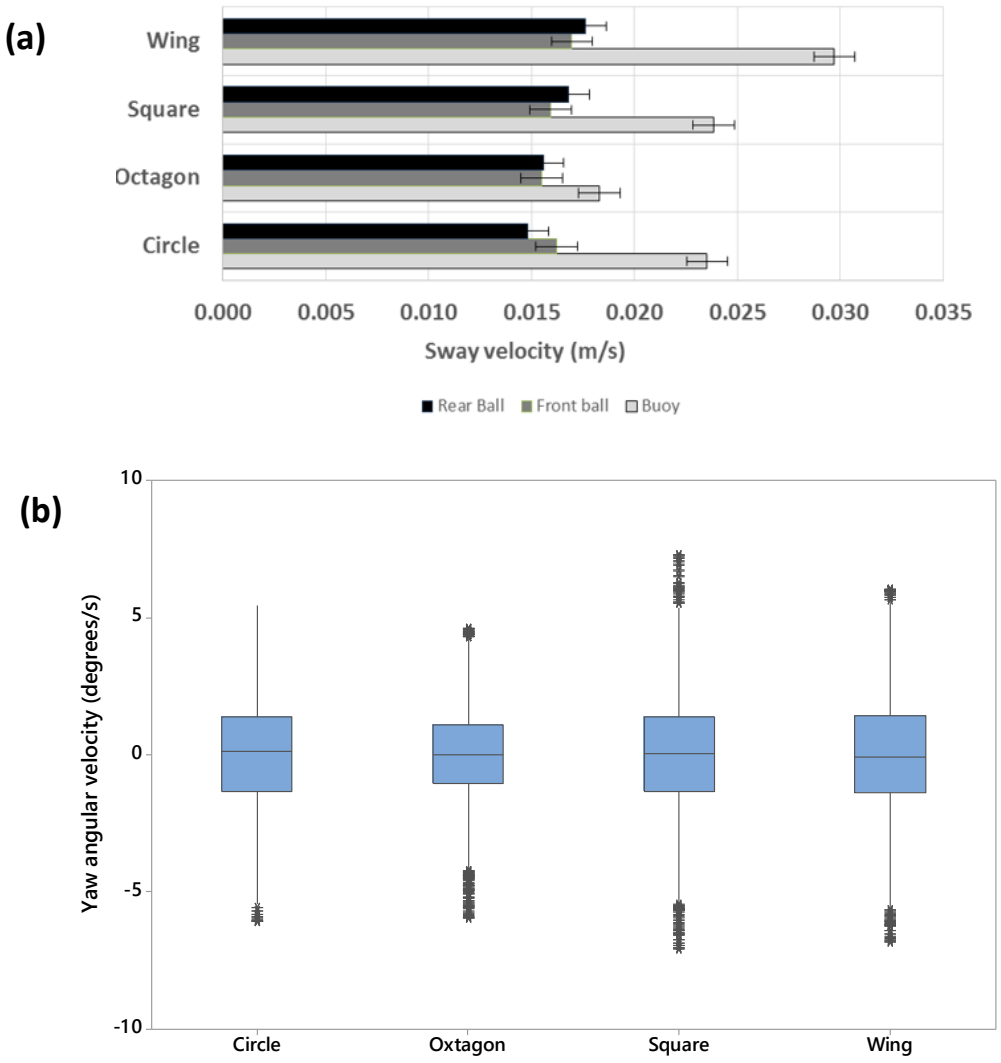

Figure 28: Effect of change in buoy shape at 1:20 scale on (a) sway (mean of three test runs DSB34-38, DSB 44-48 and DSB 49-52) and (b) yaw boxplots (DSB34-38).

Table 12: Comparison of yaw velocity and range showing the difference from 1:40 scale.

Shape	**Yaw angular velocity (degrees/s)**		**Difference (percentage)**	**Yaw range (degrees)**		**Difference (percentage)**
	1:40 scale	**1:20 scale**		**1:40 scale**	**1:20 scale**	
circle	1.96	1.59	18.6	15.04	12.64	15.98
octagon	1.86	1.40	24.9	14.15	12.31	13.00
square	2.19	1.69	22.9	17.43	13.60	21.97
wing	2.19	1.65	24.6	17.32	15.02	13.26

3.4.6 Effect of shape when no lifeboat attached to buoy

To further investigate the findings of differences between buoy shapes and sway velocity a 1:20 scale buoy series of tests were performed with a moored buoy on its own without the attachment of a lifeboat (DSB28-33). For the analysed tests there was a difference, taking into account the error bands, in the sway velocity between the five different shapes as presented in Figure 29. Nondimensionalising the velocity, using the recorded surface flow velocity, and using the circle as the benchmark figure the octagon was 10% faster, the hexagon 34% slower, the square 20% faster and wing 18% slower.

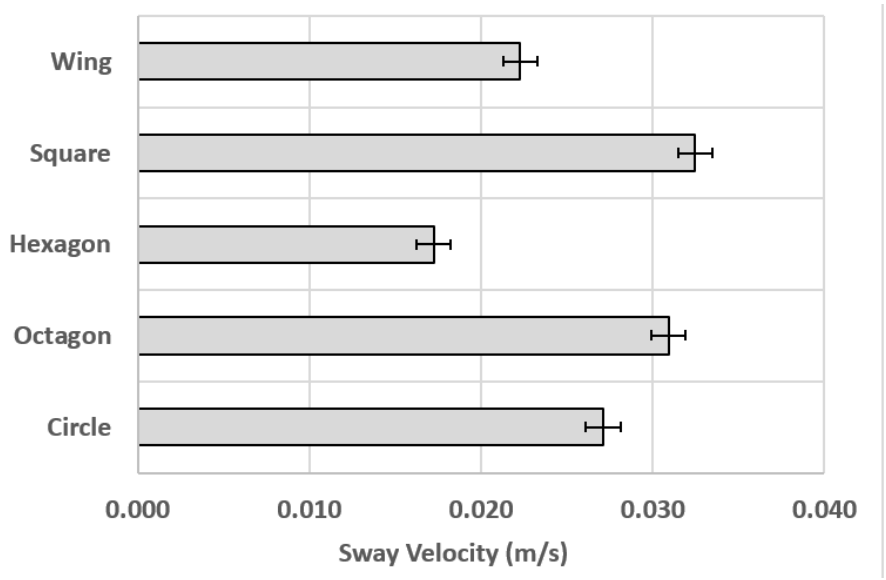

Figure 29: Sway velocities of 1:20 scale buoys unattached to a vessel.

3.5 Discussion

A series of free standing mooring configuration model tests investigating the effects of hawser length, buoy shape and buoy size on vessel and buoy motions, in current, were conducted in a flume. The experimental setup enabled the unrestricted motion of the mooring buoy and model lifeboat to be observed and avoided the influence of mechanical friction upon test results associated with using a towing tank (Simos et al., 2001). The motions of the model and buoy were captured, and validated against an IMU, using an 'off the shelf' video camera and Matlab motion tracking code. This methodology offers an adaptable, inexpensive and portable method of motion tracking with no requirement for instrument cables and a negligible degree of parallax (at this scale).

When scaling for model ship testing the experimental speed conundrum means it is impossible to simultaneously scale for the inertia, gravity and viscous forces. Reynolds similitude is "seldom invoked for most models" as gravity forces are considered to dominate in free-surface flows and viscous effects can be discounted provided "Reynolds numbers (based on flow depth) are greater than 1×10^4 " (Hughes, 2005). The flow depth range of Reynolds numbers for the experiments was 4.6×10^4 to 5.4×10^4 and therefore Froude scaling is deemed appropriate in this case. For comparison the range of flow speeds tested of 0.26m/s to 0.30m/s equates to full scale rates, using similitude of the Froude numbers, of 1.6m/s to 1.9m/s compared to 10 to 12m/s using similitude of Reynolds numbers. The small scale of the buoys used (diameters of 5 and 10cm) means that any surface roughness may lead to a higher impact of the viscous flow effects and therefore the Reynolds number may take on a greater significance for buoy motion. However the purpose of the tests was to observe any differences due to buoy shape and therefore the impact of the viscosity will have been the same for all tests. Finally, using the model beam as the length parameter, yields a Froude number range of 0.21 to 0.26 and for such values some Froude effects on the lateral force and yaw moment should be expected (Tannuri et.al. 2001) and full scale measurements are therefore required to validate the observed experimental motion responses.

A limitation of the tests performed was that the flume operation meant that it was not possible to repeat the exact depth and flow rate combinations for each set of experiments. The variability in flow rate has been shown to be more when comparing test days rather than between tests done in one session when the pumps were left running.

The results showed that the dominant motions of the model are sway and yaw, similar to the fishtailing responses reported in the literature from simulations and experiments for large scale vessels at offshore SPM. The RMS for the surge motion presented in Figure 24 is 0.03 m which is 15% of the 0.20m water depth in keeping with the findings of Isaacson and Baldwin (1996) who reported horizontal motions of 4-10% of water depth.

The effect of reducing the hawser length, for the case when the vessel was attached to a taut wire rope (i.e. no buoy present), resulted in a reduction in the sway velocity of both markers on the model, agreeing with the results of experiments of Pinkster and Remery (1975) and Halliwell and Harris (1988). Also the presence of the buoy was found to reduce the sway and yaw motions of the moored vessel at a SPM when compared to when it was moored to a rigid pole. This significant finding indicates that motion and therefore motion induced fatigue at a catenary SPM can be influenced by the size of the mooring buoy.

Changing the shape of the buoy, at a 1:40 and 1:20 scale, and thereby introducing sharp edges into the dynamic, did not result in a significant change in the model's motion. However, differently shaped 1:20 scale buoys exhibited different sway velocities when not attached to the lifeboat. This would suggest that shape had an impact on the buoys motions, in steady current, but the changes were not large enough, at this scale, to impact the motions of the moored vessel.

The observed linear correlation between the sway displacement (m) and yaw angle (°) that existed at the 1:40 scale buoy was not present at the 1:20 scale, indicating that the buoy-vessel interaction changes with buoy size. Observations showed that introducing the larger buoy and longer hawser length increased the width and vorticity of its wake as can be seen in the photograph in Figure 30. It is therefore hypothesised that this induced the larger sway excursions and reduced the yaw angle range that are presented in Figure 25.

Furthermore an increase in buoy scale resulted in a consistent decrease in the vessel's yaw angular velocity and yaw angle range. Interestingly, at the 1:40 scale, the boat exhibited the fastest sway velocity and at the larger 1:20 scale, the buoy exhibited the fastest sway velocity, suggesting that there may be a change in mode shape, as depicted by the motion arrows in Figure 31. The length of the arrows in the schematic are proportional to the mean sway velocity of the buoy, the bow and stern markers and the mode shape is drawn by connecting the extremities of the arrow heads. This change in mode shape suggests that changes in buoy size can influence the motion responses of the lifeboat and may enable mooring efficacy to be improved e.g. by a reduction in the fatigue inducing motions of the moored vessel.

Figure 30: Turbulent wake created by 1:20 scale buoy.

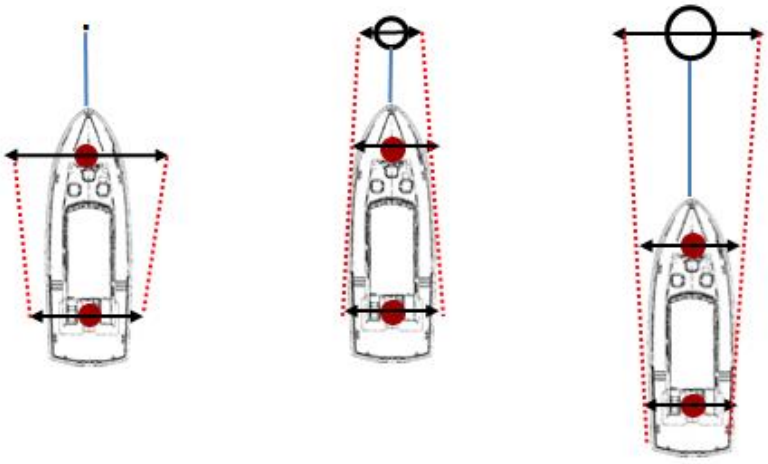

Figure 31: Change in mode shape due to buoy size.

3.6 Summary

The secure mooring of a vessel in a harbour requires the consideration of many conditions, including geographical, meteorological and oceanographic alongside functional considerations such as regulations, space availability and maintenance. A series of model tests in a circulatory flume have been performed designed to test the effect on the motion and forces experienced by a 1:40 scale lifeboat, at a SPM, of the parameters of line length, buoy shape and buoy size. Analysis of the load readings indicate that the scale was too small to accurately predict the anchor line tension as the background turbulence masked the signal and the amplitudes were too small as detailed in C.1. That said the calibration and verification has been established enabling future testing on the mooring line itself at a larger scale. The flow measurements taken in the flume indicate that there was some variability in flow rate between test runs when the pumps had been switched off

The verifications presented show that the motion tracking software and algorithm can be used to track the surge, sway and yaw of the model boat. This provides a simple, adaptable, consistent, inexpensive and portable method of motion capture which can be used for small scale testing, without the need of cabled instrumentation and allowing the free movement of the mooring configuration.

Results from the analysed experiments presented include:

- Time and frequency domain plots for motions of the vessel in steady current show the dominant translational motion to be sway and rotational motion to be yaw (Figure 24).
- The linear relationship between the coupled yaw and sway motions breaks down when the scale buoys are replaced with twice scale (Figure 25).
- The 1:40 scale buoys show consistently that in sway the stern marker ball moves faster than the bow marker ball which in turn is moving faster than the buoy (Figure 27).
- When the buoy size was doubled the bow marker ball now moved consistently faster than the stern marker ball and the buoy was predominantly the fastest of the three (Figure 28).
- These results suggest that changes in buoy size can influence the motion responses of the vessel as demonstrated in Figure 31.
- At both scales tested there was no discernible difference between the sway velocities of the vessel or buoys when a change in shape was introduced (Figure 27 and 34).
- There were significant differences in the sway velocities of the 1:20 buoys (Figure 29) when no vessel was attached.
- Both the yaw angular velocities and ranges decreased when the size of the buoy was doubled from 1:40 to a 1:20 scale (Table 12). This indicates that vessel motions at a SPM can be reduced by increasing the size of the mooring buoy.

Chapter 4: SPM REGULAR WAVE EXPERIMENTS AT 1:10.67 SCALE

> "Since it is possible to obtain results in irregular seas by linearly superimposing results from regular wave components, it is sufficient from a hydrodynamical point of view to analyse a structure in incident regular sinusoidal waves of small steepness. (Faltinsen, 1993).

This chapter details the experimental investigations into the impact of buoy size and buoy shape upon the motions of a 1:10.67 scale lifeboat in regular waves. Section 4.1 contains an introduction to the testing and scaling requirements. The experimental design of the model lifeboat, at its single point mooring, is outlined in Section 4.2 together with the test facility, key parameters, data acquisition systems and procedures. Sections 4.3, 4.4, 4.5 and 4.6 present the data acquisition verification, test results, discussion and summary respectively.

4.1 Introduction

A SPM is designed to "resist the mean mooring forces from wind, current and waves but allow the free response to wave frequency loading" (Barltrop, 1998). In order to assess the impact of the buoy shape and buoy size upon the motions experienced by a lifeboat, at a SPM, a systematic series of scaled model experiments have been performed in regular waves. The experiments were designed to examine whether the change in the characteristics of the waves radiated by different shaped buoys were significant enough to impact the model lifeboat's motions. Additionally investigated was whether changing the size of the buoy affected the shape of the catenary riser chain and the model's motions in this multibody system.

4.1.1 Scaling for experiments in waves

When scaling for tank tests the gravitational forces are considered to be dominant over the viscous forces and the wave tests were performed using the Froude scaling as described in Section 3.1.1 and detailed in Appendix H. The model lifeboat, buoys and wave parameters were scaled using the Froude similitude. The ratio of length scales, *R*, is defined as the dimension scaling ratio and is equal to the full scale length divided by the model length. Time and velocity are scaled by $1/\sqrt{R}$ and forces by $1/R^3$ and then multiplying by a correction factor for the difference in freshwater and seawater density.

The elastic properties of mooring line chains and hawsers were scaled using the Cauchy criterion which requires equality of the ratio of inertial to elastic forces in full and model scale (Hughes, 2005). The required diameter is a function of the Young's modulus of the riser and hawser materials used and these were obtained via extension tests at the University of Southampton

using an Instron E-Series Circumferential Extensometer. The stress/strain curves, linear regression lines and resultant calculations of the Young's modulus testing of the materials used in the tank tests are available in Appendix I. For a match to the RNLI hawser rope the calculation of Young's modulus dependent diameter for the hawser (fishing wire) yielded a requirement of 1.7mm and the actual diameter was 1.0mm ± 0.5mm. The calculation of diameter for the riser (brass chain) yielded a requirement of 4.0mm and the actual diameter of the available brass chain was 2.0mm ± 0.5mm.

The wave height of 0.05m, at an R = 10.67, equates to a full scale of 0.53m which compares to the recorded range of values on 7th January 2017 at Dunbar Harbour (the location of the failed mooring) of 0.3 to 0.5m (Meteo Consult Marine, 2017). The recorded swell period on that day was 2.0 to 3.0s compared to the full scale test conditions in the tank of 2.9 to 4.0s. The water depth of the Solent wave tank is 1.8m which equates to a full scale depth of 19m which is deeper than all except one of the RNLI moorings the majority of which are between 5 and 10m deep as detailed in Appendix B. Due to this increased depth the length of the mooring riser was longer than the RNLI risers detailed in Appendix A. The recommended length of a riser is at least 3 times the water depth (Bradney, 1987, Hinz, 2001), the length for the riser chain was set 6m (full scale equivalent 64m).

4.1.2 Blockage effects

A limitation of tank testing, known as the blockage effect, occurs when the tank walls and floor interfere with the fluid flow which would not occur in unrestricted water at full scale. There is a trade-off between maximising the scale of a model, in order to reduce scaling effects, and reducing the blockage effect. The wave tank at Solent University is 60m long and 3.7m wide with a water depth of 1.8m deep giving it a working cross section area of 6.66m^2. This gives a vessel to tank cross sectional area of approximately 0.7% which is fractionally above the optimal limit defined of 0.5% in Molland et. al. (2011) implying that there may be some minimal interference from the tank walls. For the particular case of tank testing of moorings, the tank wall effects on the lateral forces are negligible when the ratio of tank width to vessel length is 5 but have a noticeable effect when this is reduced to 3 (Chakrabarti and Cotter, 1994). This ratio for the 1:10.67 scale model at Solent is 2.5 (3.7/1.5m) indicating that the tank walls impacted on the lateral forces experienced by the model particularly when the model yawed. For this reason the data analysed from the tests was set at 45s in order to minimise the impact of waves reflected from the tank walls on the model's motions. As the aims of the tests were to compare the effects

of buoy shape and size this limitation is deemed acceptable as the blockage effect will be the same for each shape tested.

Furthermore for a water depth to vessel draught ratio of 5 or more, the shallow water effect is considered negligible (Chakrabarti et al., 1995). The depth to draught ratio for the current tests was 14 (1.8/0.13m) indicating that the shallow water effects were negligible.

4.2 Experimental methodology

4.2.1 Test facility and experimental set-up

The experiments were performed in April and August 2016 at Solent University's wave tank which is 60m long and 3.7m wide with a working water depth of 1.8m. Regular waves were generated using a motor-driven, single paddle HR Wallingford wavemaker with a maximum stroke length of ±180mm. A 1:10.67 scale model lifeboat and SPM were positioned in the tank; motion was recorded using an IMU and camera and wave height using a wave probe as illustrated in the schematic in Figure 32.

The initial experimental set up included a load cell attached to the hawser however the trailing cables and the weight of the load cell had a significant impact upon the model vessel and buoy's motions and the equipment was removed. Details are provided in Appendix C. This further highlights the benefits of the video method validated in chapter 3.

The full test programme and parameters are set out in Appendix G and summarised in Table 13. The motions of the lifeboat and buoy were recorded at four wave frequencies for each of the five buoy shapes that were tested in the Chilworth flume, shown in Figure 33, using buoy scales of 1:10.67 and 1:5.33.

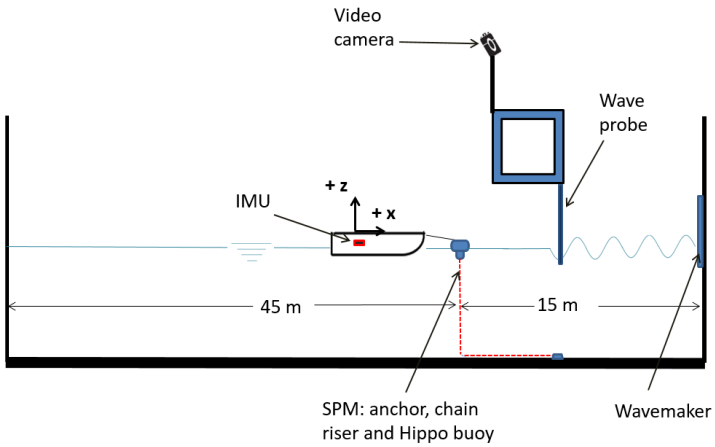

Figure 32: Schematic of experimental set in wave tank.

Table 13: Regular wave test parameters. All tests performed at constant wave height of 0.05m.

Buoy scale	Upper hawser length (m)	Lower hawser length (m)	Shape	Frequency (Hz)	Number of tests (per wave frequency)
1:10.67	0.56	0.66	Circle, octagon, hexagon, square, wing.	0.8,0.9,1.0,1.1	3
1:5.33	1.12	1.32	Circle, octagon, hexagon, square, wing.	0.8,0.9,1.0,1.1	3

Figure 33: Five 1:10.67 scale buoy shapes tested in regular waves.

4.2.2 Model Tamar class lifeboat

The representative model hull was that of a Tamar class lifeboat constructed of strip plank sheathed with glass-reinforced plastic. The full scale and 1:10.67 model scale particulars are presented in Table 14. The yaw radius of gyration of the ballasted model was measured using the suspension rig method described in Section 3.2.2. The period of ten yaw oscillations was recorded which yielded a yaw radius of gyration of 0.27 m which compares to a value of 0.34m using the estimation of 25% of the length between perpendiculars for a full scale vessel (ITTC, 2008). This reduction is to be expected as this approximation has been derived for larger vessels which typically have a length to breadth ratio of 5:1 to 8:1 (MarineWiki, 2018) compared to the ratio of a lifeboat of 3:1.

Table 14: Particulars of full and model scale Tamar lifeboat.

Particular	Full scale	1:10.67 scale model
Length overall (m)	16.3	1.53
Length between perpendiculars (m)	14.7	1.37
Beam (m)	5.3	0.49
Draught (m)	1.4	0.13
Displacement (tonnes)	32.0	0.026
Yaw radius of gyration (m)	3.67 (estimated)	0.27 (measured)

4.2.3 Data acquisition

The 6 degree of freedom motions of the model boat were recorded using an Xsens Mtw inertial motion unit (IMU) positioned at its centre of gravity. The motions of the boat and the buoy were recorded using two Go Pro Hero cameras set at 30 frames per second: one mounted above the tank in the x-y plane and the other mounted on the side wall in the x-z plane. Additionally some underwater footage was recorded capturing the change in catenary shape of the riser chain. The wave height was measured via a calibrated wave probe located in front of the SPM, as illustrated in the schematic in Figure 32.

From initial test runs it was observed that the motions of the model lifeboat were significantly affected by its initial orientation to the oncoming wave train. Therefore, in order to be able to compare the effects of the size and shape of buoy, each test was started from the same equilibrium position, as depicted in Figure 34. The model was released when the first wave reached the wave probe.

The test duration was dictated by the fact that, having reached the beach at the far end of the tank, the incident waves were reflected back towards the model. For the four wavelengths (λ) tested the wave speed, calculated using the wave number $\left(k = \frac{2\pi}{\lambda}\right)$, ranged from 1.42 to 1.95m/s, as detailed in Table 15. Having passed the buoy the wave had 88m to travel to the end of the tank and back to the stern of the model which, for the fastest wave celerity (1.95m/s), equated to 45s of data acquisition time. This duration also limited the effect of the reflected waves from the tank walls which were of shorter wavelength and therefore slower celerity.

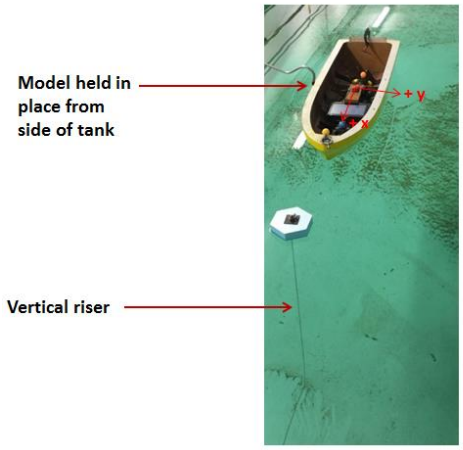

Figure 34: Equilibrium start position for experiments in regular waves.

Table 15: Wave frequency and speed data calculated assuming the deep water form of the dispersion equation (tanh (kh) ranging from 0.9998 to 1.0).

Frequency (f) (Hz)	**Period (T) (s)**	**Wavelength (λ) (m)**	**Wave number (k) (m^{-1})**	**Wave celerity (c) (m/s)**
Equation	$\frac{1}{f}$	$\frac{gT^2}{2\pi}$	$\frac{2\pi}{\lambda}$	$\frac{\omega}{k}$
0.8	1.25	2.44	2.58	1.95
0.9	1.11	1.93	3.26	1.74
1.0	1.00	1.56	4.03	1.56
1.1	0.91	1.29	4.87	1.42

4.3 Verification of data acquisition

The verification of the motion capture by the Xsens IMU has been established in Section 3.3.3; in addition a further check on the Xsens software was conducted to verify the algorithm for integrating the angular velocity (rad/s) data to roll, pitch and yaw angles (rad) as this was the primary source of boat motion recording for these experiments. The velocity data, recorded by the Xsens, was integrated using a built in Matlab function based upon the trapezoidal method. The integrand was evaluated cumulatively for 45 seconds using a unit spacing of 0.01 seconds. This was performed for tests at a wave frequency of 0.8Hz for the scale and twice scale square buoy tests (numbers 115 and 175) and the scale and twice scale hexagon buoys (tests 123 and 163). The resultant plots of angular displacements from the Matlab calculation and Xsens algorithm show close agreement but with the drift between the two increasing over time in yaw, e.g. Figure 35. Examination of the percentage difference in RMS of the two signals, presented in Table 16, confirms that the algorithm is acceptable for roll (maximum difference -2.3%) and pitch (maximum difference -0.3%) but drifts in yaw (maximum difference 18.9%).

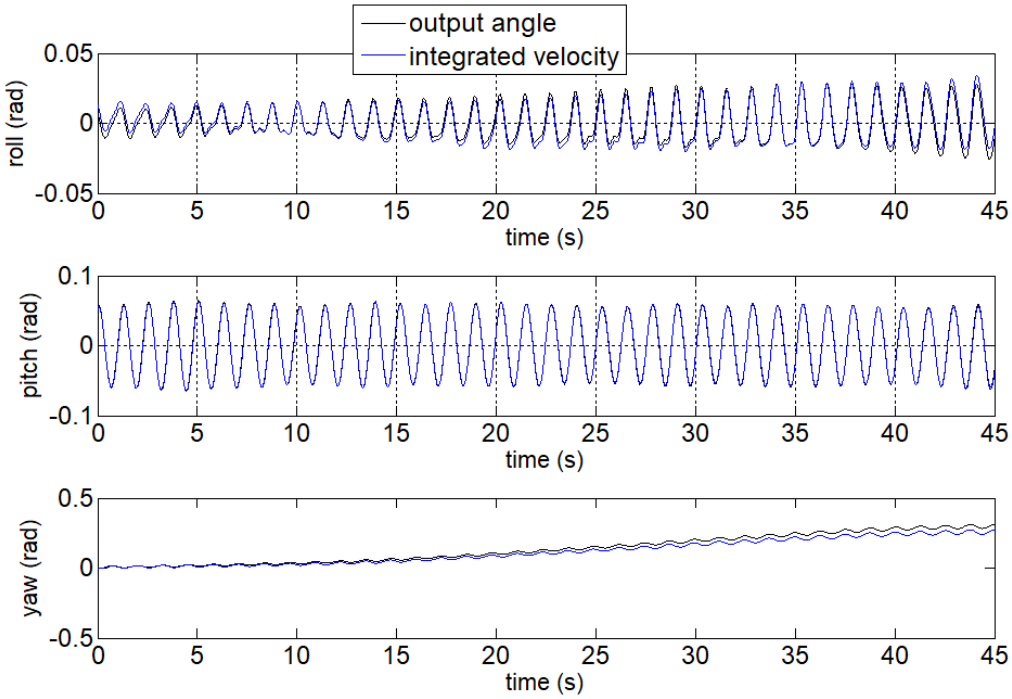

Figure 35: Comparison between Xsens angles and integrated velocity data (unfiltered data for test 115, scale square buoy, test wave frequency of 0.8Hz).

Table 16: Comparison of Xsens algorithm to Matlab integration.

Test	**Shape**	**Scale**	**Motion**	**RMS signal (rad)**	**RMS integrated data (rad)**	**Percentage difference (%)**
115	square	1:10.67	roll	0.0128	0.0131	-2.3
			pitch	0.0414	0.0413	0.2
			yaw	0.1693	0.1461	13.7
123	hexagon	1:10.67	roll	0.0171	0.0173	-1.2
			pitch	0.0403	0.0402	0.2
			yaw	0.2352	0.1907	18.9
163	hexagon	1:5.33	roll	0.0221	0.0221	0.0
			pitch	0.0385	0.0386	-0.3
			yaw	0.3874	0.4064	-4.9
175	square	1:5.33	roll	0.0242	0.0245	-1.2
			pitch	0.0376	0.0376	0.0
			yaw	0.2580	0.2736	-6.0

4.4 Results

4.4.1 Typical motion responses in regular waves

For the tests run in regular waves the effects of the buoy size and buoy shape upon the motions of a model lifeboat were investigated, at a constant wave height, over a range of four frequencies repeated three times. In order to get comparable results for changes in buoys each test run was initiated from an equilibrium starting position as illustrated in Figure 34.

For each degree of freedom results are presented for 45s of unfiltered data starting from the same time stamp which was determined by the time of the tenth peak in the pitch (°) data. At this point the regular wave was fully formed and steady state oscillations had been established, an example of which is presented in Figure 36.

Motion responses are presented in terms of a non-dimensional response amplitude operator (RAO) for each degree of freedom. For the translational motions the RAO is defined as the RMS of the acceleration (m^2/s) amplitudes divided by the RMS of the wave acceleration (m^2/s) amplitude and for the rotational motions as the RMS amplitudes (rad) divided by the wave slope RMS (Lloyd, 1989). For the yaw motion the maximum yaw angle of the model was taken rather than the RMS as the motion was not oscillatory as shown in Figure 37.

The motions of the model reached a steady state oscillatory motion in all test runs in all degrees of freedom except yaw. Pitch was the dominant rotational motion, an example of which is illustrated in Figure 37. The RMS value for pitch was 2.33° which was 5.5 times greater than the roll RMS of 0.42°. The dominant steady state oscillatory motions of the model in regular waves were pitch, surge and heave. The respective RMS values of the translational accelerations are surge $0.22m/s^2$, sway $0.04m/s^2$ and heave (having deducted the gravitational acceleration of $9.81m/s^2$) of $0.34m/s^2$.

For each test the peak frequency of oscillatory roll, pitch, surge, sway and heave motions matched the wave frequency an example of which is shown in Figure 37 in which all peak at the wave frequency of 0.8Hz.

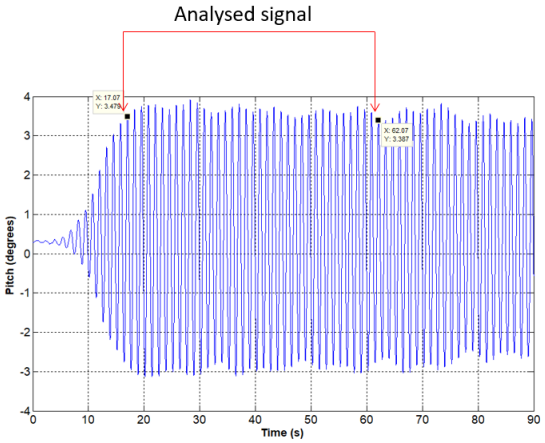

Figure 36: Example of analysed pitch data, small circle at 0.8Hz.

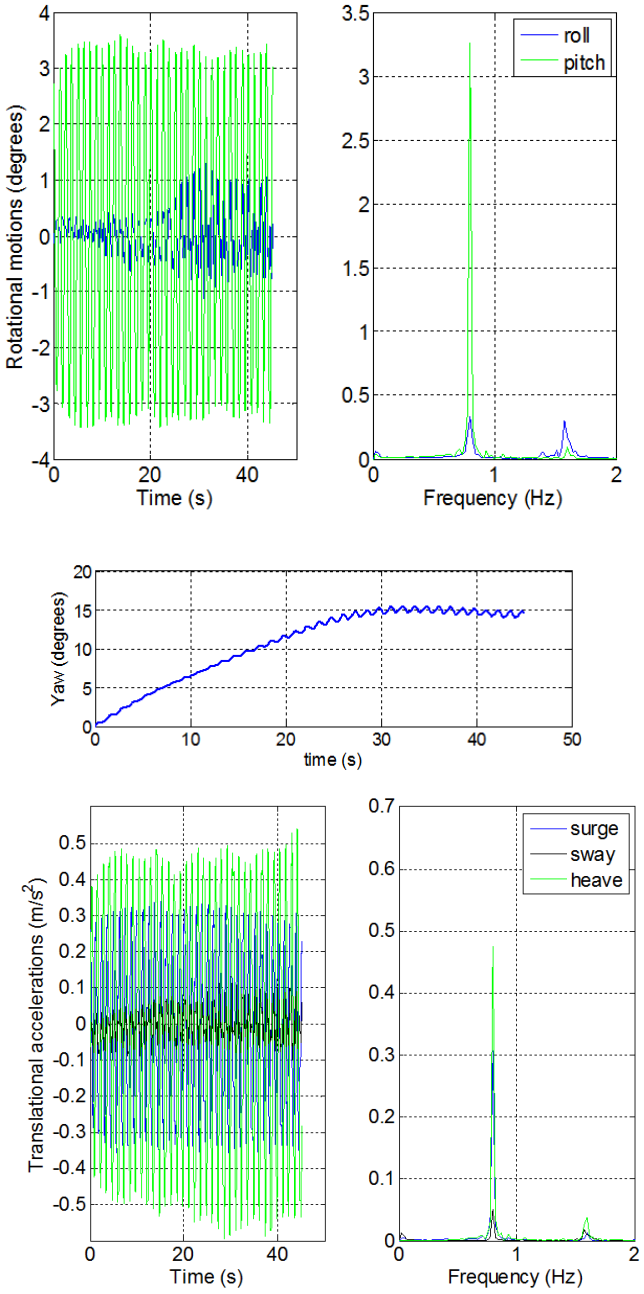

Figure 37: Translational and rotational motions at wave frequency of 0.8Hz. Circular buoy at 1:10.67 scale (test 55).

In order to compare the effect of buoy shape and size it was necessary to establish if the tests were repeatable. This was initially compared graphically for all tests and, from visual inspection, the most divergent and closest repeat runs are presented in Figure 38 (rotational motions) and Figure 39 (translational motions). No single shape emerged from the RAO graphs as the most or least repeatable but pitch and heave showed the highest repeatability over the tested frequency range.

To quantify the repeatability non-parametric Mann-Whitney U tests were performed comparing the three test runs at each frequency tested. This test was chosen as the data sets were not normally distributed and therefore a ranking of data and comparison of medians is required rather than a comparison of means. This test uses the same method as the Kruskal-Wallis test detailed in Section 3.4.4 but is adapted for the case of comparing two data sets.

From this statistical analysis the motions that showed consistent repeatability were pitch, sway and heave across all shapes and for both scales. At both scales the octagon showed the least repeatability of all the shapes and the wing the most consistent which is illustrated by the ticks and crosses of Table 17 and Table 18. The percentage of tests included in the analysis into the effect of buoy shape and size are presented in Table 19.

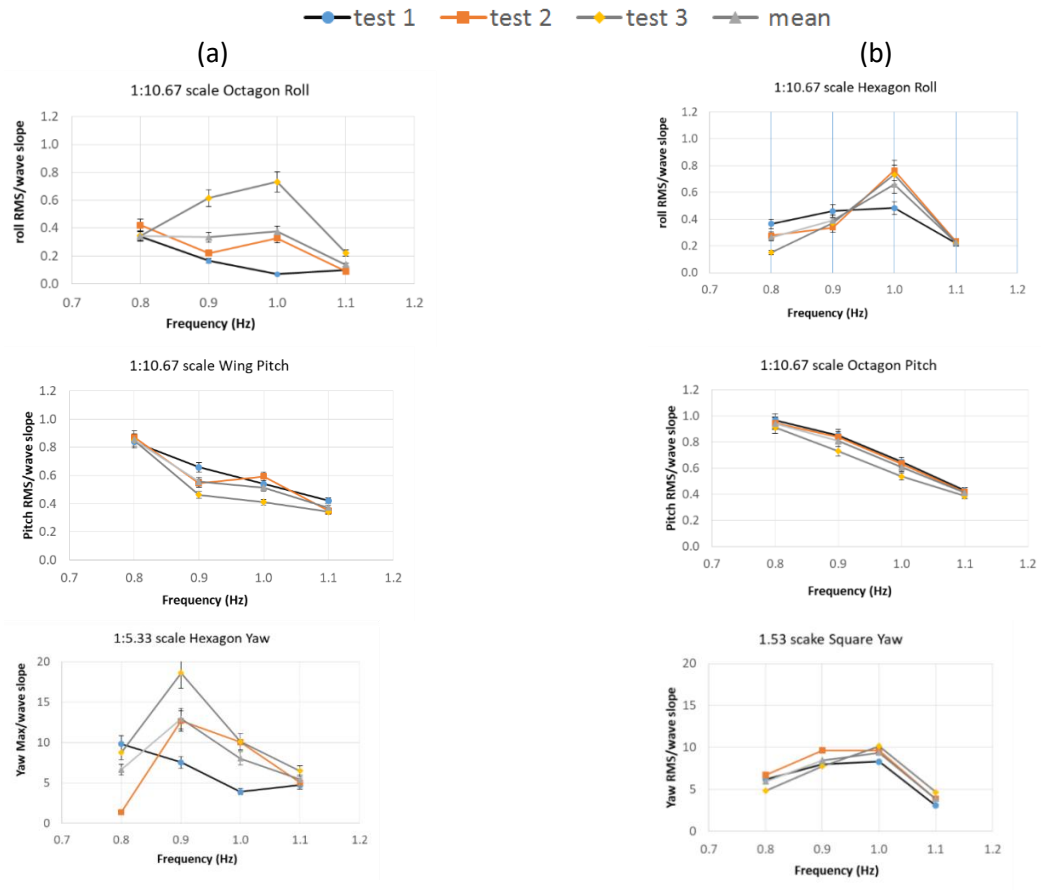

Figure 38: Comparison of rotational repeats (a) least and (b) closest repeatability.

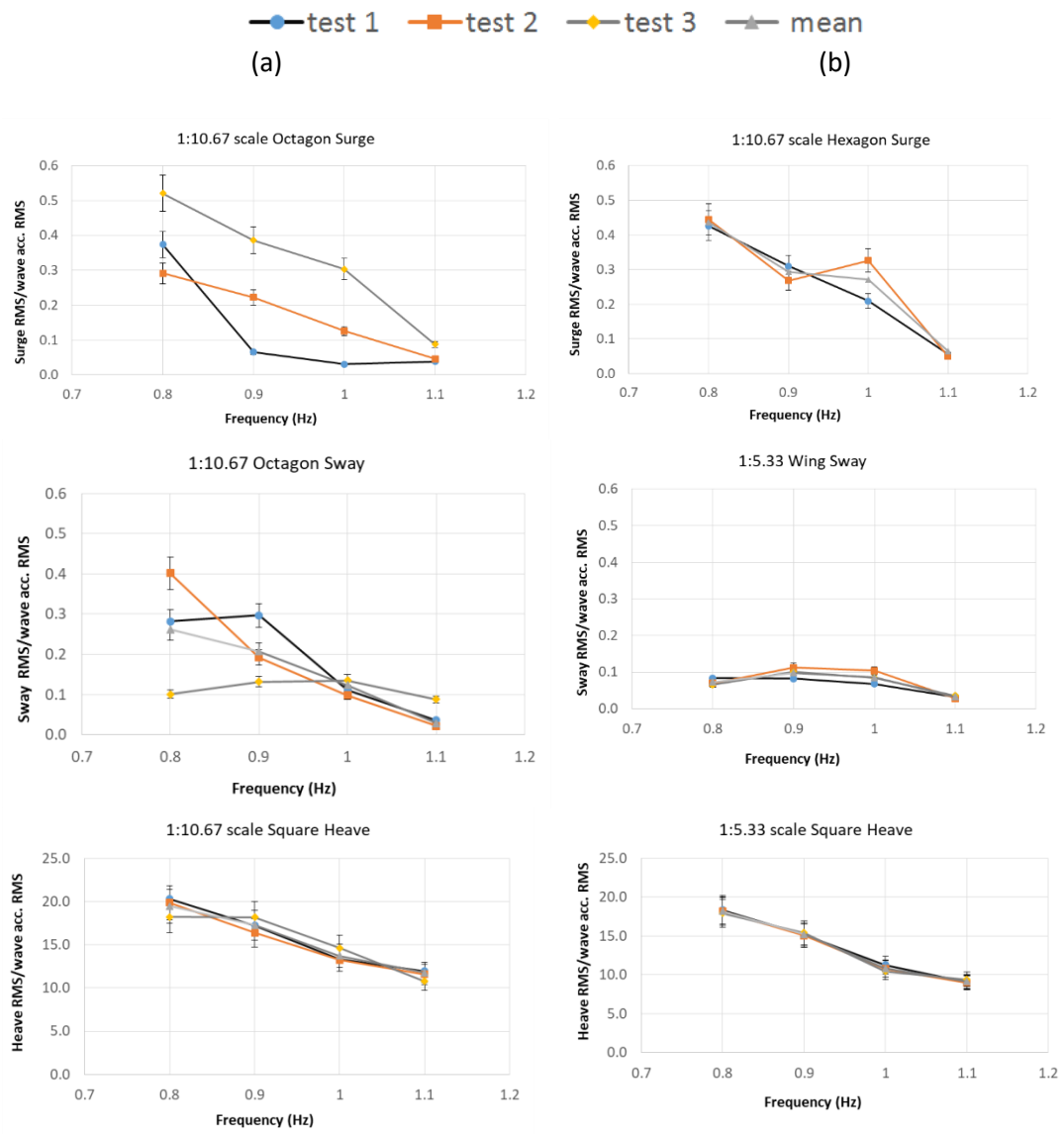

Figure 39: Comparison of translational repeats (a) least and (b) closest repeatability.

Table 17: Mann-Whitney U test results for test repeatability at 1:10.67 scale buoys.
Ticks indicate data passed the Mann-Whitney tests and crosses indicate failure. Highlighted tests are excluded from further data analysis.

	Roll			Pitch			Yaw			Surge			Sway			Heave		
Test	1	2	3	1	2	3	1	2	3	1	2	3	1	2	3	1	2	3
Circle																		
0.8 Hz	×	×	×	✓	✓	✓	✓	✓	×	✓	✓	✓	×	✓	✓	✓	✓	✓
0.9 Hz	✓	✓	✓	✓	✓	✓	×	×	×	✓	×	✓	✓	×	✓	✓	✓	✓
1.0 Hz	✓	✓	✓	✓	✓	✓	✓	✓	×	×	×	×	✓	✓	✓	✓	✓	✓
1.1 Hz	✓	✓	✓	✓	✓	✓	×	✓	✓	×	×	×	×	✓	✓	✓	✓	✓
Octagon																		
0.8 Hz	✓	×	✓	✓	✓	✓	✓	✓	✓	✓	✓	✓	✓	✓	✓	✓	✓	×
0.9 Hz	✓	✓	✓	✓	✓	✓	✓	✓	×	×	×	×	×	×	×	✓	✓	×
1.0 Hz	✓	✓	✓	✓	✓	✓	×	×	×	×	×	×	✓	×	✓	✓	✓	×
1.1 Hz	✓	✓	✓	✓	✓	✓	✓	✓	×	✓	✓	×	✓	×	✓	✓	✓	×
Hexagon																		
0.8 Hz	×	×	×	✓	✓	✓	×	✓	✓	✓	✓	✓	✓	✓	✓	✓	✓	✓
0.9 Hz	✓	✓	✓	✓	✓	✓	×	✓	✓	✓	✓	✓	✓	✓	✓	✓	✓	✓
1.0 Hz	✓	✓	✓	✓	✓	✓	×	✓	✓	✓	✓	✓	✓	✓	✓	✓	✓	✓
1.1 Hz	✓	✓	✓	✓	✓	✓	✓	✓	✓	✓	✓	×	✓	✓	✓	✓	✓	✓
Square																		
0.8 Hz	×	×	×	✓	✓	✓	✓	×	✓	✓	✓	✓	×	✓	✓	✓	✓	✓
0.9 Hz	✓	✓	✓	✓	✓	✓	✓	✓	×	×	×	×	✓	×	✓	✓	✓	✓
1.0 Hz	✓	✓	✓	✓	✓	✓	✓	✓	×	✓	✓	×	✓	×	✓	✓	✓	✓
1.1 Hz	✓	✓	✓	✓	✓	✓	×	✓	✓	×	✓	✓	✓	×	✓	✓	×	✓
Wing																		
0.8 Hz	✓	✓	✓	✓	✓	✓	×	✓	✓	✓	✓	✓	×	✓	✓	✓	✓	✓
0.9 Hz	✓	✓	✓	✓	✓	✓	✓	×	✓	✓	✓	✓	✓	✓	✓	✓	✓	✓
1.0 Hz	✓	✓	✓	✓	✓	✓	✓	✓	✓	✓	✓	✓	✓	✓	✓	✓	✓	✓
1.1 Hz	✓	✓	✓	✓	✓	✓	✓	✓	✓	✓	✓	✓	✓	✓	✓	✓	✓	✓

Table 18: Mann-Whitney U test results for test repeatability at 1:5.33 scale buoys.
Ticks indicate data passed the Mann-Whitney tests and crosses indicate failure. Highlighted tests are excluded from further data analysis.

	Roll			Pitch			Yaw			Surge			Sway			Heave		
Test	1	2	3	1	2	3	1	2	3	1	2	3	1	2	3	1	2	3
Circle																		
0.8 Hz	×	×	×	✓	✓	✓	×	×	×	✓	✓	✓	✓	✓	✓	✓	✓	✓
0.9 Hz	✓	✓	✓	✓	✓	✓	✓	✓	×	×	×	×	✓	×	✓	✓	✓	✓
1.0 Hz	✓	✓	✓	✓	✓	✓	×	✓	✓	✓	✓	✓	✓	✓	✓	✓	✓	✓
1.1 Hz	✓	✓	✓	✓	✓	✓	×	✓	✓	✓	✓	✓	✓	✓	✓	✓	✓	✓
Octagon																		
0.8 Hz	×	×	×	✓	✓	✓	×	×	×	✓	✓	✓	✓	×	✓	✓	✓	✓
0.9 Hz	×	✓	✓	✓	✓	✓	×	×	×	×	✓	✓	×	✓	✓	✓	✓	✓
1.0 Hz	✓	✓	✓	✓	✓	✓	×	✓	✓	✓	✓	✓	✓	✓	✓	✓	✓	✓
1.1 Hz	✓	✓	✓	✓	✓	✓	×	✓	✓	✓	✓	×	✓	✓	✓	✓	✓	✓
Hexagon																		
0.8 Hz	×	×	×	✓	✓	✓	✓	×	✓	✓	✓	✓	✓	✓	×	✓	✓	✓
0.9 Hz	✓	✓	✓	✓	✓	✓	×	×	×	✓	✓	✓	×	✓	✓	✓	✓	✓
1.0 Hz	✓	✓	✓	✓	✓	✓	×	✓	✓	✓	✓	✓	✓	✓	✓	✓	✓	✓
1.1 Hz	✓	✓	✓	✓	✓	✓	✓	✓	×	✓	✓	✓	✓	×	✓	✓	✓	✓
Square																		
0.8 Hz	✓	×	✓	✓	✓	✓	×	×	×	✓	✓	✓	✓	✓	×	✓	✓	✓
0.9 Hz	✓	✓	✓	✓	✓	✓	×	×	×	✓	✓	✓	✓	×	✓	✓	✓	✓
1.0 Hz	✓	✓	✓	✓	✓	✓	✓	✓	×	✓	✓	✓	✓	✓	✓	✓	✓	✓
1.1 Hz	✓	✓	✓	✓	✓	✓	✓	×	✓	✓	✓	✓	✓	✓	✓	✓	✓	✓
Wing																		
0.8 Hz	×	✓	✓	✓	✓	✓	×	✓	✓	✓	✓	✓	✓	✓	✓	✓	✓	✓
0.9 Hz	✓	✓	✓	✓	✓	✓	✓	×	✓	✓	✓	✓	✓	✓	✓	✓	✓	✓
1.0 Hz	✓	✓	✓	✓	✓	✓	✓	✓	✓	✓	✓	✓	✓	✓	✓	✓	✓	✓
1.1 Hz	✓	✓	✓	✓	✓	✓	✓	✓	✓	✓	✓	✓	✓	✓	✓	✓	✓	✓

Table 19: Percentage of tests included in analysis.

Buoy Scale	Roll	Pitch	Yaw	Surge	Sway	Heave
1:10.67	83%	100%	68%	67%	78%	92%
1:5.33	80%	100%	50%	92%	87%	100%

4.4.2 Effect of buoy shape on vessel motion at 1:10.67 scale

The Mann-Whitney statistical tests indicate which of the repeated tests, for each shape at the 1:10.67 scale, did not produce a repeated data set. These tests, which are highlighted in Table 17, are omitted from all the following analysis in order to compare the effect of buoy shape on vessel motion. The roll responses at 0.8Hz wave frequency only proved to be repeatable for two out of the five shapes, but consistently repeated at all other frequencies.

The RAO for each degree of freedom are presented in Figure 40. The three dominant oscillatory motions of pitch, surge and heave exhibit the least difference in motion response when buoy shape is changed however there are differences particularly at the 0.9 and 1.0Hz frequencies. The Wing shape is consistently the lowest for the motions of pitch and heave indicating this shape has the greatest potential to reduce vessel motions at a SPM at this buoy scale. The maximum yaw angles exhibit the largest differences again most prominently at the 0.9 and 1.0Hz frequencies.

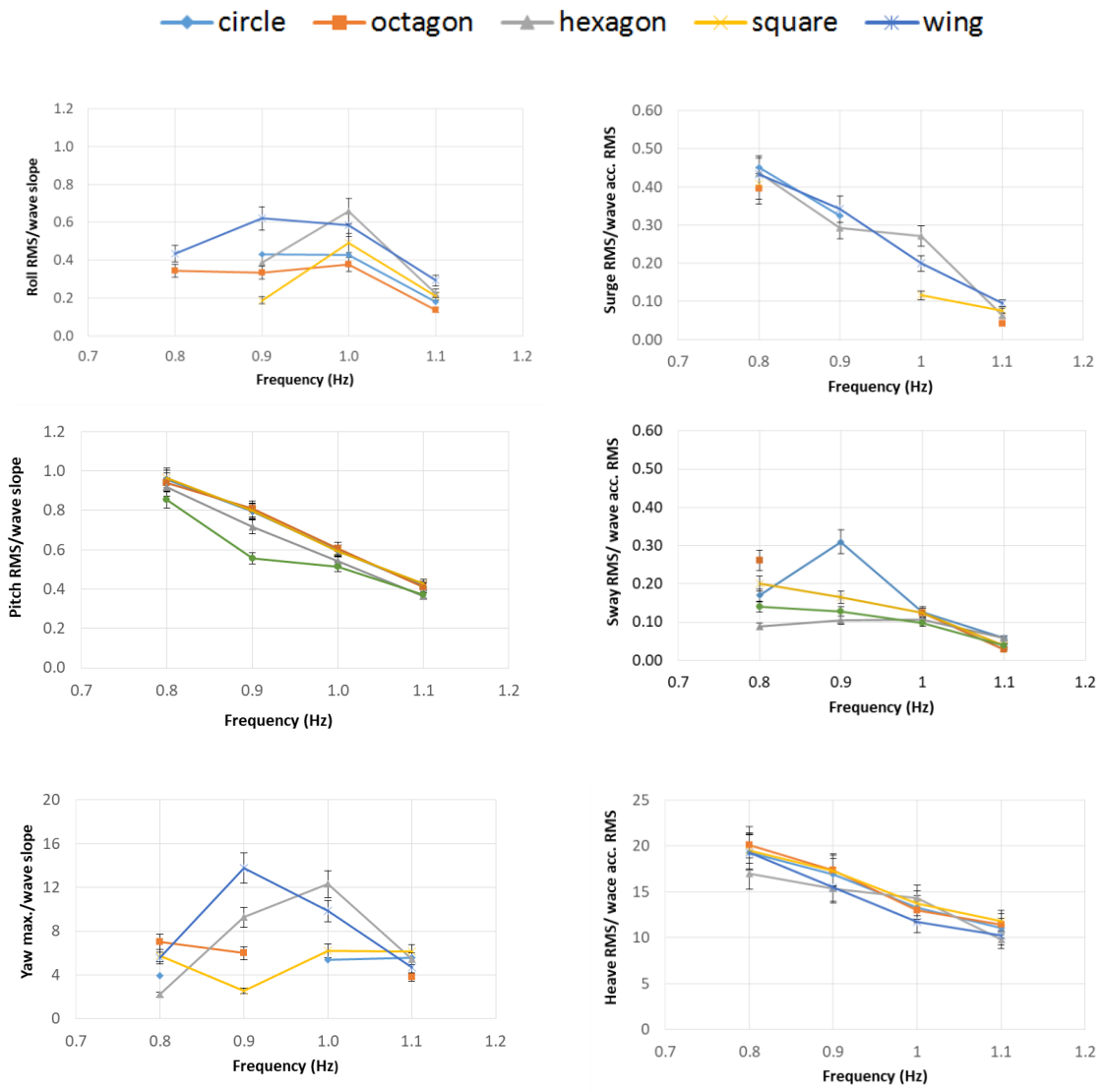

Figure 40: Comparison buoy shapes at 1:10.67 scale (RMS of repeatable tests).

4.4.3 Effect of buoy shape on vessel motion at 1:5.33 scale

The Mann-Whitney statistical tests indicate which of the repeated tests, for each shape at the 1:5.33 scale, did not produce a repeated data set. These tests, which are highlighted in Table 18, are omitted from all the following analysis in order to compare the effect of buoy shape on vessel motion. The roll and max yaw angle responses at 0.8 Hz wave frequency only proved to be repeatable for two out of the five shapes.

The RAO for each degree of freedom are presented in Figure 41. The three dominant oscillatory motions of pitch, surge and heave exhibit the least difference in motion response when buoy shape is changed however there are differences particularly at the 0.9 and 1.0Hz frequencies. The Wing shape once again is consistently the lowest for the motions of pitch and heave and also at this scale for surge. This further indicates this shape has the greatest potential to reduce vessel motions at a SPM. The maximum yaw angles exhibit the largest differences at all but the 1.0 Hz frequency.

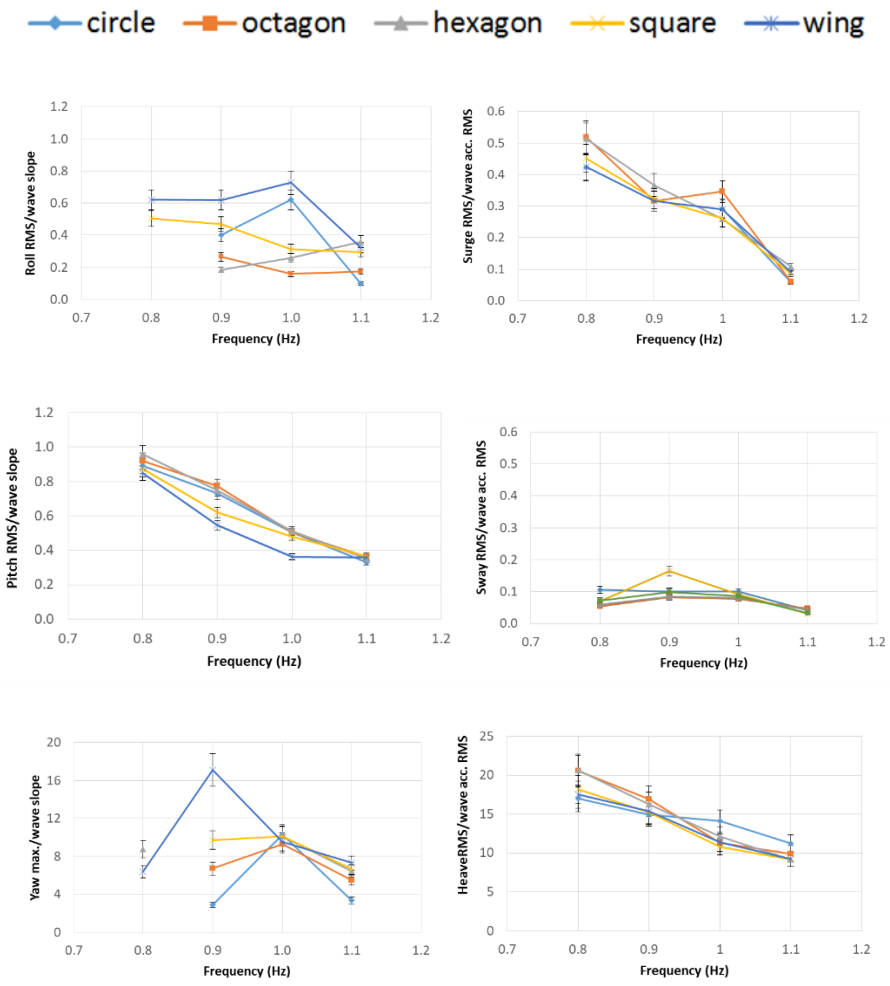

Figure 41: Comparison buoy shapes at 1:5.33 scale (RMS of repeatable tests).

4.4.4 Effect of buoy scale on vessel motion.

In order to investigate if the size of the buoy impacted upon the vessel's motions the repeatable results for the pitch, surge, sway and heave motions were compared. As presented in Sections 4.4.2 and 4.4.3 these motions demonstrated little variability between the buoy shapes tested so the results for all shapes, at the same scale, were consolidated to compare the vessel's motion between the two different sized buoys.

The resultant plots are shown in Figure 42 and percentage difference from the smaller scale are presented in Figure 43. The sway RAO exhibited the largest differences across all wave frequencies, resulting in reduced values when the larger scale buoy was used, the percentage difference decreasing with increasing wave frequency, from 53% at 0.8Hz to 1% at 1.1Hz. Surge was the only motions where tests using the larger 1:5.33 scale buoys resulted in higher RAO values, the highest difference at the 1.0Hz wave frequency.

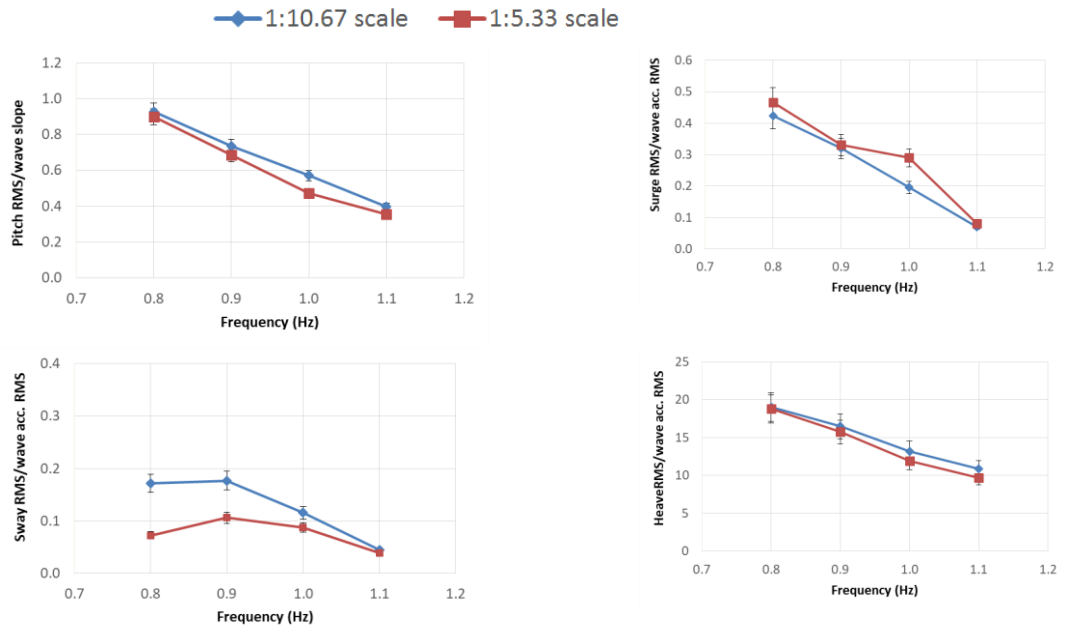

Figure 42: Comparison of vessel motions using 1:10.67 and 1:5.33 scale buoys.

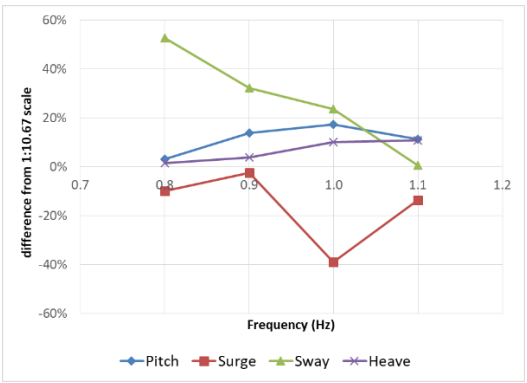

Figure 43: Percentage difference in RAO for pitch angle and surge, sway and heave accelerations.

Boxplots of the full recorded dataset of the vessel's pitch angles and translational accelerations were used to compare the effect on the vessel's motion of the 1:10.67 against the 1:5.33 scale hexagonal buoys, as presented in Figure 44. For each plot the black box is the scale buoy and the blue box the twice scale buoy for each of the tested wave frequencies of 0.8, 0.9, 1.0 and 1.1Hz. These highlight the fact that there are very few outlier measurements compared to the testing in the flume as shown in Figure 27 and Figure 28.

The pitch angle and surge acceleration plots showed no significant difference between the buoy scales as indicated by the size of the boxes at each frequency. For both sized buoys the range of pitch angles stayed constant but the range of surge accelerations reduced as the wave frequency was increased as indicated by the reduction in box size.

The range of sway accelerations for the lowest (0.8Hz) and highest (1.1Hz) wave frequencies for the larger 1:5.33 scale buoy showed a significant reduction compared to the smaller buoy. Finally the heave accelerations had a significantly different range distribution over all frequencies as shown in Figure 44. Upon investigation this reduction in heave acceleration, using the larger buoy, was recorded for all the other four shapes as illustrated in Figure 45.

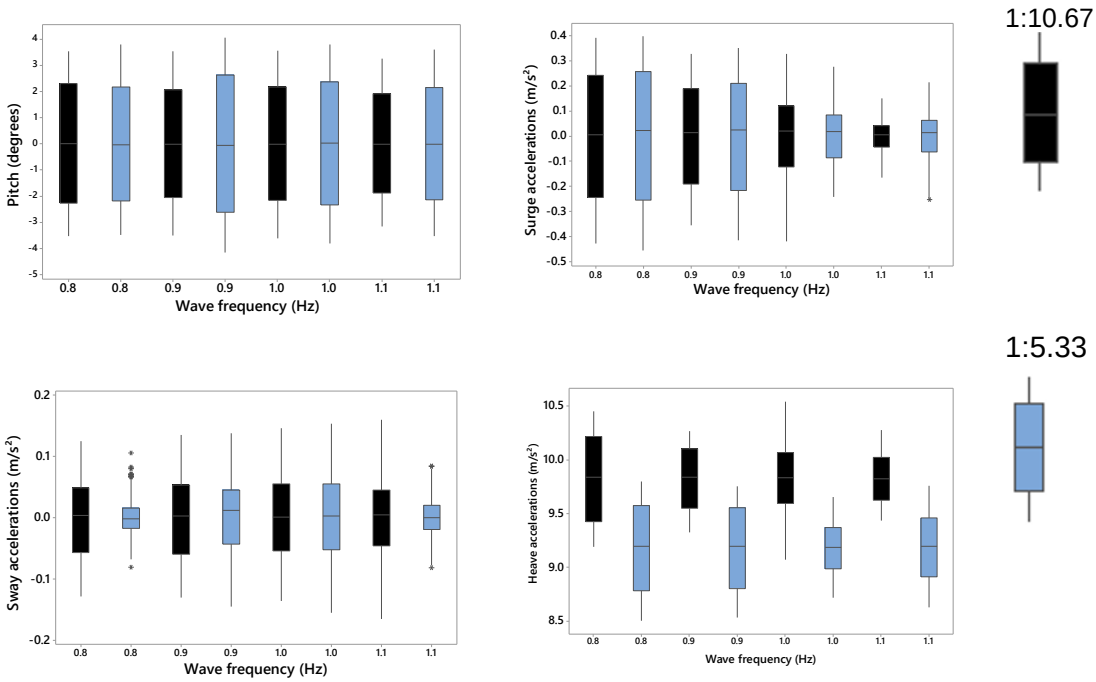

Figure 44: Boxplots of vessel pitch, surge, sway and heave using 1:10.67 scale and 1:5.33 scale hexagonal buoys.

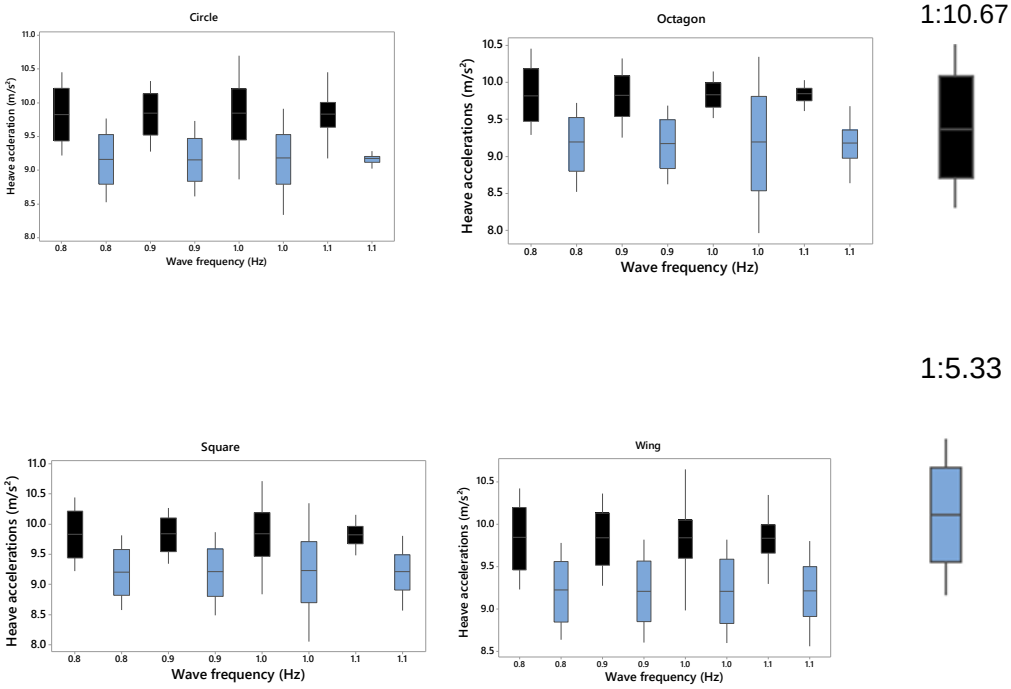

Figure 45: Boxplots of vessel heave accelerations.

4.4.5 Coupled vessel motions

In order to find if there were any coupled relationships between the five oscillatory motions, as recorded by the Xsens on the vessel, each combination of scatter plots was plotted using the translational acceleration (m/s^2) and rotational angle (°) data. The resultant plots, an example of which is shown in Figure 47, indicated a linear relationship between surge and pitch. To quantify the strength of this linear relationship the linear correlation coefficients were calculated and plotted as shown in Figure 47. At the 0.8 and 0.9Hz wave frequencies this linear correlation held for all buoy shapes and buoy scales, the drop in the value of the linear correlation coefficient at the 1.0Hz wave frequency and still further at 1.1Hz indicated that this linear relationship between the vessel's surge and pitch motions no longer held.

The scatter plots also highlighted a phase relationship between the surge and heave accelerations and the heave accelerations and pitch angle for all tests, at the 0.8Hz wave frequency. The tightly banded circular phase relationships held for all shapes at both scales at the 0.8 and 0.9Hz wave frequencies. However the relationship had begun to break down at 1.0Hz and had deteriorated still further at 1.1Hz. An example of the plots for the 1:10.67 and 1:5.33 scale square buoys is presented in Figure 49. This plot further highlights the reduced values of heave acceleration when the 1:5.33 scale buoys replaced the 1:10.67 scale ones as shown in the boxplots in Figure 45. The time series plots, an example of which is presented in Figure 49, also demonstrates this relationship highlighting the similar signal frequencies and the highest peak in heave accelerations coinciding with the lowest pitch angle and vice versa (within 0.3s).

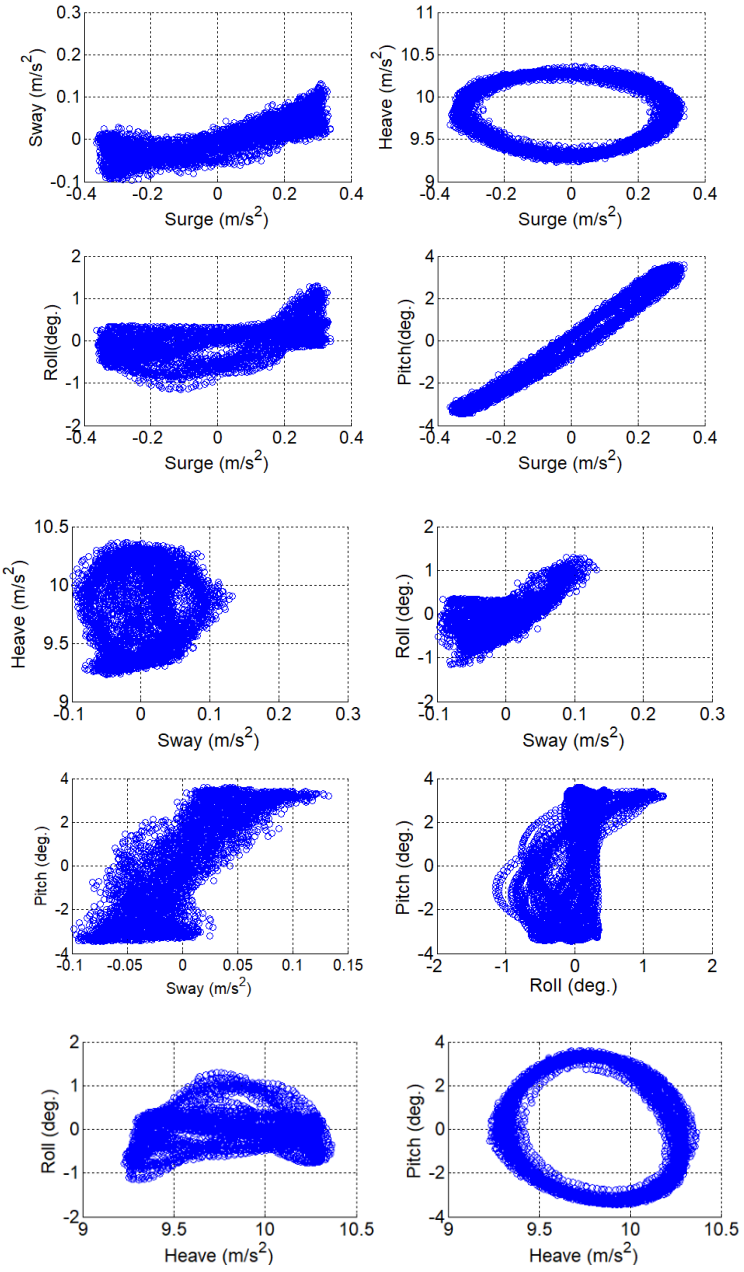

Figure 46: Coupled motions for 1:10.67 scale circular buoy at 0.8Hz (test55).

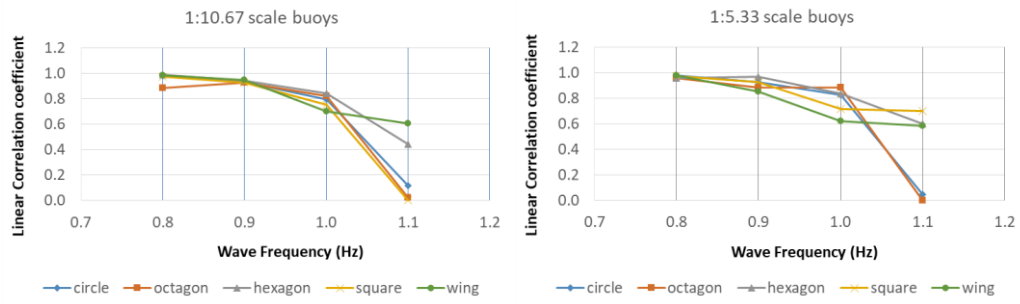

Figure 47: Linear correlation coefficients between surge and pitch motions.

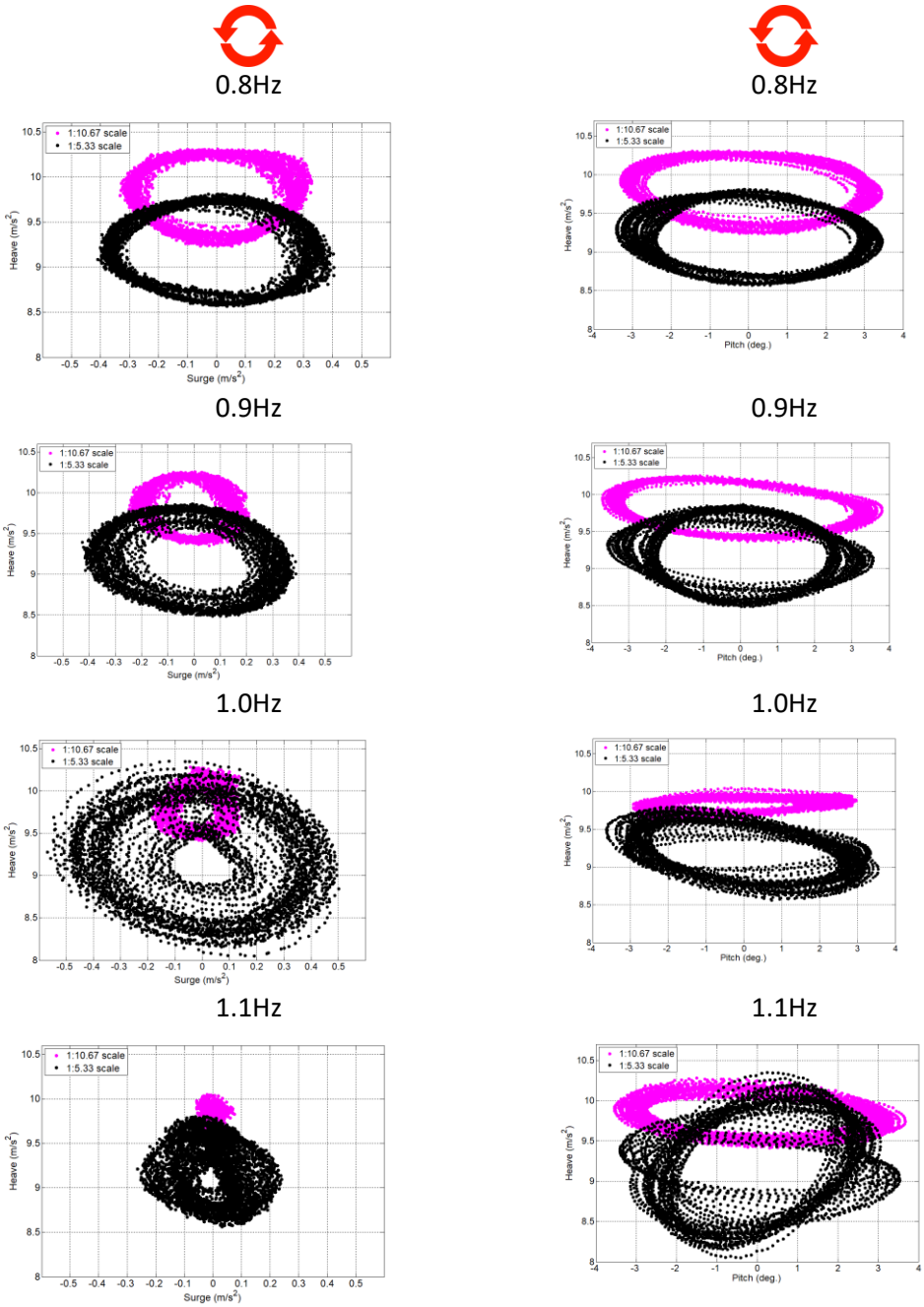

Figure 48: Surge-heave and heave-pitch relationships for 1:10.67 square shaped buoy. Red arrows indicate the anti-clockwise direction of travel.

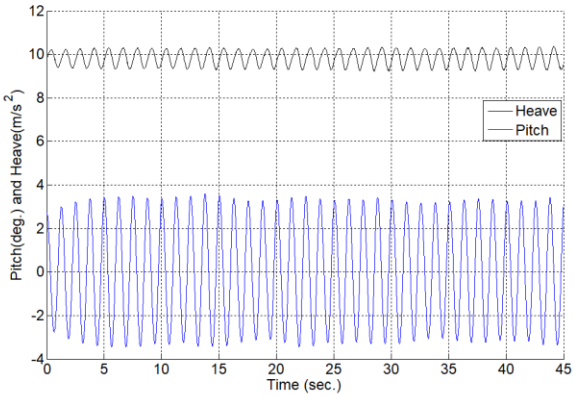

Figure 49: Heave and pitch time series, test 55 scale circular buoy at 0.8Hz.

4.4.6 Effect of buoy size on catenary riser extension

During the regular wave tests it was noted that as the wave frequency increased the buoy and model lifeboat were moving further down the tank as the catenary riser lengthened its scope, as illustrated by the schematic and underwater photograph in Figure 50a. To quantify this observation and so as not to have to run cables from the buoy the methodology using the Matlab algorithm and video capture described and verified in Chapter 3 was used.

The code, as described in Section 3.2.3, was used to locate the centroid of the buoy from the above tank video and from this its surge excursions (m) up the tank were calculated. The signal noise was removed by the implementation of a 10th order Butterworth filter set to a low pass frequency cut-off of 3Hz. A pixel factor, taken from a still image, was used to convert pixel values to distance moved down the tank in metres. This was done for all tests that had a complete image of the buoy at the start and end of the test and the maximum distance the buoy travelled from its starting position is given in Table 20. Once more there was little difference when comparing shapes with the lowest STD of 0.06m (mean 0.76m) and the highest STD of 0.19m (mean of 0.5m) as detailed in Table 20.

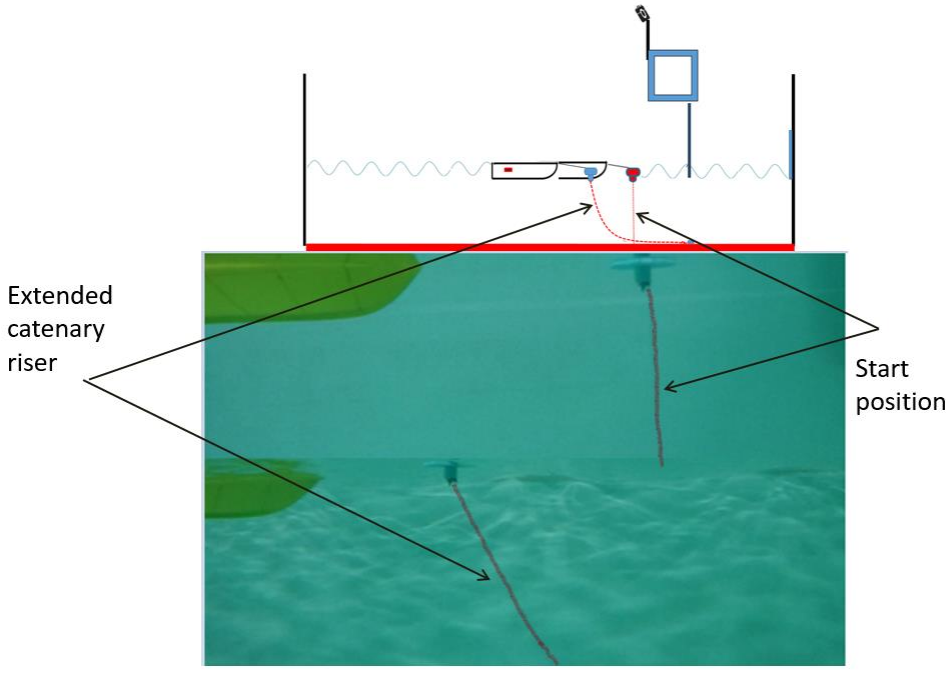

Figure 50: Schematic and underwater photograph of extended catenary mooring riser.

Table 20: Maximum surge excursion (m) of buoys.

	Wave Frequency (Hz)					Wave Frequency (Hz)			
1:10.67 Shape	**0.8**	**0.9**	**1.0**	**1.1**	**1:5.33 Shape**	**0.8**	**0.9**	**1.0**	**1.1**
circle	0.14	0.25	0.73	0.89	circle	0.51	0.58	0.71	
circle	0.22	0.63	0.92	0.78	circle	0.50	0.60	0.65	
circle	0.49		0.69	0.82	circle	0.50	0.76	0.71	
octagon	0.39	0.60	0.69	0.77	hexagon	0.47	0.72		0.81
hexagon	0.58	0.53	0.81	0.86	hexagon	0.56	0.72	0.75	0.78
hexagon		0.52	0.69	0.76	hexagon	0.59		0.80	0.93
hexagon			0.76	0.90	square	0.48	0.52	0.79	0.87
square			0.75	1.11	square	0.53	0.61	0.81	0.84
square	0.56	0.88	0.90	1.02	square	0.40	0.65	0.72	
square	0.52	0.51	0.66	0.84	wing	0.35	0.63	0.79	0.99
					wing	0.32	0.65	0.82	0.99
					wing	0.61	0.64	0.86	0.98
mean	0.41	0.56	0.76	0.88	mean	0.50	0.64	0.76	0.90
STD	0.17	0.19	0.09	0.11	STD	0.07	0.07	0.06	0.08

Plotting the mean of the maximum excursions (averaged over the five shapes for each buoy scale) against the four wave frequencies highlights that there is a very strong linear relationship as illustrated in Figure 51. The linear regression coefficient for the 1:10.67 scale is 0.9905 and for the 1:5.33 scale is 0.9992. The mean actual distance travelled, when comparing the two different sized buoys, converges as the wave frequency increases. The difference, compared to the smaller scale, starting at 22% at 0.8Hz and falling to 2% at 1.1Hz wave frequency. The data verified the observation that, as the wave frequency increased, the catenary shape lengthened and the model lifeboat moved further down the tank. Furthermore, for the tested frequencies, the maximum surge excursion of the buoy can be predicted from the wave frequency using the identified linear relationship.

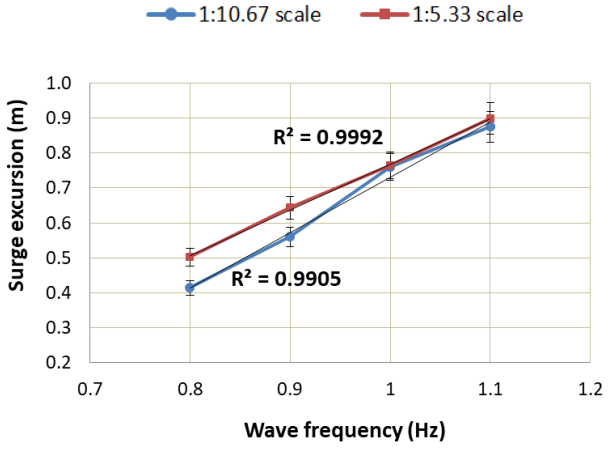

Figure 51: Mean maximum surge excursion of the buoys averaged over all shapes.

4.5 Discussion

A series of free standing SPM model tests investigating the effects of buoy shape and buoy size on vessel motions, in regular waves, have been conducted. The experimental setup enabled the unrestricted motion of the mooring buoy and model lifeboat to be observed and the motion tracking algorithm developed for the flume experiments was successfully deployed in this experimental setup. Additionally the mooring riser was able to change its scope, by extending its catenary shape, as the wave frequencies were increased.

Time domain plots of the motions show that the dominant oscillatory rotational motion of the model was pitch and translational motions were surge and heave as a result of the mooring riser chain and hawser providing a restraining mechanism against the oncoming regular waves. All motions, except for the yaw, exhibited steady state oscillatory motion at the same frequency as the regular waves. During each test the model would yaw in line with the predictions of Wehausen (1979) and Schellin (2003) who state that a freely floating elongated body will slowly drift in the direction of wave propagation and turn broadside to the waves thereby reducing the load in the mooring hawser compared to that if the heading was constrained.

In all cases the RAO of the vessel for surge, pitch, sway and heave are at their lowest value at the 1.1Hz wave frequency where the wavelength is now shorter than the LOA of the model (1.29m compared to 1.50m). This is in keeping with theory (Lloyd, 1989), namely that, as a result in the changes in buoyancy forces, a restrained ship “only experiences significant excitations in head waves when they are longer than about three quarters of the ship length.” The three cases of buoyancy changes due to wavelength are illustrated in Figure 52. For the experiments presented here three quarters of the model’s length is 1.13m which equates to a wave frequency of 1.17Hz.

This highlights a significant difference between the expected motion responses of lifeboats and offshore tankers stationed at SPMs in the same wave spectra. For example at a 1:10.67 scale three quarters of the LOA of a 175m tanker would be 12.3m which implies that significant motion responses would only occur for wave frequencies less than 0.36Hz. The two points from which significant motion responses for the two types of vessel is shown in Figure 53. The purpose of duplicating environmental conditions experienced by offshore structures at model scale is to be able “to reproduce the responses that the structure will experience when placed in operation in the offshore site” (Chakrabarti, 2005). The majority of offshore locations, where moorings operate,

have wave periods within the range of 4 to 10s (0.1 to 0.25Hz) and heights less than 2m (Halliwell and Harris, 1988). The wave periods and heights tested for offshore SPM will not be those corresponding to the LOA of lifeboats or the waves at the coastal harbour locations of RNLI SPM which are detailed in Appendix B. The results of both experimental and computer simulations conducted using large vessels must therefore be adjusted to take account of the wavelength to vessel ratio and these experimental investigations work towards providing some insight into the previously investigated motions of vessels less than 20m in length at SPM in coastal harbour wave conditions.

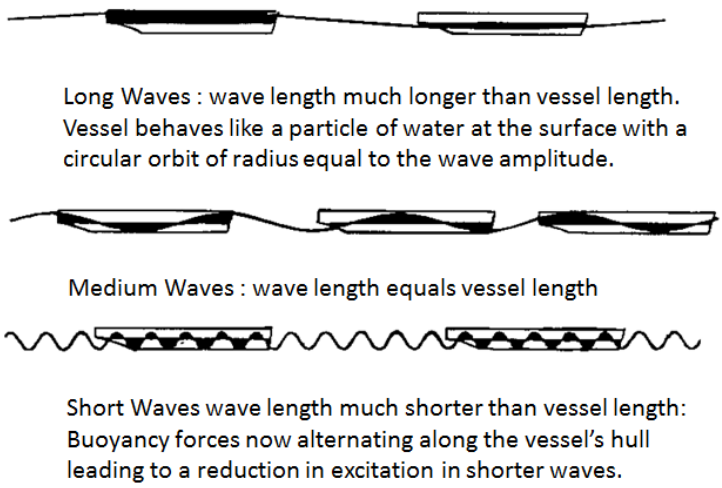

Figure 52: Buoyancy forces on a restrained ship in regular head waves, adapted from (Lloyd, 1989).

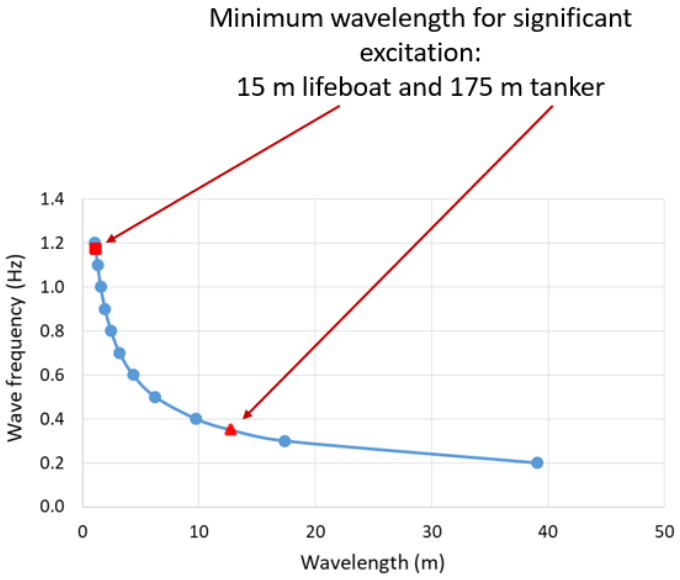

Figure 53: Minimum wavelength for significant excitation at 1:10.67 scale.

One significant contribution that these investigations showed was that increasing the wavelength to longer than the LOA of the model (wave frequencies of 1.0 and 1.1Hz) led to a breakdown of the coupling between the three pairs of motions. Namely the surge and pitch were no longer linearly correlated and the 90° out of phase relationship between surge-heave and heave-pitch broke down. In addition the results showed that the maximum surge excursion of the buoy increased linearly, for both scales, as the wave frequency was increased enabling the determination of the maximum surge from the wave frequency, and vice versa, in an engineering analysis of a lifeboat at a SPM in regular waves.

Changing the shape of the buoy, at the 1:10.67 and the 1:5.33 scale, did not result in any significant change in the model's motions but there were some trends such as the wing shape having the consistently lowest vales for some of the motions. It is therefore hypothesized that the differences in the wave patterns that were radiated from the different shapes were not significant enough to impact upon the vessel's motions at these scales. However there is the potential for further investigations at larger scale and/or more pronounced buoy shapes using the finders of wave energy converter research such as that of Hager et al., (2012), Bouali and Larbi (2013), McCabe (2013) and Goggins and Finnegan (2014) which is described in Section 2.4.

When comparing the maximum surge excursion down the tank there was not a significant difference between the buoy shapes. However, at the 0.8 and 0.9Hz wave frequencies, the larger buoys moved further down the tank, compared to the smaller ones, as the mooring riser lifted further from the tank floor. This additional suspended line weight in the water, as the scope is increased, will increase the load putting additional strain on the SPM.

Results indicate that doubling the buoy scale resulted in lower pitch, slower sway and heave RAO but faster surge RAO. In order to quantify this the percentage increase/decrease in translational accelerations were applied to the mean of the RMS of the 1:10.67 scale buoys, at each wave frequency. An overall RMS reduction was calculated for 0.8, 0.9, 1.1Hz wave frequencies and an increase at the 1.0Hz wave frequency as detailed in Table 21. Added to the fact that the pitch angle decreased for each wave frequency tested indicate that increasing the size of the buoy could lead to an overall reduction in vessel accelerations at a SPM.

Table 21: Changes in translational accelerations when comparing 1:5.33 scale buoy compared to 1:10.67 scale buoys.

	Wave Frequency (Hz)			
	0.8	**0.9**	**1.0**	**1.1**
Surge increased accelerations (m/s^2)	0.0221	0.0061	0.0741	0.0102
Sway decreased accelerations (m/s^2)	(0.0471)	(0.0342)	(0.0199)	(0.0045)
Heave decreased accelerations (m/s^2)	(0.0038)	(0.0154)	(0.0298)	(0.0186)
Total increased/(decreased) accelerations (m/s^2)	(0.0288)	(0.0436)	0.0244	(0.0129)

Boxplots highlighted that the heave accelerations significantly decreased using larger buoys. The accelerations, measured at the model's centre of gravity, are presented relative to its resting position. A possible explanation for the recorded heave reduction is the angle of the IMU on the model. If the larger heavier buoys, coupled with the longer hawser length, were pulling the bow downwards the Xsens IMU would no longer be on a horizontally flat plane and therefore the gravitational accelerations would be less than 9.81m/s^2. Taking the example of the octagon, as illustrated in the boxplots in Figure 44, the RMS of heave accelerations is 9.17m/s^2 for the 0.8, 0.9, 1.0Hz wave frequencies and 9.18m/s^2 for the 1.1Hz which implies that the Xsens was at an angle of 21°. To test this hypothesis the Xsens was positioned statically at an angle of 21° and acceleration data recorded for a 45s duration. The RMS of the heave acceleration recorded was 9.17m/s^2.

A limitation of these experiments was that the resultant motions of the model lifeboat were sensitive to its initial orientation. The larger 1:5.33 scale buoys produced a higher percentage of a complete set of three repeated tests at 71% compared to the figure of 62% for the smaller 1:10.67 scale buoys. Additionally, due to the dimensions of the tank, the length of available data recording was restricted to 45s, however with the expected response frequency equal to the wave frequencies tested this should provide sufficient detail to compare the effect of buoy shape and buoy size on the motions of the model lifeboat. Furthermore due to the non-repeatability of the roll and yaw results comparison of the effect of buoy size and buoy shape was not possible for these motions.

4.6 Summary

The stiffness and damping characteristics of a catenary mooring line are affected by a multitude of intrinsic factors such as: its material composition, diameter and length relative to water depth as well as the external factors of wind, wave and current (Chakrabarti, 2005). The investigations presented here were performed in order to evaluate if the size and shape of the mooring buoy also had an impact. The wave height was kept constant and four wave frequencies were tested in equal steps of 0.1Hz from 0.8 to 1.1Hz. Initially the experimental set up included a load cell to measure the hawser tension however both the cabling from the device and its own weight had too great an impact upon the motions of the model lifeboat and so it was removed (details are included in Appendix C.2).

Motion data were recorded using both an Xsens and video capture. Plots comparing the integrated velocity data with the Xsens algorithm for angular motions showed there was close agreement but with the drift between the two increasing over time particularly in yaw, as shown in Figure 35.

Results from the analysed motion data show:

- Time domain plots show that the dominant oscillatory rotational motion of the model was pitch and translational motions were surge and heave as a result of the mooring riser chain and hawser providing a restraining mechanism against the oncoming regular waves (Figure 37)
- All motions, except for the yaw, exhibited steady state oscillatory motion at the same frequency as the regular waves. Pitch, sway and heave showed the highest degree of repeatability. Comparing the different shapes, at both scales, the octagon showed the least repeatability and the wing the most consistent (Table 17 and Table 18).
- Changing the shape of the buoy, at the 1:10.67 and the 1:5.33 scale, did not result in any significant change in the model's motions but there were some trends such as the wing shape having the consistently lowest vales for some of the motions (Figure 40 and Figure 41).
- In all cases the RAO of the vessel for surge, pitch, sway and heave are at their lowest value at the 1.1Hz wave frequency where the wavelength is now shorter than the LOA of the model (1.29m compared to 1.50m), (Figure 42).

- Boxplots highlighted that the heave accelerations significantly decreased using larger buoys Figure 45.

- Increasing the wavelength to longer than the LOA of the model (wave frequencies of 1.0 and 1.1Hz) led to a breakdown of the coupling between surge-pitch, surge-heave and heave-pitch, Figure 47 and Figure 48.

- When comparing the maximum surge excursion down the tank there was not a significant difference between the buoy shapes. However, at the 0.8 and 0.9Hz wave frequencies, the larger buoys moved further down the tank, compared to the smaller ones, as the mooring riser lifted further from the tank floor (Figure 51).

- Results indicate that doubling the buoy scale resulted in lower pitch, slower sway and heave RAO but faster surge RAO. An overall RMS reduction was calculated for 0.8, 0.9, 1.1Hz wave frequencies and an increase at the 1.0Hz wave frequency (Table 26) indicating that increasing the size of the buoy could lead to an overall reduction in vessel accelerations at a SPM.

Chapter 5: YARMOUTH HARBOUR IN SITU DATA AQUISTION

> "Sea trials do, however, offer the definitive method of verifying theoretical calculations or predictions based on model experiments." (Lloyd, 1989).

The recorded motions of an in-situ lifeboat, at a single point mooring in Yarmouth Harbour, are presented in this Chapter. Section 5.1 provides an introduction to full scale data acquisition, the location and vessel description are outlined in Section 5.2 together with data acquisition equipment and procedures. Sections 5.3, 5.4 and 5.5 present the date acquired discussion and summary respectively.

5.1 Introduction

Data recording at full scale overcomes the limitation of model testing including: scale effects whereby it is impossible to scale all relevant variables, e.g. larger viscous forces on a small scale model leads to difference in prototype and model response and laboratory effects which require approximations such as wave spectra (Hughes, 2005). Full scale data also provides the necessary verification of the results of model experiments and computer simulations. The RNLI currently has no data on the motions of its lifeboats at SPM and the objectives of the data recording presented here were to establish the full scale motions of a lifeboat and SPM buoy, validate a GPS tracking device that records pitch and yaw and test the Matlab motion tracking algorithm in a sea trial setting.

5.2 Experimental methodology

5.2.1 Test site

The sea trials took place on Monday 23rd May 2016 at Yarmouth Harbour on the west coast of the Isle of Wight the latitudinal and longitudinal co-ordinates of which are 52°42.32.32N and 1°30.12.98W. There are 8 outer SPM, at a water depth of 1.8m relative to Chart Datum, situated north of the harbour breakwater. Each mooring is 38m apart with a 15.5m mooring chain riser as illustrated in the schematic in Figure 54.

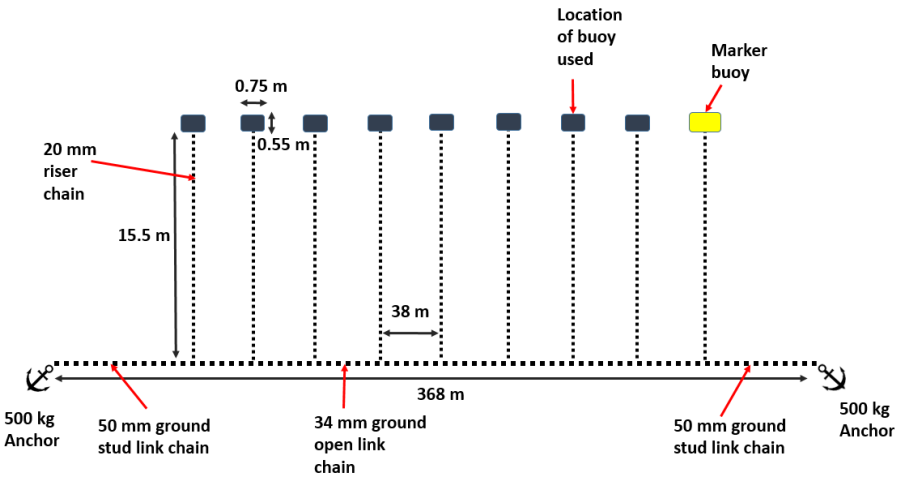

Figure 54: Schematic of Yarmouth Harbour's 'North Trot' SPM.

5.2.2 Mersey class lifeboat

Due to operational reasons the RNLI were unable to permit any data recording on one of their lifeboats but an alternative privately owned vessel was made available by Needles Pleasure Cruises Ltd. The Mersey Rose is an aluminium hull Mersey Class lifeboat, originally known as *Peggy and Alex Caird*, built in 1988 which was in active service until 1995 and was then part of the relief RNLI fleet until her sale to Needles Pleasure Cruises on 8th July 2015. A photograph of the Mersey Rose stationed at the SPM during the data collection is presented in Figure 55 and the full-scale particulars detailed in Table 22.

The Mersey Rose was moored to an in-situ buoy, belonging to the Yarmouth Harbour. Their buoys are cylindrical in shape, foam filled with an elastomer coating, with a diameter of 0.75m and a height of 0.55m.

Figure 55: The Mersey Rose at Yarmouth Harbour on 23rd May 2016.

Table 22: Full scale particulars of the Mersey Rose.

Particular		**Particular**	
Length overall (m)	11.587	Displacement (tonnes)	14.510
Length design waterline (m)	10.550	Vertical centre of gravity (m)	1.23
Beam moulded (m)	3.864	Horizontal centre of gravity (m)	-0.61
Draught moulded (m)	1.820		

5.2.3 Data acquisition

Data of the motions of the lifeboat and buoy were recorded along with the environmental parameters of wind velocity and current flow. A reading of peak hawser load was also taken and is detailed in Appendix C.3.

The 6 degree of freedom motions of the Mersey Rose were recorded using an Xsens M Ti-G-710 inertial motion unit (IMU). The sample rate was set at 100 Hz and the unit placed on inside deck at its estimated longitudinal centre gravity (0.61m aft of midships) as depicted Figure 56. The rotational and translational accelerations of the buoy were made using an Xsens MTi 10-series set at 400Hz and placed at its estimated vertical centre of gravity. Additionally a Microsoft Lumia camera phone, set at 25Hz, was used to record 20s of buoy motion in order to test the Matlab algorithm previously used in the flume and wave tank.

The latitudinal and longitudinal co-ordinates, heading of the vessel (°) and pitch angles (°) of the lifeboat were measured using a VBOX 3i Dual Antenna (VB3iSL) Global Positioning System (GPS) logging system. In addition to GPS the VB3iSL tracks the Russian GLONASS range of satellites thereby maintaining a robust satellite connection and increasing the accuracy of the system. The VB3iSL measures the azimuth and elevation between the antennas, i.e. the direction the antennas are pointing and the angle between them measured from the horizontal. The unit was set at a sample frequency of 100 Hz and data were recorded onto a SD (secure digital) card. The GPS antennas were placed 1.8 m apart on the roof of the lifeboat's wheelhouse as depicted in Figure 56. The elevation mask was set to 30°, to improve GPS signal quality when nearby obstacles such as trees and buildings reflect or temporarily obscure the signal from satellites. As no on-board power was available during the data recording the VB3iSL was powered by a HQ 12V 7.2Ah Universal Sealed Rechargeable Lead Acid Battery via a female 12v cigarette socket.

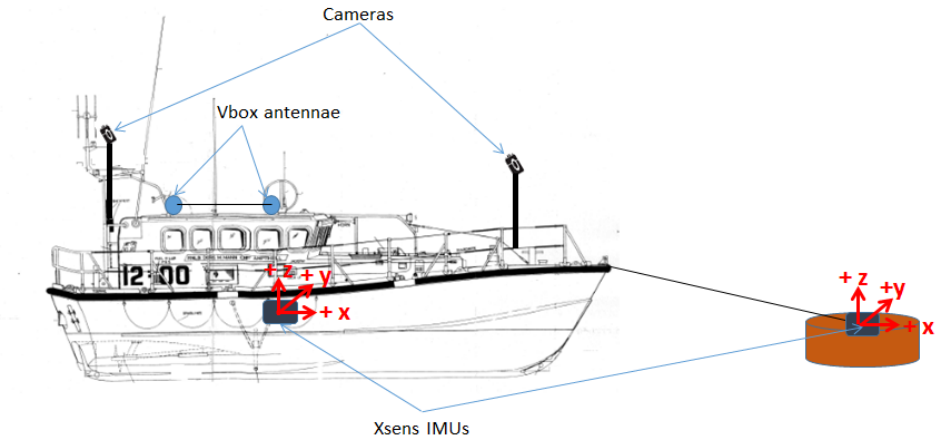

Figure 56: Schematic of in-situ data recording.

Two Go-pro cameras were used; the first was placed at the bow overlooking the buoy and set to take a photograph every 2s and the second was set to video record and attached to the rigging above the ship's wheel with a view across the wheelhouse. The location of the cameras is depicted in the schematic in Figure 56.

The current flow was measured using a Valeport Model 801 Electromagnetic Flow Meter. The meter measures the flow twice every second, and calculates the real time flow every second as the average of the half second readings. The average speeds (m/s) are computed as the average of the one second real time values over the averaging period which was set at 60s; the standard deviation (STD) is also calculated. The flow was measured using the Valeport 801 held at arm's length over the stern of the vessel.

The recorded wind speed and direction were downloaded from the website 'weatherfile.com' for which an administrative login was provided by Richard Paul Russell Ltd. Data are uploaded from their weather station located on Yarmouth Pier (Latitude 50.750845, Longitude -1.529369) for sample lengths of 10 minutes and at a logging rate of 1Hz. Additionally wind speed and direction readings were taken using a handheld N96GY Weather Station which has a touch screen weather station (WH1080PC), base station receiver, transmitter unit, wind direction sensor, wind speed sensor and rain gauge.

A summary of the acquired data is presented in Table 23 along with the location of the device on-board, on the buoy or based upon the shore.

Table 23 : Data acquired at Yarmouth Harbour SPM.

Data acquired	Device	Location
Vessel accelerations and angles	Xsens 710-series	Vessel (longitudinal centre of gravity)
Vessel yaw angle	VBOX3i 100Hz Data Logger	On roof of wheelhouse
Buoy accelerations	Xsens 10-series	Buoy (longitudinal centre of gravity)
Current flow speed	Valeport 801 Flow Meter	Held overside
Wind speed	(Weatherfile, 2017) https://weatherfile.com/?loc_id=GBR00003	Yarmouth Pier
Air Temperature, wind speed and direction	N96GY Weather station	On shore.
Video capture	Two GoPro Hero cameras	Bow, Stern
Hawser load	Telemetry Load Shackle	Hawser between boat and buoy

5.3 Results

Data recording took place aboard the Mersey Rose, a Mersey class lifeboat, moored at Yarmouth Harbour on Monday 23rd May 2016 commencing at 10:24 and ending at 12:07 British Summer Time (BST).

5.3.1 Environmental conditions

A low tide of 1.0m was due at 04:52 followed by a high tide of 2.9m at 11:31 returning to a 1.0m low at 17:08. Cloud cover moved from 2 oktas at the start to 7 oktas at the end of the data recording. Observed wave heights were estimated to be less than 0.15m. There was no rain and the measured temperature inside the boat was 21.4 ° and at harbour side was 19.4 °.

The lowest, average and highest wind speed recorded at Yarmouth pier is presented in Figure 57. The lowest speed of 0.70m/s was recorded during the ten minute interval ending at 10:10 and the highest of 7.82m/s at 10:40. The wind direction blew from a north-westerly to northerly direction varying from a maximum of 316° at 10:30 to a minimum of 6° at 11:30. The speeds measured using the N96GY Weather Station at the Yarmouth Harbour Commission Offices on the harbourside are detailed in Table 24.

The current flow readings at the stern of the Mersey Rose that were taken at 10:15 and at 12:40 are presented in Table 25.

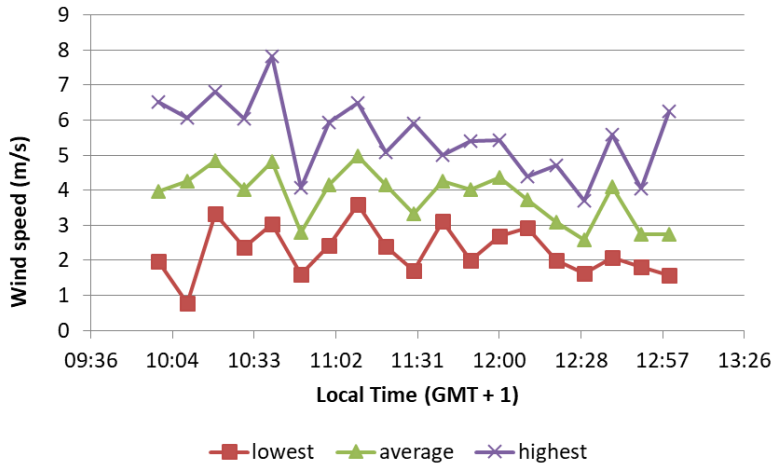

Figure 57: Wind speed recorded at Yarmouth pier on 23rd May 2016.

Table 24: Recorded wind speed at Yarmouth harbourside

Time	Direction	Speed (m/s)
12:04	N	6.1
12:05	N	8.6
12:06	N	7.2
12:07	NE	7.2
12:08	N	5.0

Table 25: Current flow readings in Yarmouth Harbour on 23rd May 2016.

Time (BST)	Mean flow (m/s)	Standard deviation (m/s)
10:15	0.078	0.202
10:19	0.058	0.258
12:40	0.831	0.057
12:44	0.861	0.053

5.3.2 GPS location of the lifeboat

The GPS co-ordinates of the lifeboat were recorded, by the Vbox, for 6,180s (1 hour 43 minutes) starting at 10:24 and ending at 12:07. The path of the vessel is presented in Figure 58a. The vessel's heading is presented in Figure 58b showing a starting position at 315°and ending at a heading of 35° equating to an 80° turn. A visual representation of the vessel's orientation is provided by the photographs presented in Figure 58c.

(a)

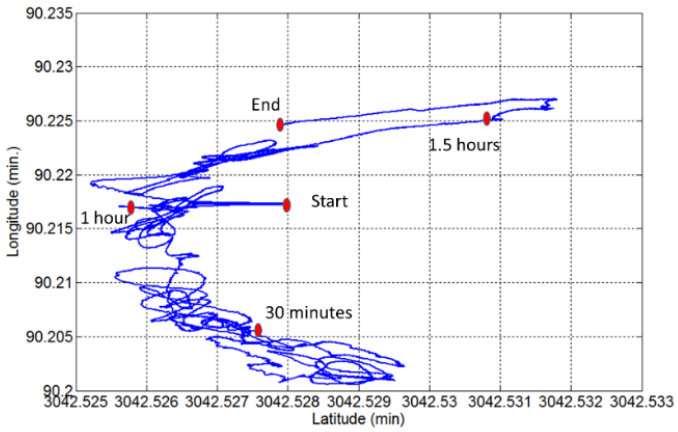

(b)

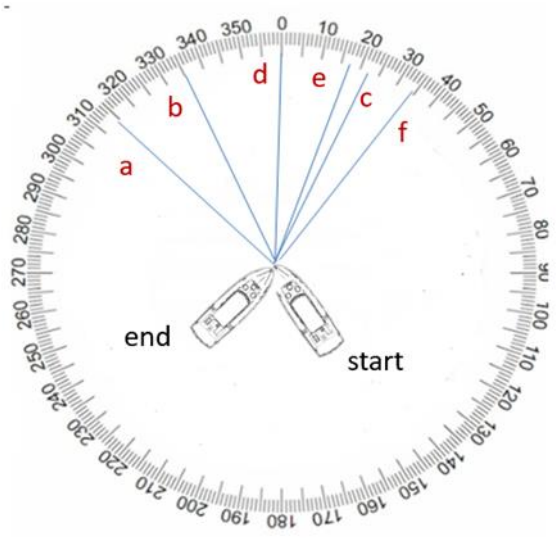

(c)

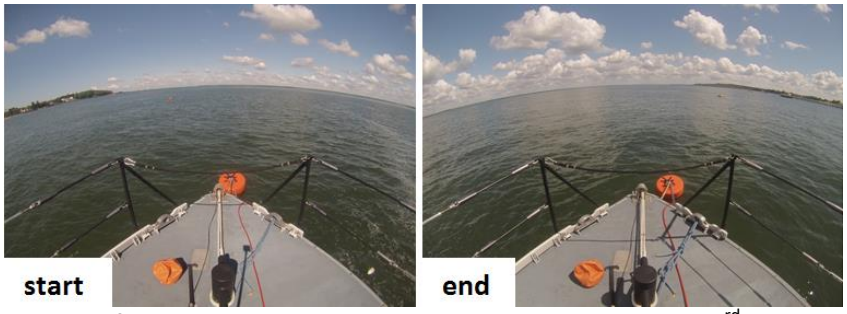

Figure 58: Position of Mersey Rose at a SPM in Yarmouth harbour on 23rd May 2016. (a) Route map, (b) vessel heading. The letters represent the times a= 10:24, b= 10:54, c= 11:24, d= 11:31. (high tide), e=11:54, f= 12:07 and (c) photographs of heading at start and end of sea trials.

5.3.3 Rotational motions of the lifeboat

The roll angle (degrees) was measured using the Xsens IMU and the results show that the vessel rolled between ± 2.0° with one 30s excursion when it reached +7.4° and – 7.7° at 10:32. The roll RMS was 0.60° and the peak frequency was 0.34Hz. The plots in the time and frequency domains are shown in Figure 59.

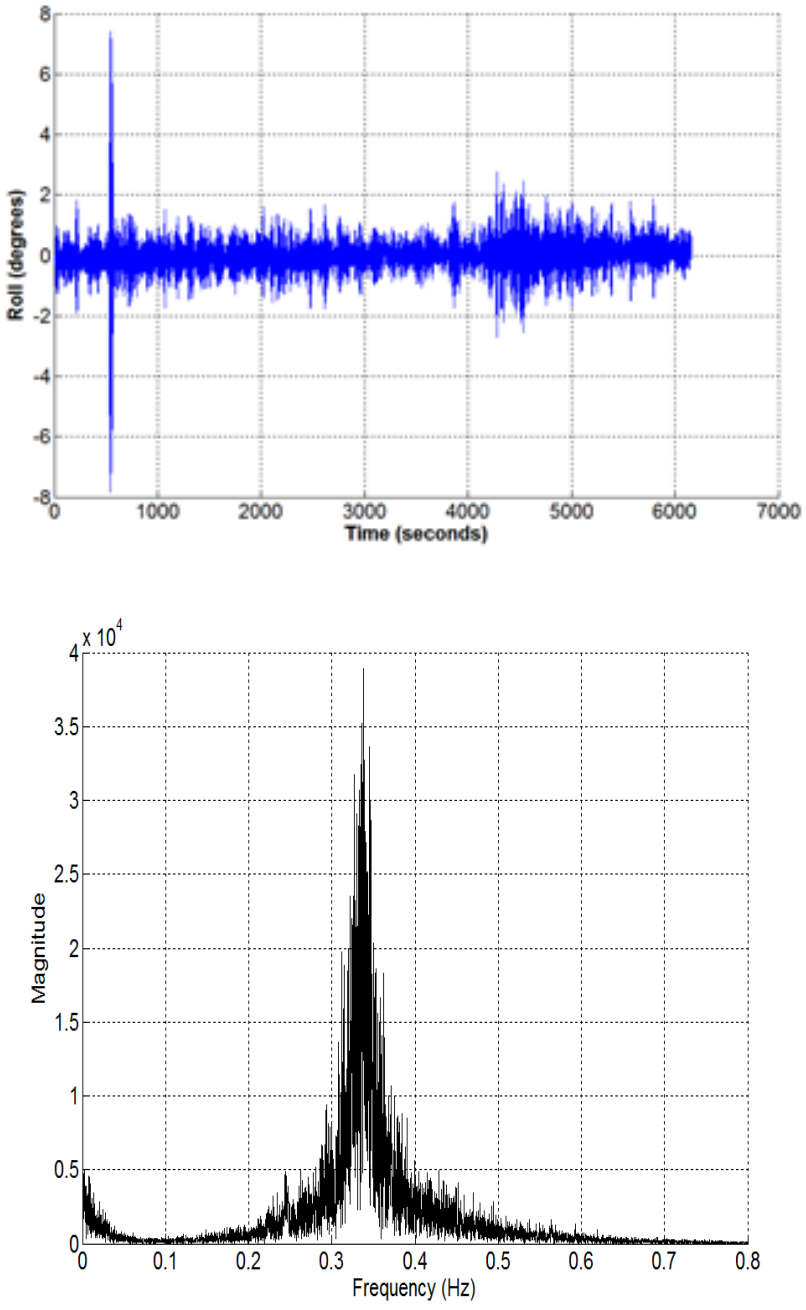

Figure 59: Roll angles of Mersey Rose with a low pass Butterworth filter at 0.5Hz.

The pitch angle (°) was measured using the Xsens IMU and the Vbox GPS devices. The results show that the vessel pitched between ± 0.5° until 11:35 when it increased to ± 1.0° and then continued to pitch at higher angles. The pitch RMS measured by both devices was 0.60° and the peak frequency was between 0.3 and 0.5Hz. The plots in time and frequency domain are shown in Figure 60.

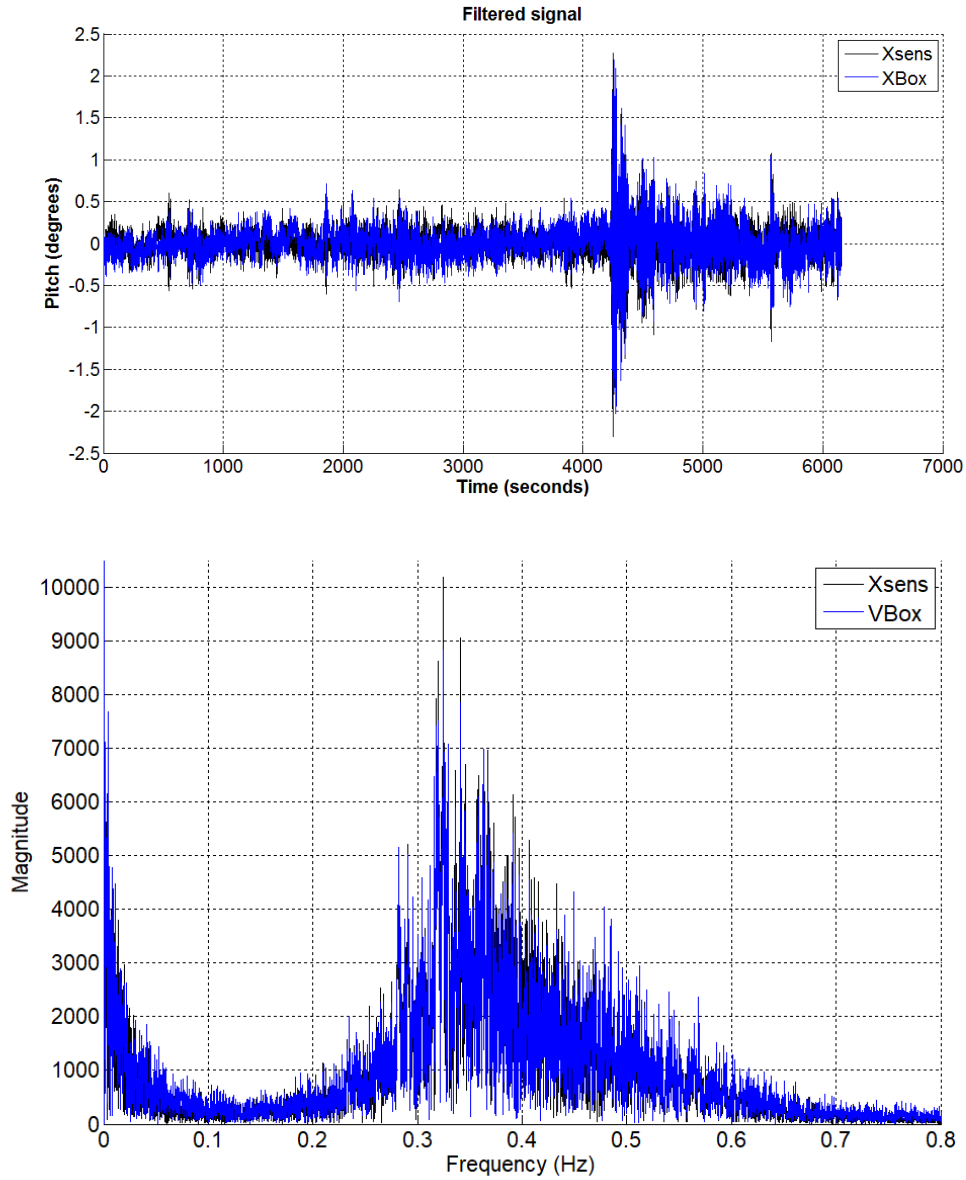

Figure 60: Pitch angles of Mersey Rose with a low pass Butterworth filter at 0.5Hz.

The yaw angle was measured using the Xsens IMU and the Vbox GPS devices. The verification of the yaw data presented in Section 3.3.2 and Figure 35 showed that the yaw angle calculated by the Xsens algorithm was prone to drift over time. The Xsens yaw data was therefore obtained by integration of the recorded yaw angular velocity data as presented in Figure 61a. Comparison of the yaw angle data shows close agreement but the time series are a mirror image of each due to the opposite orientation of the measurement devices, this is shown in Figure 61b.

(a)

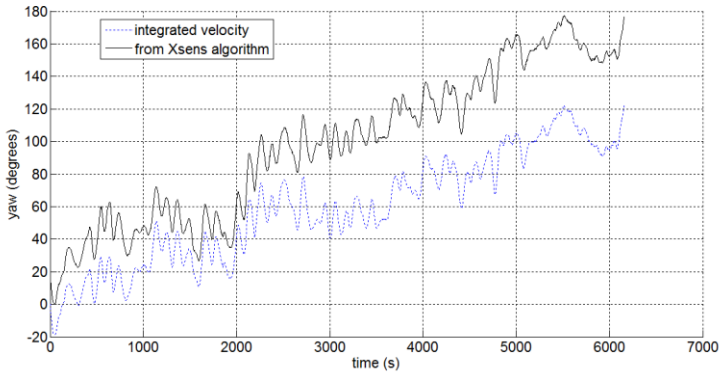

(b)

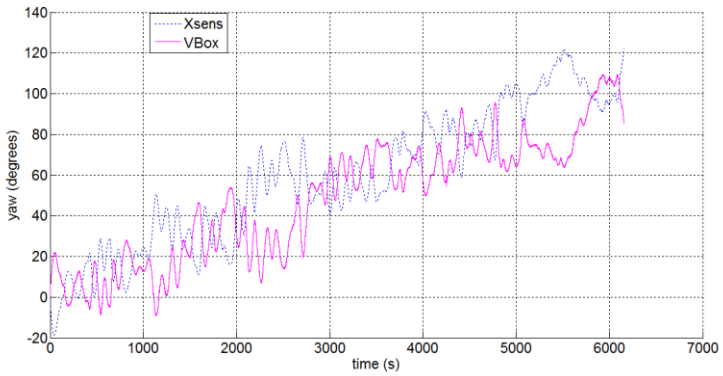

Figure 61: Yaw angles of Mersey Rose with a low pass Butterworth filter at 3Hz.
(a) yaw angle from Xsens algorithm compared to integration of angular velocity
(b) yaw angle from the Xsens and Vbox recoding equipment.

5.3.4 Translational motions of the lifeboat

The translational accelerations of the lifeboat were measured using the Xsens IMU. The surge accelerations were between ± 0.05m/s^2 until 11:35, then accelerating to ± 0.25m/s^2 for 30s and then exhibiting a higher range afterwards, coinciding with the pattern of pitch. The surge RMS was 0.02m/s^2. The sway accelerations were between ± 0.3m/s^2 accelerating to ± 1.3m/s^2 at 10:32 coinciding with the roll excursion. The sway RMS was 0.10m/s^2. The heave accelerations were between + 9.9m/s^2 and +9.7m/s^2 with peak excursions at 10:32, 10:55 and 11:35. The heave RMS was 9.8m/s^2. Time and frequency domain plots for all translational motions are presented in Figure 62.

(a)

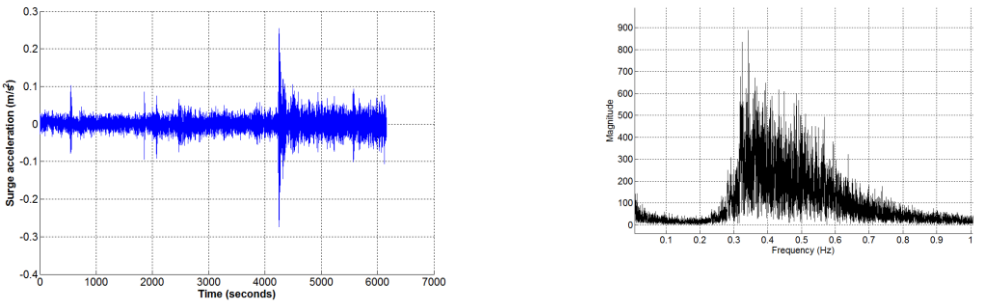

(b)

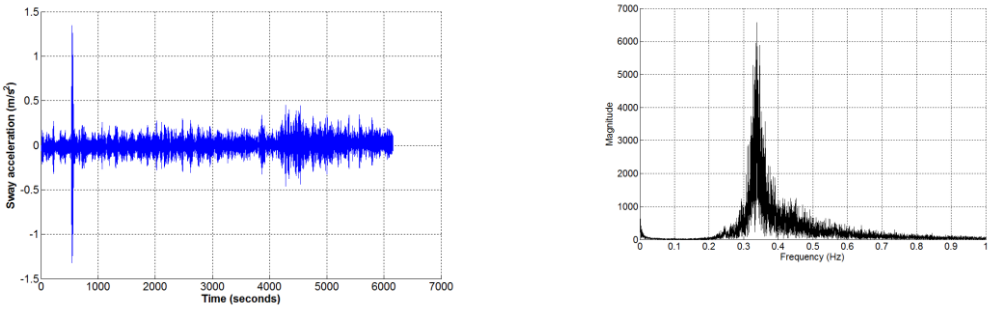

(c)

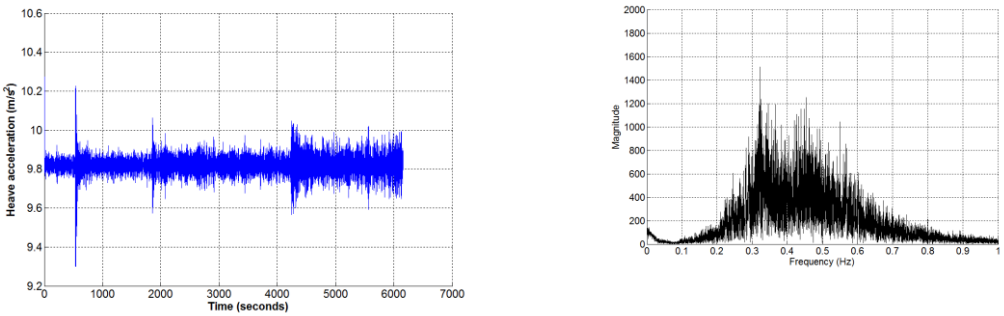

Figure 62: Translational acceleration of the Mersey Rose. All data are Butterworth low pass filtered: surge at 0.6Hz, sway at 0.5Hz and heave at 0.7Hz.

5.3.5 Motion of the buoy

Data on the accelerations of the buoy were recorded by the Xsens Mti 10 for 1,967s (32 minutes 47s) starting at 10:15, one hour and 16 minutes before high tide. The recording period was cut short due to data storage issues on the laptop.

The buoy's x direction translational accelerations ranged between ± 2.0 m/s^2, the y between ± 1.0m/s^2 and the z between + 8.5 and + 10.5m/s^2. The buoy's x direction rotational angular velocity ranged between ± 9.0deg./s, the y between ± 10.0deg./s, and the z between ± 5.5deg./s. The RMS values are presented in Table 26 and the time and frequency domain plots are presented Figure 63 and Figure 64 respectively.

Table 26: RMS of buoy motions

	Motion RMS.
x translational (m/s^2)	0.73
y translational (m/s^2)	0.34
z translational (m/s^2)	9.59
x rotational (deg./s)	3.00
y rotational (deg./s)	3.84
z rotational (deg./s)	2.94

(b)

(c)

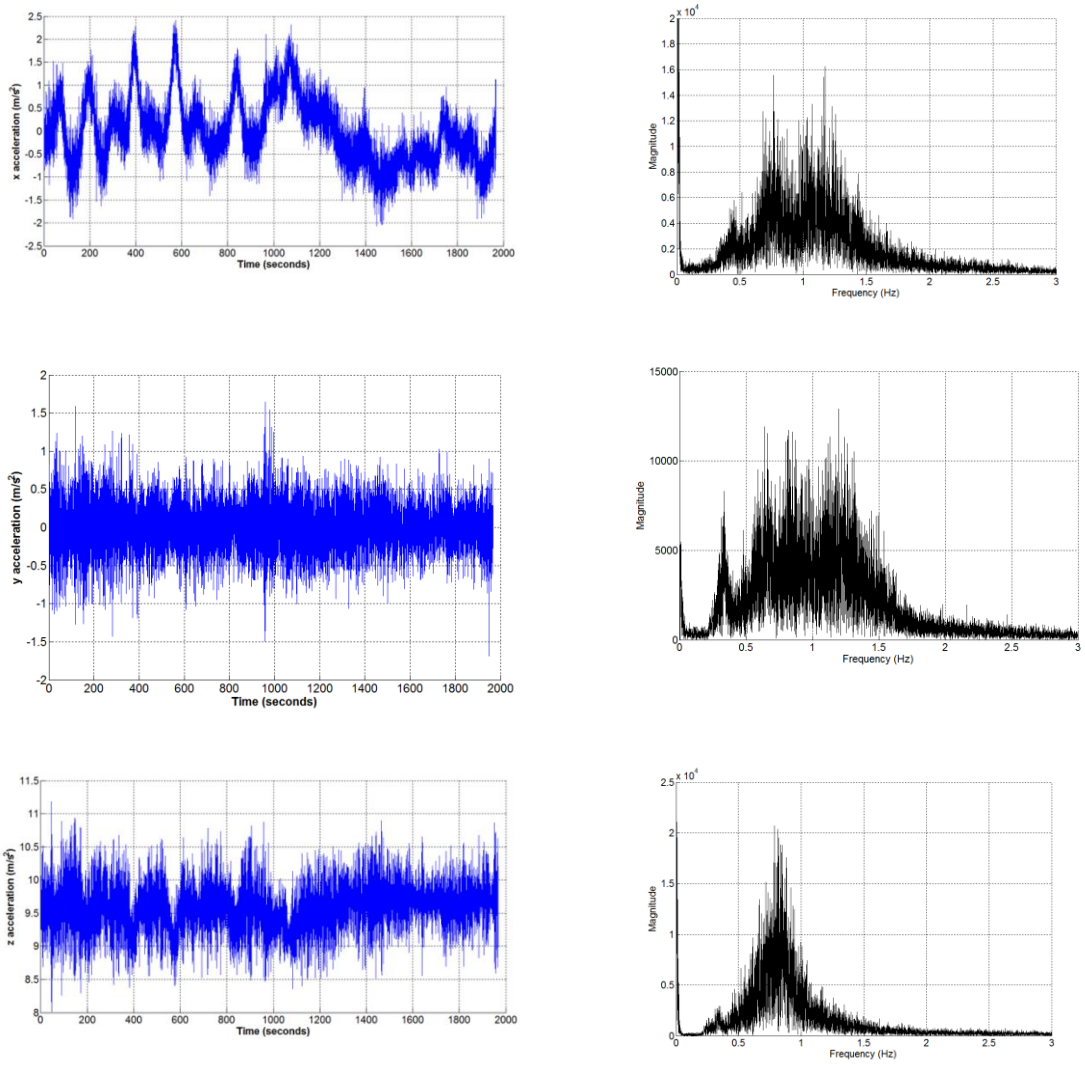

Figure 63: Translational motions of buoy starting at 10:15.
(a) x accelerations Butterworth low-pass 1.5Hz, (b) y accelerations Butterworth low-pass 1.5Hz (c) z accelerations Butterworth low-pass 1.5Hz.

(a)

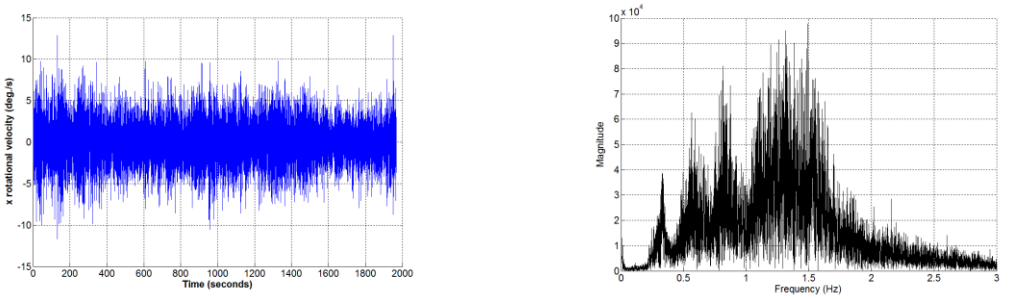

(b)

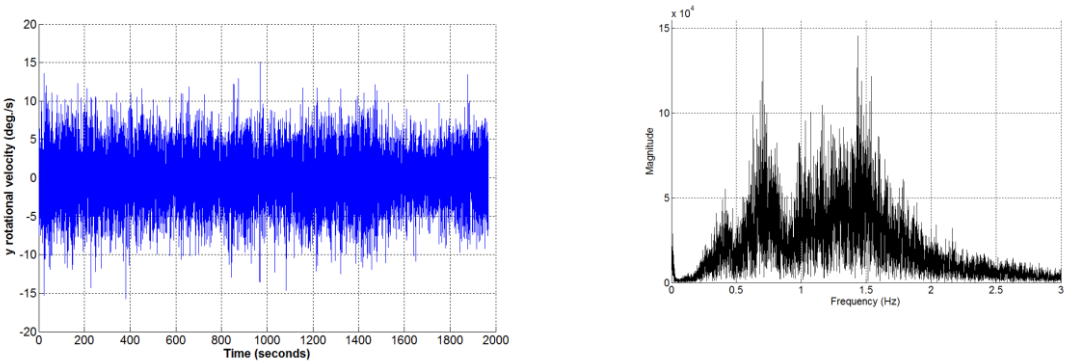

(c)

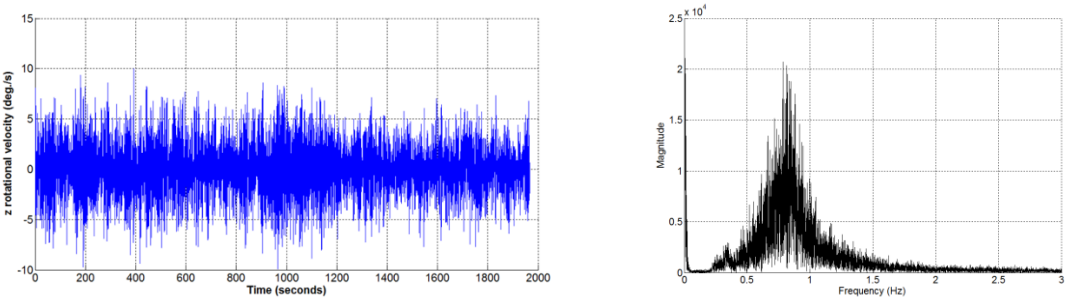

Figure 64: Rotational motions of buoy starting at 10:15.
(a) x rotational velocity Butterworth low-pass 1.7Hz, (b)y rotational velocity Butterworth low-pass 2.0Hz (c) z rotational velocity Butterworth low-pass 1.0Hz.

5.4 Discussion

Data recording of the motions of a full scale lifeboat and buoy were recorded on Monday May 23rd 2016 at Yarmouth Harbour off the coast of the Isle of Wight.

The results of the motion capture of the vessel showed peak excursions in the pitch angle and surge accelerations at 11:35. The images taken by the GoPro camera over the bow show that at 11:35 the Wightlink car ferry passed close by as depicted in Figure 65a which created a wash as depicted in Figure 66b. These increased motions continued for the remainder of the recording period after the passing of the ferry. The RMS of the pitch before the Wightlink ferry passed was 0.14°, for the period of passing was 1.12° and after was 0.24°. The corresponding figures for the RMS values for the sway accelerations were 0.02, 0.12 and 0.03m/s^2.

The peak in the recorded heave acceleration at 10:55 is explained by the passing of a fish vessel as depicted in Figure 65b which created a wash as depicted in Figure 66d. The peak in the roll and sway excursions at 10:32 is explained by the tender carrying the research personnel away from the vessel on the port side of the lifeboat.

No comparative literature has been found presenting the motions of any vessels at SPM in harbours. However model experiments performed on the effect of the passage of a larger tanker upon a tanker, moored on an open jetty in shallow water, showed a doubling in longitudinal force when the passing distance was reduced from 60m to 30m and that the induced forces and moments were proportional to the square of speed of the passing tanker (Remery, 1974).

From the twenty seconds of buoy motion data captured by a Lumia camera phone the Matlab algorithm, built at the University of Southampton and described in Section 3.2.3, has been used to track the buoy's motion at full scale. The angle of the footage is shown in Figure 66a along with the frame of reference. Using the isolated centroid of the buoy its path can be plotted as illustrated in Figure 66b. The frequency domain plot for the y direction is presented in Figure 66c showing a peak at the normalised frequency of 0.0129, equating to 0.2Hz. The buoy's excursion (cm) in the y direction is shown in the time domain in Figure 66d. Taking the excursion from 16.0s to 18.6s, for example, the buoy travelled 36.82cm equivalent to a velocity of 0.14m/s. This method could be used to track the in-situ motions of wave energy conversion devices which is required in order to assess the impact on engineering issues and optimise control parameters (Tyrberg et al., 2011).

(a)

(b)

(c)

(d)

Figure 65: Video capture of vessels passing the Mersey Rose.

(a) Wightlink ferry passing at 11:35 (b) subsequent wash from ferry (c) passing fishing vessel at 10:55 (d) subsequent wash from fishing vessel.

(a)

(b)

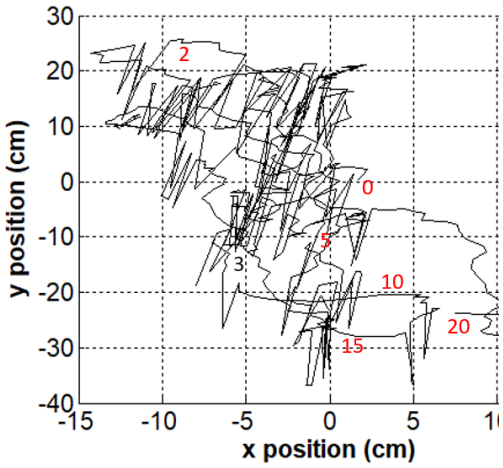

(c)

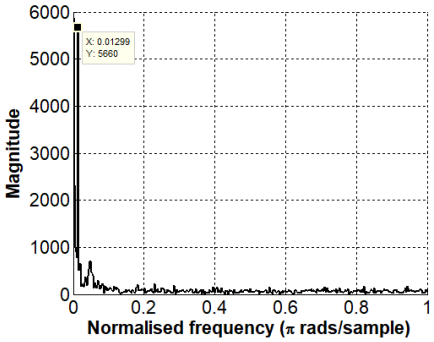

(d)

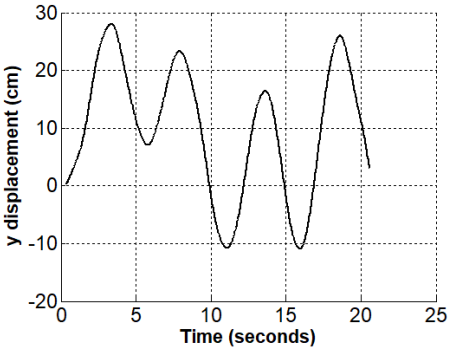

Figure 66: Buoy motion captured from camera phone
(a) Picture of video footage showing frame of reference and video shot from Matlab algorithm,
(b) Position (cm) in x and y direction of the buoy,
(c) Frequency domain and
(d) Time signal for y direction (cm) filtered at 1.2Hz.

Two independent methods of motion capture were used to record the pitch and yaw angles of the lifeboat and resultant plots, shown in Figure 60 and Figure 61 , show close agreement but provide further evidence that the yaw angle should be obtained from the Xsens by integrating the velocity data rather than using the inbuilt algorithm.

In terms of providing comparable data for the RNLI to use it should be pointed out that the volume of the Yarmouth Harbour buoys is significantly smaller than their Hippo buoys and the results of Chapters 3 and 4 indicate that this would have an impact on the motions of both the vessel and the buoy. However there is now a proven procedure for recording motion data via this inexpensive and unobtrusive methodology.

5.5 Summary

Motion data were recorded for one and three quarter hours, one hour and seven minutes before a high tide of 2.9m, with estimated wave heights of 0.15m and a mean wind speed of 3.8m/s on Monday 23rd May 2016. The results of the motion of the lifeboat and its buoy were as follows:

- The pitch and yaw data of the lifeboat were recorded and compared using an IMU and a GPS device. A mobile phone was used to record the motions of the buoy and the verified Matlab motion tracking algorithm used to plot its motion.
- The pitch angles varied between ± 0.5° until 11:35 when a car passenger ferry passed close by and subsequently pitched at angles ± 1.0°. The RMS was 0.22°. The roll angles varied between ± 2.0° with one 30s excursion when it reached +7.4° and – 7.7° at 10:32 as the launch left from its port side. The roll RMS was 0.60°.
- The vessel yawed to a maximum angle of 177.1° at 11:56 and was at a yaw angle of 135° at the time of high tide at 11:31.
- The surge accelerations were between ± 0.05m/s^2 until 11:35, then accelerating to ± 0.2 m/s^2. The surge RMS was 0.02m/s^2. The sway accelerations were between ± 0.3m/s^2 accelerating to ± 1.3m/s^2 at 10:32 coinciding with the roll excursion. The sway RMS was 0.10m/s^2. The heave accelerations were between +9.9m/s^2 and +9.7m/s^2 with peak excursions at 10:32 and 10:55 when a fishing trawler passed close by and 11:35 when a car ferry passed by. The heave RMS was 9.8m/s^2.
- The buoy's x direction translational accelerations ranged between ± 2.0m/s^2, the y between ± 1.0m/s^2 and the z between + 8.5 and + 10.5m/s^2. The rotational angular velocity ranged between ± 9.0deg./s, the y between ± 10.0deg./s, and the z between ± 5.5deg./s.

Chapter 6: DISCUSSION

> "Knowledge and experience may therefore limit our view. An example in the field of hydrodynamics is the low frequency motion behaviour of moored vessels, which may be caused by non-linearities of the mooring system or by excitation by drift forces. Before drift forces were recognised as a physical reality, low frequency motions were often wrongly attributed to the properties of the mooring system (although in other cases this interpretation is correct)." (Oortmerssen, 1991).

This thesis presents the experimental methodology and results of investigations into the effect of hawser length, buoy shape and buoy size upon the motions of vessels, less than 20 m in length, at SPMs in water depths, wave and current conditions that are typical of the coastal harbours of the United Kingdom.

A moored vessel is in dynamic equilibrium between the resultant of all external forces and the inertial force it exhorts (van Dorn, 1974). Increases in the horizontal motions of a moored body can cause very large instantaneous tensions (snap loading) and increased probability of SPM failure (Webster, 1995). The period of the pendulum like fishtailing motion of a vessel at a SPM may arise due to "inherent instabilities in the system, non-linearities in the hawser characteristics, variations in the wave drift force and, in some cases, wind gust loading" (Bowers and Standing, 1982). If a mooring configuration can be economically adapted to reduced vessel motion then there is the potential to increase its lifespan and reduce the risks of mooring failure.

The size of a mooring buoy is largely governed by the buoyancy requirements to support the mooring chain, the weight of which is determined by the vessel size, water depth and sea conditions (Barltrop, 1998). Full scale buoy diameters range from 1.24 to 1.85m for coastal locations and 2.4 to 4.0m for ports and deep sea locations (Hydrosphere, 2017) and different buoy shapes include spherical, cylindrical, barrel and modular (Budder, 2017). The diameter of the RNLI Hippo buoys, at 2m, are significantly larger than the average harbour buoys and their mushroom Hippo buoys are a customised design (Manuplas, 2017). The analysed experimental results, in both steady current and regular waves, indicate that the shape of the buoy has no significant impact, but increasing its geometric size does. The results presented indicate that introduction of a twice scale buoy into a SPM may reduce lifeboat motions and therefore reduce the risk of failure from reduced motioned induced fatigue.

An examination of which physical variables have an impact upon the mooring-induced damping experienced by an offshore floating platform, using Dimensional Analysis, is presented in Webster (1995). Simulations for a range of pre-tensions and motion amplitudes were performed testing the dimensionless parameters of scope, line drag coefficient, excitation period, stiffness and current. The excitation period was found to have a very strong effect on damping and, at low pre-tensions, shorter periods produced higher damping. This would suggest that the larger scale buoys, which had a higher velocity, would produce higher damping than the smaller ones.

The experiments which changed the size of the buoy in regular waves showed that, for wavelengths less than the LOA of the model lifeboat, increasing the size of the buoy resulted in a 0.08 – 0.09m (14% - 22%) increase in the excursion of the buoy in the direction of the wave train. As the buoy moves the change in shape of the catenary riser results in less chain lying on the tank floor as depicted in the schematic in Figure 67. From a static point of view, as the buoy moves from point A1 to A4, the cable tension at the point it is attached to the buoy is due to the total weight in sea water of the suspended line length (Faltinsen, 1993; Chakrabarti, 2005). The increase in suspended line weight when the larger buoys were used will result in an increase in line tension thereby adversely affecting the lifespan of the SPM. Therefore the reduction in fatigue due to reduced vessel motion, from incorporating a larger buoy, must be offset against the increase in tension at the attachment point of the SPM to the vessel.

From the documented environmental conditions in Appendix B it is apparent that the tide induced current flow is a constant factor and the location of coastal harbours are not in areas of extreme wave conditions around the UK. However the calculation of fatigue of mooring lines is "strongly dependent upon the tension oscillations induced by wave frequency motions" (Barltrop, 1998). The data acquired of the motions of a full scale lifeboat at a Yarmouth Harbour SPM indicate that it is the wake from the passing ships that had the most significant effect on the day of data recording. It is therefore imperative that the SPM is designed to be able to withstand the wave induced motion from frequent harbour traffic. This is of particular relevance for the RNLI as the crews, responding to an emergency call, will approach the moored lifeboat at high speed in their Rigid Inflatable Boats.

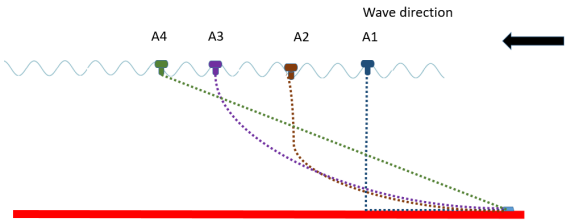

Figure 67: Schematic of catenary mooring line of SPM.

Motions of a 1:40 model scale, a 1:10.67 model scale and a full scale lifeboat have been recorded in laboratories and an in-situ environment. A motion tracking algorithm was successfully employed and validated against data from an IMU allowing tank testing without the influence of instrument cabling. The motions of the model and buoy were captured using an 'off the shelf' video camera and so this methodology offers an adaptable, inexpensive and portable method of motion tracking. This allowed an extensive series of experimental conditions to be undertaken within very tight budgetary requirements and timescales. Furthermore verification of the Xsens IMU against both the video and Vbox (GPS) data indicated that the built in algorithm in the Xsens outputs yaw angle values (°) that drift over time and direct integration of the Xsens's acceleration data is recommended.

The devised methodologies of motion capture, using free standing SPM, have been verified at three experimental scales. Due to operational and budgetary constraints there have been some limitations in terms of comparability between the model experiments in current, regular waves and full scale data acquisition. In particular the class of lifeboat in the three scenarios tested were different (namely a Severn, Tamar and Mersey) and the mooring buoy used in the full scale sea trials was neither the shape nor size of those used in the experimental set-up. Whilst these differences do not invalidate the results of the research their usefulness to the RNLI is somewhat compromised. Furthermore no tank testing facilities were available to test the combined effect of current and waves or for testing the environment component of wind, however, as stated above, it is the current induced motions that are considered to be dominant in coastal harbours. Finally the recording of load data was unsuccessful as the load cells interfered with the lifeboat's motions at the two scales tested and therefore the analysed results are for motion only.

SPM design is a trade-off between making it compliant enough to avoid excessive forces and stiff enough to avoid difficulties from excessive offsets in mooring risers (Chakrabarti, 2005). There are still many unanswered questions as to the optimal size of a SPM buoy in terms of optimising mooring efficiency and minimising fatigue. Nonetheless this thesis and corresponding research has shown there is the potential to reduce vessel motion and improve mooring efficacy and ensure system lifetime integrity.

Chapter 7: CONCLUSION

> *"Thus despite continuous publication of papers over the past 30 years by a variety of authors, analysis techniques for the assessment of mooring system stability are still evolving."* (Paton et al., 2006)

In order to achieve their purpose to "save lives at sea" the Royal National Lifeboat Institution (RNLI) owns and maintains forty single point moorings (SPM) around the coasts of the United Kingdom (U.K.) and Ireland, the location and configuration of which has been determined by local knowledge of wind, tide, current, fetch and topography. On the 23rd March 2008, in Dunbar's Torness harbour, the *Sir Ronald Pechell BT* a Trent class lifeboat slipped her mooring and was damaged beyond economic repair during a force 8 storm.

Additionally there are significant numbers of other small vessels at SPM around the coasts of the United Kingdom which employ a variety of hawser lengths and buoy shapes, including spherical, cylindrical, barrel and modular. Despite a number of reported accidents and rescue callouts at these SPM, the experimental investigations and computer simulations of the motions of moored vessels is largely confined to offshore tankers in deep open waters. The roll, pitch and yaw of a vessel will depend upon the resonance period of the ship and the wave spectrum, both of which differ when comparing lifeboats to tankers and coastal to offshore environments. The motivations for this thesis were this reported loss of human life, damage to vessels and the lack of consistent SPM configurations and safe mooring guidelines. The aim of the experimental work was to improve the understanding of the motions of a vessel and buoy at a SPM and gain insight into the key influencing factors in order to provide guidance for full scale SPMs.

The use of scientific investigation and full scale measurements at sea in terms of both financial and time scale investments is usually prohibitive and so physical interactions are best modelled at a smaller scale giving the advantage of a controlled environment to test new hypotheses. This thesis investigates the impact of changes in mooring line (hawser) length, buoy shape and buoy size upon the motions of a lifeboat at a SPM. The experimental methodologies were designed to record the motions of a lifeboat and buoy in different configurations in order to establish whether mooring efficacy could be improved by optimising these parameters. The experiments presented here reflect the wave and current conditions of the United Kingdom's coastal harbours and use a free catenary SPM configuration which allow changes in the mooring riser scope and the unrestricted motion of the mooring buoy and model lifeboat to be recorded.

A motion tracking algorithm has been successfully employed and validated against data from an inertial measuring unit allowing adaptable, inexpensive and portable method of motion tracking which enables small scale testing without the influence of instrument cabling.

The results from tests in steady current are presented Chapter 3 and those in regular waves in Chapter 4. Furthermore the motions of a full scale lifeboat and buoy at SPM were recorded over a tidal cycle at Yarmouth Harbour and the results are presented in Chapter 5.

- **Flume Tests**

A SPM allows the moored vessel the freedom to self-align to the prevailing wind and current. A series of freestanding 1:40 scale tests were performed in a circulatory flume at Chilworth research laboratory. The experimental setup enabled the unrestricted motion of the mooring buoy and model lifeboat to be observed and comparison between the effects of changes in line length, buoy shape and buoy size to be quantified. The presented results and discussion highlight the dominant motions and examine whether changing the size and shape of a SPM buoy impacts upon the motions of the attached lifeboat.

Results and conclusions from the analysed experiments in steady current presented include:

- The dominant translational motion of the model lifeboat was sway and the dominant rotational motion was yaw. This results in fishtailing responses similar to those reported in the literature from simulations and experiments for large scale vessels at offshore SPM.
- The effect of reducing the hawser length, when there was no buoy in the SPM, resulted in a reduction in the sway velocity of both markers on the model, agreeing with the results of published experiments.
- The observed linear correlation between the sway displacement (m) and yaw angle (°) that existed at the 1:40 scale buoy was not present when the larger 1:20 scale were used, indicating that the buoy-vessel interaction changes with buoy size. The larger buoy and longer hawser length increased the width and vorticity of its wake that induced larger sway excursions and reduced the yaw angle range.
- The mode shape of the SPM changed when a larger scale buoy was introduced: using the 1:40 scale buoys the stern marker ball moves faster than the bow marker ball which in turn is moving faster than the buoy. Conversely using the 1:20 scale buoys the buoy had the fastest sway velocity followed by the bow marker and the stern marker was the slowest. These results suggest that changes in buoy size can influence the motion responses of the vessel.

- At both scales tested there was no discernible difference between the sway velocities of the vessel when a change in shape was introduced.
- There were significant differences in the sway velocities of the 1:20 buoys when no vessel was attached. These results suggest that buoy shape had an impact on its own motions but the changes were not large enough, at this scale, to impact the motions of the moored vessel.
- Both the yaw angular velocities and ranges decreased when the size of the buoy was doubled from 1:40 to a 1:20 scale. Therefore increasing the size of a SPM buoy could lessen the risk of failure by reducing motion induced fatigue.

- **Regular wave tests**

A SPM is designed to "resist the mean mooring forces from wind, current and waves but allow the free response to wave frequency loading" (Barltrop, 1998). A series of freestanding 1:10 scale tests were performed in regular waves at the Solent University towing tank facility. The presented results and discussion highlight the dominant motions and examine whether changing the size and shape of a SPM buoy impacts upon the motions of the attached lifeboat.

The results and conclusions of the investigations are:

- All motions, except for the yaw, exhibited steady state oscillatory motion at the same frequency as the regular waves. The dominant rotational motion was pitch and the dominant translational motions were surge and heave as a result of the mooring riser chain and hawser providing a restraining mechanism against the oncoming regular waves.
- During each test the model slowly drifted in the direction of wave propagation and turned broadside to the waves thereby reducing the load in the mooring hawser compared to that if the heading was constrained.
- As a result of the changes in buoyancy forces the restrained model experienced significant excitations when head waves were longer than three quarters of the model length.
- Changing the shape of the buoy, at the 1:10.67 and the 1:5.33 scale, did not result in any significant change in the model's motions but there were some trends such as the wing shape having the consistently lowest values.

- Boxplots highlighted that the heave accelerations significantly decreased as the larger heavier buoys and longer line lengths were pulling the bow of the model lifeboat downwards at an angle of approximately 21°.
- Increasing the wavelength to longer than the LOA of the model led to a breakdown of the coupling between surge-pitch, surge-heave and heave-pitch.
- The maximum surge excursion of the buoy increased linearly, for both scales, as the wave frequency was increased enabling the determination of the maximum surge from the regular wave frequency in an engineering analysis of a lifeboat at a SPM.
- Results indicate that doubling the buoy scale resulted in lower pitch, slower sway and heave RAO but faster surge RAO. An overall RMS reduction, in motion, was calculated for 0.8, 0.9, 1.1Hz wave frequencies and an increase at the 1.0Hz wave frequency. These results indicated that increasing the size of the buoy would lead to an overall reduction in vessel accelerations at a SPM.

Full scale data acquisition

Data recording at full scale overcomes the scaling limitations of model testing and provides the necessary verification of the results of both model experiments and computer simulations. This thesis presents data on the motions of an RNLI lifeboat at a SPM. Two independent methods of motion capture were used to record the pitch and yaw angles of the lifeboat. Data were recorded on either side of high tide at Yarmouth Harbour off the coast of the Isle of Wight and the results and conclusions of the investigations are:

- The pitch and yaw data of a full scale lifeboat were recorded and compared using an IMU and a GPS device. A mobile phone was used to record the motions of the buoy and the verified Matlab motion tracking algorithm used to plot its motion.
- Peak excursions in the lifeboat's motions were correlated to passing by of harbour vessels.

- **Summary**

The secure mooring of a vessel in a harbour requires the consideration of many conditions, including geographical, meteorological and oceanographic alongside functional considerations such as regulations, space availability and maintenance. This thesis addresses the gaps in the literature, for small vessels at SPM in coastal waters, by presenting the experimental methodology and results of investigations into the effect of hawser length, buoy shape and buoy size upon the motions of vessels, less than 20m in length, at SPM.

The findings for experiments in both steady current and regular waves, for the scales investigated, indicate that the shape of the buoy has no significant impact but the geometric size does. Full scale buoy diameters range from 1.24 to 1.85m for coastal locations and 2.4 to 4.0m for ports and deep sea locations (Hydrosphere, 2017). The diameter of the RNLI Hippo buoys, at 2 m, are therefore significantly larger than the average of these harbour buoys and this series of tests were designed to assess the impact of size on the motions of a lifeboat. Increases in the horizontal motions of a moored body can cause very large instantaneous tensions and increased probability of SPM failure (Webster, 1995). The results presented in this thesis indicate that introduction of a twice scale buoy onto an RNLI SPM may therefore reduce the risk of failure by a reduction of the horizontal motions of a lifeboat at a SPM.

The data acquired of the motions of a full scale lifeboat at a Yarmouth Harbour SPM indicate that it is the passing ships that had the most significant effect on the motions of the lifeboat on the day of data acquisition. This data suggests that a position in a coastal harbour that is not in the path of regular vessel routes would significantly reduce lifeboat motion thereby reducing fatigue and extending the life of their SPM. The SPM should be positioned at an optimum point between (a) time taken for the crew to reach the lifeboat and (b) the minimum expected interaction of harbour traffic to the boat at SPM.

REFERENCES

ABS 2014. Rules for Building and Classing Single Point Moorings 2014 Houston, Texas: American Bureau of Shipping.

AGHAMOHAMMADI, F. & THOMPSON, J. 1990. An experimental study of the large amplitude fish-tailing instabilities of a tanker at a single point mooring. *Applied ocean research,* 12**,** 25-33.

ALVES, M., TRAYLOR, H. & SARMENTO, A. 2007. Hydrodynamic optimization of a wave energy converter using a heave motion buoy. *Proceedings of the 7th European Wave and Tidal Energy Conference, Porto, Portugal***,** 11-14.

BARLTROP, N. D. 1998. *Floating Structures: a guide for design and analysis*, Oilfield Pubns Inc.

BEHROOZI, F., 2014. A fresh look at the catenary. *European Journal of Physics*, *35*(5), p.055007.

BOUALI, B. & LARBI, S. 2013. Contribution to the geometry optimization of an oscillating water column wave energy converter. *Energy procedia,* 36**,** 565-573.

BOWERS, E. & STANDING, R. 1982. *Environmental loading and response*, Thomas Telford Limited.

CHAKRABARTI, S. 2005. *Handbook of Offshore Engineering (2-volume set)*, Elsevier.

CHAKRABARTI, S. & COTTER, D. 1994. Tank wall effects on broadside current forces on barge models. *Ocean Engineering,* 21**,** 489-497.

CHAKRABARTI, S., LIBBY, A. & PALO, P. 1995. Small-scale testing on current-induced forces on a moored tanker. *Ocean engineering,* 22**,** 271-300.

FALTINSEN, O. 1993. *Sea loads on ships and offshore structures*, Cambridge university press.

FERRERAS, J., SÁNCHEZ-TEMBLEQUE, F., PEÑA, E., PRIEGUE, L., SANDE, J., COSTA, F. & RABUÑAL, J. 2013. Field monitoring of Ship Moored motions and Mooring Loads at Punta Langosteira Port (A Coruna, Spain). *6th SCACR - International Short Courses on Applied Coastal Research*.

FITZGERALD, J. & BERGDAHL, L. 2008. Including moorings in the assessment of a generic offshore wave energy converter: A frequency domain approach. *Marine Structures,* 21**,** 23-46.

GAYTHWAITE, J. W. 2004. Design of Marine Facilities for Berthing, Mooring and Repair of Vessels. 2nd revised ed.: ASCE Press.

GOGGINS, J. & FINNEGAN, W. 2014. Shape optimisation of floating wave energy converters for a specified wave energy spectrum. *Renewable Energy,* 71**,** 208-220.

HAGER, R., FERNANDEZ, N. & TENG, M. H. 2012. Experimental Study Seeking Optimal Geometry of a Heaving Body for Improved Power Absorption Efficiency. *The Twenty-second International Offshore and Polar Engineering Conference*.

HALLIWELL, A. & HARRIS, R. 1988. A parametric experimental study of low-frequency motions of single point mooring systems in waves. *Applied ocean research,* 10**,** 74-86.

HINZ, E. R. 2001. *The complete book of anchoring and mooring. (Rev. 2nd ed.)*, Cornell Maritime Press Centreville, Maryland.

HOLLYHEAD, C.J., TOWNSEND, N.C. & BLAKE, J.I. 2017. Experimental investigations into the current-induced motion of a lifeboat at a single point mooring. *Ocean Engineering,* 146, 192-201.

HUANG, C.-C. & LEE, M.-F. 2012. Experimental Study on a Single-point-mooring Floating Structure. *The Twenty-second International Offshore and Polar Engineering Conference*.

HUGHES, S. A. 2005. *Physical Models and Laboratory Techniques in Coastal Engineering*, World Scientific Publishing Co Pte Ltd, Singapore.

ISAACSON, M. & BALDWIN, J. 1996. Moored structures in waves and currents. *Canadian Journal of Civil Engineering,* 23**,** 418-430.

KITNEY, N. & BROWN, D. T. 2001. Experimental investigation of mooring line loading using large and small-scale models. *Journal of Offshore Mechanics and Arctic Engineering,* 123**,** 1-9.

LANG, S. 2001. Review of Lifeboat and Launching Systems' Accidents. *Southampton: Marine Accident Investigation Branch*.

LANG, S. 2002. Report on the analysis of fishing vessel accident data, 1992 to 2000. *Southampton: Marine Accident Investigation Branch*.

LLOYD, A. R. J. M. 1989. *Seakeeping: ship behaviour in rough weather* Chichester, Ellis Horwood.

LUAI, A. & ZHI, Y. 2013. Comparison of laboratory and predicted motions and mooring line forces for a container ship moored to a dock. *Proceedings of the 18th Offshore Symposium, Houston, Texas.*

McCabe, A. P. 2013. Constrained optimization of the shape of a wave energy collector by genetic algorithm. *Renewable Energy,* 51**,** 274-284.

MOLLAND, A. F., TURNOCK, S. R. & HUDSON, D. A. 2011. *Ship Resistance and Propulsion: Practical Estimation of Propulsive Power.* Cambridge University Press.

MYERS, L. E. & BAHAJ, A. S. 2010. Experimental analysis of the flow field around horizontal axis tidal turbines by use of scale mesh disk rotor simulators. *Ocean Engineering,* 37**,** 218-227.

O.C.I.M.F. 2008. Oil Companies International Marine Forum Mooring Equipment Guidelines. Livingston, United Kingdom: Witherby Seamanship International.

OORTMERSSEN, G. V. 1991. Assessment of the Validity of Computer Models for the Prediction of Dynamics of Floating Structures. *Dynamics of Marine Vehicles and Structures in Waves.* Elsevier Science Publishers.

OPPENHEIM, B. & WILSON, P. 1982. Static 2-D solution of a mooring line of arbitrary composition in the vertical and horizontal operating modes. *International Shipbuilding Progress,* 29**,** 142-153.

PAPAZOGLOU, V.J., MAVRAKOS, S. A. & TRIANTAFYLLOU, M. S. 1990. Nonlinear cable response and model testing in water. *Journal of Sound and Vibration,* 140, 103-115.

PASTOR, J. & LIU, Y. 2014. Frequency and time domain modeling and power output for a heaving point absorber wave energy converter. *International Journal of Energy and Environmental Engineering,* 5**,** 1-13.

PATON, C., CARRA, C., SINCOCK, P. & CONSULTING, A. 2006. Investigation of sway/yaw motions of deepwater FPSOs. *Proceedings Offshore Tech Conf, Paper OTC,* 18039.

PATTISON, J. H. 1977. Components of Force Generated by Harmonic Oscillations of Small-Scale Mooring Lines in Water. David W Taylor Naval Ship Research and Development Centre, Bethesda MD Ship Performance Department, No. SPD-589-01.

PINKSTER, J. 2004. The influence of a free surface on passing ship effects. *International shipbuilding progress,* 51**,** 313-338.

PINKSTER, J. & REMERY, G. 1975. The role of model tests in the design of single point mooring terminals. *Offshore Technology Conference*.

REMERY, G. 1974. Mooring forces induced by passing ships. *Offshore technology conference*.

SCHELFN, T. & ÖSTERGAARD, C. 1995. The vessel in port: Mooring problems. *Marine structures,* 8**,** 451-479.

SCHELLIN, T. 2003. Mooring load of a ship single-point moored in a steady current. *Marine structures,* 16**,** 135-148.

SHARMA, S., JIANG, T. & SCHELLIN, T. 1988. Dynamic instability and chaotic motions of a single-point-moored tanker. *17th Symposium on Naval Hydrodynamics*.

SIMOS, A. N., TANNURI, E. A., ARANHA, J. A. P. & LEITE, A. J. P. 2001. Theoretical analysis and experimental evaluation of the fishtailing phenomenon in a single-point moored tanker. *Proceedings of the Eleventh International Offshore and Polar Engineering Conference.*

SORHEIM, H. R. 1980. Analysis of Motion in Single-Point mooring systems. *Modelling Identification and Control,* 1**,** 165-186.

SUNDARAVADIVELU, R., BABU, M. H. & MURUGAGANESH, R. 1991. Experimental investigation on a single point buoy mooring system. *Ocean Engineering,* 18**,** 405-&.

TANNURI, E. A., SIMOS, A. N., LEITE, A. J. & ARANHA, J. A. P. 2001. Experimental validation of a quasi-explicit hydrodynamic model: Fishtailing instability of a single-point moored tanker in rigid-hawser configuration. *Journal of Ship Research,* 45**,** 302-314.

TROESCH, A. & BECK, R. F. 1974. Experiments on Ship Motions in Shallow Water. DTIC Document.

TYRBERG, S., SVENSSON, O., KURUPATH, V., ENGSTRÖM, J., STRÖMSTEDT, E. & LEIJON, M. 2011. Wave buoy and translator motions—on-site measurements and simulations. *Oceanic Engineering, IEEE Journal of,* 36**,** 377-385.

VAN DORN, W. G. 1974. *Oceanography and seamanship*, Dodd, Mead New York, NY, USA.

VELEGRAKIS, A., VOUSDOUKAS, M., VAGENAS, A., KARAMBAS, T., DIMOU, K. & ZARKADAS, T. 2007. Field observations of waves generated by passing ships: a note. *Coastal Engineering,* 54**,** 369-375.

VIGGOSSON, G. 1988. Field Observations of Ship Behaviour at Berth. *In:* BRATTELAND, E. (ed.) *Advances in Berthing and Mooring of Ships and Offshore Structures*

WANG, J., LI, H., LI, P. & ZHOU, K. 2007. Nonlinear coupled analysis of a single point mooring system. *Journal of Ocean University of China,* 6**,** 310-314.

WEBSTER, W. C. 1995. Mooring-induced damping. *Ocean Engineering,* 22, 571-591.

WEHAUSEN, J. 1971. Motion of Floating Bodies. *Annual Review of Fluid Mechanics,* 3**,** 237-&.

WICHERS, J. E. W. 1976. On the Slow motions of Tankers Moored to Single Point Moorings Systems. *Offshore Technology Conference. ,* OTC 2548.

WICHERS, J. E. W. 1988. *A simulation model for a single point moored tanker.* Thesis, Technische Universiteit Delft.

Websites (working links as at 27th May 2018):

A&D.2015a. Load cell used. Available: http://www.appmeas.co.uk/dbbsm-s-beam-load-cell.html accessed on 16th August 2015.

A&D. 2015b. Load cell used. Available: http://www.aandd.jp/products/weighing/loadcell/introduction/pdf/6-1.pdf accessed on 16th August 2015.

BBC. 2008a. News report on mooring failure of RNLI lifeboat. Available: http://news.bbc.co.uk/1/hi/scotland/7309579.stm accessed on 28th March 2017.

BBC. 2008b. Four rescued as boat runs aground. Available: http://news.bbc.co.uk/1/hi/england/kent/7272434.stm accessed on 3rd September 2017.

BBC. 2012. Yacht breaks from harbour mooring in Port St Mary. Available: http://www.bbc.co.uk/news/world-europe-isle-of-man-18952895 accessed on 21st August 2017.

BBC. 2013. Two rescued after yacht breaks its moorings. Available: http://www.bbc.co.uk/news/world-europe-guernsey-21739188 accessed on 21st August 2017.

Budder, 2017. Types of mooring buoy. Available: http://www.buoder.com/products/list-en1-1.html accessed on 21st August 2017.

Bradney. 1987. A practical guide to the mooring and anchoring of small boats. Available https://dbscweb.files.wordpress.com/2013/08/bradney-mooring-and-anchoring-leaflet.pdf accessed on 21st August 2017.

Hydrosphere. 2017. Mooring buoys. Available: http://hydrosphere.co.uk/datasheets/product-services-summaries/hydrosphere_mooring_buoys_v_2_01_sep_14_web.pdf accessed 20th July 2017.

ITTC. 2008. Testing and Extrapolation Methods Loads and Responses, Seakeeping. Available: http://ittc.info/media/1667/75-02-07-021.pdf accessed on 6th February 2017

ITTC. 2011. Table of fresh water density. Available: https://ittc.info/media/4048/75-02-01-03.pdf accessed on 27th May 2018.

IWCP, 2012. Boats sink in heavy seas. News feed now deleted but referred to in: http://www.ybw.com/forums/archive/index.php/t-314183.html accessed on 27th May 2018.

Lost Dunbar. 2009. Report of the loss of Trent class lifeboat. Available: http://www.lostdunbar.co.uk/lifeboat-history.html accessed on 27th March 2017.

Manuplas (2017). Types of mooring buoy. Available: http://www.manuplas.co.uk/commercial-mooring-buoys accessed on 14th October 2017.

Meteo Consult Marine. 2017. Sea conditions for Dunbar Harbour. Available: http://marine.meteoconsult.co.uk/marine-weather-forecast/weather-harbour-approaches/bassin-par-defaut/weather-forecast-dunbar-harbour-trust-840-1.php# accessed on 9th January 2017

MarineWiki, 2018. Hull Proptyions. Available: http://www.marinewiki.org/index.php?title=Hull_Proportions accessed 11th September 2018.

Percuil River Mooring Ltd. 2010. Implementation of the Mooring Contractor Guidelines. Available: http://www.percuilriver.co.uk/implementation-mooring-contractor-guidelines accessed 21st June 2017.

RNLI. 2015. RNLI Principal Activities 2015. Available: https://www.rnli.org/aboutus/aboutthernli/rnli-annual-report-and-accounts-2015/Pages/our-plans-and-purpose.aspx accessed on 11th July 2016.

SeaSurveys. 2013. Newspage. Available: http://www.turbolink.co.uk/seasurveys2011/news.html accessed on 21st June 2017.

UDEL. 2015. University of Delaware – definition of hydraulic diameter. Available: http://udel.edu/~inamdar/EGTE215/Open_channel.pdfl accessed on 17th September 2015.

VPG. 2015. Load cell errors. Available: http://www.vishaypg.com/doc?11864 accessed on 11th September 2015.

Weatherfile. 2017. Website for wind data. Available: https://weatherfile.com/?loc_id=GBR00003 accessed on 14th October 2017.

Which-Marina. 2015. Registered UK marinas. Available: http://www.which-marina.com/Default.asp accessed on 21st June 2017.

Yachting and Boating World. 2016a. May Dream aground in Plockton. Available: http://www.ybw.com/news-from-yachting-boating-world/may-dream-aground-plockton-23755 accessed on 21st June 2017.

Yachting and Boating World. 2016b. Yacht smashes and sinks in Portland Harbour. Available: http://www.ybw.com/news-from-yachting-boating-world/yacht-smashes-and-sinks-in-portland-harbour-39858 accessed 21st June 2017.

APPENDICES

Appendix A Configurations of RNLI SPM

P and S indicate a primary and secondary SPM with specific characteristics presented in Figure 2.

Station	Lifeboat	Used	Ground chain	Ground chain length	Chain Riser length	Anchor or Sinker	Upper hawser	Lower hawser
	(type)		(no.)	(m)	(m)	(A) (S)	(m)	(m)
Achill Islands	Trent	P	4	27.5	20	A and S	5	6
Alderney	Trent	P	3	27.5	5	S	chain and sliphook	
Angle	Tamar	S	3	27.5	20	A	6	7
Appledore	Tamar	S	1	0	25	S	8	8
Arranmore	Severn	P	4	27.5	20	A	chain and sliphook	
Ballyglass	Severn	P	4	27.5	15	A	6	10
Baltimore	Tamar	S	3	27.5	20	A	chain and sliphook	
Barra	Severn	P	4	20	15	A	6	8
Barrow	Tamar	S	3	20	25	A	8	10
Bembridge	Tamar	S	3	27.5	25	A	6	8
Courtmacsharry	Trent	P	4	27.5	15	A	chain and sliphook	
Dunbar	Trent	P	5	27.5	15	A and S	chain and sliphook	
Exmouth	Shannon	S	2	27.5	15	A	3	4
Fishguard	Trent	P	3	20	20	A	8	10
Fleetwood	Tyne	P	3	27.5	20	A	6	7
Humber	Severn	P	3	20	35	S	8	10
Larne	Trent	P	4	27.5	25	A	6	8
Lizard	Tamar	S	3	20	15	A	10	10
Lough Swilly	Tyne	P	4	27.5	20	A	6	8
Moelfre	Tamar	S	3	27.5	35	A	6	7
New Quay	Mersey	S	3	20	15	A	6	7
Padstow - trevose	Tamar	S	3	27.5	10	A	6	8
Padstow - town	Tamar	S	2	20	10	A	6	7
Porthdinllaen	Tamar	S	3	20	15	A	5	7
Portree	Trent	P	3	20	20	A	8	10
Salcombe	Tamar	P	2	20	10	A	3	4
Selsey	Tyne	S	3	20	30	A	6	8
Sheerness	Trent	P	4	20	15	A	6	8
St Davids	Tamar	S	3	25	30	A	6	7
St Mary's	Severn	P	4	27.5	20	A	5	6
St Peter Port	Severn	P	3	27.5	5	S	chain and sliphook	
Swanage	Mersey	S	3	20	15	A	6	8
Tenby	Tamar	S	4	27.5	15	A	4	6
The Mumbles	Tamar	S	3	27.5	35	A	6	7
Tobermory	Severn	P	4	27.5	35	A	4	6
Valentia	Severn	P	4	27.5	20	A	6	8

Appendix B Environmental factors of documented RNLI stations

Lifeboat Station	Max. water depth	Max. wave height	Highest tide	Available swing	Wind Fetch and direction	Current flow and direction
	(m)	(m)	(m)	(m)	(Nm), (deg.)	(m/s), (deg.)
Achill Islands	5	1.2	5.2	50	1.5 from 015	2.6 from 184
Alderney	5	2.0	6.8	45	6 from 045	no details
Angle	10	2.0	7.0	20	5 from 300	no details
Appledore	2	3.0	8.7	30	3 from 310	3.1
Arranmore	2	2.0	4.0	37	0.2 from 215	0.3 from 180
Ballyglass	10	2.0	11.0	340	10 from 009	1.0 from 190
Baltimore	2	1.3	4.3	25	1 from 315	1.8 from 270
Barra	10	1.5	5.0	30	0.1 from 135	no details
Barrow	5	1.5	12.0	32	8.5 from 175	1.5 from 345
Bembridge	2	2.0	5.1	30	25 from 095	1.5 from 135
Courtmacsherry	2	0.8	7.7	25	1.75 from 290	2.3 from 125
Dunbar	3	5.0	11.0	25	200 from 045	1
Exmouth	5	1.5	9.0	30	1 from 130	3.1 from 130 and 310
Fishguard	5	1.5	5.6	110	1.3 from 115	no details
Fleetwood	2	2.0	10.8	40	20 from 0	2.6
Humber	10	2.5	8.0	95	13 from 315	3.1 from 035
Larne	5	2.0	3.8	100	2.5 from 135	0.8 from 115 and 300
Lizard	10	10.0	13.2	40	100 from 180	0.8 from 23 and 200
Lough Swilly	10	2.5	10.0	350	6.5 from 315, 5.5 from 225	0.3 from 180
Moelfre	2	2.0	8.0	30	60 from 045	"very little"
New Quay	2	4.0	5.6	330	no details	0.3
Padstow	5	5.0	11.0	350	40 from 035	0.5
Padstow	2	2.0	9.5	24	60 from 345	3.1 from 180
Porthdinllaen	3	5.0	11.0	26	11 from 045	0.9 from 023
Portree	2	10.0	12.0	100	45 from 122	1.5 from 190
Salcombe	1	3.0	5.6	18	1 from 225	1.3 from 055 to 235
Selsey	2	5.0	5.2	50	90 from 115-120	2.6 from 220
Sheerness	10	0.0	6.3	45	100 from 22.5 to 90	1
St Davids	10	4.0	12.5		50 from 220	no details
St Mary's	2	3.0	8.1	20	6 from 278	2.6 from 270 to 355
St Peter Port	5	1.0	15.0	40	0.2 from 135	0.3
Swanage	2	3.0	2.5		23 from 095	1.0 from 90 & 270
Tenby	2	2.0	5.2	30	1.2 from 210	1.8 from 180 & 50
The Mumbles	5	4.0	9.3	350	50 from 135	1.0 from 246
Tobermory	25	1.5	4.4	7	4.5 from 045	no details
Valentia	5	1.5	11.3	350	1.25 from 270	0.8 from 270

Appendix C Recording of load

C.1 Tests in steady current

The tension on the mooring ground chains was recorded using 5kg rated tension miniature ‘S' Beam load cells sealed to IP67 provided by Strainstall UK Ltd (A&D, 2015a). Each cell was connected, via an embedded analogue amplifier, to a National Instruments 9205 voltage logging module on a CompactRIO. For the scale and twice scale buoy tests two load cells were positioned on the tank floor in line with the mooring ground chain. For the tests with no buoy one load cell was suspended vertically on wire rope.

The factors which influence a load cell’s performance capability and accuracy are defined by the manufacturer as (A&D, 2015b):

- ϵ_L (%) nonlinearity – the deviation of the calibration line from a straight line connecting the zero load and the rated load output values.
- ϵ_H (%) hysteresis error - the difference between load cell output readings for the same applied load, one reading obtained by increasing the load from minimum load and the other by decreasing the load from maximum load (VPG, 2015).
- ϵ_R(%) repeatability.
- ϵ_Z (%/°C) temperature effect on zero balance.
- ϵ_S (%/°C) temperature effect on span.
- RC rated capacity of load cell.
- W_1 maximum load to be measured.
- Zero balance.
- t temperature range.

These factors are combined into a single error equation (A&D, 2015b).

$$\epsilon > \sqrt{\epsilon_L^2 + \epsilon_H^2 + \epsilon_R^2 + \left(\frac{\epsilon_Z (RC) t}{W_1}\right)^2 + (\epsilon_S t)^2}$$

For the ‘S’ beam load cell used this equates to an error of 0.0587%.

The voltage readings were recorded via a timed loop in LabVIEW set at 250Hz which yielded 25 readings per second. The zero reading for the conversion from recorded volts to Newtons was taken as an average of load readings when the cells were left to run with nothing attached. To filter out the noise in the signal the measurements were filtered using a low pass tenth order Butterworth filter set at a normalised frequency of 0.05Hz.

Plots in the time domain show that both cells were recording the same periodic signal with a mean difference of 0.34N (STD 0.05N) and those in the frequency domain show signal peaks at the same frequencies as shown in Figure 68. The load readings are verified as being an accurate measurement of the tension they were recording but there is uncertainty, at this small scale, as to whether they are measuring the changes in tension on the mooring ground chains and so a set of experiments were performed to test this.

Series 2 included a test which just recorded the load fluctuations recorded by the load cells in the current with no model or mooring attached. The time domain plots show the cells recording periodic signals as shown in Figure 69. The results show that there was little difference in the range recorded with and without the mooring namely 0.086 N increased for cell 0 with it attached and a decrease of 0.003 N for cell 2. Furthermore plots in the frequency domain also showed the dominant magnitudes to be at similar frequencies as shown in Figure 69. It is therefore concluded that at this scale of experimentation the load readings could not be used as a measured parameter. However the fact that the readings are verified, but not validated, means the equipment is suitable for testing load on mooring chains at the larger scales.

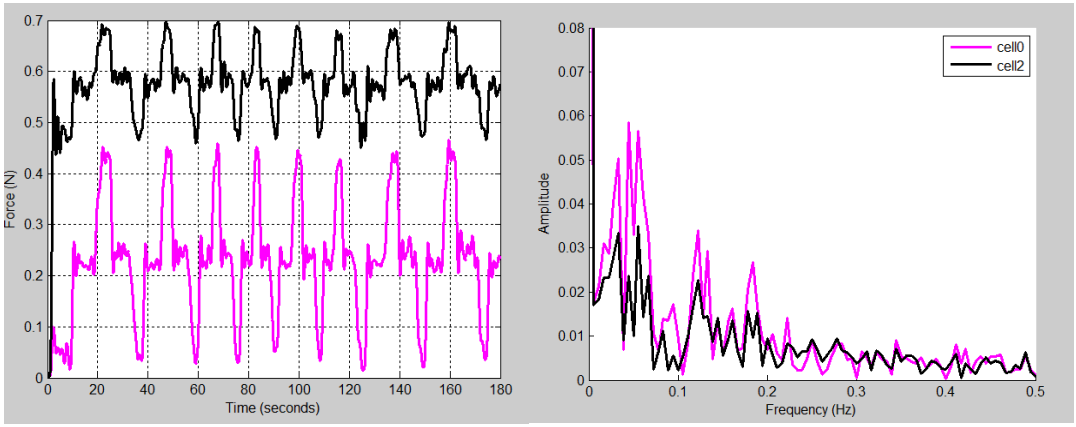

Figure 68: Time and frequency plots of two load cells test (ADB1).

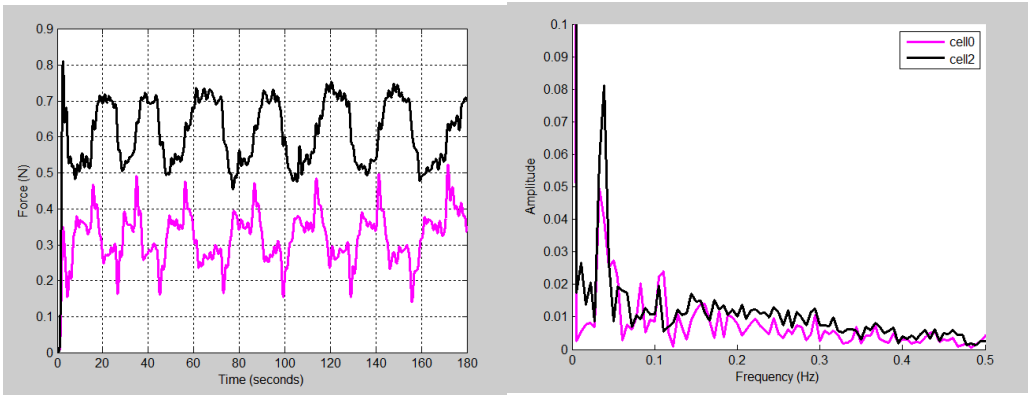

Figure 69: Time and frequency plots of two load cells test (NBB1).

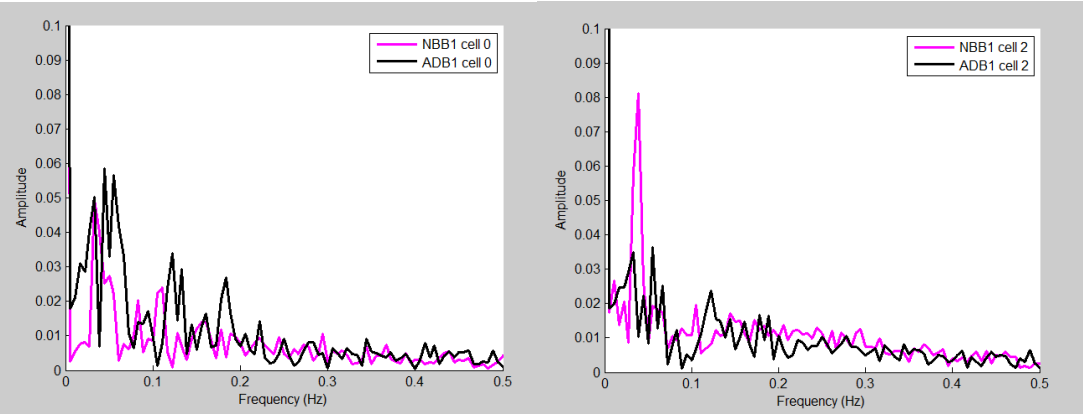

Figure 70: Comparison in frequency domain of measured load for mooring attached (ADB1) and with nothing attached (NBB1).

C.2 Tests in regular waves

The tension in the hawser was recorded using a 5kg rated tension miniature 'S' Beam load cell sealed to IP67 provided by Strainstall UK Ltd (A&D, 2015a). It was attached to the hawser at the bow of the model, as depicted in Figure 71, and connected, via an embedded analogue amplifier, to a National Instruments 9205 voltage logging module on a CompactRIO located on the carriage. The load cells were those used in the Chilworth flow experiments the verification for which is discussed in C.1. The calibration was checked by recording the voltage reading whist hanging three masses (1kg, 2kg, and 3kg) vertically downwards. The resultant linear plots showed a correlation coefficient (goodness of fit) of 0.9970, 0.9806 and 0.9998 between mass and voltage output.

However load recording was unsuccessful as the cabling required from the load cells to the towing carriage had a significant impact on the motions of the vessel and buoy. In addition the load cell was too heavy compared to the fishing wire hawser e.g. Figure 71. Therefore only two test runs with the load recording equipment were made and then the load cell was removed and the computer logging the Xsens data was moved into the model thereby removing all cabling to the carriage. The wave frequency was set at 0.8Hz and the 1:10.67 circular buoy was used, repeated once. Over the 45s test the load fluctuated from a minimum of 3.6N to a maximum of 4.3N. The repeat runs show close agreement, as illustrated in Figure 72; test 1 resulted in a RMS of 3.97N and test 2 a RMS of 3.95N. These values scale up to a full scale lifeboat's hawser load of 4.8kN in 4s period waves.

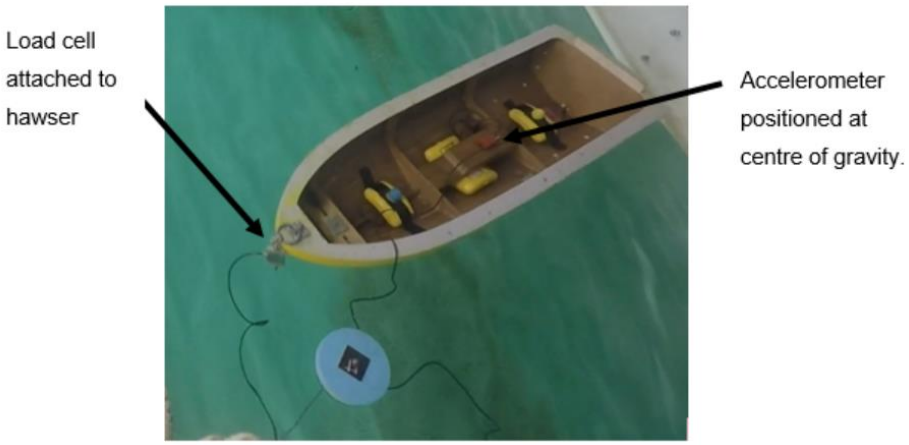

Figure 71: Location of the motion and loading recording on Tamar model.

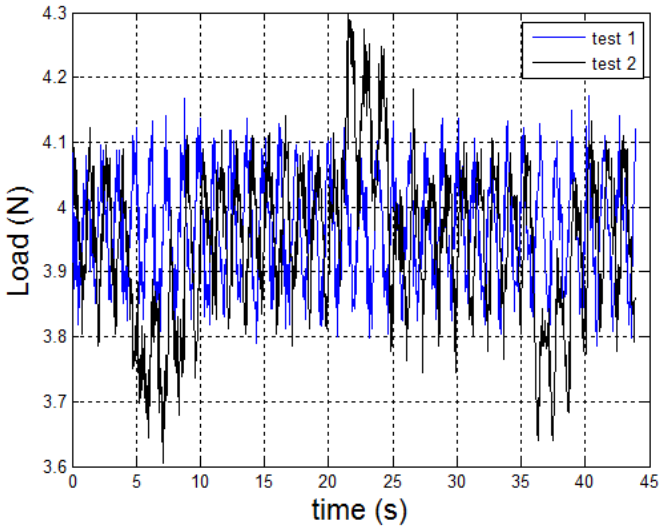

Figure 72: Recorded hawser load.

C.3 Sea trials at Yarmouth Harbour

The peak load on the hawser was measured using a 12 tonne load shackle with a 5900 Portable Load Indicator kindly loaned, free of charge, from Strainstall Ltd. on the Isle of Wight. The shackle was placed between two upper hawser ropes and the Indicator placed on deck as illustrated in Figure 73. The Indicator records in increments of 0.1tonnes, i.e. 100kg steps, and returns the peak reading during the recorded period.

The peak load recorded by the shackle load cell was 0.02, which can be seen in the photograph in Figure 73b, this equates to a reading of 20kg or a load of 196N. A test of the peak load, whilst the lifeboat was reversed on half power, gave a reading of 0.33 equating to 3.2kN force on the hawser.

Figure 73: Load shackle and Portable Load Indicator.

Appendix D Parameters of Chilworth flume tests

D.1 Series 1: August 2014

1:40 scale Severn all-weather lifeboat, varied hawser length. Depth set using an adjustable weir, set at B=bottom, M=middle and T=top. SB = Small Buoy, BB= Big Buoy, FB = Fixed Buoy.

						Upper	Lower	Water	Flow	Flow	Mass Flow	Full scale	Full scale
Test	**Date**	**Time**	**Buoy**	**Weir**	**Pump**	**hawser**	**hawser**	**depth**	**time**	**speed**	**Rate**	**depth**	**flow**
			(scale)	(setting)	(setting)	(m)	(m)	(m)	(s)	(m/s)	(kg/s)	(m)	(m/s)
SB1	18.08.14	14:00	1:40	B	half	0.200	0.250	0.165	4.1	0.24	54.61	6.60	1.52
SB2	18.08.14	14:25	1:40	M	half	0.200	0.250	0.190	4.3	0.24	62.88	7.60	1.52
SB3	18.08.14	14:45	1:40	T	half	0.200	0.250	0.240	5.1	0.20	66.19	9.60	1.26
SB4	18.08.14	15:20	1:40	T	full	0.200	0.250	0.251	4.3	0.23	79.61	10.04	1.45
SB5	18.08.14	15:50	1:40	M	full	0.200	0.250	0.220	3.2	0.31	94.04	8.80	1.96
SB6	18.08.14	16:20	1:40	B	full	0.200	0.250	0.202	3.1	0.32	89.13	8.08	2.02
SB7	19.08.14	11:50	1:40	B	half	0.150	0.175	0.168	4.1	0.24	55.60	6.72	1.52
SB8	19.08.14	13:45	1:40	M	half	0.150	0.175	0.195	4.8	0.21	56.47	7.80	1.33
SB9	19.08.14	14:00	1:40	T	half	0.150	0.175	0.238	5.9	0.17	55.79	9.52	1.08
SB10	19.08.14	14:15	1:40	T	full	0.150	0.175	0.235	6.2	0.16	51.85	9.40	1.01
SB11	19.08.14	14:40	1:40	M	full	0.150	0.175	0.195	4.4	0.23	61.84	7.80	1.45
SB12	19.08.14	15:15	1:40	B	full	0.150	0.175	0.180	3.4	0.30	74.46	7.20	1.90
SB13	19.08.14	15:45	1:40	B	half	0.125	0.150	0.185	3.4	0.30	76.53	7.40	1.90
SB14	19.08.14	16:10	1:40	M	half	0.125	0.150	0.210	3.7	0.27	78.19	8.40	1.71
SB15	19.08.14	16:20	1:40	T	half	0.125	0.150	0.245	4.4	0.23	77.70	9.80	1.45
SB16	19.08.14	16:30	1:40	T	full	0.125	0.150	0.255	4.1	0.24	84.39	10.20	1.52
SB17	19.08.14	16:45	1:40	M	full	0.125	0.150	0.215	3.2	0.31	91.91	8.60	1.96
SB18	19.08.14	16:55	1:40	B	full	0.125	0.150	0.195	3.0	0.33	88.73	7.80	2.09
BB19	20.08.14	10:00	1:20	B	half	0.200	0.250	0.185	3.2	0.31	79.08	7.40	1.96
BB20	20.08.14	10:10	1:20	M	half	0.200	0.250	0.205	3.8	0.26	73.50	8.20	1.64
BB21	20.08.14	10:20	1:20	T	half	0.200	0.250	0.250	4.7	0.21	72.39	10.00	1.33
BB22	20.08.14	10:50	1:20	T	full	0.200	0.250	0.265	3.9	0.26	95.01	10.60	1.64
BB23	20.08.14	11:10	1:20	M	full	0.200	0.250	0.220	3.2	0.31	94.04	8.80	1.96

Test	Date	Time	Buoy	Weir	Pump	Upper hawser	Lower hawser	Water depth	Flow time	Flow speed	Mass Flow Rate	Full scale depth	Full scale flow
			(scale)	(setting)	(setting)	(m)	(m)	(m)	(s)	(m/s)	(kg/s)	(m)	(m/s)
BB24	20.08.14	11:20	1:20	B	full	0.200	0.250	0.200	2.8	0.35	96.52	8.00	2.21
BB25	20.08.14	12:40	1:20	B	half	0.150	0.175	0.185	3.3	0.30	76.53	7.40	1.90
BB26	20.08.14	12:50	1:20	M	half	0.150	0.175	0.208	3.6	0.28	80.31	8.32	1.77
BB27	20.08.14	13:05	1:20	T	half	0.150	0.175	0.260	4.8	0.21	75.29	10.40	1.33
BB28	20.08.14	13:20	1:20	T	full	0.150	0.175	0.275	3.8	0.27	102.39	11.00	1.71
BB29	20.08.14	13:35	1:20	M	full	0.150	0.175	0.232	3.1	0.32	102.37	9.28	2.02
BB30	20.08.14	13:45	1:20	B	full	0.150	0.175	0.215	2.9	0.35	103.76	8.60	2.21
BB31	20.08.14	15:10	1:20	B	half	0.125	0.150	0.196	3.3	0.30	81.08	7.84	1.90
BB32	20.08.14	15:25	1:20	M	half	0.125	0.150	0.220	3.8	0.26	78.87	8.80	1.64
BB33	20.08.14	15:40	1:20	T	half	0.125	0.150	0.262	4.5	0.22	79.48	10.48	1.39
BB34	20.08.14	15:50	1:20	T	full	0.125	0.150	0.275	4.1	0.24	91.01	11.00	1.52
BB35	20.08.14	16:05	1:20	M	full	0.125	0.150	0.233	3.2	0.31	99.60	9.32	1.96
BB36	20.08.14	16:15	1:20	B	full	0.125	0.150	0.210	2.9	0.35	101.35	8.40	2.21
FB2	21.08.14	12:20	none	B	half	0.150		0.193	3.3	0.31	82.50	7.72	1.96
FB3	21.08.14	13:55	none	M	half	0.150		0.219	3.9	0.26	78.52	8.76	1.64
FB4	21.08.14	14:15	none	T	half	0.150		0.261	4.8	0.21	75.58	10.44	1.33
FB5	21.08.14	14:25	none	T	full	0.150		0.270	4.2	0.24	89.35	10.80	1.52
FB6	21.08.14	14:35	none	M	full	0.150		0.220	3.0	0.33	100.11	8.80	2.09
FB7	21.08.14	14:45	none	B	full	0.150		0.200	2.9	0.35	96.52	8.00	2.21
FB8	21.08.14	15:05	none	B	half	0.125		0.187	3.3	0.31	79.94	7.48	1.96
FB9	21.08.14	15:20	none	M	half	0.125		0.207	3.7	0.27	77.07	8.28	1.71
FB10	21.08.14	15:30	none	T	half	0.125		0.250	4.6	0.22	75.84	10.00	1.39
FB13	21.08.14	10:30	none	T	full	0.125		0.260	4.0	0.25	89.63	10.40	1.58
FB14	22.08.14	10:50	none	M	full	0.125		0.222	3.0	0.33	101.02	8.88	2.09
FB15	22.08.14	11:00	none	B	full	0.125		0.200	2.8	0.36	99.28	8.00	2.28
FB16	22.08.14	12:50	none	B	half	0.200		0.182	3.5	0.29	72.78	7.28	1.83
FB17	22.08.14	13:00	none	M	half	0.200		0.203	4.0	0.25	69.98	8.12	1.58
FB18	22.08.14	13:10	none	T	half	0.200		0.245	4.7	0.21	70.95	9.80	1.33
FB19	22.08.14	13:30	none	T	full	0.200		0.260	3.9	0.25	89.63	10.40	1.58

Test	Date	Time	Buoy	Weir	Pump	Upper hawser	Lower hawser	Water depth	Flow time	Flow speed	Mass Flow Rate	Full scale depth	Full scale flow
			(scale)	(setting)	(setting)	(m)	(m)	(m)	(s)	(m/s)	(kg/s)	(m)	(m/s)
FB22	22.08.14	14:40	none	B	full	0.200		0.196	3.0	0.33	89.19	7.84	2.09
FB23	22.08.14	14:55	none	M	full	0.200		0.220	3.4	0.30	91.01	8.80	1.90
FB24	22.08.14	15:20	none	T	full	0.125		0.255	4.6	0.22	77.36	10.20	1.39
FB25	22.08.14	15:30	none	M	full	0.125		0.217	3.3	0.31	92.76	8.68	1.96
FB26	22.08.14	15:45	none	B	full	0.125		0.196	3.2	0.29	78.38	7.84	1.83

D.2 Series 2: April 2015

1:40 scale Severn all-weather lifeboat, different 1:40 scale buoy shapes. Tests with moored boat attached to SPM and buoy only.
ADB = Additional Different Shaped Buoys, NBB = No Buoy or Boat.

Test	Date	Time	Buoy	hawser	hawser	depth	time	speed	Rate	depth	flow
			(shape)	(m)	(m)	(m)	(s)	(m/s)	(kg/s)	(m)	(m/s)
Buoy and boat, no Xsens											
ADB1	13.04.15	16:10	circle	0.15	0.175	0.204	3.5	0.29	81.65	8.16	1.83
ADB2	13.04.15	16:30	octagon	0.15	0.175	0.203	3.6	0.28	78.45	8.12	1.77
ADB3	13.04.15	16:45	hexagon	0.15	0.175	0.203	3.7	0.27	75.65	8.12	1.71
ADB4	13.04.15	17:00	square	0.15	0.175	0.203	3.8	0.27	75.65	8.12	1.71
ADB5	13.04.15	17:15	triangle	0.15	0.175	0.203	3.6	0.28	78.45	8.12	1.77
ADB6	13.04.15	17:30	wing	0.15	0.175	0.203	3.6	0.28	78.45	8.12	1.77
Repeat 1 to 6											
ADB7	14.04.15	16:50	circle	0.15	0.175	0.204	3.5	0.29	81.65	8.16	1.83
ADB8	14.04.15	17:05	octagon	0.15	0.175	0.203	3.6	0.28	78.45	8.12	1.77
ADB9	14.04.15	17:20	hexagon	0.15	0.175	0.203	3.7	0.27	75.65	8.12	1.71
ADB10	14.04.15	17:30	square	0.15	0.175	0.203	3.8	0.27	75.65	8.12	1.71
ADB11	14.04.15	17:45	triangle	0.15	0.175	0.203	3.6	0.28	78.45	8.12	1.77
ADB12	14.04.15	18:00	wing	0.15	0.175	0.203	3.6	0.28	78.45	8.12	1.77
Buoy only no boat attached											

Test	Date	Time	Buoy	hawser	hawser	depth	time	speed	Rate	depth	flow
			(shape)	(m)	(m)	(m)	(s)	(m/s)	(kg/s)	(m)	(m/s)
ADB13	15.04.15	10:32	circle	0.15	0.175	0.203	3.7	0.27	75.65	8.12	1.71
ADB14	15.04.15	10:43	octagon	0.15	0.175	0.202	3.8	0.27	75.27	8.08	1.71
ADB15	15.04.15	10:55	hexagon	0.15	0.175	0.202	3.9	0.26	72.49	8.08	1.64
ADB16	15.04.15	11:10	square	0.15	0.175	0.202	3.8	0.26	72.49	8.08	1.64
ADB17	15.04.15	11:25	triangle	0.15	0.175	0.201	3.7	0.27	74.90	8.04	1.71
ADB18	15.04.15	11:35	wing	0.15	0.175	0.201	3.6	0.27	74.90	8.04	1.71
Buoy and boat, with Xsens											
ADB25	15.04.15	14:50	circle	0.15	0.175	0.203	3.9	0.26	72.85	8.12	1.64
ADB26	15.04.15	15:00	octagon	0.15	0.175	0.203	3.6	0.28	78.45	8.12	1.77
ADB27	15.04.15	15:15	hexagon	0.15	0.175	0.202	3.6	0.28	78.06	8.08	1.77
ADB28	15.04.15	15:35	square	0.15	0.175	0.203	3.5	0.28	78.45	8.12	1.77
ADB29	15.04.15	16:15	triangle	0.15	0.175	0.203	3.6	0.28	78.45	8.12	1.77
ADB30	15.04.15	16:30	wing	0.15	0.175	0.204	3.5	0.28	78.84	8.16	1.77
Just load cell in water											
NBB1	16.04.15	10:50		load cells located at top left and right corner sinkers							
NBB2	16.04.15	11:00		moved clockwise							
NBB3	16.04.15	11:10		moved clockwise							
NBB4	16.04.15	10:20		moved clockwise							
NBB5	16.04.15	11:40		back to start position							
Repeat 25-30											
ADB43	17.04.15	10:45	circle	0.15	0.175	0.204	3.4	0.30	84.47	8.16	1.90
ADB44	17.04.15	11:10	octagon	0.15	0.175	0.204	3.4	0.30	84.47	8.16	1.90
ADB45	17.04.15	11:15	hexagon	0.15	0.175	0.204	3.4	0.29	81.65	8.16	1.83
ADB46	17.04.15	11:25	square	0.15	0.175	0.203	3.4	0.29	81.25	8.12	1.83
ADB47	17.04.15	11:35	triangle	0.15	0.175	0.203	3.5	0.29	81.25	8.12	1.83
ADB48	17.04.15	11:45	wing	0.15	0.175	0.203	3.4	0.29	81.25	8.12	1.83

D.3 Series 3: August 2015

1:40 scale Severn all-weather lifeboat, different 1:20 and 1:40 scale buoy shapes. Tests with moored boat attached to SPM and buoy only. DSB = Different Shaped and sized Buoys.

				Upper	Lower	Water	Flow	Flow	Mass Flow	Full scale	Full scale
Test	**Date**	**Time**	**Buoy**	**hawser**	**hawser**	**depth**	**time**	**speed**	**Rate**	**depth**	**flow**
			(shape)	(m)	(m)	(m)	(s)	(m/s)	(kg/s)	(m)	(m/s)
1:40 buoy with Xsens not recording											
DSB1	18.08.15	11:00	circle	0.15	0.175	0.203	3.2	0.32	88.59	8.12	2.00
DSB2	18.08.15	11:30	octagon	0.15	0.175	0.203	3.2	0.32	88.79	8.12	2.01
DSB3	18.08.15	12:45	hexagon	0.15	0.175	0.203	3.3	0.30	84.96	8.12	1.92
DSB4	18.08.15	13:15	square	0.15	0.175	0.203	3.2	0.31	87.16	8.12	1.97
DSB5	18.08.15	13:35	wing short	0.15	0.175	0.201	3.4	0.29	81.12	8.04	1.85
DSB6	18.08.15	14:00	wing long	0.15	0.175	0.201	3.2	0.31	85.47	8.04	1.95
1:40 buoy with no boat flow meter only											
DSB7	19.08.15	15:00	circle			0.201				8.04	
DSB8	19.08.15	15:15	octagon			0.201				8.04	
DSB9	19.08.15	15:30	hexagon			0.201				8.04	
DSB10	19.08.15	15:45	square			0.201				8.04	
DSB11	19.08.15	16:00	wing short			0.201				8.04	
DSB12	19.08.15	16:15	wing long			0.201				8.04	
Repeat 7-12											
DSB13	20.08.15	10:20	barrel			0.200				8.00	
DSB14	20.08.15	10:35	circle			0.200				8.00	
DSB15	20.08.15	10:50	octagon			0.200				8.00	
DSB16	20.08.15	11:30	hexagon			0.200				8.00	
DSB17	20.08.15	11:45	square			0.200				8.00	
DSB18	20.08.15	12:00	wing short			0.200				8.00	
DSB19	20.08.15	12:15	wing long			0.200				8.00	

				Upper	Lower	Water	Flow	Flow	Mass Flow	Full scale	Full scale
Test	**Date**	**Time**	**Buoy**	**hawser**	**hawser**	**depth**	**time**	**speed**	**Rate**	**depth**	**flow**
			(shape)	(m)	(m)	(m)	(s)	(m/s)	(kg/s)	(m)	(m/s)
DSB20	20.08.15	12:30	barrel			0.200				8.00	
Repeat 7-12											
DSB21	20.08.15	13:25	barrel			0.200				8.00	
DSB22	20.08.15	13:55	wing long			0.200				8.00	
DSB23	20.08.15	14:10	wing short			0.200				8.00	
DSB24	20.08.15	14:25	square			0.200				8.00	
DSB25	20.08.15	14:45	hexagon			0.200				8.00	
DSB26	20.08.15	15:00	octagon			0.200				8.00	
DSB27	20.08.15	15:15	circle			0.200				8.00	
1:20 scale buoy and riser only											
DSB28	21.08.15	11.25	circle			0.200	3.4	0.30	81.87	8.00	1.88
DSB29	21.08.15	12:10	octagon			0.200	3.3	0.31	84.35	8.00	1.93
DSB30	21.08.15	13:00	hexagon			0.200	3.4	0.29	80.69	8.00	1.85
DSB31	21.08.15	13:55	square			0.200	3.3	0.30	82.90	8.00	1.90
DSB32	21.0815	15:30	barrel			0.200	3.4	0.30	81.89	8.00	1.88
DSB33	21.08.15	15:40	wing			0.200	3.3	0.30	83.61	8.00	1.92
1:20 scale buoy, riser, hawser and Xsens											
DSB34	24.08.15	11:05	circle	0.30	0.400	0.200	3.4	0.29	79.16	8.00	1.82
DSB35	24.08.15	11:20	wing	0.30	0.400	0.200	3.5	0.32	87.98	8.00	2.02
DSB36	24.08.15	11:40	barrel	0.30	0.400	0.200	3.6	0.31	84.40	8.00	1.94
DSB37	24.08.15	12:00	square	0.30	0.400	0.200	3.7	0.29	79.16	8.00	1.82
DSB38	24.08.15	12:15	octagon	0.30	0.400	0.200	3.8	0.29	79.43	8.00	1.82
repeat DSB34 to DSB38											
DSB44	26.08.15	16:15	barrel	0.30	0.400	0.200	3.4	0.30	82.26	8.00	1.89
DSB45	26.08.15	16:25	wing	0.30	0.400	0.200	3.6	0.28	77.15	8.00	1.77
DSB46	26.08.15	16:35	square	0.30	0.400	0.200	3.6	0.28	76.77	8.00	1.76
DSB47	26.08.15	16:45	octagon	0.30	0.400	0.200	3.7	0.27	75.11	8.00	1.72
DSB48	26.08.15	17:00	circle	0.30	0.400	0.200	3.6	0.28	77.37	8.00	1.77

				Upper	Lower	Water	Flow	Flow	Mass Flow	Full scale	Full scale
Test	**Date**	**Time**	**Buoy**	**hawser**	**hawser**	**depth**	**time**	**speed**	**Rate**	**depth**	**flow**
			(shape)	(m)	(m)	(m)	(s)	(m/s)	(kg/s)	(m)	(m/s)
2nd repeat											
DSB49	26.08.15	10:40	circle	0.30	0.400	0.200	3.6	0.28	76.83	8.00	1.76
DSB50	26.08.15	11:25	octagon	0.30	0.400	0.200	3.7	0.27	73.73	8.00	1.69
DSB51	26.08.15	12:00	square	0.30	0.400	0.200	3.7	0.27	74.01	8.00	1.70
DSB52	26.08.15	13:00	wing	0.30	0.400	0.200	3.7	0.27	75.11	8.00	1.72
DSB53	26.08.15	14:00	barrel	0.30	0.400	0.200	3.3	0.31	84.27	8.00	1.93

Appendix E Scaling at 1:40 of RNLI Severn lifeboat, mooring parts and environmental factors

Severn Lifeboat Model scale									
			Full scale	**Length**	**Mass**	**Depth**	**Time**	**Velocity**	**Force**
	R=scale factor = 40			R	$\frac{\rho_m}{\rho_s R^3}$	R	$\frac{1}{\sqrt{R}}$	$\frac{1}{\sqrt{R}}$	$\frac{\rho_m}{\rho_s R^3}$
VESSEL	Displacement	kg	42,000		0.64				
WATER	Depth	m	2			0.05			
	Depth	m	5			0.13			
	Depth	m	10			0.25			
	Current	m/s	0.26					0.04	
	Current	m/s	1.28					0.20	
	Current	m/s	2.58					0.41	
CHAIN	Ground: mass	g/m	20,300		12.38				
	Riser: mass	g/m	12,500		7.63				
	Ground: diameter	mm	31	0.78					
	Riser: diameter	mm	26	0.65					
	Young's modulus	G Pa	180						4.4
MOORING RING	Mass	g	11900		0.18				
	Outer diameter	mm	52	1.30					
	Inner diameter	mm	187	4.68					
	R=scale factor = 40			R	$\frac{\rho_m}{\rho_s R^3}$	R	$\frac{1}{\sqrt{R}}$	$\frac{1}{\sqrt{R}}$	$\frac{\rho_m}{\rho_s R^3}$
	Total diameter	mm	291	7.28					
SHACKLE	Mass	g	7300		0.11				
	Width	mm	139	3.48					
	Height	mm	249	6.23					
HAWSER	Mass	g/m	220		0.13				

Severn Lifeboat Model scale									
			Full scale	**Length**	**Mass**	**Depth**	**Time**	**Velocity**	**Force**
	Young's modulus	G Pa	2						0.04
	Length: upper	mm	5,000	125					
	Length: lower	mm	6,000	150					
	Length: upper	mm	6,000	150					
	Length: lower	mm	7,000	175					
	Length: upper	mm	8,000	200					
	Length: lower	mm	10,000	250					
	Diameter	mm	44	1.1					
BUOY	Mass	kg	245		0.004				
	Height of segment	mm	500	13					
	Top diameter	mm	2,000	50					
	R=scale factor = 40			R	$\frac{\rho_m}{\rho_s R^3}$	R	$\frac{1}{\sqrt{R}}$	$\frac{1}{\sqrt{R}}$	$\frac{\rho_m}{\rho_s R^3}$
	Bottom diameter	mm	500	13					
SINKER	Mass	kg	3,230		0.05				
	Height	mm	600	15					
	Width	mm	1,500	38					
	Length	mm	1,500	38					

Appendix F Results of 1:40 scale Young's modulus testing flume materials

The Young's modulus for each material is the gradient of the strain vs. stress curves from the tested samples, examples of one sample per material type is presented in Figure 74. The calculations of the Youngs modulus and linear regression correlation coefficients are presented below: The strain is calculated as the ratio of extension to original gauge length and the stress (GPa) as the ratio of load (N) to the surface area of the material (m^2).

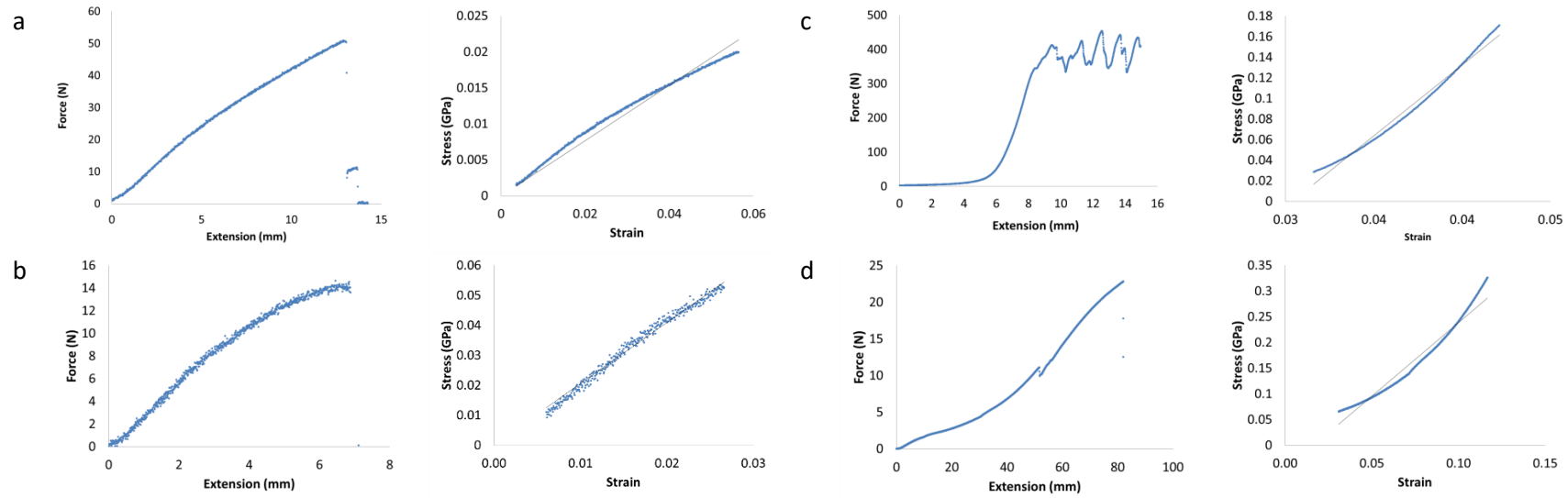

Figure 74: Stress vs. strain curves for flume test materials.
(a) 1.8mm nylon filled rubber (b) 0.5mm chain (c) 1.5mm wire rope (d) 0.2mm fishing wire.

Specimen		Gauge length (mm)	Max Load (N)	Max Extension (mm)	Young's Modulus (GPa)	Correlation coefficient
1.8 mm Nylon filled rubber test speed 5mm/min						
1		230	51	13	0.3837	0.9757
2		297	52	22	0.3377	0.9764
3		302	78	31	0.3329	0.9640
4		274	72	33	0.2964	0.9554
5		286	82	27	0.3145	0.9623
				Arithmetic mean	0.3330	
				Standard deviation	0.0327	
0.8 mm Chain test speed 5mm/min						
1		150	14	7.0	2.1030	0.9875
2		190	14	9.0	2.6170	0.9791
3		188	12	5.0	2.3129	0.9831
4		183	14	6.5	2.3835	0.9864
5		222	13	7.5	3.1801	0.9947
				Arithmetic mean	2.5193	
				Standard deviation	0.4125	
1.5 mm Steel wire rope test speed 5mm/min						
1		190	350	8.5	13.781	0.9852
2		180	600	8.5	14.997	0.9926
3		203	450	8.5	16.673	0.9912
4		192	150	failed		
5		321	380	10.0	14.624	0.9074
				Arithmetic mean	15.0188	
				Standard deviation	1.2145	
0.20 mm Fishing wire test speed 20mm/min						

Specimen		Gauge length	Max Load	Max Extension	Young's Modulus	Correlation
		(mm)	(N)	(mm)	(GPa)	coefficient
1		425	23	82	2.868	0.9608
2		506	22	101	3.481	0.9762
3		441	28	144	4.132	0.9714
4		456	17	74	3.381	0.9714
5		386	22	130	3.055	0.9714
				Arithmetic mean	3.3834	
				Standard deviation	0.4856	

Appendix G Parameters of Solent University regular wave tests

Wave RMS is calculated from the recorded wave height, wave amplitude is taken from the fft of the data.

G.1 Series 1: April 2016

Test	Date	Time	Buoy (scale)	Buoy (shape)	Wave frequency (Hz)	Wave RMS (m)	Wave amplitude (m)
55	28.04.16	10:33	1:10.67	circle	0.8	0.016	0.022
56	28.04.16	10:45	1:10.67	circle	0.8	0.016	0.022
57	28.04.16	10:56	1:10.67	circle	0.9	0.015	0.015
58	28.04.16	11:13	1:10.67	circle	0.9	0.015	0.015
59	28.04.16	11:23	1:10.67	circle	1.0	0.015	0.020
60	28.04.16	11:38	1:10.67	circle	1.0	0.015	0.020
61	28.04.16	11:54	1:10.67	circle	1.1	0.015	0.015
62	28.04.16	12:06	1:10.67	circle	1.1	0.015	0.014
79	29.04.16	09:21	1:10.67	octagon	0.8	0.016	0.022
80	29.04.16	09:55	1:10.67	octagon	0.9	0.015	0.015
81	29.04.16	10:09	1:10.67	octagon	1.0	0.014	0.020
82	29.04.16	10:22	1:10.67	octagon	1.1	0.015	0.015
83	29.04.16	10:35	1:10.67	octagon	0.8	0.016	0.022
84	29.04.16	10:45	1:10.67	octagon	0.9	0.015	0.014
85	29.04.16	10:55	1:10.67	octagon	1.0	0.014	0.020
86	29.04.16	11:08	1:10.67	octagon	1.1	0.015	0.015
95	29.04.16	14:15	1:10.67	square	0.8	0.015	0.021
96	29.04.16	14:25	1:10.67	square	0.9	0.015	0.015
97	29.04.16	14:33	1:10.67	square	1.0	0.014	0.020
98	29.04.16	14:43	1:10.67	square	1.1	0.015	0.014
99	29.04.16	14:54	1:10.67	square	0.8	0.016	0.022

Test	Date	Time	Buoy (scale)	Buoy (shape)	Wave frequency (Hz)	Wave RMS (m)	Wave amplitude (m)
100	29.04.16	15:02	1:10.67	square	0.9	0.015	0.015
101	29.04.16	15:11	1:10.67	square	1.0	0.015	0.020
102	29.04.16	15:20	1:10.67	square	1.1	0.015	0.015

G.2 Series 2: August 2016

Test	Date	Time	Buoy (scale)	Buoy (shape)	Wave frequency (Hz)	Wave RMS (m)	Wave amplitude (m)
106	22.08.16	13:09	1:10.67	circle	0.8	0.017	0.024
107	22.08.16	14:47	1:10.67	circle	0.9	0.016	0.016
108	22.08.16	14:57	1:10.67	circle	1.0	0.016	0.023
110	22.08.16	15:22	1:10.67	circle	1.1	0.019	0.022
111	22.08.16	15:37	1:10.67	octagon	0.8	0.018	0.024
112	22.08.16	15:49	1:10.67	octagon	0.9	0.016	0.017
113	22.08.16	16:03	1:10.67	octagon	1.0	0.016	0.022
114	22.08.16	16:18	1:10.67	octagon	1.1	0.019	0.021
115	22.08.16	16:31	1:10.67	square	0.8	0.018	0.024
116	22.08.16	16:43	1:10.67	square	0.9	0.018	0.024
117	22.08.16	16:54	1:10.67	square	1.0	0.016	0.022
118	22.08.16	17:08	1:10.67	square	1.1	0.018	0.021
123	22.08.16	10:52	1:10.67	hexagon	0.8	0.018	0.025
124	22.08.16	11:05	1:10.67	hexagon	0.8	0.018	0.025
125	22.08.16	11:19	1:10.67	hexagon	0.8	0.018	0.025
126	22.08.16	11:32	1:10.67	hexagon	0.9	0.016	0.017
127	22.08.16	11:46	1:10.67	hexagon	0.9	0.016	0.016
128	22.08.16	12:10	1:10.67	hexagon	0.9	0.017	0.017
129	22.08.16	12:24	1:10.67	hexagon	1.0	0.016	0.021
130	22.08.16	12:39	1:10.67	hexagon	1.0	0.016	0.022
131	22.08.16	12:50	1:10.67	hexagon	1.0	0.016	0.021
132	22.08.16	13:02	1:10.67	hexagon	1.1	0.019	0.022
133	22.08.16	13:12	1:10.67	hexagon	1.1	0.019	0.022
134	22.08.16	13:26	1:10.67	hexagon	1.1	0.019	0.022
135	23.08.16	14:41	1:5.33	circle	0.8	0.019	0.026

Test	Date	Time	Buoy (scale)	Buoy (shape)	Wave frequency (Hz)	Wave RMS (m)	Wave amplitude (m)
136	23.08.16	14:53	1:5.33	circle	0.8	0.018	0.026
137	23.08.16	15:03	1:5.33	circle	0.8	0.018	0.025
138	23.08.16	15:13	1:5.33	circle	0.9	0.017	0.018
139	23.08.16	15:23	1:5.33	circle	0.9	0.017	0.018
140	23.08.16	15:34	1:5.33	circle	0.9	0.017	0.018
141	23.08.16	15:45	1:5.33	circle	1.0	0.017	0.023
142	23.08.16	15:56	1:5.33	circle	1.0	0.016	0.022
143	23.08.16	16:08	1:5.33	circle	1.0	0.017	0.023
146	24.08.16	10:25	1:5.33	circle	1.1	0.017	0.019
147	24.08.16	10:35	1:5.33	circle	1.1	0.018	0.021
148	24.08.16	10:46	1:5.33	circle	1.1	0.018	0.020
149	24.08.16	10:57	1:5.33	octagon	0.8	0.017	0.023
150	24.08.16	11:10	1:5.33	octagon	0.8	0.017	0.023
151	24.08.16	11:20	1:5.33	octagon	0.8	0.016	0.023
152	24.08.16	11:29	1:5.33	octagon	0.9	0.016	0.017
153	24.08.16	11:40	1:5.33	octagon	0.9	0.016	0.017
154	24.08.16	11:50	1:5.33	octagon	0.9	0.016	0.017
156	24.08.16	12:13	1:5.33	octagon	1.0	0.017	0.024
157	24.08.16	12:24	1:5.33	octagon	1.0	0.018	0.025
158	24.08.16	12:34	1:5.33	octagon	1.0	0.020	0.023
159	24.08.16	14:06	1:5.33	octagon	1.1	0.019	0.020
160	24.08.16	14:18	1:5.33	octagon	1.1	0.019	0.021
161	24.08.16	14:30	1:5.33	octagon	1.1	0.019	0.022
163	24.08.16	14:55	1:5.33	hexagon	0.8	0.016	0.023
164	24.08.16	15:04	1:5.33	hexagon	0.8	0.016	0.022
165	24.08.16	15:14	1:5.33	hexagon	0.8	0.016	0.022
166	24.08.16	15:25	1:5.33	hexagon	0.9	0.017	0.018

Test	Date	Time	Buoy (scale)	Buoy (shape)	Wave frequency (Hz)	Wave RMS (m)	Wave amplitude (m)
167	24.08.16	15:37	1:5.33	hexagon	0.9	0.016	0.017
168	24.08.16	15:49	1:5.33	hexagon	0.9	0.016	0.016
169	24.08.16	15:59	1:5.33	hexagon	1.0	0.017	0.023
170	24.08.16	16:08	1:5.33	hexagon	1.0	0.018	0.025
171	24.08.16	16:18	1:5.33	hexagon	1.0	0.018	0.025
172	24.08.16	16:27	1:5.33	hexagon	1.1	0.020	0.024
173	24.08.16	16:37	1:5.33	hexagon	1.1	0.022	0.023
174	24.08.16	16:47	1:5.33	hexagon	1.1	0.020	0.022
175	25.08.16	09:44	1:5.33	square	0.8	0.017	0.023
176	25.08.16	09:55	1:5.33	square	0.8	0.017	0.023
177	25.08.16	10:08	1:5.33	square	0.8	0.017	0.023
178	25.08.16	10:16	1:5.33	square	0.9	0.017	0.018
179	25.08.16	10:26	1:5.33	square	0.9	0.017	0.018
180	25.08.16	10:39	1:5.33	square	0.9	0.016	0.017
181	25.08.16	10:49	1:5.33	square	1.0	0.017	0.024
182	25.08.16	11:06	1:5.33	square	1.0	0.019	0.026
183	25.08.16	11:18	1:5.33	square	1.0	0.019	0.026
184	25.08.16	11:30	1:5.33	square	1.1	0.020	0.023
185	25.08.16	11:40	1:5.33	square	1.1	0.021	0.024
186	25.08.16	11:51	1:5.33	square	1.1	0.020	0.023
190	25.08.16	14:05	1:5.33	wing	0.8	0.017	0.024
191	25.08.16	14:15	1:5.33	wing	0.8	0.017	0.023
192	25.08.16	14:25	1:5.33	wing	0.8	0.017	0.023
193	25.08.16	14:41	1:5.33	wing	0.9	0.016	0.016
194	25.08.16	14:52	1:5.33	wing	0.9	0.016	0.017
195	25.08.16	15:02	1:5.33	wing	0.9	0.016	0.017
196	25.08.16	15:13	1:5.33	wing	1.0	0.019	0.026

Test	Date	Time	Buoy (scale)	Buoy (shape)	Wave frequency (Hz)	Wave RMS (m)	Wave amplitude (m)
197	25.08.16	15:23	1:5.33	wing	1.0	0.019	0.026
198	25.08.16	15:33	1:5.33	wing	1.0	0.018	0.025
199	25.08.16	15:48	1:5.33	wing	1.1	0.020	0.022
200	25.08.16	15:58	1:5.33	wing	1.1	0.019	0.021
201	25.08.16	16:08	1:5.33	wing	1.1	0.021	0.023
202	26.08.16	09:21	1:10.67	wing	0.8	0.017	0.024
203	26.08.16	09:31	1:10.67	wing	0.8	0.017	0.023
204	26.08.16	09:41	1:10.67	wing	0.8	0.017	0.023
205	26.08.16	09:52	1:10.67	wing	0.9	0.017	0.018
206	26.08.16	10:03	1:10.67	wing	0.9	0.017	0.018
207	26.08.16	10:22	1:10.67	wing	0.9	0.017	0.017
208	26.08.16	10:39	1:10.67	wing	1.0	0.017	0.023
209	26.08.16	10:49	1:10.67	wing	1.0	0.017	0.023
210	26.08.16	11:01	1:10.67	wing	1.0	0.017	0.024
211	26.08.16	11:12	1:10.67	wing	1.1	0.017	0.024
212	26.08.16	11:24	1:10.67	wing	1.1	0.021	0.024
213	26.08.16	11:34	1:10.67	wing	1.1	0.021	0.025

Appendix H Scaling at 1:10.67 of RNLI Tamar lifeboat, mooring parts and environmental factors.

Tamar Lifeboat Model scale									
			Full scale	**Length**	**Mass**	**Depth**	**Time**	**Velocity**	**Force**
	R=scale factor = 10.67			R	$\frac{\rho_m}{\rho_s R^3}$	R	$\frac{1}{\sqrt{R}}$	$\frac{1}{\sqrt{R}}$	$\frac{\rho_m}{\rho_s R^3}$
VESSEL	Displacement	kg	32,000		25.7				
WATER	Depth	m	19			1.8			
	Wave height	m	0.53	0.05					
	Wave period	s	3.0				0.92		
	Wave period	s	3.3				1.01		
	Wave period	s	3.6				1.10		
	Wave period	s	3.7				1.13		
CHAIN	Riser: mass	g/m	12,500		107.36				
	Riser: diameter	mm	26	2.44					
	Riser: length	Mm	64,000	601					
	Young's modulus	G Pa	180						16.48
MOORING RING	Mass	g	11,900		9.59				
	Outer diameter	mm	52	4.88					
	Inner diameter	mm	187	17.54					
	Total diameter	mm	291	27.30					
SHACKLE	Mass	g	7,300		5.88				
	Width	mm	139	13.04					
	Height	mm	249	23.36					
	R=scale factor = 10.67			R	$\frac{\rho_m}{\rho_s R^3}$	R	$\frac{1}{\sqrt{R}}$	$\frac{1}{\sqrt{R}}$	$\frac{\rho_m}{\rho_s R^3}$
HAWSER	Mass	g/m	0.22		1.89				
	Young's modulus	G Pa	2						0.14
	Length: upper	mm	6,000	563					
	Length: lower	mm	7,000	657					

Tamar Lifeboat Model scale									
			Full scale	**Length**	**Mass**	**Depth**	**Time**	**Velocity**	**Force**
	Diameter	mm	44	4.1					
BUOY	Mass	kg	245		0.197				
	Height of segment	mm	500	47					
	Top diameter	mm	2,000	188					
	Bottom diameter	mm	500	47					

Appendix I **Results of Young's modulus testing, wave materials**

The Young's modulus for each material is the gradient of the strain vs. stress curves from the tested samples, examples of which are presented in Figure 75. The strain is calculated as the ratio of extension to original gauge length and the stress (GPa) as the ratio of load (N) to the surface area of the material (m^2).

(a)

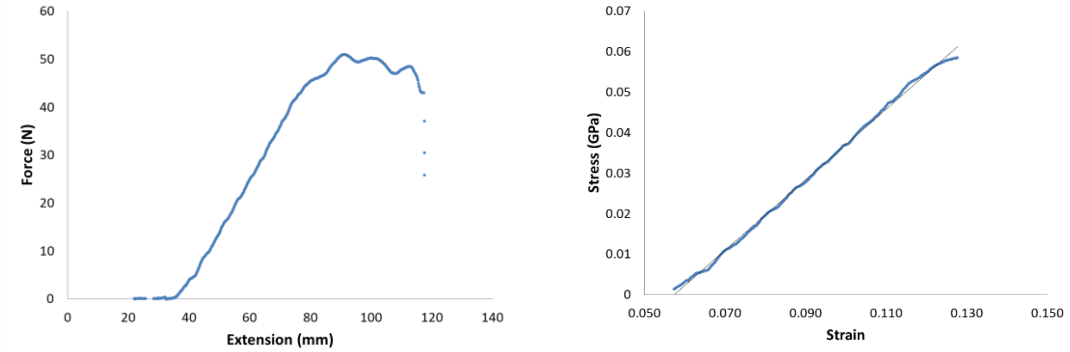

(b)

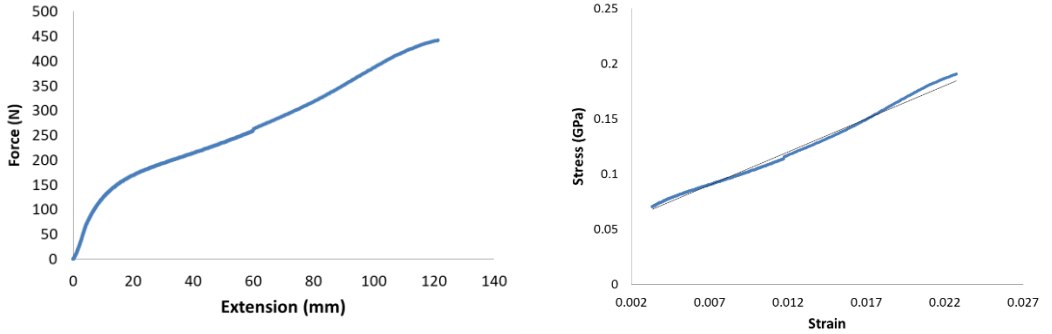

Figure 75: Young's modulus for wave experiment materials (a) 1.0mm fishing wire (b) 2.0mm chain.

Specimen		Gauge length (mm)	Max Load (N)	Max Extension (mm)	Young's Modulus	Correlation coefficient
1.0 mm fishing wire 100mm/min						
1		640	51	92	0.8735	0.9906
2		640	43	53	0.8330	0.9955
3		553	38	37	0.7594	0.9916
				Arithmetic mean	0.8220	
				Standard deviation	0.0578	
2.0 mm brass chain at 20 mm/s						
1		510	433	116.0	5.9863	0.9888
2		490	450	115.0	6.1707	0.9951
3		520	383	105.0	5.8919	0.9880
				Arithmetic mean	6.0163	
				Standard deviation	0.1418	

Bibliography

1.1 Catherine J. Hollyhead, Nicholas C. Townsend, James I.R. Blake. "Experimental investigations into the current-induced motion of a lifeboat at a single point mooring." *Ocean Engineering* 146 (2017): 192-201.

Experimental investigations into the current-induced motion of a lifeboat at a single point mooring.

Catherine J. Hollyhead*, Nicholas C. Townsend, James I.R. Blake.

Faculty of Engineering and the Environment, University of Southampton, UK.

* Corresponding author: cjh1g08@soton.ac.uk

ABSTRACT

This paper presents a series of model experiments on the current-induced motions of a 1:40 scale lifeboat at a single point mooring (SPM). The influence upon vessel and buoy motion of the mooring configuration factors of (a) three mooring line (hawser) lengths, (b) four buoy shapes and (c) two buoy sizes have been investigated. A motion tracking algorithm was successfully employed and validated against data from an inertial measuring unit allowing small scale testing without the influence of instrument cabling. The results show that the dominant translational motion, of the model lifeboat at a SPM, is sway and the rotational motion is yaw, with double pendulum-like fishtailing behaviour prevalent. Increasing the hawser length, when no buoy was present, resulted in an increase in the vessel's sway velocity. No significant effects on vessel motion were observed from changes in the shape of the 1:40 and 1:20 scale buoys. However, the presence and increasing size of the buoy was found to increase the sway velocity of the buoy and reduce the motions of the model lifeboat. These results suggest that changes in buoy size influence the motions of the model lifeboat which may enable mooring efficacy to be improved.

Key words:

Single point mooring (SPM), Moored ship responses, Buoy shape, Lifeboat, Tank testing.

Introduction

1.1 Motivation

A Single Point Mooring (SPM), defined by the American Bureau of Shipping as “a system which permits a vessel to weathervane while the vessel is moored to a fixed or floating structure anchored to the seabed by a rigid or an articulated structural system or by catenary spread mooring” (ABS, 2014), allows a vessel to self-align to the prevailing waves and reduce the mooring hawser load compared to that if its heading was constrained (Schellin, 2003; Oil Companies International Marine Forum, 2008). To date, the motions of large scale tankers at SPM’s, in deep off-shore waters, has been extensively investigated, due to the expansion of offshore oil and gas extraction (Gaythwaite, 2004; Fan et al., 2017).

At the smaller scale, e.g., boat lengths of less than 20m, there is limited published data on the efficacy of SPM moorings. There are significant numbers of SPM moored boats around the world, including forty belonging to the Royal National Lifeboat Institution (RNLI) and 389 listed marinas in the U.K (Which-Marina, 2015), which employ a variety of hawser lengths and buoy shapes, including spherical, cylindrical, barrel and modular. Coupled with the numerous media reports of yachts breaking free from their moorings resulting in damage and/or rescue crews being called out (for example (BBC, 2008; Percuil River Moorings Ltd., 2010; BBC, 2012; IWCP, 2012; BBC, 2013; SeaSurveys, 2013; Yachting and Boating World, 2016a; Yachting and Boating World, 2016b). In addition the U.K’s Marine Accident Investigation Branch have reported that, in the ten year period to 2001, eighty five fishermen lost their lives of which six were due to “whiplash from failed mooring lines, mooring lines slipping from fairleads or being struck by failed mooring ropes” (Lang, 2001). There is a need to understand the motion responses of small vessels at SPM moorings.

1.2 Background

The displacement of a rigid floating body can be described by six degrees of freedom: the translational motions along the axes of surge, sway and heave and the rotational ones around them of roll, pitch and yaw Fig. 1. For an unconstrained vessel these can be subdivided into oscillatory (heave, pitch and roll) that invoke restoring forces due to a change in the vessel's equilibrium displacement and non-oscillatory (surge, sway and yaw), (van Dorn, 1974). However when a vessel is moored at a SPM the catenary mooring chain provides a restoring force and oscillations can additionally occur in surge, sway and yaw, each mode with its own natural frequency providing the potential for large amplitude motions at their resonant frequencies (van Dorn, 1974). One of the observed behaviours in wind and current, both in experiments and from mathematical modelling, is termed "fishtailing" (e.g. Aghamohammadi and Thompson, 1990; Luai and Zhi, 2013; Schellin, 2003; Sharma et al., 1988; Wang et al., 2007; Wichers, 1988). This slowly varying drift motion, in the horizontal plane, is described by a combination of the oscillatory motions of surge, sway and yaw around the buoy (Fig. 2).

Experiments performed using model offshore tankers in deep water show this swinging double pendulum-like motion can be reduced by reducing the hawser length (Pinkster and Remery, 1975) or increasing the hawser tension (Sorheim, 1980). A literature review has found numerous publications detailing experimental data on the motion responses of offshore tankers at SPM but only one relating to small vessels which examined the motion of a fishing boats moored at jetties (Oosugi *et. al.*, 2007). The authors are unaware of any literature presenting experimental data on the effect of buoy shape or buoy size upon the motions of small vessels, such as those of the RNLI, stationed at catenary SPM in coastal harbours.

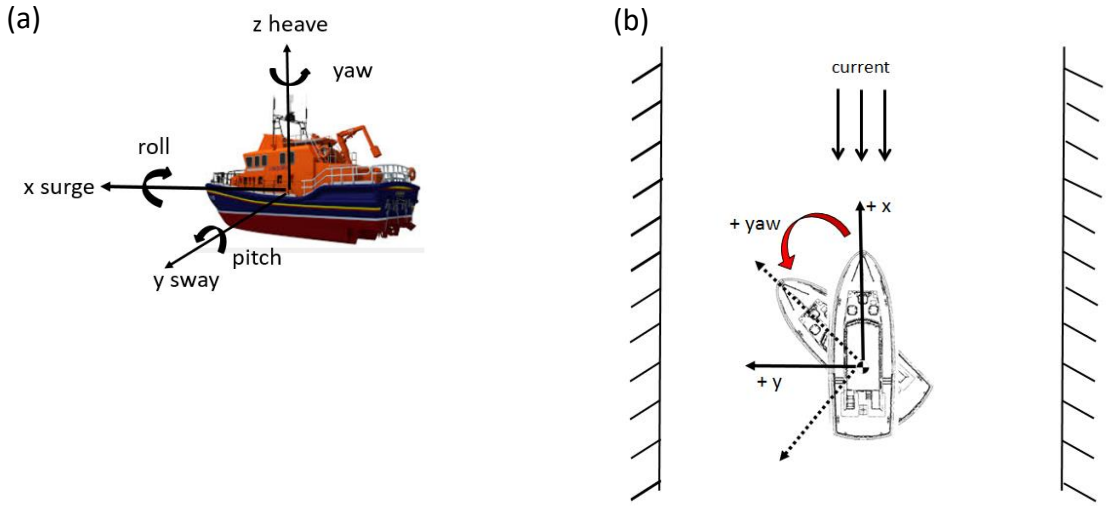

Fig. 1: The right handed frame of reference in the flume (a) three-dimensional and (b) two-dimensional representations.

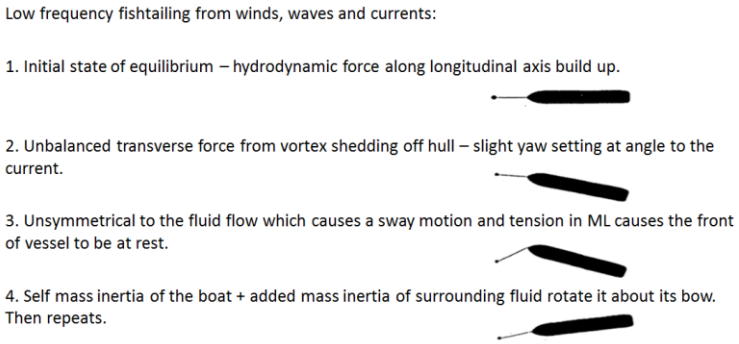

Fig. 2: Fishtailing motion of a vessel at a single point mooring adapted from Aghamohammadi and Thompson (1990).

1.3 Paper Contribution

This paper presents the results from a series of 1:40 model scale experimental investigations into the effect of hawser length, buoy scale and shape on small boats (considered sub 20m) with free catenary SPM configurations (i.e., without the use of fixed spring-mass-damper mooring line). The paper structure is as follows; In Section 2 the experimental setup and methodology is described. In Section 3 the experimental results are presented and discussed in Section 4. The conclusions are presented in Section 5.

Methodology

2.1 Experimental Setup

A series of 1:40 model scale experimental investigations into the effect of hawser length, buoy scale and buoy shape on small boats (considered sub 20 m) with a free catenary SPM configuration were conducted in the circulatory flume at the Chilworth research laboratory, University of Southampton (21 m in length, 1.35 m width and depths up to 0.4 m). The flume is a conventional gravity fed system in which water is lifted from a large sump via three centrifugal pumps each with a radial clock valve to control the flow rates (Myers and Bahaj, 2010).

When conducting ship tank experiments it is recognised that gravity forces predominate in free-surface flows (Hughes, 2005) and Froude similitude was used to determine the model scales. The geometric scaling factor, R, was defined as the ratio of the full scale length divided by the model length which also defines the depth scaling. The flow velocity was scaled at $1/\sqrt{R}$. In this particular case of model testing cables in water it is usual to violate exact geometric scaling for practical reasons however the correct value for the Young's modulus of the material should be used as its violation, in dynamic testing, is extremely significant (Papazoglou et al., 1990). The ground and riser chains were scaled using the Cauchy criterion which facilitates the similitude of the ratio of inertial to elastic forces using the Young's modulus of the material (Hughes, 2005). Tensile tests, using an Instron E-Series Circumferential Extensometer, yielded a required diameter using the Cauchy criteria of 0.92 mm compared to a geometrically scaled diameter of 0.65 mm.

The experimental setup, a four sinker SPM configuration arrangement, as shown in Fig. 3a, was chosen to represent those of the RNLI. The model (Fig. 3b) used was chosen as representative of an RNLI lifeboat, the closest class being that of the Severn. Although not all particulars (Table 1) were an accurate match the two deemed most important for the testing conditions, *i.e.* length overall and yaw radius of gyration, were within a 2% error.

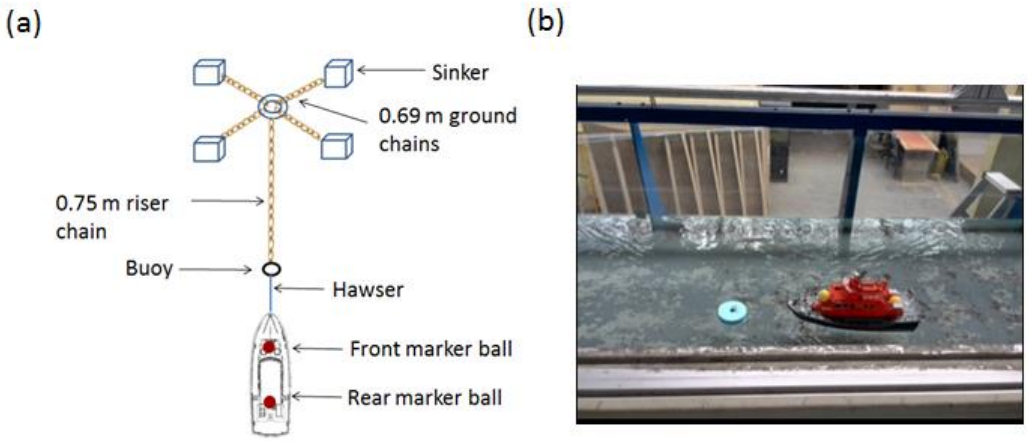

Fig. 3: (a) Aerial schematic of experimental set up. (b) Photograph of model boat in flume (1:20 scale buoy).

Table 1: Principle characteristics of RNLI Severn lifeboat and measured values of model with percentage difference of model values compared to full scale at a ratio of 1:40.

Particular	Full scale	Model actual	Percentage difference to 1:40 scale
Length overall (m)	17.30	0.443	2%
Beam (m)	5.92	0.164	10%
Draught (m)	1.78	0.0520	-14%
Displacement (tonnes)	42,300	0.856	-23%
Yaw radius of gyration (m)	4.32 (estimated)	0.1061 (measured)	2%

Four hawser lengths, two buoy scales (1:20 and 1:40 scale) and four shapes (circle, octagon, hexagon and square) were investigated as summarised in Table 2 and shown in Fig. 4. The Froude scaled flow speeds and depth ranges were chosen as representative of those documented at RNLI's SPM at full scale equivalents of 1.45 to 2.09 m/s and 8 to 10 m.

In tank tests the established assumption is that, in order that the tank walls and floor do not interfere with the fluid flow, the model's cross-sectional area should not be more than 0.5% of the tank cross-sectional area (Molland et al*.,* 2011)). There is thus a trade-off between maximising the scale of a model in order to reduce scaling effects and reducing the blockage effect. This ratio for the 1:40 scale model at Chilworth is between 0.02 – 0.05% indicating that these blockage effects were negligible. Furthermore for a water depth to vessel draft ratio of 5 or more, the shallow water effects of

increased wave-making resistance are negligible (Chakrabarti et al., 1995). The shallowest depth to draught ratio for the current tests was 5 (0.2/0.04 m) indicating that the shallow water effects were negligible.

For the particular case of tank testing of moorings in current, tank wall effects on the lateral forces are considered negligible when the ratio of tank width to vessel length is 5 but have a noticeable effect when this is reduced to 3 (Chakrabarti and Cotter, 1994). The tank width to vessel length ratio for the 1:40 scale model is 3.18 (1.4/0.44 m) indicating that the experimental set up should not have a noticeable effect from the tank walls.

Table 2: Summary of flume tests performed. Figures in brackets are the hawser length (m).

Test set up	Buoy shape and hawser length
No buoy	(0.125)
Normal buoy size (1:40)	circle (0.125,0.150,0.200) octagon (0.150) hexagon (0.150) square (0.150)
Large buoy size (1:20)	circle (0.125,0.150,0.200,0.300) octagon (0.300) square (0.300)
Large buoy (1:20) and no boat	circle, octagon, hexagon, square

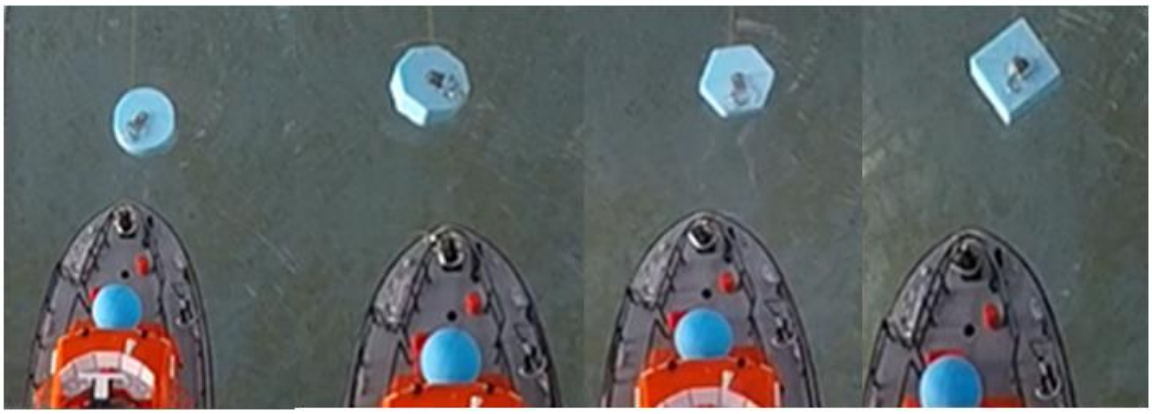

Fig. 4: 1:40 scale buoy shapes.

2.2 Motion capture

Motions of both the model lifeboat and buoy were captured using a GoPro Hero camera set at 30 frames per second mounted on a gantry above the tank. In order to provide an adaptable, inexpensive and portable method of tracking motion a bespoke motion tracking algorithm was created at the University of Southampton. The Matlab code uses video footage to track the centroid of an object via a mask created from its unique red, green, and blue colour combination. Three positional co-ordinates were tracked; two fluorescent markers (blue and yellow) on the centreline of the model and the buoy (blue) as depicted in Fig. 3b.

For a rigid hawser the dynamics of the vessel's translational motions can be described by a pair of angles controlled by the hawser length (L_H) and the length to a reference point along its centerline (L_V) as illustrated in Fig. 5. The two degrees of freedom, double pendulum-like motion can be defined in terms of: ϕ the angle between the hawser and the vertical from the buoy and θ the angle between the vessel's centreline and the vertical from the bow tip i.e. the yaw angle (Halliwell and Harris, 1988). From this two dimensional representation the model's motion in relation to the flume's fixed frame of reference were calculated as:

$$x = L_H \sin\phi + L_V \sin\theta \quad (1)$$

$$y = L_H (1-\cos\phi) + L_V (1-\cos\theta) \quad (2)$$

with small yaw angles, x ≈ surge, y ≈ sway. This method allowed for the direct measurement of displacement rather than the double integration of acceleration data from an accelerometer. Furthermore, this approach avoided the use of cabled instrumentation, which (at this 1:40 scale) was observed to have a significant impact on the motions of the lifeboat.

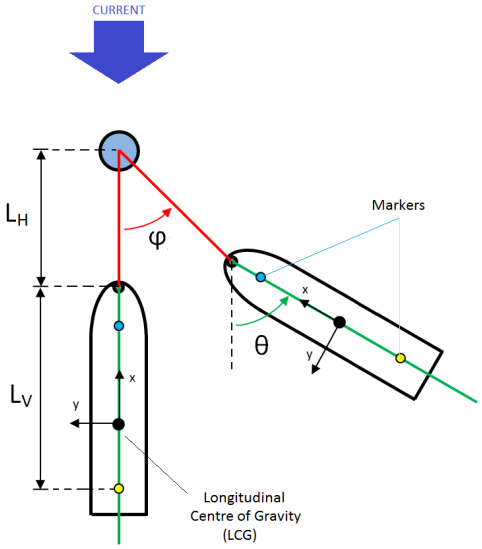

Fig. 5: Schematic of double pendulum model with fixed hawse Results

3.1 Verification

3.1.1 Motion capture

In order to verify the motion capture and Matlab algorithm the yaw angle of the model was also measured using a wireless Xsens MTw-G-710 inertial motion tracker for a sample of fourteen tests. The sensor houses rate gyroscopes with an angular resolution of 0.05° which was set at a sampling rate of 120 Hz. This unit weighs 20 g adding 0.02% additional mass to the model.

The root mean square of the fourteen yaw signals, using both measurement methods, showed a maximum difference of 0.67° and a mean difference across all the tests of 9.2%. An example plot comparing the signals using both methods is presented in Fig. 6.

The fisheye distortion from the GoPro video was removed, before implementing the tracking algorithm, using GoPro Studio software. Furthermore in order to quantify the amount of parallax, in the video footage, a calibration plot of the variation in millimetres per pixel for the various object lengths on the model lifeboat and the buoy is presented Fig. 7. There was a negligible degree of parallax with a difference of 0.4 (mm per pixel) between the two marker balls which represents an error of 0.8% for a sway excursion of 5 cm. The specific pixel factor (cm per pixel) for each object in each test was used in the algorithm and so no parallax correction was deemed necessary.

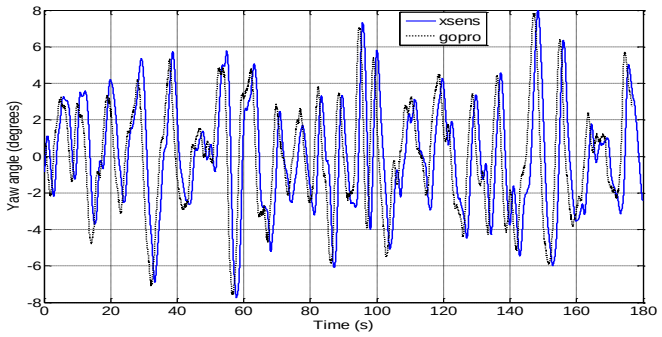

Fig. 6: Comparison of yaw angles. Angles are calculated from GoPro camera and Matlab code (dotted line) and measured by Xsens triaxial accelerometer (solid line).

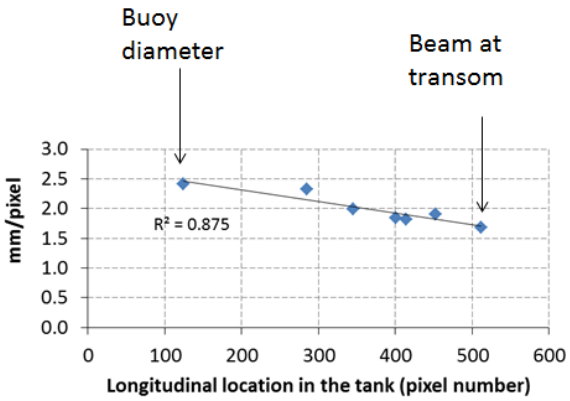

Fig. 7: Calibration plot of ratio of mm per pixel.

3.1.2 Mass Flow Rate

The experiments were designed to test the effect on vessel and buoy motions from changes in hawser length and buoy shape and buoy size at a constant flow speed. The test flow speeds were compared using the Mass Flow Rate ($\dot{M}$) calculated by multiplication of the cross-sectional area (A) of the tank by the water density (ρ) and surface flow speed (v). The surface flow speed was measured ten times per test run by recording the time taken for a ping pong ball to travel one meter. The standard deviations for each set of ten recordings, a measure of the steadiness of the flow, is presented in Fig. 8. The minimum value was 0.002 m/s (for a 0.27 m/s flow speed) and the maximum value was 0.014 (for a 0.30 m/s flow speed).

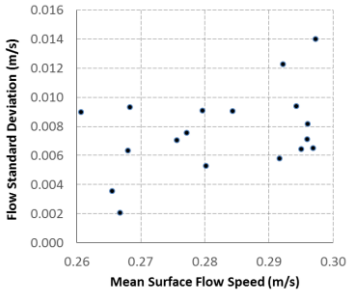

Fig. 8: Standard deviation of flow speed for ten repeat measurements for 27 tests.

The error of the $\dot{M}$ is calculated by the addition of the fractional measurement errors in quadrature (the square root of the sum of the squares):

$$\dot{M}\ error = \sqrt{\left(\frac{\delta\rho}{\rho}\right)^2 + \left(\frac{\delta A}{A}\right)^2 + \left(\frac{\delta v}{v}\right)^2} \qquad (3)$$

The results were a percentage measurement error ranging between 3.02% and 3.73%. Furthermore for a range of $\dot{M}$ of 74 to 90 kg/s there was a maximum standard deviation of 2.74 kg/s when comparison is made between experiments within a specific configuration, 7.65 kg/s when comparing the effect of hawser length tests between scales and 4.38 kg/s when comparing the effect of different shaped buoys at 1:40 scale (Table 3).

Table 3: Mass flow rates of tests at Chilworth flume (a) changes in hawser length and (b) changes in buoy shape and size.

(a)

Hawser length (m)	Mass flow rate (kg/s)				
	1:40 scale buoy	1:20 scale buoy	no buoy	mean	standard deviation
0.125	77.70	78.87	89.35	81.97	6.42
0.150	74.46	80.31	89.63	81.47	7.65
0.200	79.61	79.08	89.19	82.63	5.69
mean	77.26	79.42	89.39		
standard deviation	2.60	0.78	0.22		

(b)

Buoy shape	Mass flow rate (kg/s)							
	1:40 scale buoy	1:40 scale buoy	1:20 scale buoy	1:20 scale buoy	1:20 scale buoy	Buoy only	mean	standard deviation
circle	72.85	84.47	79.16	83.30	76.83	81.87	79.75	4.38
octagon	78.45	84.47	79.43	79.99	73.73	84.35	80.07	4.02
hexagon	78.06	81.65				80.69	80.13	1.86
square	78.45	81.25	79.16	78.61	74.01	82.90	79.06	3.02
mean	76.95	82.96	79.25	80.63	74.86	82.45	79.52	3.16

standard deviation	2.74	1.75	0.16	2.41	1.71	1.55	1.72	0.89

3.2 Typical Motion Responses

Experimental results presented are for a duration of 100 s, similar to those presented by Chakrabarti and Cotter (1994) and Huang and Lee (2012). With expected yaw and surge oscillations of a full scale tanker at a SPM subjected to steady current of 0.8 Hz (Aghamohammadi and Thompson, 1990) this should provide sufficient detail to compare the effects of changes in hawser length and buoy characteristics. Fig. 9 shows the typical motion responses of the 1:40 scale lifeboat. The dominant rotational motion was found to be yaw and the translational motion sway. The yaw angle ranged from -7.9° to +4.2° with a frequency range of 0.08 to 0.23 Hz. The maximum sway excursion was approximately 0.10 m with a frequency range of 0.05 to 0.23 Hz. Fishtailing motion was also observed for all the tests, similar to that described in the experiments and simulations of tankers at SPM.

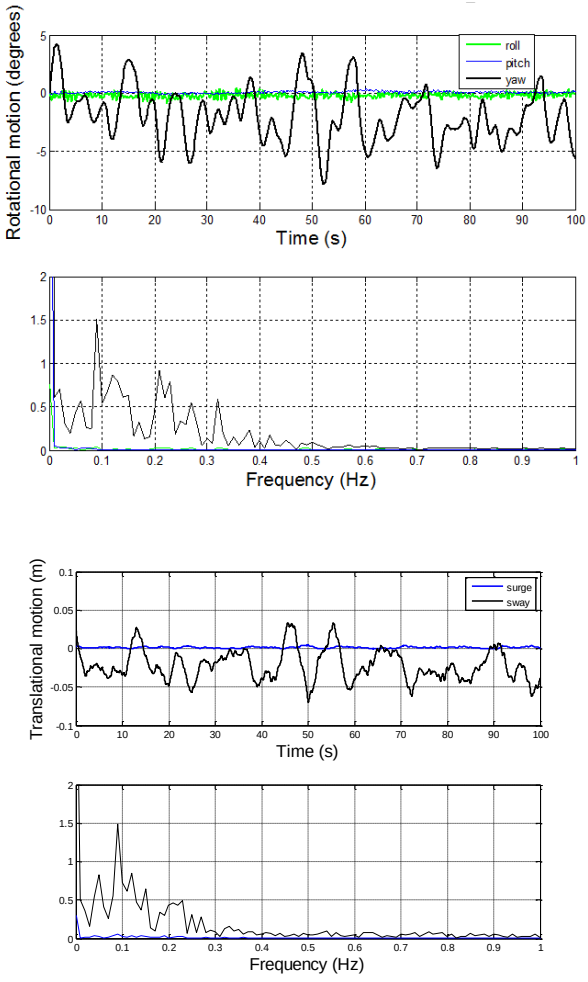

Fig. 9: 100 seconds of the motions of a 1:40 scale Severn lifeboat (1:40 scale circular buoy with a 0.15 m hawser, surface flow 0.26 m/s).

Interestingly, the correlation between the dominant motions of sway (m) and yaw (degrees) between the 1:40 and 1:20 scale buoys showed a marked difference (Fig. 10). For all three buoy shapes, at the 1:40 scale, the results showed a significant linear correlation. However, for the all buoy shapes at the larger 1:20 scale, this relationship was no longer observed: the linear correlation coefficient (R^2) for the 1:40 scaled buoys ranged from 0.76 to 0.81 and for the 1:20 scale buoys fell to between 0.29 and 0.41.

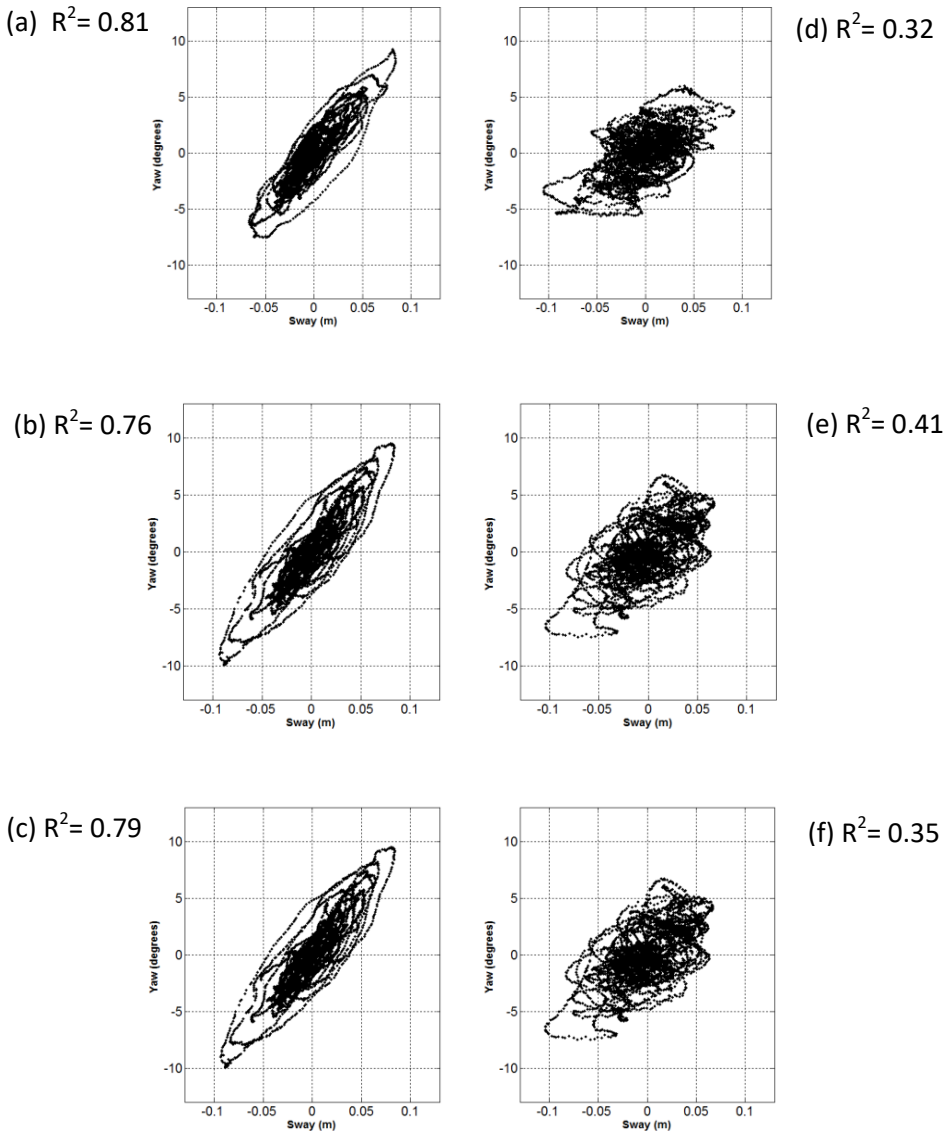

Fig. 10: Model lifeboat's sway (m) and yaw angle (degrees) (a) 1:40 circular (b) 1:40 octagon (c) 1:40 square (d) 1:20 circular (e) 1:20 octagon and (f) 1:20 square buoy with associated coefficient of determination (R^2) value indicating the

closeness of fit. (Note: The hawser lengths scaled with the buoys, i.e., at the 1:40 scale the hawser length = 0.15 m, at the 1:20 scale the hawser length =0.30 m. The full scale length was 6m).

3.3 Effect of line length and buoy scale.

Tests were designed to investigate the effect of hawser length (three lengths at a 1:40 scale of 0.125, 0.150 and 0.200 m) and of the size of the circular buoy (three scenarios of 1:40 scale, 1:20 scale and no buoy) upon the current-induced motion of a 1:40 scale lifeboat. The results show no discernible trend for changes in line length. Though, for the tests where no buoy was present (when the lifeboat was moored to a taut 1.5 mm diameter wire rope) there was observed a decrease in the sway velocity for both the front and rear marker balls placed on the vessel (Fig. 11). The sway and yaw velocities, over the 100 second interval, show significantly higher values when there was no buoy on the mooring, reducing when a 1:40 scale buoy was introduced and further reducing when a larger 1:20 scale buoy was introduced (Fig. 11). For example, when using a 0.125 m hawser and moving from no buoy to a 1:20 scale buoy, the recorded sway velocity of the front marker reduced from 0.030 to 0.013 m/s, the rear marker from 0.210 to 0.015 m/s and the yaw angular velocity from 2.90°/s to 1.84°/s. These findings directed the future experiments towards the examination of size and shape of mooring buoy and its effect on the lifeboat's motions.

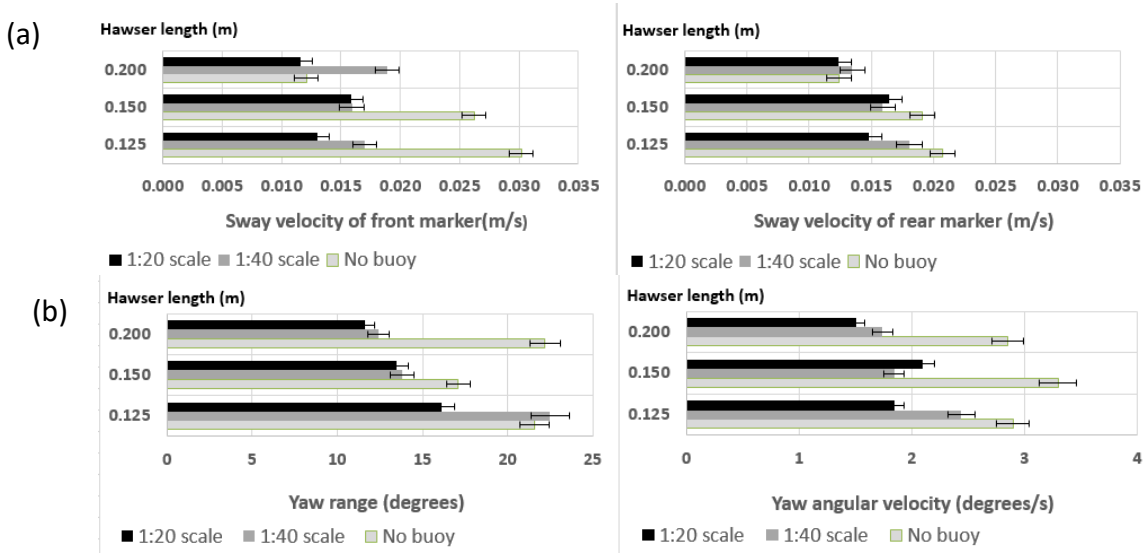

Fig. 11: Effect of change in line length on (a) sway (m) and (b) yaw range (degrees) and yaw angular velocity (degrees/s) of the vessel for a 100 second duration.

3.4 Effect of buoy shape at 1:40 scale with a 0.15 m hawser.

In addition to the size of the buoy, the motions of the vessel may also be influenced by the shape of the buoy. This hypothesis was tested by using four shapes, of equal immersed volume with increasing number of sides. The four 1:40 scale buoy shapes that were tested were a circle, octagon, hexagon and square (Fig. 4). For each test, the hawser length was fixed at a length of 0.15 m.

At this small scale, and within the calculated error bars, the results showed little difference between the sway velocities with different shaped buoys (Fig. 12a). Although, the results consistently showed that the sway velocity of the buoy was slower than the front marker on the model lifeboat, with the rear marker showing the fastest sway velocity.

The yaw angular velocity of the lifeboat was also compared by the use of boxplots (Fig. 12b). The plots are centered on the median value with an interquartile range box and upper and lower whiskers extending to the maximum and minimum data point that are 1.5 box heights away. Overall there is little difference between the distributions of the yaw angular velocities of the lifeboat due to a change in buoy shape, at the investigated scale. As the yaw angular velocity for each experimental data set failed a Kolmogorov-Smirnov test for a Gaussian distribution a non-parametric comparison of medians was required. The Kruskal-Wallis test performed returned a probability of 0.3013 implying that there is a significant probability that the data sets of yaw velocities come from distributions with the same medians. That is, buoy shape was found to have no significant effect on the average yaw angular velocity of the model lifeboat, at this scale.

(a)

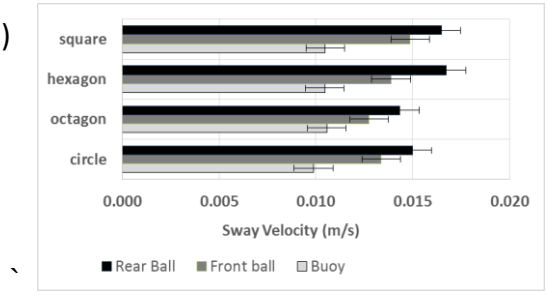

(b)

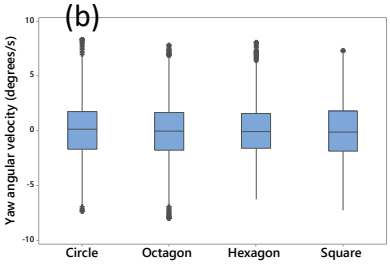

Fig. 12: Effect of change in buoy shape at 1:40 scale on (a) sway (mean of two test runs) and (b) yaw boxplots of the first run.

3.5 Effect of buoy shape at 1:20 scale with a 0.3 m hawser.

Increasing the buoy and hawser scale, to 1:20, the results found the interaction between buoy and lifeboat to have changed, with the buoy now exhibiting the highest sway velocity (Fig. 13a). Compared to that of the 1:40 scale, the sway velocity of the 1:20 scale buoys increased significantly (circle 138%, octagon 73%, square 128%). Furthermore, the yaw angular velocities and range of yaw angles of the model lifeboat, were found to consistently decrease, when the scale of the buoy was increased. The percentage differences in mean values are presented in Table 4.

The boxplots (Fig. 13b) and Kruskal Wallis probability (of 0.1892), showed that the yaw angular velocities have similar distributions and equal medians, for all investigated buoy shapes, at this scale.

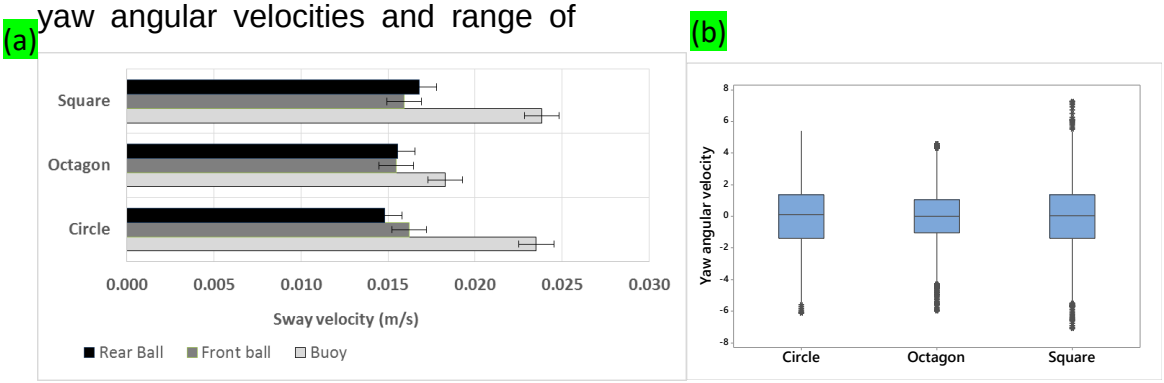

Fig. 13: Effect of change in buoy shape at 1:20 scale on (a) sway (mean of three test runs) and (b) yaw boxplots of the first run.

Table 4: Comparison of yaw for 1:40 and 1:20 scaled buoys

Shape	Yaw angular velocity (deg./s)	Yaw angular velocity (deg./s)	Difference 1:40 to 1:20 (%)	Yaw range (degrees)	Yaw range (degrees)	Difference 1:40 to 1:20 (%)
	1:40 scale buoy	1:20 scale buoy		1:40 scale buoy	1:20 scale buoy	
square	2.19	1.69	22.9	17.43	13.60	21.97
octagon	1.86	1.40	24.9	14.15	12.31	13.00
circle	1.96	1.59	18.6	15.04	12.64	15.98

3.6 Effect of shape when no lifeboat attached to buoy.

The observed differences in buoy behaviour lead to a set of experiments, at a 1:20 scale, where the motion of the buoys in current were tracked when not attached to the vessel. For the tests analysed there was a difference, taking into account the error bands, in the sway velocity between the four different shapes (Fig. 14). Non dimensionalising the velocity, using the recorded surface flow velocity, and using the circle as the benchmark figure then the octagon was 6% faster, the hexagon 29% slower and the square shape 25% faster over the 100 second test.

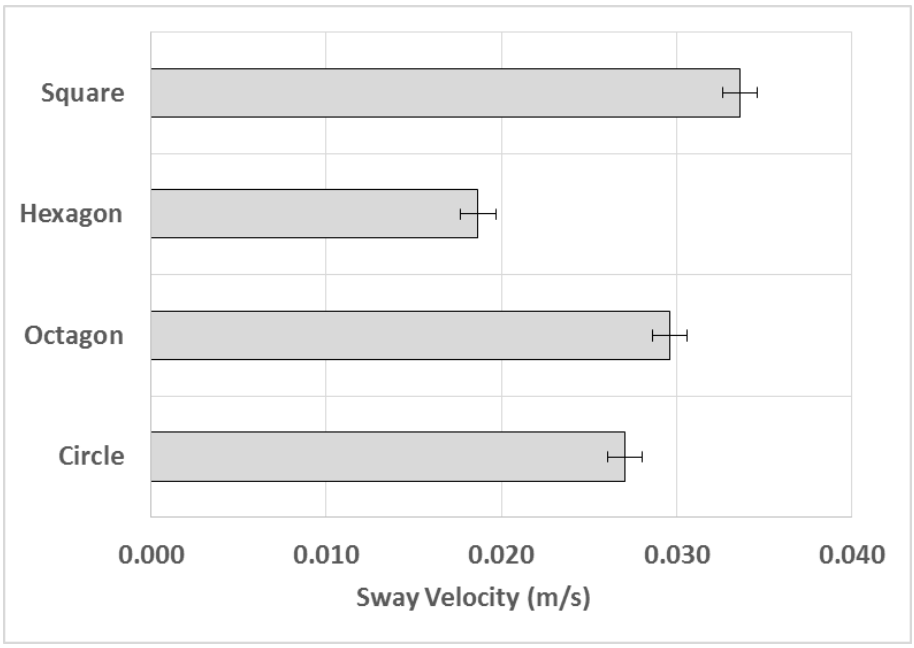

Fig. 14: Sway velocity, during 100 s, of the 1:20 scale buoys unattached to the vessel.

4. Discussion

A series of free standing mooring configuration model tests investigating the effects of hawser length, buoy shape and buoy size on vessel and buoy motions, in current, were conducted in a flume. The experimental setup enabled the unrestricted motion of the mooring buoy and model lifeboat to be observed and avoided the influence of mechanical friction upon test results associated with using a towing tank (Simos et al., 2001). The motions of the model and buoy were captured, and validated against an inertial measuring unit, using an ‘off the shelf’ video camera and Matlab motion tracking code. This

methodology offers an adaptable, inexpensive and portable method of motion tracking with no requirement for instrument cables and a negligible degree of parallax (at this scale).

When scaling for model ship testing it is impossible to simultaneously scale for the inertia, gravity and viscous forces. Reynolds similitude is “seldom invoked for most models “as gravity forces are considered to dominate in free-surface flows and viscous effects can be discounted provided “Reynolds numbers (based on flow depth) are greater than 1×10^4 (Hughes, 2005). The flow depth range of Reynolds numbers for the experiments was 4.6×10^4 to 5.4×10^4 and therefore Froude scaling is deemed appropriate in this case. For comparison the range of flow speeds tested of 0.26 m/s to 0.30 m/s equates to full scale rates, using similitude of the Froude numbers, of 1.6 m/s to 1.9 m/s compared to 10 to 12 m/s using similitude of Reynolds numbers. The small scale of the buoys used (diameters of 5 and 10 cm) means that any surface roughness may lead to a higher impact of the viscous flow effects and therefore the Reynolds number may take on a greater significance for buoy motion. However the purpose of the tests was to observe any differences due to buoy shape and therefore the impact of the viscosity will have been the same for all tests. Finally, using the model beam as the length parameter, yields a Froude number range of 0.21 to 0.26 and for such values some Froude effects on the lateral force and yaw moment should be expected (Tannuri et.al. 2001) and full scale measurements are therefore required to validate the observed experimental motion responses.

The results showed that the dominant motions of the model are sway and yaw, similar to the fishtailing responses, reported in the literature, from simulations and experiments for large scale vessels at offshore SPM. The effect of reducing the hawser length, for the case when the vessel was attached to a taut wire rope (i.e. no buoy present), showed a reduction in the sway velocity of both markers on the model, agreeing with the results of experiments of Pinkster and Remery (1975) and Halliwell and Harris (1988). Also the presence of the buoy was found to reduce the sway and yaw motions of the moored vessel at a SPM when compared to moored to a rigid pole. Changing the shape of the buoy did not result in a significant change in the model’s motion, at either scale (1:40 and 1:20

scale). However, differently shaped 1:20 scale buoys exhibited different sway velocities when not attached to the lifeboat. This would suggest that shape had an impact on the buoys motions, in steady current, but the changes were not large enough, at this scale, to impact the motions of the moored vessel.

The observed linear correlation between the sway displacement (m) and yaw angle (degrees) that existed at the 1:40 scale buoy was not present at the 1:20 scale, indicating that the buoy-vessel interaction changes with buoy size. Observations showed that introducing the larger buoy and longer hawser length increased the width and vorticity of its wake (Fig. 15) and it is therefore hypothesised that this induced the larger sway excursions and reduced the yaw angle range (as shown in Fig. 10). Furthermore an increase in buoy scale resulted in a consistent decrease in the vessel's yaw angular velocity and yaw angle range. Interestingly, at the 1:40 scale, the boat exhibited the fastest sway velocity and at the larger 1:20 scale, the buoy exhibited the fastest sway velocity, suggesting that there may be a change in mode, as depicted by the motion arrows in Fig. 16. This change in mode shape suggests that changes in buoy size can influence the motion responses of the lifeboat and may enable mooring efficacy to be improved.

Fig. 15: Turbulent wake created by 1:20 scale buoy.

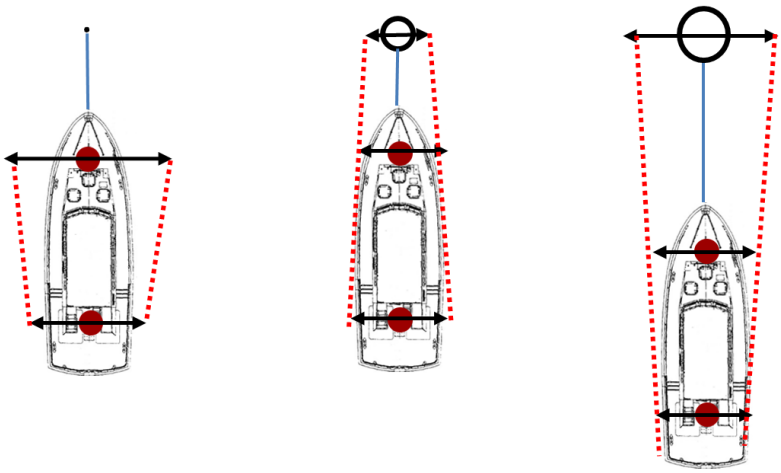

Fig. 16: Change in mode shape using no buoy, 1:40 scale buoy and 1:20 scale buoy.

An examination of which physical variables have an impact upon the mooring-induced damping experienced by an offshore floating platform, using Dimensional Analysis, is presented in Webster (1995). Simulations for a range of pre-tensions and motion amplitudes were performed testing the dimensionless parameters of scope, line drag coefficient, excitation period, stiffness and current. The excitation period was found to have a very strong effect on damping and, at low pre-tensions, shorter period produced higher damping. This would suggest that the larger scale buoys, which had a higher velocity, would produce higher damping than the smaller ones.

The size of a mooring buoy is largely governed by the buoyancy requirements to support the mooring chain, the weight of which is determined by the vessel size, water depth and sea conditions (Barltrop, 1998). Full scale diameters range from 1.24 to 1.85 m for coastal locations (and 2.4 to 4.0 m for ports and deep sea locations) (Hydrosphere, 2017). The diameter of the RNLI HIPPO buoys, at 2 m, are therefore significantly larger than the average of these harbour buoys and this series of tests were designed to assess the impact of size on the motions of a lifeboat. Increases in the horizontal motions of a moored body can cause very large instantaneous tensions and increased probability of SPM failure (Webster, 1995), these results indicate that introduction of a twice scale buoy may therefore reduce the risk of failure by a reduction of the horizontal motions of a lifeboat at a SPM.

5. Conclusion

This paper presents a series of model experiments on the current-induced motions of a 1:40 scale lifeboat at a single point mooring (SPM). The experimental set up enabled the unrestricted motions of the model and SPM buoy to be observed using a single ‘off the shelf’ video camera and a verified Matlab algorithm.

The results show the dominant motions of the lifeboat are sway and yaw and that a fishtailing motion is prevalent. The linear correlation between the sway (m) and yaw (degrees) that existed at the 1:40 scale buoy was not observed at the 1:20 scale indicating the buoy-vessel interaction had changed when the larger buoy was tested. When the buoy scale was increased the yaw angular velocities and range of yaw angles of the model lifeboat were found to consistently decrease. The sway velocity of the larger buoy, compared to the smaller one, increased resulting in a change in mode shape. The results suggest that changes in buoy size can influence the motion responses and may enable mooring efficacy to be improved.

Acknowledgements:

The provision of EngD funding from the RNLI & EPSRC (grant EP/G036896/1 the Industry Doctoral Training Centre in Transport and the Environment) is gratefully acknowledged.

The Matlab motion tracking code was written by Dr Christopher Phillips of Imperial College, University of London.

REFERENCES

ABS, 2014. Rules for Building and Classing Single Point Moorings 2014. American Bureau of Shipping, Houston, Texas.

Aghamohammadi, F., Thompson, J., 1990. An experimental study of the large amplitude fish-tailing instabilities of a tanker at a single point mooring. Applied Ocean Research 12 (1), 25-33.

Barltrop, N. D. 1998. *Floating Structures: a guide for design and analysis*, Oilfield Pubns Inc.

BBC, 2008. Four rescued as boat runs aground. Available: http://news.bbc.co.uk/1/hi/england/kent/7272434.stm (Accessed 21.06.17)

BBC, 2012. Yacht breaks from harbour mooring in Port St Mary. Available: http://www.bbc.co.uk/news/world-europe-isle-of-man-18952895 (Accessed 21.06.17).

BBC, 2013. Two rescued after yacht breaks its moorings. Available: http://www.bbc.co.uk/news/world-europe-guernsey-21739188 (Accessed 21.06.17).

Chakrabarti, S. & Cotter, D., 1994. Tank wall effects on broadside current forces on barge models. Ocean Engineering 21 (5), 489-497.

Chakrabarti, S., Libby, A., Palo, P., 1995. Small-scale testing on current-induced forces on a moored tanker. Ocean Engineering 22 (3), 271-300.

Fan, T., Qiao, D., Yan, J., Chen, C., Ou, J., 2017. An improved quasi-static model for mooring-induced damping estimation using in the truncation design of mooring system. Ocean Engineering 136, 322-329.

Gaythwaite, J.W., 2004. Design of Marine Facilities for Berthing, Mooring and Repair of Vessels, 2nd revised ed. ASCE Press, p. 560.

Halliwell, A. & Harris, R. 1988. A parametric experimental study of low-frequency motions of single point mooring systems in waves. *Applied ocean research,* 10, 74-86.

Huang, C.C. & Lee, M.F. 2012. Experimental Study on a Single-point-mooring Floating Structure. *The Twenty-second International Offshore and Polar Engineering Conference*.

Hughes, S. A. 2005. *Physical Models and Laboratory Techniques in Coastal Engineering*, World Scientific Publishing Co Pte Ltd, Singapore.

Hydrosphere, 2017. Mooring buoys. http://hydrosphere.co.uk/datasheets/product-services-summaries/hydrosphere_mooring_buoys_v_2_01_sep_14_web.pdf (Accessed 20.07.17).

IWCP, 2012. Boats sink in heavy seas. Available: http://www.iwcp.co.uk/news/news/boats-sink-in-heavy-seas-44153.aspx (Accessed 21.06.17).

Lang, S., 2001. Review of Lifeboat and Launching Systems' Accidents. Southampton: Marine Accident Investigation Branch.

Luai, A., Zhi, Y., 2013. Comparison of laboratory and predicted motions and mooring line forces for a container ship moored to a dock. Proceedings of the 18th Offshore Symposium, Houston, Texas.

Molland, A.F., Turnock, S.R., Hudson, D.A., 2011. Ship Resistance and Propulsion: Practical Estimation of Propulsive Power Cambridge University Press.

Myers, L. E. & Bahaj, A. S. 2010. Experimental analysis of the flow field around horizontal axis tidal turbines by use of scale mesh disk rotor simulators. *Ocean Engineering,* 37, 218-227.

Oil Companies International Marine Forum, 2008. Oil Companies International Marine Forum Mooring Equipment Guidelines. Witherby Seamanship International, Livingston, United Kingdom.

Oosugi, Y., Kimura, N., Hujimori, Y. & Abeshima, N. 2007. A fundamental study concerning mooring disaster of small fishing boats at fishing ports: an interrelation between the ship motion induced by the wind and tension of mooring lines. *Journal of Japan Institute of Navigation,* 116, 249-54.

Orcaflex, 2018. Orcaflex Example- C Moorings. Available: https://www.orcina.com/SoftwareProducts/OrcaFlex/Examples/C%20Moorings/index.php (Accessed 20.08.18)

Papazoglou, V.J., Mavrakos, S. A. & Triantafyllou, M. S. 1990. Nonlinear cable response and model testing in water. *Journal of Sound and Vibration,* 140, 103-115.

Percuil River Moorings Ltd., 2010. Implementation of the Mooring Contractor Guidelines. Available: http://www.percuilriver.co.uk/implementation-mooring-contractor-guidelines (Accessed 21.06.17).

Pinkster, J., Remery, G., 1975. The role of model tests in the design of single point mooring terminals, Offshore Technology Conference.
Schellin, T., 2003. Mooring load of a ship single-point moored in a steady current. Marine Structures 16 (2), 135-148.
SeaSurveys, 2013. News page. Available: http://www.turbolink.co.uk/seasurveys2011/news.html (Accessed 21.06.17).
Sharma, S., Jiang, T., Schellin, T., 1988. Dynamic instability and chaotic motions of a single-point-moored tanker, 17th Symposium on Naval Hydrodynamic.
Simos, A. N., Tannuri, E. A., Aranha, J. A. P. & Leite, A. J. P. 2001. Theoretical analysis and experimental evaluation of the fishtailing phenomenon in a single-point moored tanker. *Proceedings of the Eleventh International Offshore and Polar Engineering Conference.*
Sorheim, H.R., 1980. Analysis of Motion in Single-Point mooring systems. Modelling Identification and Control 1 (3), 165-186.
Tannuri, E. A., Simos, A. N., Leite, A. J. & Aranha, J. A. P. 2001. Experimental validation of a quasi-explicit hydrodynamic model: Fishtailing instability of a single-point moored tanker in rigid-hawser configuration. *Journal of Ship Research,* 45, 302-314.
van Dorn, W. G. 1974. *Oceanography and seamanship*, Dodd, Mead New York, NY, USA.
Wang, J., Li, H., Li, P., Zhou, K., 2007. Nonlinear coupled analysis of a single point mooring system. Journal of Ocean University of China 6 (3), 310-314.
Webster, W. C. 1995. Mooring-induced damping. *Ocean Engineering,* 22, 571-591.
Which-Marina, 2015. Registered UK marinas. . Available: http://www.which-marina.com/Default.asp (Accessed 21.06.17).
Wichers, J.E.W., 1988. A Simulation Model for a Single Point Moored Tanker. PhD Dissertation, Delft University of Technology, Delft, The Netherlands.
Yachting and Boating World, 2016a. May Dream aground in Plockton. Available: http://www.ybw.com/news-from-yachting-boating-world/may-dream-aground-plockton-23755 (Accessed 21.06.17).
Yachting and Boating World, 2016b. Yacht smashes and sinks in Portland Harbour. Available: http://www.ybw.com/news-from-yachting-boating-world/yacht-smashes-and-sinks-in-portland-harbour-39858 (Accessed 21.06.17).

1.2 Catherine J. Hollyhead, Nicholas C. Townsend, and James IR Blake. "Experimental investigations into the motions of a lifeboat in regular waves at a single point mooring." *Ocean Engineering* (in preparation).

Experimental investigations into the motions of a lifeboat in regular waves at a single point mooring.

Catherine J. Hollyhead*, Nicholas C. Townsend, James I.R. Blake.

Faculty of Engineering and the Environment, University of Southampton, UK.

* Corresponding author: cjh1g08@soton.ac.uk

ABSTRACT

This paper presents a series of model experiments on the wave-induced motions of a 1:10.67 scale lifeboat at a single point mooring (SPM). The hypothesis that changing the shape and/or size of the mooring buoy would have an impact upon the motions of the model lifeboat has been tested. Five buoy shapes and two buoy scales have been investigated. The dominant oscillatory rotational motion of the model lifeboat, at a SPM in regular waves, was pitch and translational oscillatory motions were surge and heave. No significant effects on vessel motion were observed from changes in the shape of the buoys at both scales tested. However doubling the size of the buoy resulted in the model lifeboat exhibiting lower pitch angles, slower sway and heave accelerations and faster surge accelerations. Consolidating the impacts of the changes in translational accelerations indicated an overall reduction in total accelerations at three of the four wave frequencies tested. These results when combined with previous experimental results, from the current-induced motion of a lifeboat at a SPM, suggest that changes in buoy size influence the motions of the model lifeboat which may enable mooring efficacy to be improved.

Key words:

Single point mooring (SPM), Moored ship responses, Buoy shape, Lifeboat, Tank testing.

1. Introduction

1.1 Motivation

There are significant numbers of Single Point Moorings (SPM) around the world's coasts, including 388 listed marinas in the U.K (Which-Marina, 2015) and forty belonging to the Royal National Lifeboat Institution (RNLI). There are numerous media reports of yachts breaking free from their SPM resulting in damage and/or rescue crews being called out around the coats of the United Kingdom (Hollyhead *et al.*, 2017). There is a need to understand the motion responses of small vessels at SPM moorings. The use of scientific investigation and full scale measurements at sea in terms of both financial and time scale investments is usually prohibitive and so physical interactions are best modelled at a smaller scale giving the advantage of a controlled environment to test new hypotheses.

The experiments presented here extend the research into the effect of buoy shape and buoy size upon the motion of a lifeboat at a SPM which are detailed in Hollyhead *et al.* (2017). The conclusions of the paper, which investigated the current-induced motion responses of a lifeboat at a SPM, were that when the buoy scale was increased the yaw angular velocities and range of yaw angles of the model lifeboat consistently decreased suggesting that changes in buoy size can influence motion responses and may enable mooring efficacy to be improved.

1.2 Background

A SPM is designed to "resist the mean mooring forces from wind, current and waves but allow the free response to wave frequency loading" (Barltrop, 1998). The vessel is free to weathervane around its mooring buoy allowing it to self-align to the prevailing waves and reduce the mooring hawser load compared to that if its heading was constrained (Schellin, 2003; Oil Companies International Marine Forum, 2008).

The displacement of a rigid floating body can be described by six degrees of freedom: the translational motions along the axes of surge, sway and heave and the rotational ones around them of roll, pitch and yaw (Fig. 1a). For an unconstrained vessel these can be subdivided into oscillatory (heave, pitch and roll) that invoke restoring forces due to a change in the vessel's equilibrium displacement and non-oscillatory (surge, sway and yaw), (van Dorn, 1974). However when a vessel is moored at a SPM the catenary mooring chain provides a restoring force and oscillations can additionally occur in surge, sway and yaw (van Dorn, 1974).

The scope, of the mooring riser, is defined as the chain length from the point it rises from the seabed up to the point at which it is attached to the buoy. When a vessel is attached to a SPM the restoring force from changes in the shape of the catenary line changes the scope of the line and therefore the suspended line weight (Fig. 1b).

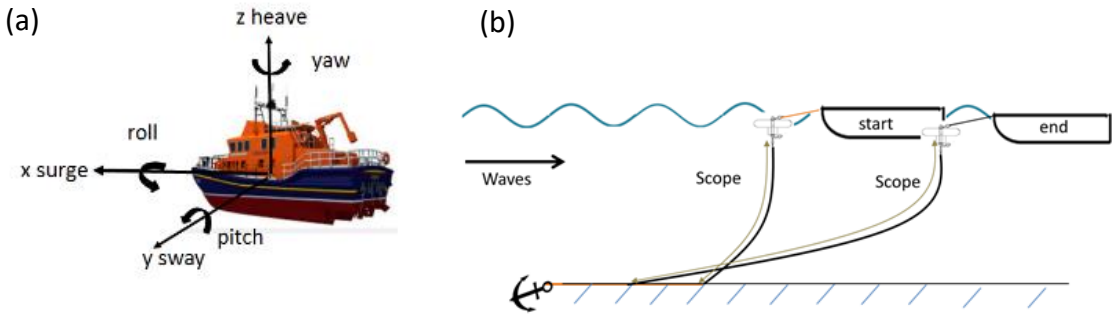

Fig. 1: The right handed frame of reference in the flume (a) three-dimensional and (b) schematic of change in scope.

Due to the expansion of offshore oil and gas extraction the motions of large scale tankers at SPM's has been extensively investigated (Gaythwaite, 2004) and the purpose of duplicating environmental conditions experienced by offshore structures at model scale is to be able "to reproduce the responses that the structure will experience when placed in operation in the offshore site" (Chakrabarti, 2005). The majority of offshore locations where SPM operate have wave periods within the range of 4 to 10s (0.1 to 0.25Hz) and heights 2 to 9m (Halliwell and Harris, 1988). The length of vessels and environmental conditions tested for offshore SPM differ from the lifeboats and lifeboat station locations of the RNLI. As an example wave data recorded at Swanage Pier, since 2007, has a mean significant wave height of 0.2m and mean significant wave period of 4s (Channel Coastal Observatory, 2017).

Furthermore wave experiments, using SPM, have traditionally been conducted using a fixed spring-mass damper mooring riser (e.g. Halliwell and Harris, 1988; Aghamohammadi and Thompson, 1990; Carpenter *et al.,* 1995, Jenkins *et al.,* 1995; Eriksson *et al.*, 2006). The experiments presented here reflect the wave conditions of coastal harbours and use a free catenary SPM configuration which allow changes in the mooring riser scope and the unrestricted motion of the mooring buoy and model lifeboat to be recorded.

1.3 Paper Contribution

This paper presents the results from a series of 1:10.67 model scale experimental investigations into the effect of buoy scale and shape on small boats (considered sub 20m) with free catenary SPM configurations (i.e., without the use of fixed spring-mass-damper mooring line). The paper structure is as follows; In Section 2 the methodology and experimental setup is described. In Section 3 the experimental results are presented and discussed in Section 4. The conclusions are presented in Section 5.

Methodology

2.1 Model Tamar lifeboat

A series of 1:10.67 model scale experimental investigations into the effect of buoy shape and buoy scale on small boats (considered sub 20m) with a free catenary SPM configuration were conducted in the wave tank at the Solent University (60m in length, 3.7m width and 1.8m depth). When conducting ship tank experiments it is recognised that gravity forces predominate in free-surface flows (Hughes, 2005) and Froude similitude was used to determine the model and wave parameters. The representative model hull was that of a Tamar class lifeboat constructed of strip plank sheathed with glass-reinforced plastic, the full scale and 1:10.67 model scale particulars of which are presented in Table 1. The wave height was kept constant for all tests at 0.05m (full scale Froude equivalent of 0.53m).

In tank tests the established assumption is that, in order that the tank walls and floor do not interfere with the fluid flow, the model's cross-sectional area should not be more than 0.5% of the tank cross-sectional area (Molland *et al.,* 2011). The wave tank at Solent University has a working cross section area of 6.66m^2 which gives a vessel to tank cross sectional area of approximately 0.7% which is fractionally above this prescribed optimal limit. Furthermore for a water depth to vessel draught ratio of 5 or more, the shallow water effect is considered negligible (Chakrabarti *et al.*, 1995). The depth to draught ratio for the current tests was 14 (1.8/0.13m) indicating that the shallow water effects were negligible.

Table 1: Particulars of full and model scale Tamar lifeboat.

Particular	Full scale	1:10.67 scale model
Length overall (m)	16.3	1.53
Length between perpendiculars (m)	14.7	1.37
Beam (m)	5.3	0.49
Draught (m)	1.4	0.13
Displacement (tonnes)	32.0	0.026
Yaw radius of gyration (m)	3.67 (estimated)	0.27 (measured)

2.2 Mooring configuration and buoy shapes

The experiments were conducted using a free catenary SPM configurations (i.e., without the use of fixed spring-mass-damper riser chain). In the particular case of model testing cables in water it is usual to violate exact geometric scaling of the materials however the correct value for the Young's modulus of the material should be used as its violation, in dynamic testing, is extremely significant (Papazoglou *et al*., 1990). The riser chains and mooring hawser materials were scaled using the Cauchy criterion which facilitates the similitude of the ratio of inertial to elastic forces using the Young's modulus of the material (Hughes, 2005). The Young's modulus of the materials used was measured using an Instron E-Series Circumferential Extensometer. The riser chain length was 6m (full scale Froude equivalent 64m) which is the recommended length of a riser being at least 3 times the water depth (Bradney, 1987; Hinz, 2001). The hawser length for the 1:10.67 buoys was 0.56m and for the 1:5.33 buoys was 1.12m (full scale Froude equivalents 6m).

The effect on the model lifeboat's motions of five buoy shapes (circle, octagon, hexagon, square and (ogival delta) wing, (Fig. 2)) and two buoy scales (1:10.67 and 1:5.33) was investigated (Table 2).

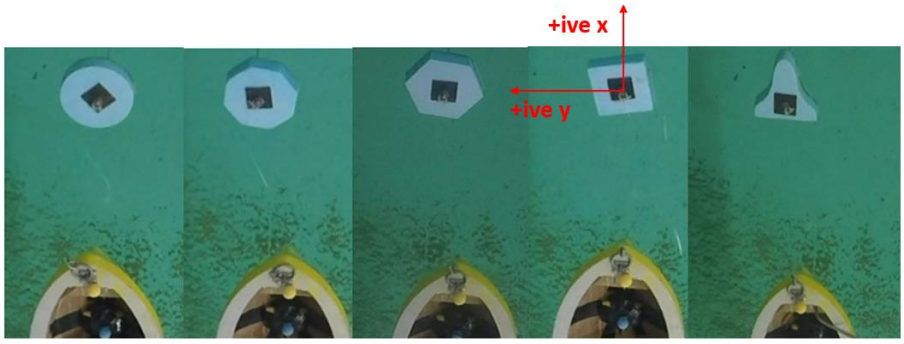

Fig. 2: 1:10.67 scale buoy shapes and 2D frame of reference.

Table 2: Regular wave test parameters. All tests performed at constant wave height of 0.05m.

Buoy scale	Upper hawser length (m)	Lower hawser length (m)	Shape	Wave frequency (Hz)	Number of tests (per wave frequency)
1:10.67	0.56	0.66	circle, octagon, hexagon, square, wing.	0.8,0.9,1.0,1.1	3
1:5.33	1.12	1.32	circle, octagon, hexagon, square, wing.	0.8,0.9,1.0,1.1	3

2.3 Experimental setup and test programme

The 1:10.67 scale model lifeboat and SPM were positioned in the tank (Fig. 3) and regular waves were generated using a motor-driven, single paddle HR Wallingford wavemaker with a maximum stroke length of ±180mm. Each buoy was tested at four wave frequencies (0.8, 0.9, 1.0, 1.1 Hz, (Table 2)).

The 6 degrees of freedom motions of the model lifeboat were recorded using an Xsens Mtw inertial motion unit (IMU) positioned at the measured centre of gravity of the model lifeboat (Fig. 3). The excursions of the buoys were recorded using a Go Pro Hero camera set at 30 frames per second mounted above the tank (Fig. 3) in the x-y plane (Fig. 2). In order to avoid the use of cabled instrumentation, which would have had a significant impact on the motions of the buoys at this

scale, a bespoke motion tracking algorithm was created at the University of Southampton the details of which are given in Hollyhead *et.al.* 2017.

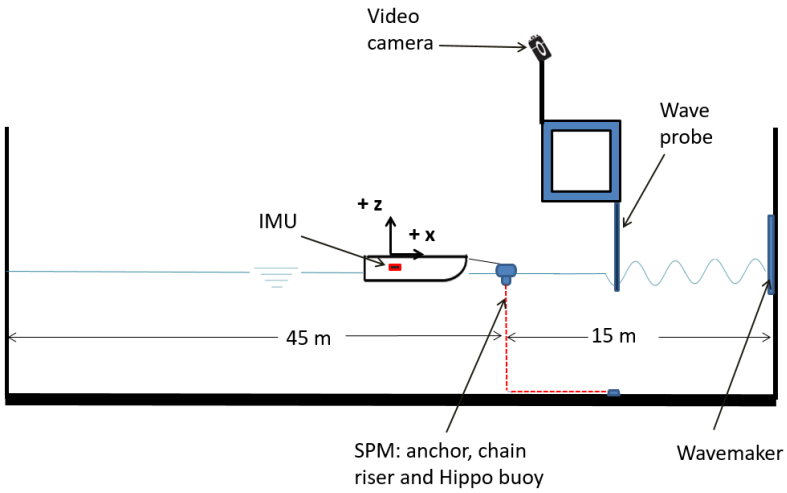

Fig. 3: Schematic of experimental set-up.

From initial test runs it was observed that the motions of the model lifeboat were significantly affected by its initial orientation to the oncoming regular waves. In order to compare the effects of the size and shape of buoy, each test was started from the same equilibrium position (Fig. 4). The model was released from this initial start position when the first wave reached the wave probe (Fig. 3).

The test duration was dictated by the time taken for the incident waves to be reflected back from the end of the wave tank. For the four wavelengths (λ) tested the wave speed, calculated using the wave number ($k= 2\pi/(\lambda)$), ranged from 1.42 to 1.95m/s (Table 3). Having passed the buoy the wave travelled 88m to the end of the tank and back to the stern of the model which, for the fastest wave celerity (1.95 m/s), equated to an available 45s of data acquisition time.

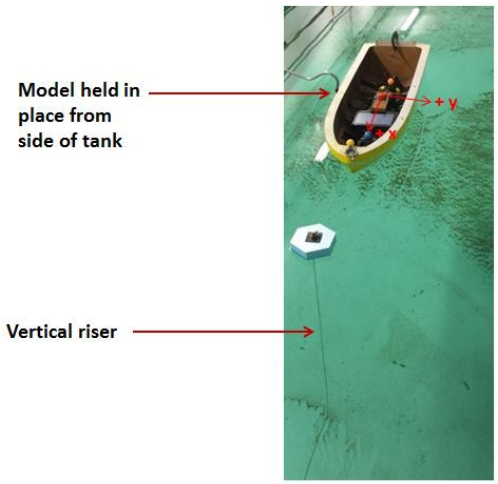

Fig. 4: Equilibrium start position for experiments in regular waves.

Table 3: Wave frequency and speed data

Frequency (Hz)	Period (s)	Wavelength (m)	Wave number (m^{-1})	Wave celerity (m/s)
0.8	1.25	2.44	2.58	1.95
0.9	1.11	1.93	3.26	1.74
1.0	1.00	1.56	4.03	1.56
1.1	0.91	1.29	4.87	1.42

3. Results

3.1 Typical Motion Responses

The effects of the buoy shape and buoy size upon the motions of a model lifeboat in regular waves were investigated, at a constant wave height, over a range of four frequencies repeated three times. For each degree of freedom results are presented for 45s of unfiltered data starting from the same time stamp which was determined by the tenth peak in the pitch (deg.) data (Fig. 5). At this point the regular wave was fully formed and steady state oscillations had been established.

The motions of the model lifeboat reached a steady state oscillatory motion in all test runs in all degrees of freedom except yaw. For each test the peak frequency of roll, pitch, surge, sway and

heave motions matched the wave frequency. Pitch was the dominant rotational motion and surge and heave were the dominant translational motions. The results for the 1:10.67 scale circular buoy, at 0.8Hz wave frequency, are presented in Fig. 6. The RMS value for pitch angle was 2.33° which was 5.5 times greater than the roll angle RMS of 0.42°. The respective RMS values of the translational accelerations are surge 0.22m/s^2, sway 0.04m/s^2 and heave of 0.34m/s^2 (having accounted for gravitational acceleration).

To quantify the repeatability of the experiments non-parametric Mann-Whitney U tests were performed comparing the three test runs at each frequency. This test was chosen as the data sets were not normally distributed and a ranking of data and comparison of medians is required rather than means. Test results of the motions of the model lifeboat that were shown not to have been repeated were excluded from the analysis of the effect of buoy size and buoy shape (Table 4).

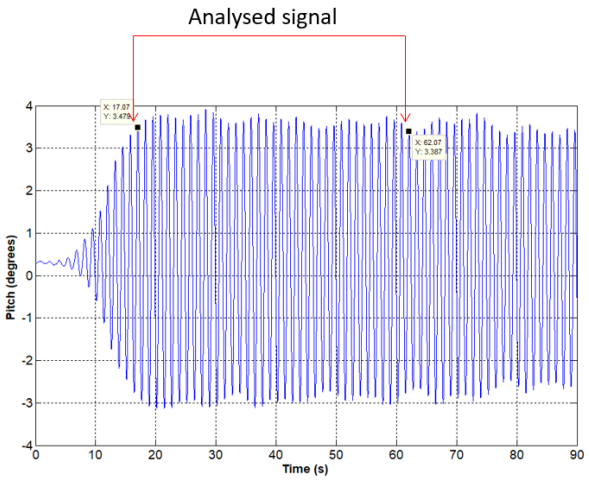

Fig. 5: Example of analysed pitch data (1:10.67 scale circular buoy at wave frequency 0.8Hz).

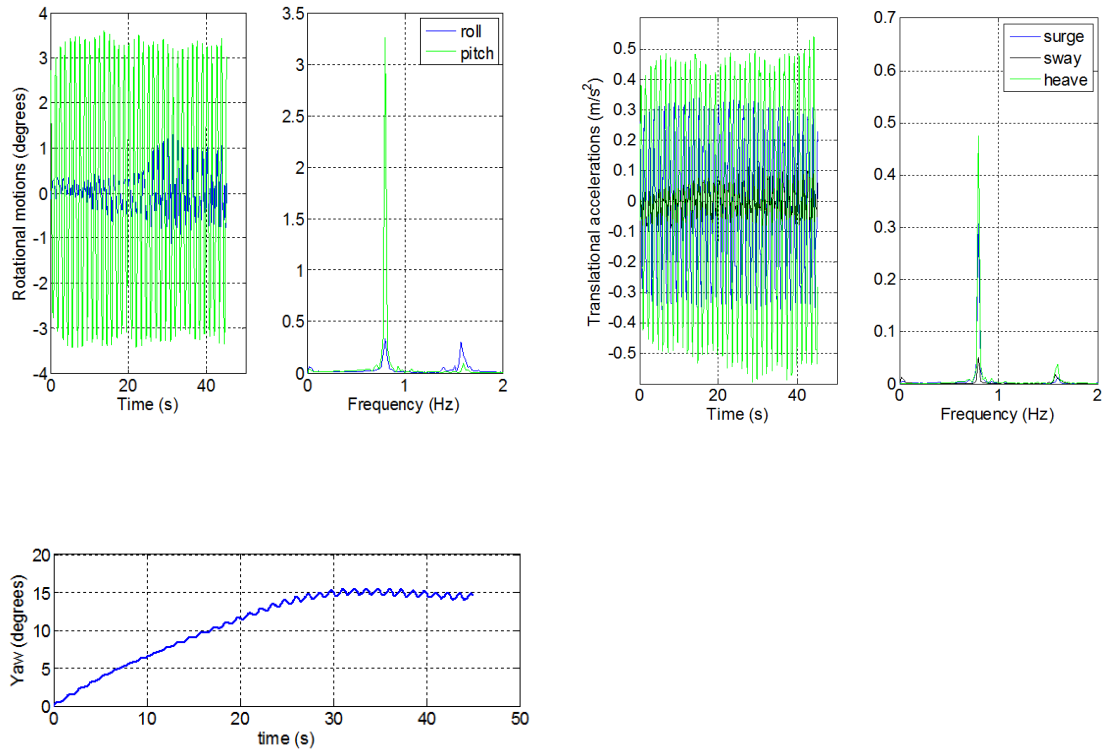

Fig. 6: Motions of model lifeboat (1:10.67 scale circular buoy at wave frequency 1.0Hz).

Table 4: Percentage of tests included in analysis.

Buoy Scale	Roll	Pitch	Yaw	Surge	Sway	Heave
1:10.67	83%	100%	68%	67%	78%	92%
1:5.33	80%	100%	50%	92%	87%	100%

3.2 Effect of buoy shape on vessel motion

Motion responses are presented in terms of a non-dimensional response amplitude operator (RAO) for each degree of freedom. For the translational motions the RAO is defined as the RMS of the acceleration (m^2/s) amplitudes divided by the RMS of the wave acceleration (m^2/s) amplitude and for the rotational motions as the RMS amplitudes (rad) divided by the wave slope RMS (Lloyd, 1989). For the yaw motion the maximum yaw angle of the model was taken rather than the RMS as the motion was not oscillatory as shown in Fig. 6.

The RAO, using different shaped buoys, at a 1:10.67 scale, are presented in Fig. 7. For each motion response the largest differences, when comparing the different shapes, are at the 0.9 and 1.0 Hz wave frequencies with all results converging at the 0.8 and 1.1Hz frequencies. The three dominant oscillatory motions of pitch, surge and heave exhibit the least difference in motion response when buoy shape is changed. The maximum yaw angles exhibit the largest differences.

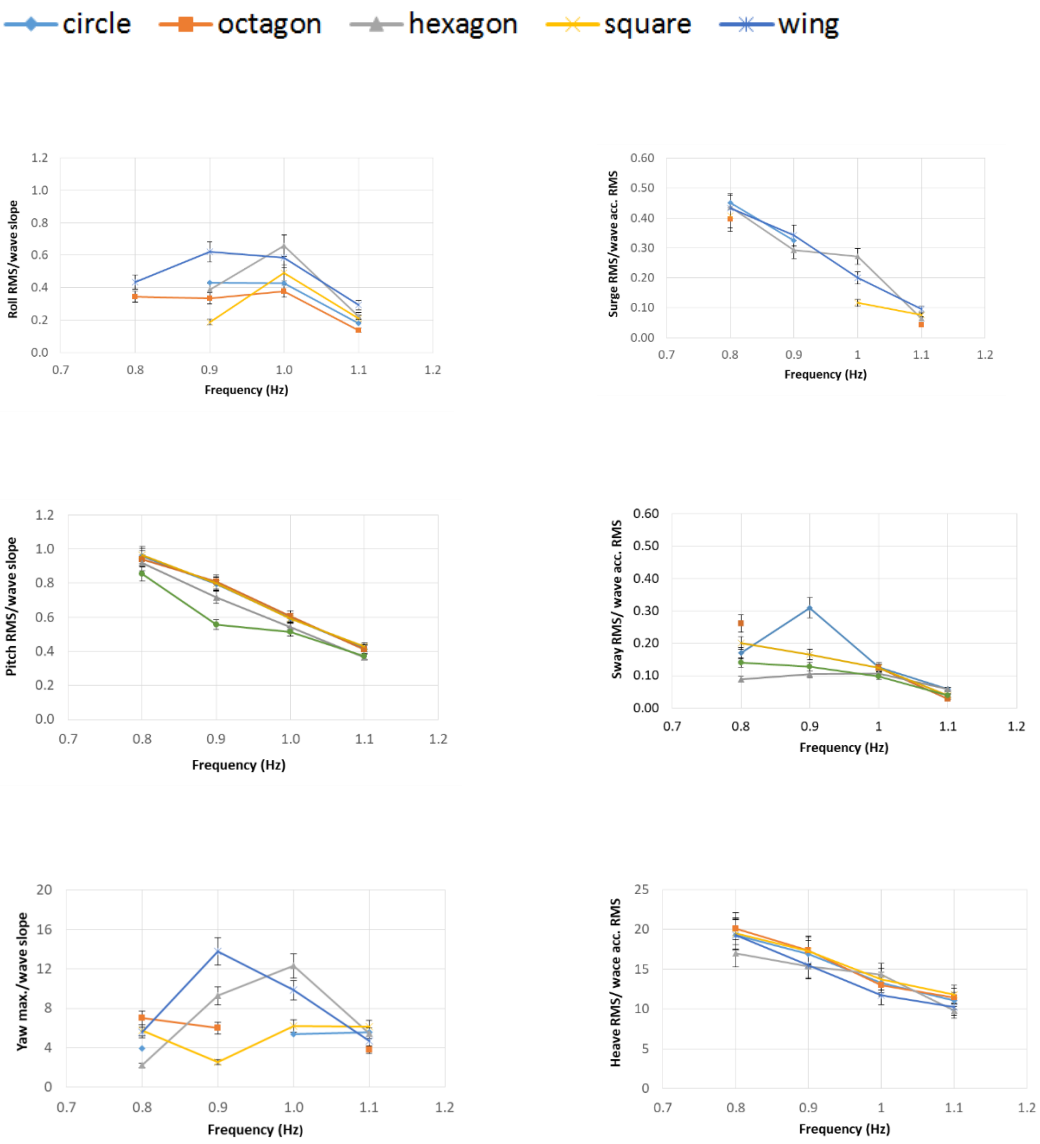

Fig. 7: Comparison buoy shapes at 1:10.67 scale (RMS of repeatable tests).

The RAO, using different shaped buoys, at a 1:5.33 scale are presented in Fig. 8. For each motion response the largest differences, when comparing the different shapes, are at the 0.9 and 1.0Hz wave frequencies with all results converging at the 0.8 and 1.1Hz frequencies. The three dominant oscillatory motions of pitch, surge and heave exhibit the least difference in motion response when buoy shape is changed. The maximum yaw angles and roll RMS exhibit the largest differences.

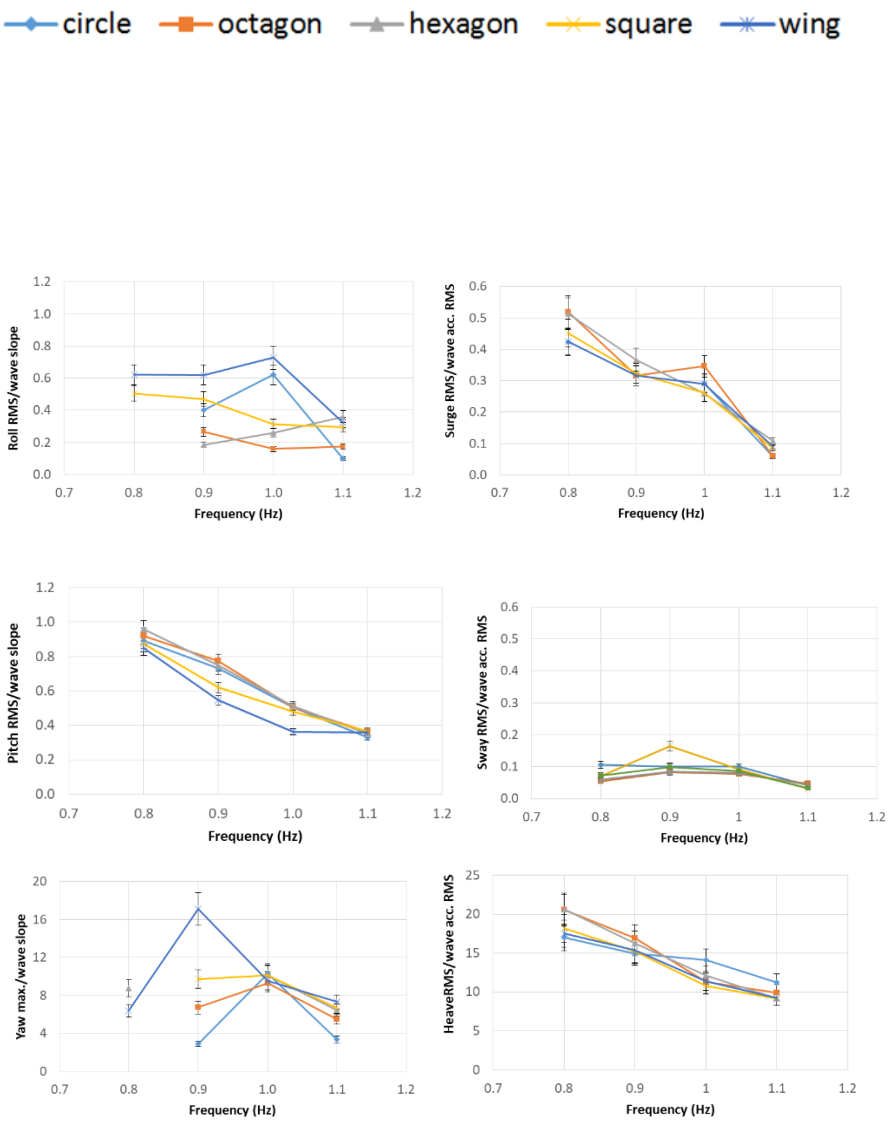

Fig. 8: Comparison buoy shapes at 1:5.33 scale (RMS of repeatable tests).

3.3 Effect of buoy scale

In order to assess if the size of the buoy impacted upon the vessel's motions the repeatable results for pitch, surge, sway and heave motions were compared. As presented in Fig. 7 and Fig. 8 these motions demonstrated little variability between the buoy shapes tested so the results for all shapes, at the same scale, were consolidated to compare the vessel's motion between the two different scaled buoys.

The resultant plots of percentage difference from the 1:10.67 scale buoys are presented in Fig. 9. The sway RAO exhibited the largest differences across all wave frequencies, resulting in reduced values when the larger scale buoy was used, the percentage difference decreasing with increasing wave frequency. Surge was the only motion where tests using the larger 1:5.33 scale buoys resulted in higher RAO values, the highest difference at the 1.0Hz wave frequency.

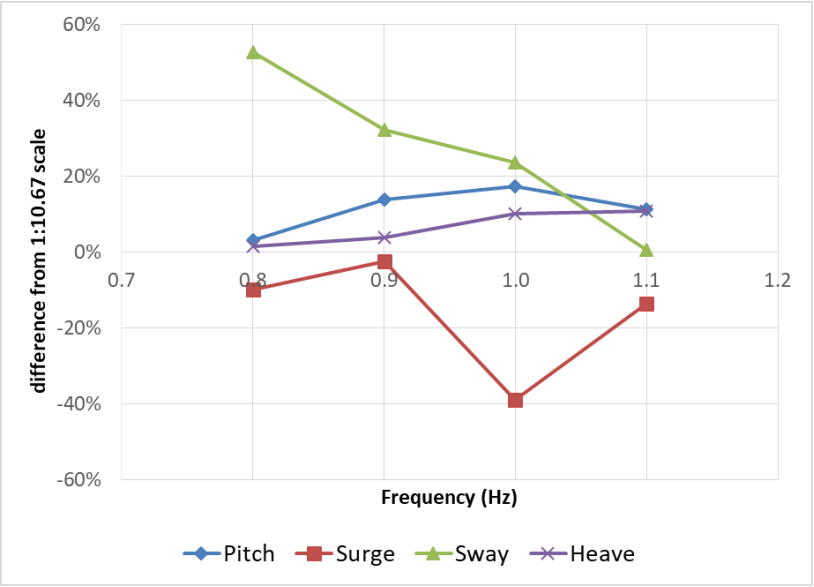

Fig. 9: Percentage difference in RAO for pitch angle and surge, sway and heave accelerations using 1:10.67 and 1:5.33 scale buoys.

Boxplots of the full recorded dataset of the vessel's pitch angles and translational accelerations were used to compare the effect on the vessel's motion of the different sized buoys. The plots showed no significant difference in the median and range of pitch, surge and sway values when comparing sizes. The heave accelerations had a significantly different range distribution over all frequencies when comparing the two sizes of buoy for all shapes tested (e.g. the circular shaped buoy, Fig. 10). The plot is centred on the median value with associated interquartile range boxes. The upper whiskers extend to the maximum data point within 1.5 box heights from the top of the box and the lower 1.5 box heights away from the bottom. The black boxes are the 1:10.67 scale buoys and the blue boxes the 1:5.33 scale buoys for each of the tested wave frequencies of 0.8, 0.9, 1.0 and 1.1Hz.

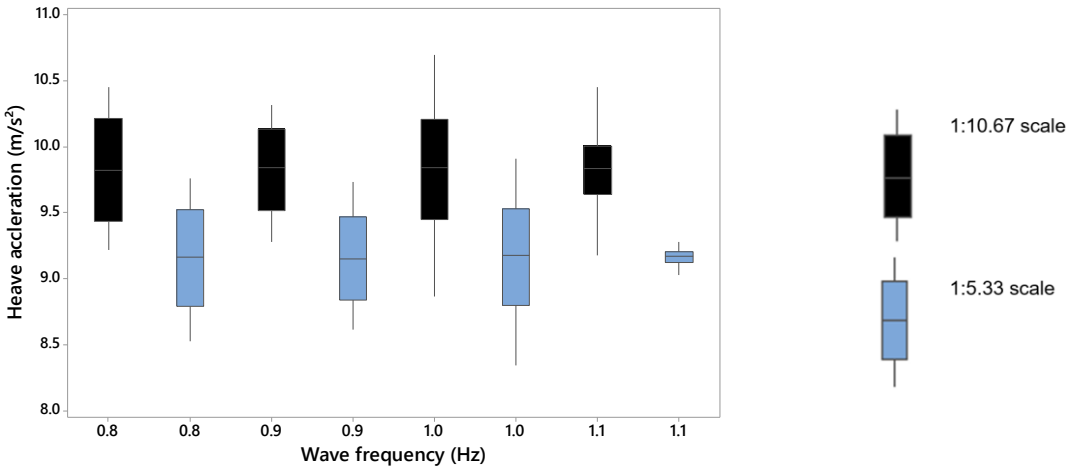

Fig. 10: Boxplots of vessel heave accelerations for 1:10.67 and 1:5.33 circular shaped buoys.

3.4 Effect of buoy scale on catenary riser extension

Observations of the motions of the buoys in the tanks revealed that as the wave frequency was increased the buoy and model lifeboat was moving further down the tank as the catenary riser lengthened its scope, as illustrated by the schematic and underwater photograph in Fig. 11. To quantify this observation the methodology using the Matlab algorithm described and verified in Hollyhead *et al.* (2017) was used to track the centroid of the buoy in the x-y plane, as videoed from above the tank. The signal noise was removed by the implementation of a 10^{th} order Butterworth filter set to a low pass frequency cut-off of 3Hz. A pixel factor, taken from a still image, was used to convert pixel values to distance moved down the tank (x direction) in metres.

Plotting the mean of the maximum excursions for the two scales against the four wave frequencies highlights that there is linear relationship as illustrated in Fig. 12. The linear regression coefficient for the 1:10.67 scale is 0.9905 and for the 1:5.33 scale is 0.9992. The mean actual distance travelled, when comparing the two different sized buoys, converges as the wave frequency increases. The difference, compared to the smaller scale, starting at 22% at 0.8Hz and falling to 2% at 1.1Hz wave frequency.

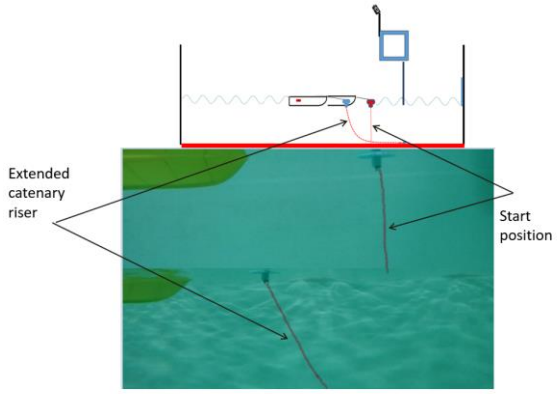

Fig. 11: Schematic and underwater photograph of extended catenary mooring riser.

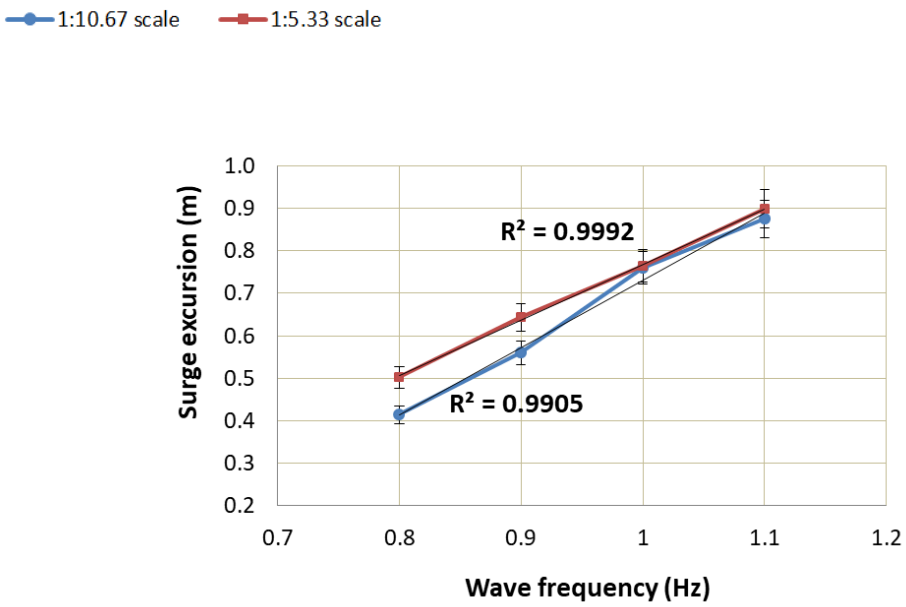

Fig. 12: Mean maximum surge excursion of the buoys averaged over all shapes.

4. Discussion

A series of free standing SPM model tests investigating the effects of buoy shape and buoy size on vessel motions, in regular waves, have been conducted. The experimental setup enabled the unrestricted motion of the mooring buoy and model lifeboat to be observed and the motion tracking algorithm (Hollyhead *et al.*, 2017) was successfully deployed in this experimental setup. Additionally the mooring riser was able to change its scope, by extending its catenary shape, as the wave frequencies were increased.

Time domain plots of the motions show that the dominant oscillatory rotational motion of the model was pitch and translational motions were surge and heave as a result of the mooring riser chain and hawser providing a restraining mechanism against the oncoming regular waves. All motions, except for the yaw, exhibited steady state oscillatory motion at the same frequency as the regular waves. During each test the model would yaw in line with the predictions of Wehausen (1979) and Schellin (2003) who state that a “floating elongated body will slowly drift in the direction

of wave propagation and turn broadside to the waves" thereby reducing the load in the mooring hawser compared to that if the heading was constrained.

In all cases the RAO of the vessel for surge, pitch, sway and heave are at their lowest value at the 1.1Hz wave frequency where the wavelength is now shorter than the LOA of the model (1.29m compared to 1.50m). This is in keeping with theory (Lloyd, 1989), namely that, as a result in the changes in buoyancy forces, a restrained ship only experiences significant excitations in head waves when they are longer than about three quarters of the ship length. For the experiments presented here three quarters of the model's length is 1.13m which equates to a wave frequency of 1.17Hz. This highlights a significant difference between the expected motion responses of lifeboats and offshore tankers stationed at SPMs in the same wave spectra. For example at a 1:10.67 scale three quarters of the LOA of a 175m tanker would be 12.3m which implies that significant motion responses would only occur for wave frequencies less than 0.36Hz.

Changing the shape of the buoy, at the 1:10.67 and the 1:5.33 scale, did not result in any significant change in the model's motions. It is therefore hypothesized that the differences in the wave patterns that were radiated from the different shapes were not significant enough to impact upon the vessel's motions.

When comparing the maximum surge of the buoy excursion down the tank there was not a significant difference between the buoy shapes. However, at the 0.8 and 0.9Hz wave frequencies, the larger buoys moved further down the tank, compared to the smaller ones, as the mooring riser lifted further from the tank floor (Fig. 11). As this results in an increase in suspended riser chain weight (Fig. 13) this would place an additional strain on the SPM buoy.

Results indicate that doubling the buoy scale resulted in lower pitch, slower sway and heave RAO but a higher surge RAO. In order to quantify this the percentage increase/decrease in translational accelerations were applied to the mean of the RMS of the 1:10.67 scale buoy, at each wave frequency (Table 5). An overall RMS reduction was calculated for 0.8, 0.9, 1.1 wave frequencies and an increase at the 1.0 wave frequency due to the peak in surge RAO. Added to the fact that the pitch angle decreased for each wave frequency tested indications are that increasing the size of the buoy could lead to an overall reduction in vessel motions at a SPM.

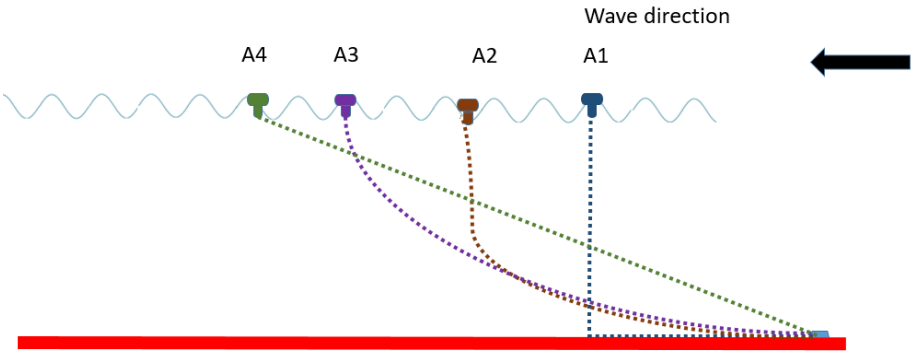

Fig. 13: Schematic of catenary mooring line of SPM.

Table 5: Changes in translational accelerations when comparing a 1:5.33 scale buoy to 1:10.67 scale buoys.

	Wave Frequency (Hz)			
	0.8	0.9	1.0	1.1
Surge increased accelerations (m/s^2)	0.0221	0.0061	0.0741	0.0102
Sway decreased accelerations (m/s^2)	(0.0471)	(0.0342)	(0.0199)	(0.0045)
Heave decreased accelerations (m/s^2)	(0.0038)	(0.0154)	(0.0298)	(0.0186)
Total increased/(decreased) accelerations (m/s^2)	(0.0288)	(0.0436)	0.0244	(0.0129)

Boxplots highlighted that the heave accelerations, including the gravitational accelerations, significantly decreased using larger buoys. The accelerations, measured at the model's centre of gravity, are presented relative to its resting position. A possible explanation for the recorded heave reduction is the angle of the IMU on the model. If the larger heavier buoys were pulling the bow downwards the Xsens IMU would no longer be on a horizontally flat plane and therefore the gravitational accelerations would be less than 9.81m/s^2. Taking the example of the 1:5.33 scale octagonal shaped buoys the RMS of heave accelerations was 9.17m/s^2 for the 0.8, 0.9, 1.0Hz wave frequencies and 9.18m/s^2 for the 1.1Hz which implies that the Xsens was at an angle of 21°. To test this hypothesis the Xsens was positioned statically at an angle of 21° and acceleration data recorded for a 45s duration. The RMS of the heave acceleration recorded was 9.17m/s^2.

A limitation of these experiments was that the resultant motions of the model lifeboat were sensitive to its initial orientation in the tank. The larger 1:5.33 scale buoys produced a higher percentage of a complete set of three repeated tests at 71% compared to the figure of 62% for the smaller 1:10.67 scale buoys. Additionally, due to the dimensions of the tank, the length of available data recording was restricted to 45s, however with the expected response frequency equal to the wave frequencies tested this should provide sufficient detail to compare the effect of buoy shape and buoy shape on the motions of the model lifeboat. Furthermore due to the non-repeatability of the roll and yaw results comparison of the effect of buoy size was not possible for these motions

5. Conclusion

This paper presents a series of model experiments on the regular wave induced motions of a 1:10.67 scale lifeboat at a single point mooring (SPM). The experimental set up enabled the unrestricted motions of the SPM buoy to be observed using a single 'off the shelf' video camera and a verified Matlab algorithm.

The results show the dominant oscillatory rotational motions of the model lifeboat was pitch and oscillatory translational motions were surge and heave as a result of the mooring riser chain and hawser providing a restraining mechanism at the SPM. The RAO of the model lifeboat's surge, pitch, sway and heave were at their lowest value at the 1.1Hz wave frequency where the wavelength is shorter than the length overall of the model. Changing the shape of the buoy, did not result in any significant change in the model's motions. Results indicate that doubling the buoy scale resulted in lower pitch, slower sway and heave RAO but higher surge RAO and quantification of these changes indicated that an overall acceleration RMS reduction was observed for wave frequencies of 0.8, 0.9, 1.1Hz and an increased RMS acceleration at the 1.0Hz wave frequency. The results suggest that changes in buoy size can influence the motion responses and may enable mooring efficacy to be improved.

Acknowledgements:

The provision of EngD funding from the RNLI and EPSRC (grant EP/G036896/1 the Industry Doctoral Training Centre in Transport and the Environment) is gratefully acknowledged.

The Matlab motion tracking code was written by Dr Christopher Phillips of Imperial College, University of London.

REFERENCES

Aghamohammadi, F. & Thompson, J. 1990. An experimental study of the large amplitude fish-tailing instabilities of a tanker at a single point mooring. Applied ocean research, 12, 25-33.

Barltrop, N. D. 1998. *Floating Structures: a guide for design and analysis*, Oilfield Pubns Inc.

Bradney. 1987. A practical guide to the mooring and anchoring of small boats. Available https://dbscweb.files.wordpress.com/2013/08/bradney-mooring-and-anchoring-leaflet.pdf (accessed on 17.09.17).

Carpenter, E.B., Leonard, J.W. and Yim, S.C.S., 1995. Experimental and numerical investigations of tethered spar and sphere buoys in irregular waves. *Ocean engineering*, *22*(8), 765-784.

Chakrabarti, S. 2005. Handbook of Offshore Engineering (2-volume set), Elsevier.

Chakrabarti, S., Libby, A., Palo, P., 1995. Small-scale testing on current-induced forces on a moored tanker. Ocean Engineering 22 (3), 271-300.

Channel Coastal Observatory. Wave data for Swanage Pier. https://www.channelcoast.org/data_management/real_time_data/charts/?chart=93&tab=stats&disp_option= (Accessed 01.10.17).

Eriksson, M., Isberg, J. and Leijon, M., 2006. Theory and experiment on an elastically moored cylindrical buoy. *IEEE Journal of Oceanic Engineering*, *31*(4), 959-963.

Gaythwaite, J.W., 2004. Design of Marine Facilities for Berthing, Mooring and Repair of Vessels, 2nd revised Ed. ASCE Press, p. 560.

Halliwell, A. & Harris, R. 1988. A parametric experimental study of low-frequency motions of single point mooring systems in waves. *Applied ocean research,* 10, 74-86.

Hinz, E. R. 2001. The complete book of anchoring and mooring. (Rev. 2nd ed.), Cornell Maritime Press Centreville, Maryland.

Hollyhead, C.J., Townsend N.C. and Blake J.I.R., 2017. Experimental investigations into the current-induced motions of a lifeboat at a single point mooring. Ocean Engineering. *Ocean engineering*, 146, 192-201.

Hughes, S. A. 2005. *Physical Models and Laboratory Techniques in Coastal Engineering*, World Scientific Publishing Co Pte Ltd, Singapore.

Schellin, T. 2003. Mooring load of a ship single-point moored in a steady current. *Marine structures,* 16**,** 135-148.

Jenkins, C.H., Leonard, J.W., Walton, J.S. and Carpenter, E.B., 1995. Experimental investigation of moored-buoys using advanced video techniques. *Ocean engineering*, *22*(4), 317-335.

Lloyd, A. R. J. M. 1989. *Seakeeping : ship behaviour in rough weather* Chichester, Ellis Horwood.

Oil Companies International Marine Forum, 2008. Oil Companies International Marine Forum Mooring Equipment Guidelines. Witherby Seamanship International, Livingston, United Kingdom.

Molland, A.F., Turnock, S.R., Hudson, D.A., 2011. Ship Resistance and Propulsion: Practical Estimation of Propulsive Power Cambridge University Press.

Papazoglou, V.J., Mavrakos, S. A. & Triantafyllou, M. S. 1990. Nonlinear cable response and model testing in water. *Journal of Sound and Vibration,* 140, 103-115.

Schellin, T., 2003. Mooring load of a ship single-point moored in a steady current. Marine Structures 16 (2), 135-148.

van Dorn, W. G. 1974. *Oceanography and seamanship*, Dodd, Mead New York, NY, USA.

Wehausen, J. 1971. Motion of Floating Bodies. *Annual Review of Fluid Mechanics,* 3**,** 237-&.

Which-Marina, 2015. Registered UK marinas. . Available: http://www.which-marina.com/Default.asp (Accessed 08.10.17).